

Some pages of this thesis may have been removed for copyright restrictions.

If you have discovered material in Aston Research Explorer which is unlawful e.g. breaches copyright, (either yours or that of a third party) or any other law, including but not limited to those relating to patent, trademark, confidentiality, data protection, obscenity, defamation, libel, then please read our [Takedown policy](#) and contact the service immediately (openaccess@aston.ac.uk)

Cellular and molecular consequences of S100A4-induced motility in rat breast tumour Rama 37 cells

Connie Goh Then Sin

Doctor of Philosophy

Aston University

July 2013

©Connie Goh Then Sin, 2013

Connie Goh Then Sin asserts her moral right to be identified as the author of this thesis

This copy of the thesis has been supplied on condition that anyone who consults it is understood to recognise that its copyright rests with its author and that no quotation from the thesis and no information derived from it may be published without proper acknowledgement.

Cellular and molecular consequences of S100A4-induced motility in rat breast tumour Rama 37 cells

Connie Goh Then Sin

A thesis submitted for the Doctor of Philosophy

2013

Thesis Summary

Since the first discovery of S100 members in 1965, their expressions have been affiliated with numerous biological functions in all cells of the body. However, in the recent years, S100A4, a member of this superfamily has emerged as the central target in generating new avenue for cancer therapy as its overexpression has been correlated with cancer patients' mortality as well as established roles as motility and metastasis promoter. As it has no catalytic activity, S100A4 has to interact with its target proteins to regulate such effects. Up to date, more than 10 S100A4 target proteins have been identified but the mechanical process regulated by S100A4 to induce motility remains vague. In this work, we demonstrated that S100A4 overexpression resulted in actin filaments disorganisation, reduction in focal adhesions, instability of filopodia as well as exhibiting polarised morphology. However, such effects were not observed in truncated versions of S100A4 possibly highlighting the importance of C terminus of S100A4 target recognition. In order to assess some of the intracellular mechanisms that may be involved in promoting migrations, different strategies were used, including active pharmaceutical agents, inhibitors and knockdown experiments. Treatment of S100A4 overexpressing cells with blebbistatin and Y-27632, non muscle myosin IIA (NMMIIA) inhibitors, as well as knockdown of NMMIIA, resulted in motility enhancement and focal adhesions reduction proposing that NMMIIA assisted S100A4 in regulating cell motility but its presence is not essential. Further work done using Cos 7 cell lines, naturally lacking NMMIIA, further demonstrated that S100A4 is capable of regulating cell motility independent of NMMIIA, possibly through poor maturation of focal adhesion. Given that all these experiments highlighted the independency of NMMIIA towards migration, a protein that has been put at the forefront of S100A4-induced motility, we aimed to gather further understanding regarding the other molecular mechanisms that may be at play for motility. Using high throughput imaging (HCI), 3 compounds were identified to be capable of inhibiting S100A4-mediated migration. Although we have yet to investigate the underlying mechanism for their effects, these compounds have been shown to target membrane proteins and the externalisation of S100 proteins, for at least one of the compounds, leading us to speculate that preventing externalisation of S100A4 could potentially regulate cell motility.

[Keywords: cancer, filopodia, focal adhesion, migration, non muscle myosin IIA]

Acknowledgements

I would like to take this opportunity to express my gratitude towards those who participate directly or indirectly throughout the academic years and ultimately, compiling this thesis.

My deepest gratitude goes to my supervisors, Dr. Stephane R. Gross and Professor Martin Griffin, for showering me with their wisdom, dedication and patience. Their concerns and constructive comments made the project's aims achievable.

I am highly thankful to Professor Phillip Rudland, Dr. Roger Barraclough, and Dr. Bernd Hoffmann for sharing their broad knowledge, experiences and laboratory skills throughout the entire project. Their patience with my never-ending doubts has broadened my knowledge and triggered my curiosity to explore even deeper into the researched area. A sincere gratitude is offered towards Charlotte Bland from ARCHA for her expertise in using confocal microscope. My warmest appreciation goes to Dr. Zita Baklava for her useful suggestions, encouragements, sympathetic ear, generosity and kindness ever since I met her.

I am thankful to all the colleagues who share their expertise (and chocolates!) without hesitation. Their amazing dedication towards the research has not only boosted my interest in the project, but also made me strive for excellence standards. Besides, I am grateful to those who offered me their friendships, especially the Shahid Miah and family. Their presence has made this journey enjoyable, fun and lively.

Last but not least, my heartfelt gratitude to my beloved family, Mum, Dad, Raymond, Alice, Shirley and Christine, who showered me with their unconditional love, care, moral and financial support regardless of the distance. Thank you, Mum, for being the listener and the best friend. Thank you, Dad, for your financial support and being the pillar of strength. Loving appreciation is extended to my maternal grandfather who had never failed to remind me of my capabilities. Without any of these mentioned people, I would never have completed my thesis. For this, I am forever indebted.

List of Publications

Goh Then Sin, C. Hersch, N., Rudland, P.S., Barraclough, R., Hoffmann, B. and Gross, .S. R. 2011. S100A4 downregulates filopodia formation through increased dynamic instability. Cell Adhesion and migration, 5, 439 - 47

Gross, S.R., Goh Then Sin, C., Barraclough, R. and Rudland, P. S. 2013. Joining S100 proteins and migration: for better or for worse, in sickness and in health. Cellular and Molecular Life Sciences. (In Press)

Ismail, T., Gross, S. R., Goh Then Sin, C., Fenig, D. G., Wilkinson, M. C., Rudland, P. S., and Barraclough, R. The C-terminal amino acid of S100P plays a role in S100P-induced cell migration and metastasis. (In preparation)

Table of Contents

Acknowledgement	3
List of Publications	4
Table of Content.....	5
List of Figures	6 - 9
List of Tables.....	10 - 11
List of Abbreviations	12 - 15
Chapter 1: Introduction.....	16 - 57
Chapter 2: Materials and Methods	58 - 91
Chapter 3: Upregulation of S100A4 promotes cell migration and filopodia instability.....	92 - 128
Chapter 4: Independency of non muscle myosin II pathway in S100A4-induced cell migration	129 - 180
Chapter 5: Targeting S100A4 protein in high throughput screen technology.....	181 - 213
Chapter 6: General Discussion	214 - 224
References.....	225 - 264

List of Figures

Figure 1.1	Illustration showing the changes in position of helix 3 and helix 4 of S100A4 in a calcium-dependent manner.....	22
Figure 1.2	Schematic representation of consequences of S100A4 interacting with its target protein	33
Figure 1.3	Illustration of non muscle myosin II (NMMII) homodimer	35
Figure 1.4	Actomyosin contraction	38
Figure 1.5	Interaction of S100A4 dimer with 45-residue long NMMIIA tail fragment ...	41
Figure 1.6	Formation of lamellipodia through various signalling proteins.....	45
Figure 1.7	Formation of filopodium	47
Figure 1.8	Integrin transducing extracellular cues which led to recruitment of cytoplasmic protein signalling	51
Figure 1.9	Different types of stress fibers distinguished by focal adhesions	54
Figure 1.10	Signalling proteins involved in regulating focal adhesion dynamicity through actin filaments to facilitate cell migration	56
Figure 2.2.1	Illustration of C terminus region of S100A4 protein.....	66
Figure 2.2.2	Western blot reconfirming level of S100A4 expression	66
Figure 2.2.3	Representative image of Rama 37 control cells assigned into respective class using CellIQ imaging system.....	71
Figure 2.2.4	Layout of cell types seeded in 24 well plates for preliminary screening.....	72
Figure 2.2.5	Layout of cell types seeded in 24 well plates for secondary and tertiary screening.....	72

Figure 2.2.6	Illustration showing how a wound area closure rate is calculated from raw data obtained	73
Figure 3.2.1	Full length S100A4 protein expression promotes cellular migration in wound healing assay	98
Figure 3.2.2	Low mitotic index during wound healing assay	99
Figure 3.2.3	Overexpression of wild type S100A4 but not the C-terminal truncated forms of $\Delta 2$ and $\Delta 6$ prevents the formation of mature vinculin clusters	101
Figure 3.2.4	Maturation of paxillin clusters was observed in Rama 37 control, R37 S100A4 $\Delta 2$ and R37 S100A4 $\Delta 6$	102
Figure 3.2.5	Truncated forms of S100A4 protein (S100A4 $\Delta 2$ and $\Delta 6$) did not affect the localisation of fascin within filopodia as observed in Rama 37 control cells.....	107
Figure 3.2.6	Cells expressing full length of S100A4 protein display prominent lamellipodium structure	108
Figure 3.2.7	Elevation of vinculin and paxillin expressions in R37 S100A4 WT cells	112
Figure 3.2.8	Distinguishing matured from nascent focal adhesion in Rama 37 cells	115
Figure 3.2.9	Establishment of stably adhered filopodia, retraction fibers and unstable filopodia in Rama 37 cells	116
Figure 3.2.10	Reduction of NMMIIA expressions in wild type S100A4 expressing cells	122
Figure 4.2.1	Blebbistatin and BDM, but not Y-27632 post 24 hours treatment on Rama 37 control cells reduces cell viability	136
Figure 4.2.2	Blebbistatin (25 μ M) and Y-27632 (50 μ M) resulted in alteration of cell morphology and actin filaments disorganisation	137

Figure 4.2.3	Inhibition of NMMII with blebbistatin or Y-27632 promotes wound healing in both Rama 37 control cells and R37 S100A4 WT cells	139
Figure 4.2.4	Reduction of paxillin clusters and disassembly of actin stress fibers in Rama 37 cells as a consequence of NMMII inhibition by blebbistatin	142
Figure 4.2.5	Reduction of paxillin clusters and disassembly of actin stress fibers in Rama 37 cells as a consequence of NMMII inhibition by Y-27632	143
Figure 4.2.6	Treatment with 25 μ M of blebbistatin resulted in loss of transverse arcs and distribution of NMMII throughout the cytoplasm of the cells	146
Figure 4.2.7	NMMII inhibition by Y-27632 resulted in loss of actin stress fibers and distribution of NMMIIA throughout the cytoplasm of the cells	147
Figure 4.2.8	Level of NMMIIA expression is significantly reduced after knockdown with SiRNA2.....	150
Figure 4.2.9	Knockdown of NMMIIA has opposing motility effects in Rama 37 control cells and R37 S100A4 WT cells	151
Figure 4.2.10	Inhibition of NMMIIA resulted in overall loss of paxillin clusters while promoting polarisation of Rama 37 cells.....	153
Figure 4.2.11	Inhibition of NMMIIA resulted in loss of colocalisation of NMMIIA with actin stress fibers	154
Figure 4.2.12	Jetpei transfection reagents gives the highest transfection efficiency in Cos 7 cells.....	156
Figure 4.2.13	High level of NMMIIA and S100A4 protein expression in Cos 7 cells transfected with PeGFP NMMIIA and PeCFP S100A4 WT	157
Figure 4.2.14	Rescue of NMMIIA in Cos 7 reduces migration	159
Figure 4.2.15	Inhibition of NMMIIA in Cos 7 PeGFP NMMIIA restored its original phenotype.....	161

Figure 4.2.16	Blebbistatin inhibition causes disassembly of NMMIIA localisation along actin stress fibers	163
Figure 4.2.17	Blebbistatin inhibition causes reduction of paxillin clusters in NMMIIA transfected Cos 7 cells	164
Figure 4.2.18	Y-27632 inhibition disassembly of NMMIIA along actin stress fibers in Cos 7 cells transfected with NMMIIA.....	165
Figure 4.2.19	Y-27632 inhibition resulted in reduction of paxillin clusters in Cos 7 cells transfected with NMMIIA	166
Figure 4.2.20	Introduction of S100A4 enhance migration	168
Figure 4.2.21	Restoration of NMMIIA in Cos 7 cells leads to increment of stress fibers whereas introduction of S100A4 resulted in polarisation	171
Figure 4.2.22	Introduction of S100A4 protein into Cos 7 cells leads to polarisation while significant increase of paxillin clusters were observed in NMMIIA expressing Cos 7 cells.....	172
Figure 5.2.1	Preliminary screening showing different effects of chemical compounds on S100A4 protein through wound healing.....	188
Figure 5.2.2	Specificity of compounds to S100A4 protein can be shown through wound healing based-HCl	193
Figure 5.2.3	Compounds demonstrating reproducibility and specificity for S100A4 protein whilst not affecting cell viability	200
Figure 5.2.4	Optimisation of working concentration of the selected compounds through wound healing assay shows 5 μ M as optimal.....	203
Figure 5.2.1	Mobilisation of calcium through GPCRs triggered pathway	208
Figure 5.2.2	Mechanism of uptake of serotonin through SERT	211

List of Tables

Table 2.1	Densities of different cell lines to be seeded in each well of 24 well plate for scratch assay.	70
Table 2.2	Density of respective cells to be seeded in each well of 24 well plate for transfection.....	75
Table 2.3	Density of respective cells to be seeded in 60 mm culture dish for transfection prior to conducting western blot.	75
Table 2.4	Ratios of different reagents to be added in either 24 well or 6 well transfections	77
Table 2.5	Dilutions of antibodies used for immunofluorescence staining.....	78
Table 2.6	Formulations used for making 1L of cytoskeleton buffer (1x).....	78
Table 2.7	Formulations to prepare 1L of Lennox Broth and 100ml of Transformation and Storage Solutions (1X).....	82
Table 2.8	Formulations of 1L of Tris-Acetate-EDTA (1X) and 10ml of DNA tracking dye.....	84
Table 2.9	Appropriate percentage of gels to be used to separate different protein size.....	87
Table 2.10	Appropriate amount of different reagents to make up specific gel percentages.....	87
Table 2.11	Formulations to prepare 1L of running buffer (1X) and 50ml Laemmli buffer (4X)	87
Table 2.12	Formulations for preparing different buffers used in Western Blot	89
Table 2.13	Dilutions of different primary antibodies used in Western Blot	90
Table 2.14	Preparation of stripping buffer	90

Table 3.2.1	Overexpression of S100A4 protein resulted in loss of vinculin clusters.....	103
Table 3.2.2	Significant reduction of number of paxillin clusters in cells expressing full length of S100A4 protein.....	104
Table 3.2.3	Number of filopodia protusions was significantly lowered in R37 S100A4 WT cells.....	109
Table 3.2.4	Overexpression of S100A4 protein reduced the number of fascin-mediated filopodia projections.....	110
Table 3.2.5	Significantly lower count of focal adhesions observed in live cell analysis of R37 S100A4 WT cells.....	117
Table 3.2.6	R37 S100A4 WT displays lower focal adhesion formation	118
Table 3.2.7	Cells overexpressing full length of S100A4 protein show higher filopodia dynamics	119
Table 3.2.8	R37 S100A4 WT cells exerts significantly lower contractile force	121
Table 4.2.1	Inhibition of NMMII resulted in loss of paxillin clusters	144
Table 4.2.2	Introduction of NMMIIA and S100A4 into Cos 7 cells causes opposing effect on focal adhesion clusters	173
Table 5.2.1	Out of 30 hits, compounds that slow migration occupy the largest group, followed by causing cell death, inhibition of wound healing and accelerate wound healing.....	189 - 190
Table 5.2.2	High reproducibility of primary screen result is achieved and detailed calculation of wound area closure rate correlates with the wound healing curves	194 - 196
Table 5.2.3	Tertiary screen showing 3 drugs having significant specificity towards R37 S100A4 WT cells but not Rama 37 control cells	199

List of Abbreviations

5-HT – 5-hydroxytryptamine

[Ca²⁺] – Calcium concentration

A2AR - α_{2a} adrenergic receptor

ADC - adenylyl cyclase

ADP - Adenosine diphosphate

Arp - Actin-related protein

ATP - Adenosine triphosphate

BDM - 2,3-Butanedione monoxime

Ca²⁺ - calcium

cAMP - cyclic adenosine monophosphate

CCN3 - nephroblastoma overexpressed

cdk2 - cell division-stimulating protein

CH - calponin homology

CKII - casein kinase II

CP – capping protein

CRK - Rac GTP-exchange factor

DAG - diacyl glycerol

DIP - Dia interacting protein

DMEM - Dulbecco minimal Eagle's medium

DMSO - dimethylsulphoxide

DPC - detergent dodecyl phosphocholine

DR2 - dopamine 2 receptor

EDTA - Ethylenediaminetetraacetic acid

ELC - essential myosin light chains

EMT - epithelial-mesenchymal transition

Ena/VASP - Enabled/vasodilator-stimulated phosphoprotein

ER - endoplasmic reticulum

ERK - extracellular signal-regulated kinase

ES - null embryonic stem

EVH1 - ENA/VASP homology

F-actin - filamentous actin

FAT - focal adhesion targeting

FAK - focal adhesions kinase

FERM - protein 4.1, ezrin, radixin and moesin homology

FLN-A - non-muscle filamin

FN - fibronectin

Formazan - 1-(4,5-dimethylthiazol-2-yl)-3,5-diphenylformazan

formin mDia2 - mammalian Diaphanous –related formins

FSP1 - fibroblast-specific protein

G418 - geneticin

G-actin – globular actin

G-protein coupled receptor (GPCR)

HCI - High Content Imaging

hPA-SMCs - human pulmonary arterial smooth muscle cells

HTS - High throughput screening

IP₃ - inositol 1,4,5-triphosphate

IP₃R - IP3 receptor

IRSp53 - insulin receptor tyrosine kinase substrate p53

K_d - dissociation constant

K⁺ - potassium

LIMK1 - LIM-domain kinase 1

LAR - leukocyte common antigen-related

M₁₋₃ - muscarinic 1-3 receptor

MBS - myosin binding subunit

Mena - mammalian Enabled

MetAP2 - methionine aminopeptidase 2

MLCK - myosin light chain kinase

MMPs - matrix metalloproteinases

MTT - 3-(4,5-dimethylthiazol-2-yl)-2,5-diphenyl tetrazolium bromide

Mts1 – metastasin

NMM - non muscle myosin

NMMHCII – non muscle myosin heavy chain II

NaOH - Sodium hydroxide

NaCl – Sodium chloride

PAH - pulmonary arterial hypertension

PAK - p21-GTPase-activated kinase

PBS – phosphate buffered saline

PFA - Paraformaldehyde

PH - pleckstrin homology

PIP₂ - phosphatidylinositol 4,5-bisphosphate

PIP 5-kinase - phosphatidylinositol 4-phosphate 5-kinase

PIN1 - peptidyl-prolyl cis/trans isomerase

PKA - protein kinase A

PKC - protein kinase C

PLC - phospholipase C

PP1M - myosin protein phosphatase 1

RAGE - Receptor for Advanced Glycation Endproducts

RIF - Rho in filopodia

RLC - regulatory light chains

ROCK - Rho-associated protein kinase

R_{YR2} - ryanodin receptor 2

SERT - serotonin reuptake transporter

SDS - sodium dodecyl sulphate

SFKs - Src family kinases

SiRNA – Small interfering RNA

TAE - Tris-Acetate-EDTA

TEMED - N,N,N',N'-Tetramethylethylenediamine

TG - thapsigargin

TIMPs - tissue inhibitor of metalloproteinases

TMs - tropomyosins

TM2 - non muscle tropomyosin 2

TM5 - non muscle tropomyosin 5

WASP - Wiskott-Aldrich syndrome protein

WAVEs - Wiskott-Aldrich syndrome protein (WASP) family verprolin-homologous protein

Chapter 1: Introduction

Chapter 1 Introduction

1.1 S100 family proteins	18
1.1.1 S100A4 proteins	20
1.1.1.1 Protein structure	21
1.1.1.2 Distribution of S100A4 in tissues and cells.....	23
1.1.1.3 S100A4 in tumourigenesis and metastasis.....	25
1.1.1.4 S100A4 molecular mechanism	26
1.1.1.4.1 S100A4 and non cytoskeletal proteins.....	27
1.1.1.4.2 S100A4 and cytoskeletal proteins.....	31
1.2 Non muscle myosin II	34
1.2.1 Non muscle myosin II isoforms	35
1.2.2 Regulation of non muscle myosin IIA	36
1.2.3 Actomyosin contraction	37
1.2.4 Myosin and S100A4.....	39
1.3 Migration	42
1.3.1 Cell polarisation	42
1.3.1.1 Lamellipodia	43
1.3.1.2 Filopodia	45
1.3.2 Stabilisation of extended leading edge.....	47
1.3.2.1 Integrins and downstream signalling	48
1.3.3 Contraction of cell body	52
1.3.4 Tail retraction and disintegration of focal complexes.....	55
1.4 Aims	57

Chapter 1: Introduction

According to statistical data provided by Cancer Research UK, death caused by breast cancer account up to 7% of all cancers in both genders and is currently the second most common cancer among female after lung cancer. A year after diagnosis and treatment, the patients' survival rate is 95.8%, but this rate dropped to 85.1% after 5 years of treatment and 10 years post treatment, this rate dropped to 77.0% (<http://www.cancerresearchuk.org/cancer-info/cancerstats/types/breast/survival/>). The main cause of reduction in patients' survival is due to the progression of benign tumour into malignant tumour through a process known as metastasis. Generally, this process requires tumour to 1) breakdown basal membrane, 2) invade adjacent tissues, 3) infiltrate blood stream (intravasation), 4) invade into tissue (extravasation) and finally proliferate as secondary tumour by harvesting nutrients through angiogenesis (Chaffer and Weinberg, 2011, Leber and Efferth, 2009, Oppenheimer, 2006, Yokota, 2000, Gupta and Massague, 2006, Mack and Marshall, 2010). In order to tackle tumour malignancies, a myriad of research have been dedicated to each of these chronological steps (evasion from immune systems, invasion, migration, angiogenesis and aberrant proliferations) to provide better understanding and ultimately, to generate new therapeutic avenues. In this work, we focused on some aspect of cell migration and its relevancy in malignancy progression.

1.1 S100 family proteins

S100 gene family is the largest subgroup within the superfamily of the proteins, with more than 25 family members found specifically distributed in human tissue and characterised by possession of calcium binding EF-hand motif at either end of the protein (Barraclough et al., 1987). The name S100 is derived from the fact that they are soluble in 100% saturated

ammonium sulphate. These 25 members of the S100 family share 22% to 57% sequence identity (Marenholz et al., 2004, Gross et al., 2013). Although S100 family spans widely among vertebrates, no S100-like family has ever been detected in invertebrates, suggesting that this gene is a relatively new gene which only occurs during vertebrate evolution (Shang et al., 2008).

Most S100 proteins, with the exception of S100A10, bind to their intracellular target proteins in a calcium dependent manner (Rescher and Gerke, 2008). The insensitivity of S100A10 to calcium is a result of mutations in both EF hand motifs (calcium binding sites of helix E and helix F) causing the protein to remain in calcium-bound configuration (Lewit-Bentley et al., 2000). As for the rest of the S100 members, conformational shifts from closed hydrophilic to hydrophobic were attained in the presence of calcium, with higher calcium binding affinity at the C terminus EF-hand motif than those of N terminus. These motifs demonstrate highest levels of amino acid conservation throughout the protein (Donato, 1986, Gribenko and Makhatadze, 1998, Barraclough et al., 1990). Binding of calcium to these motifs resulted in conformational change, which exposes a hydrophobic region with the least amount of sequence homology, suggesting their specificity in binding to other target proteins which has been shown to have direct interaction with lipid vesicles (Bhattacharya et al., 2004, Mueller et al., 1999). For instance, S100G has been shown to directly interact with detergent dodecyl phosphocholine (DPC), S100B has been shown to bind to cardiolipin vesicles while S100A1 has been shown to increase L-type calcium channel current in cardiomyocytes which suggests the potential role of S100 proteins to bind to natural membranes (Malmendal et al., 2005, Zolese et al., 1988, Reppel et al., 2005)

Due to the vast diversity of S100 family proteins, they have been shown to be involved in various cell's functions such as cell cycle, differentiation, survival, apoptosis, motility and

intracellular calcium homeostasis via intracellular and extracellular activities (Brozzi et al., 2009, Tsoporis et al., 2010, Cheng et al., 2008, Beccafico et al., 2011, Lin et al., 2010, Chen et al., 2001, Donato et al., 2009). Besides, S100 family proteins have been implicated in different pathological conditions such as cancer, hypertension, arthritis and neurodegeneration (Barraclough, 1998, Rudland et al., 2000, Ambartsumian et al., 2001, Donato, 2001, Donato et al., 2009). For instance, it was reported that S100A1 has been linked to heart failure and hypertension whereas S100A4 has been linked to metastasis promotion (Most et al., 2013, Boye and Mælandsmo, 2010). Recently, with the advancement of gene therapy, S100A1 has been introduced in clinical trials to treat patients with heart failure (Most et al., 2013) whereas S100A4 has been proposed to be used as a prognostic marker in breast cancer (Ismail et al., 2008a). Other members of S100 proteins has also been shown to be involved in cellular migration where S100A6 is thought to act as motility inhibitor whereas S100A7, S100A8, S100A9 and S100B as motility promoter (van Dieck et al., 2009, Wolf et al., 2011, Rescher and Gerke, 2008, Brozzi et al., 2009). Due to the cosmic effects caused by S100 proteins, researches have been dedicated to provide in depth understanding of their mechanisms and functions.

1.1.1 S100A4

S100A4, one of the member of S100 protein superfamily, has been independently named as metastasin (Mts1), fibroblast-specific protein (FSP1), 18A2, pEL98, p9Ka, 42A, CAPL, calvasculin and Placental Calcium Binding Protein (reviewed by Mishra et al., 2012). Due association of S100A4 with different cancer types, this 101-amino acids-containing-polypeptide generated much attention in the field of carcinogenesis. Although S100A4 is expressed in various tissues, overexpression of S100A4 has been reported to correlates

with breast, esophageal, lung, gastric, colorectal, pancreatic and skin cancer (Rudland et al., 2000, Andersen et al., 2011, Goh Then Sin et al., 2011, Ninomiya et al., 2001, Kimura et al., 2000, Yonemura et al., 2000b, Takenaga et al., 1997b, Rosty et al., 2002, Andersen et al., 2004).

1.1.1.1 Protein structure

S100A4 is a relatively small molecule, with a molecular weight of 10 – 12 kDa and is expressed in cytoplasm, within the cell nucleus as well as secreted extracellularly (Barraclough, 1998, Flatmark et al., 2003). This protein may present as a monomer, heterodimer, symmetric homodimer and oligomer where interaction with target proteins has only been associated with homodimeric conformation (Vallely et al., 2002, Kim and Helfman, 2003, House et al., 2011, Kiss et al., 2012). S100A4 has been found to form heterocomplex with S100A1 through yeast two-hybrid system in the absence of calcium. Although no known cellular functions has been demonstrated as a consequence of this heterodimerisation, it was proposed that this heterocomplex could possibly have cellular targets different than those of the S100A4 and S100A1 homodimers as homodimerisation of S100A1 and S100B, in the presence of zinc, has been shown to inhibit the assembly of brain microtubule whereas S100A1 homodimer did not exhibited such effects (Tarabykina et al., 2000, Tarabykina et al., 2001, Donato et al., 1985). Addition of exogenous S100A4 oligomer has been shown to induce endothelial cell motility, stimulate the production of matrix metalloproteinases (MMPs) of synovial fibroblast, as well as induce differentiation of rat hippocampal neurons (Ambartsumian et al., 2001, Senolt et al., 2006, Novitskaya et al., 2000). However, interactions of S100A4 oligomer with target proteins have not been established and their binding mechanisms have yet to be resolved. On the other hand,

S100A4 homodimer is well characterised and a few of its target proteins will be mentioned in the preceding sections. S100A4 homodimer comprises of two alpha and two beta chains joined by noncovalent interaction.

Dimerisation of S100A4 monomer occurs via antiparallel alignment of helix 1 with helix 1' and helix 4 with helix 4'. C terminus binding domain of S100A4, located between helix 1 and helix 2, contains 12 residues and has higher affinity toward calcium (Kd 10 - 50 μ M) than the 14 residues containing N terminus, located between helix 3 and helix 4 (Kd 200 - 500 μ M) (Kligman and Hilt, 1988, Vallely et al., 2002, Dutta et al., 2002). S100A4 undergoes conformational change in the presence of calcium where a hydrophobic binding pocket is formed by helices 3 and 4, the hinge region and the C terminal loop (Figure 1.1) (Garrett et al., 2006).



Figure 1.1 Illustration showing the changes in position of helix 3 and helix 4 of S100A4 in a calcium-dependent manner. This conformational change is needed for S100A4 to bind to target proteins such as Myosin IIA, p53, and annexin II. Dimerisation of S100A4 occurred through interaction of helix 1 with helix 1' and helix 4 with helix 4'. (Prime (') indicating the other monomer) (Adapted from Garrett et al., 2006).

1.1.1.2 Expression of S100A4 in different pathological diseases

S100A4 expression has only been implicated in a some of normal ovary and prostate cells and has not been detected in normal breast, colon, thyroid, lung, kidney and pancreas cells (Mazzucchelli, 2002). Higher levels of S100A4 are detected in more motile cells such as monocytes, macrophages and leukocytes when compared to levels of S100A4 detected in keratinocytes, melanocytes, Langerhans' cells and sweat glands suggesting the possibility of S100A4 in regulating cell motility (Gibbs et al., 1995, Takenaga et al., 1994, Boni et al., 1997, Li et al., 2010). Besides, up-regulation of S100A4 has been reported in most carcinomas as well as some pathological diseases which may emphasize the reputation of S100A4 as indicator of these abnormalities (Kimura et al., 2000, Lo et al., 2011, Moriyama-Kita et al., 2005, Rosty et al., 2002, Saleem et al., 2006, Takenaga et al., 1997b, Yonemura et al., 2000b, Zou et al., 2005).

Overexpression of S100A4 has been found to be correlated to the severity of pulmonary arterial hypertension (PAH) disease (Greenway et al., 2004). In S100A4 transgenic mice, S100A4 was found to be concentrated in the endothelial cell lining of the occluded vessels with increased level of circulating inflammatory cells. As inflammatory cells were found to highly express S100A4 protein, it was suggested that this could be the reason affecting S100A4 concentration in the vessels. This hypothesis was supported by the finding demonstrating that in human pulmonary arterial smooth muscle cells (hPA-SMCs), secretion of S100A4 to the extracellular matrix is dependent on both serotonin (5-HT) receptor and serotonin transporter which increases human pulmonary arterial smooth muscle cells (hPA-SMCs) migration and proliferation (Lawrie et al., 2005).

In another study, it has been demonstrated that cross-breeding of transgenic mice overexpressing S100A4 in the mammary gland with GRS/A mice (GRS/A strain is

characterised by high incidence of non-metastatic tumours) resulted in offspring developing metastatic tumours with a marked elevation of S100A4 in the blood (Ambartsumian et al., 2005). These observations demonstrated that extracellular S100A4 is responsible for stimulating tumourigenesis, metastasis and angiogenesis in the transgenic offspring via an unknown mechanism.

Besides, expressions of S100A4 were detected in synovial fluid of rheumatoid arthritis patients and articular chondrocytes of osteoarthritis patients but not in normal synovium suggesting that S100A4 may be involved in these pathological conditions (Senolt et al., 2006). It was found that addition of exogenous S100A4 oligomer to normal synovium resulted in upregulation of MMPs in the cell culture supernatants which led to speculation of S100A4 may regulate osteoarthritis and rheumatoid arthritis via MMPs (Senolt et al., 2006, Yammani et al., 2006). Decreased bone matrix mineralisation has been implicated in patients suffering from osteoarthritis where S100A4 may be involved as S100A4 was found to inhibit mineralisation (Cox et al., 2012). It was found that periodontal ligament cells which remain unmineralised, has lower expression of osteopontin, osteocalcin and the osteoblastic-specific transcriptors (Runx2/Cbfa1 and Osterix) and inhibition of S100A4 expression led to restoration of the osteoblastic markers expression (Kato et al., 2005). In another report, it was found that level of S100A4 decreases as level of osteoblast extracellular matrix mineralisation increases. These observations further strengthen the role of S100A4 in delaying mineralisation and/or differentiation of osteoblasts (Duarte et al., 1999, Duarte et al., 2003).

Also, S100A4 was found to be expressed in astrocytes of the spinal cord and addition of oligomeric form of S100A4 has been found to coincide with differentiation of cultured hippocampal neurons (Kozlova and Lukanidin, 1999, Novitskaya et al., 2000, Belot

et al., 2002). Oligomeric form of S100A4 was found to interact with G_{αq/11} subunit of G-protein coupled receptor (GPCR) which resulted in activation of phospholipase C β (PLCβ) and subsequently causing influx of calcium, leading to alteration of neuron's morphology (Kiryushko et al., 2006). However, it was unknown whether this oligomeric form of S100A4 is present in vivo, raising the speculation if S100A4 dimer could interact directly with GPCRs.

1.1.1.3 S100A4 in tumourigenesis and metastasis through clinical evidences

The reason behind much gained attention of S100A4-based research is due to its association with cancer and metastasis. Evidently, S100A4 has been shown to promote metastasis in different carcinomas (Ismail et al., 2008a, Davies et al., 1994, Andersen et al., 2011, Cabezón et al., 2007, Xue et al., 2003, Rudland et al., 2000, McKiernan et al., 2011).

Using immunohistochemistry to test normal and malignant breast tissues from 216 subjects, S100A4 was found to be absent in normal breast tissues whereas approximately 50% of the cancer tissues overexpresses S100A4 (Ismail et al., 2008a). In another report, 349 breast cancer patients were assessed for S100A4 overexpression. Similarly, less than half of the carcinogenic samples stained positive for S100A4. In the follow up of the experiments which was conducted 19 years later, it was found that 80% of the S100A4-negative patients and only 11% of the S100A4-positive patients are still alive (Rudland et al., 2000). Although these studies revealed the correlation between up-regulation of S100A4 and severity of breast cancer, other proteins such as matrix metalloproteinases (MMPs), CD44, methionine aminopeptidase 2 (MetAP2), integrins and p53 has also been shown to be up-regulated in malignant breast cancer (Andersen et al., 2011, Sternlicht et al., 1999, Afify et al., 2009, Chou et al., 2013). However, direct link between S100A4 and metastasis was

established when non-metastatic cancer cell lines acquired metastatic characteristic via specific introduction of S100A4 in vivo and ex vivo (Xue et al., 2003, Ismail et al., 2008b).

Beside breast cancer, severity and overexpression of S100A4 has also been implicated in patients suffering from advanced gastric (Wang et al., 2010, Yonemura et al., 2000b), pancreatic (Ikenaga et al., 2009), colorectal (Takenaga et al., 1997b), lung (Kimura et al., 2000) and thyroid carcinoma (Zou et al., 2004, Zou et al., 2005). For instance, consequences of S100A4 overexpression in these carcinomas are; 1) gastric cancer patients have higher incidence of metastatic lesions, 2) pancreatic cancer patients have lower survival chances, 3) lung cancer patients have higher incidence of metastasis with poor survival rate and 4) thyroid cancer patients with high incidence of lymph nodes metastases. Collectively, these studies also revealed the inverse correlation of S100A4 expression with adhesion-associated protein expression such as E-cadherin, α -catenin, and tissue inhibitor metalloproteinases (TIMPs) (Andersen et al., 2011, Moriyama-Kita et al., 2005, Rodriguez et al., 2012, Yonemura et al., 2000b, Yonemura et al., 2000a, Bjornland et al., 1999, Kimura et al., 2000). Although it is unknown whether S100A4 is capable of regulating the expressions of these proteins, it is confirmed that this inverse correlations promote epithelial-mesenchymal transition (EMT), an important tumour progression and invasion event (Schneider et al., 2008, Lo et al., 2011, Matsuzaki and Darcha, 2012).

1.1.1.4 S100A4 molecular mechanism

As S100A4 possess no enzymatic activity, it is believed that the pathological effects observed due to S100A4 upregulation could possibly be due to its interactions with other target proteins such as S100A1, non muscle myosin (NMM) IIA and -IIB, actin, tropomyosins (TMs), p53, liprin β 1, methionine aminopeptidase 2 (MetAP2), and CCN3 protein (Cysteine-

rich protein, Cyr61, Connective tissue growth factor, CTGF, and Nephroblastoma overexpressed gene, Nov) (Figure 1.2) (reviewed by Boye and Mælandsmo, 2010). The target proteins mentioned will be classified into non cytoskeletal proteins (p53, S100A1, CCN3, liprin β 1 and MetAP2) and cytoskeletal proteins (actin and TMs) where their interactions with S100A4 will be briefly discussed here.

1.1.1.4.1 S100A4 and non cytoskeletal proteins

Tumour suppressor p53 is a transcriptional factor which plays an important role in maintaining and regulating overall cellular functions by inducing cell cycle arrest, repair of damaged DNA, apoptosis due to cell stress signals, angiogenesis, senescence and cell differentiation (reviewed by Sionov and Haupt, 1999). P53 limits tumourigenic transformation by binding to DNA which led to stimulation of another protein known as p21. The p21 protein in turn, forms a complex with cell division-stimulating protein (cdk2), halting the G1 stage of cell division from proceeding to S phase (Gervais et al., 1998). It has been reported that p53 mutation occurred in diverse human tumour types and mice with p53 deficiency are more susceptible to tumour development which led to speculation that cells with mutated p53 protein are unable to halt cell division resulting in replication of mutated DNA which may, ultimately, lead to tumour formation (Nigro et al., 1989, Donehower et al., 1992, Loayza-Puch et al., 2013, Tamaki et al., 2013). N-terminal domain of p53 protein reveals a proline rich region (from 61 – 97 residues) which has been shown promote apoptosis, a central part which acts as DNA binding region (from 102 - 292 residues) and lastly, a C-terminal domain which contain nuclear localisation domain (313 – 332 residues), tetramerisation domain (320 – 356 residues) and negative regulatory

domain (367 – 393 residues) (Cho et al., 1994, Venot et al., 1998). S100A4 has been shown to bind to the 364 - 393 amino acid residues of C terminal region of p53, inhibiting phosphorylation by protein kinase C (PKC) in a calcium independent manner as opposed to S100B, S100A2 and S100A6 binding to p53 in which the presence of calcium is essential (Grigorian et al., 2001, Grigorian and Lukanidin, 2003, Chen et al., 2001, Berge and Mælandsmo, 2011). Binding of S100A4 to p53 has been shown to suppress the DNA binding activity of p53, proposing that the possible regulatory mechanism of S100A4 on p53 activity (Grigorian et al., 2001). Immunohistochemistry of breast tumour specimens revealed higher percentage of positively-stained p53 correlates with positive staining of S100A4 than the S100A4 negatively-stained specimens suggesting that these two protein may have inter-regulatory roles (Rudland et al., 2000). Recently, through immunocytochemical staining, it was found that S100A4 colocalises with p53 in the nucleus and S100A4 knockdown increased the expressions of p53 associated proteins such as p21 and mdm21 without altering the expression level of p53 (Tamaki et al., 2013).

As mentioned in Section 1.1.1.1, S100A4 has been demonstrated to form heterocomplex with S100A1 where S100A1 prevents the binding of S100A4 to NMMIIA and reduce S100A4 induced motility in vitro as well as reducing metastasis in vivo (Wang et al., 2004). Although there was no structural analysis of this heterocomplex, it was revealed that specific mutations of S100A4 at Phe 71 and Tyr 75 to glutamine resulted in complete abolishment of this heterodimerisation. However, dimerisation of S100A4 was only partially disrupted in Tyr 75 mutants suggesting that S100A4 may not be binding to S100A1 monomer as observed in homodimerisation of S100A4 (Wang et al., 2000).

Beside p53 and S100A1, CCN3 has also been identified as one of the target proteins of S100A4 through the yeast two hybrid system (Lin et al., 2003). CCN3 is a matricellular protein which plays a pivotal role in internal/external cell signalling, inducing angiogenesis in vivo as well as promotes cell survival. Its aberrant expression is thought to regulate tumourigenesis (Planque and Perbal, 2003, Gupta et al., 2001). As S100A4 has no enzymatic activities, it was proposed that S100A4-CCN3 interactions may be involved in tumourigenesis associated with CCN3 up-regulation (Lombet et al., 2003, Gupta et al., 2001, Manara et al., 2002, Sin et al., 2009, Chen et al., 2013). As no study has been conducted on direct consequence of this interaction on tumourigenesis, one can only speculate the possible results from this interaction.

Liprins are identified as the binding partner of the leukocyte common antigen-related tyrosine phosphatase (LAR) receptor protein, which consists of α -liprins and β -liprins where the subfamilies might form homo and heterodimers (Serra-Pagès et al., 1998). Although α -liprins are well characterised, the biological significance of liprin β 1 which has been shown to interact with S100A4, remains unclear. While LAR receptor protein is implicated in axon guidance and mammary gland development, liprins are known to regulate cell migration, adhesion as well as synaptic development through LAR receptor where the deactivation of liprins has been shown to impair motoneuron growth cone guidance and terminal differentiation of alveoli in *Drosophila* and mouse respectively (reviewed by Wei et al., 2011, de Curtis, 2011, Kriajevskaja et al., 2002, Krueger et al., 1996, Serra-Pages et al., 1995). S100A4 has been shown to bind to the C-terminus of liprin β 1 (938 – 1005 residues) which modulates in vitro phosphorylation of PKC (Thr 891, Ser 932 and Thr 962 residues) and inhibit CK2-mediated phosphorylation of liprin β 1 (Ser 997 residue) (Kriajevskaja et al., 2002). As

Liprin α 1- β 1 heterodimer has been found to colocalise with LAR at the integrin-mediated focal adhesion sites, the colocalisation of S100A4 and liprin β 1 at the protrusion sites of the plasma membrane, proposed that binding of S100A4 to liprin β 1 could inhibit its heterodimerisation with liprin α 1, thereby affecting its subsequent interaction with LAR to promote LAR-dependent cell adhesion signalling (Kriajevska et al., 2002).

Another recently identified target protein of S100A4 is MetAP2 which catalyses the removal of methionine residue from nascent peptides in eukaryotes to prevent initiation of protein translation. It was demonstrated that mammalian cell growth is strictly dependent on both MetAP1 and MetAP2 as treatment with MetAP inhibitors or knockdown of either MetAP1 or MetAP2 in HUVEC and A549 cells resulted in reduced cell proliferation (Chang et al., 1989, Bernier et al., 2005). Interestingly, it was found that treatments with MetAP2 inhibitors (fumagillin and ovalicin), in vitro, led to inhibition of angiogenesis and synthetic analogs of fumagillin, TNP-470 and NC2213 are currently undergoing clinical trial for treatment of various cancer types (Griffith et al., 1998, Selvakumar et al., 2009, Sin et al., 1997, Bhargava et al., 1999). S100A4 is now known to be capable of binding to MetAP2 at N-terminus region (170 - 229 residues) and colocalised at the perinuclear region of murine endothelial MSS31 cells. Upon stimulation with basic fibroblast growth factor (bFGF), a motility inducer, S100A4-MetAP2 was found to be distributed throughout the cytoplasm (Endo et al., 2002). Although the direct consequence of this interaction remained elusive, it was speculated that the redistribution of MetAP2 by S100A4 may be regulating endothelial cell growth and metastasis.

1.1.1.4.2 S100A4 and cytoskeletal proteins

The cellular cytoskeleton is a dynamic network of intracellular filaments which is crucial for modulating/maintaining cell shape and functions such as division and migration (Howard, 2009, Wickstead and Gull, 2011). This network consists of three groups of filamentous protein, known as filamentous actin (F-actin), microtubules and intermediate filaments which are assisted by extensive accessory proteins. Interactions of S100A4 with some these proteins have been reported and due to the involvement of these proteins to the cytoskeletal structure, it was speculated that these interactions could be the culprit behind the S100A4-induced metastasis.

In an experiments conducted with NH3T3 cell line, it was found that S100A4 binds directly to non muscle tropomyosin 2 (TM2) (39 – 107 residues) and non muscle tropomyosin 5 (TM5) (81 – 107 residues) in a calcium dependent manner (Takenaga et al., 1994). However, in another contradictory report using optic biosensor approach, it was found that there were no direct interaction between S100A4 and non muscle tropomyosin (TMs) either in presence or absence of calcium (Chen et al., 2001). Nonetheless, TMs will be briefly introduced here to speculate the effect of S100A4-TM2/TM5 interaction, if any. TM2 and TM5 belong to non-muscle tropomyosin (TMs) where they are classified into high molecular weight group and low molecular weight group respectively where they play an important role in organisation of actin filament during cell migration, division, and differentiation (Kee et al., 2004). Moreover, it was demonstrated that TMs binds to actin in high affinity which resulted in recruitment of non muscle myosin IIA (NMMIIA) to the existing actin filaments to promote stress fibers formation (Bryce et al., 2003, Moraczewska et al., 1999). One of the TM isoforms, Tm5NM1, antagonises the activities of ADF/cofilin by inactivating it through

phosphorylation and displacing it from the cell periphery as well as preventing Actin-related protein (Arp) 2/3 complex from nucleating actin filament (Bryce et al., 2003, Ono and Ono, 2002). From the mentioned functions of TMs, it is speculated that if S100A4-TMs interaction is valid, S100A4 may be regulating actin polymerisation through TMs which may subsequently affect cell motility.

Up to date, association of S100A4 with actin in calcium dependent manner has been demonstrated in two independent studies using co-sedimentation assay (Watanabe et al., 1993, Li et al., 2003). Watanabe et al. demonstrated that S100A4, but not S100B is capable of bundling F-actin in vitro. In the study conducted by Li et al., it was found that S100A4 binds to NMMIIA at the highest affinity (K_d 2.7 μ M), followed by NMMIIB (K_d 23.1 μ M) and finally F-actin (K_d 34 μ M) proposing that S100A4 may preferentially exert its effect on cytoskeleton through NMMIIA rather than actin (Li et al., 2003). However, discrepancy of this interaction has been demonstrated where S100A4 was only reported to interact with NMMIIA and p53 as well as weak association with tubulin, but not with actin using optical biosensor approach (Chen et al., 2001). Nonetheless, if S100A4-actin interaction is valid as proposed, S100A4 may be capable of remodelling the entire cytoskeletal structure to facilitate migration and metastasis as actin polymerisation is a crucial process of most protrusive structures as well as focal adhesions which will be further discussed in Chapter 1.3.

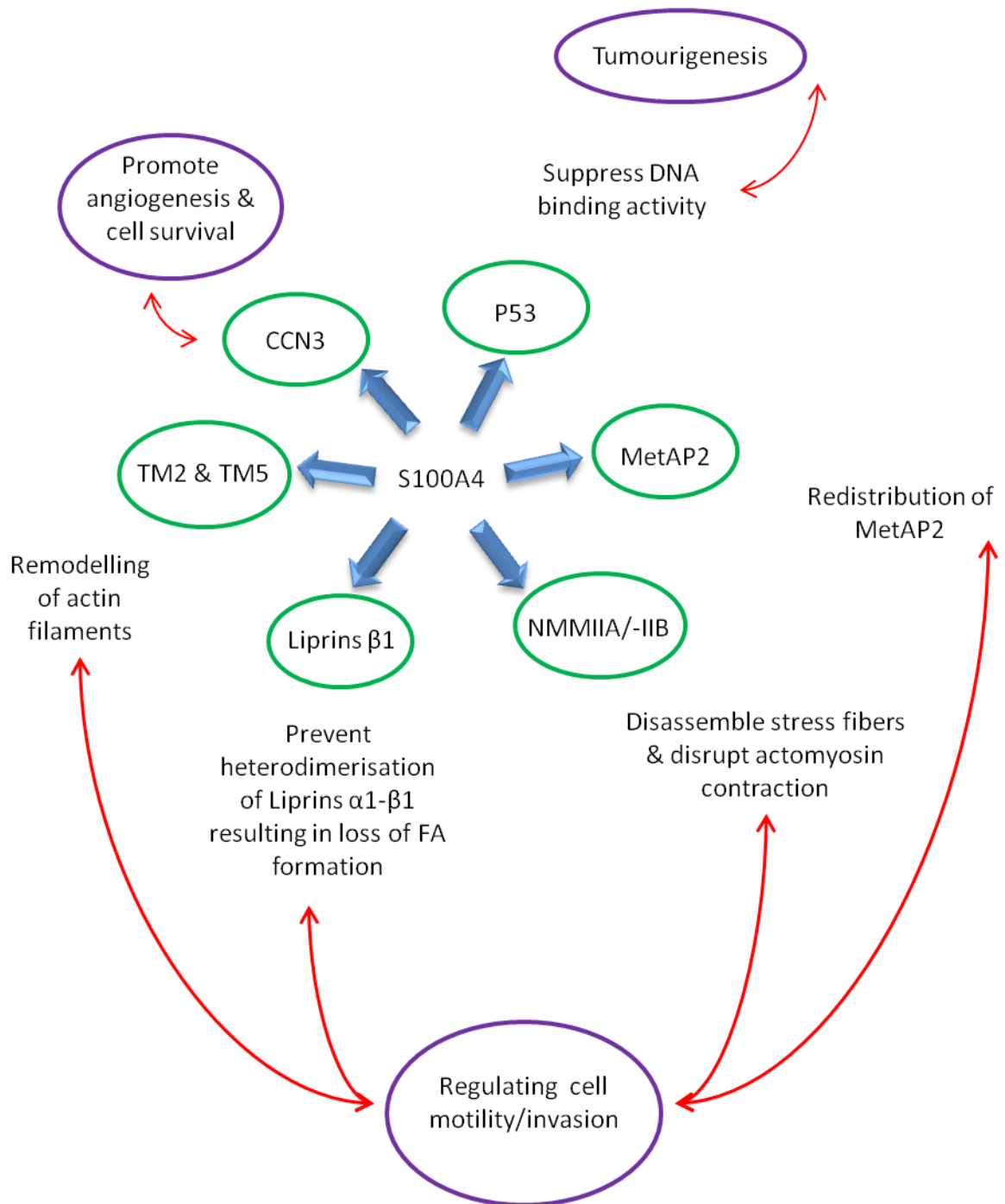


Figure 1.2 Schematic representation of consequences of S100A4 interacting with its target proteins.

1.2 Non muscle myosin II

Myosin superfamily is divided into 15 classes where only 9 classes (I, II, III, V, VI, VII IX, X and XV) have been detected in mammals. Myosin II, also known as 'conventional' myosins, were subclassified into four groups; 1) sarcomeric myosins, 2) smooth and non muscle myosins, 3) myosins from lower eukaryotic species and 4) myosins from fungi (reviewed by Sellers, 2000).

The non-muscle myosin II (NMMII) complex is an ATP-dependent molecule containing six peptides chains; two of each heavy chain (NMMHCII), two essential myosin light chains (ELC) and two regulatory light chains (RLC). NMMII is assembled into two bipolar filaments with globular head, a neck region consisting of ELC and RLC, and α helical coiled-coil region with a non helical C terminal tail piece (Figure 1.3) (Sellers, 2000, Bresnick, 1999). The globular head of each NMMHCII consist of an ATP binding site as well as an actin binding region which allow it to move in anti parallel manner via conformational changes induced by ATP hydrolysis. In the neck region, ELC serves to stabilise the NMMHC, while RLC acquire both stabilisation role and regulating NMMII functions via reversible phosphorylation activity (Bresnick, 1999). In the rod-like helical coiled-coil region, alternating charge were distributed, which serves to assemble homodimers of NMMII into higher order filaments (McLachlan and Karn, 1982). The repetitive assembly of bipolar NMMII and actin filament form the actomyosin network resulting in formation stress fibres where bundles of actin filaments are localised at the plasma membrane (Matsumura, 2005, Burridge and Wittchen, 2013). Such association forms belts of actin filament which encircle epithelial cells associated with adhering junctions. Similarly, during cytokinesis, actin filament bundles form a structure known as contractile ring (Asano et al., 2009).

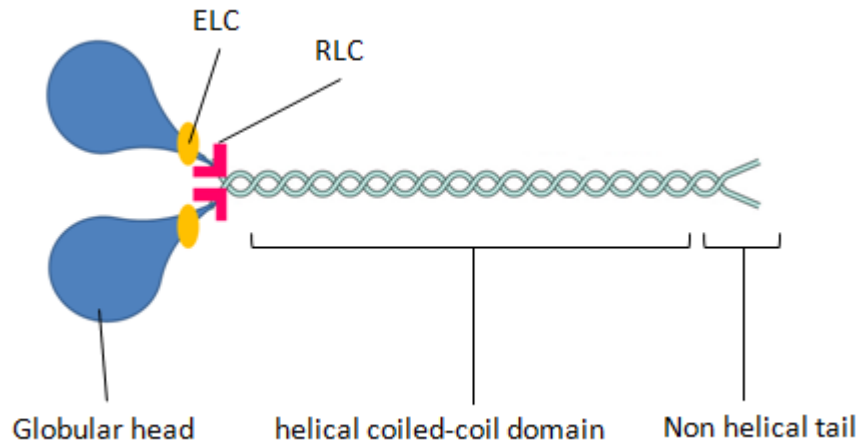


Figure 1.3 Illustration of non muscle myosin II (NMMII) homodimer: comprises of two of each non muscle myosin II heavy chain (NMMHCII), essential light chain (ELC) and regulatory light chain (RLC) followed by an α helical coiled-coil region and a non helical tailpiece.

1.2.1 Non muscle myosin II isoforms

There are three NMMII isoforms found in mammals; -IIA, -IIB and -IIC each encoded by different genes, *MYH9*, *MYH10* and *MYH14* respectively, sharing 60 – 80% amino acid sequence identity (Simons et al., 1991, Golomb et al., 2004). The two major isoforms of non muscle myosin, refer to NMMIIA and NMMIIB, are expressed at comparable levels in variety of vertebrate cells with an exception of neuronal cells in which NMMIIB is predominantly expressed (Lo et al., 2004, Sandquist and Means, 2008, Sandquist et al., 2006, Betapudi et al., 2006). NMMIIC, on the other hand, may be induced during hemopoietic differentiation (Lo et al., 2004).

Although comparable levels of NMMIIA and NMMIIB are expressed in mammalian cells, both have distinct distributions; NMMIIA is distributed around the edge of the cells and concentrated at the leading edge whereas myosin IIB is found to be distributed

around the perinuclear and concentrated at the rear end of migrating cells (Cai et al., 2006, Kolega, 1998). It has been demonstrated that NMMIIA is responsible for generating retraction force during cell migration whereas NMMIIB serves to stabilise the polarity and stress fibres of the cell (Cai et al., 2006, Betapudi, 2010, Kolega, 1998, Vicente-Manzanares et al., 2008). As a consequence, NMMIIA exert higher contractile force (2.6 fold) at faster velocity (3.3 fold) than NMMIIB with NMMIIA being more dynamic and is involved in the initial stages of focal complex formations (Kelley et al., 1996, Vicente-Manzanares et al., 2007).

1.2.2 Regulation of non muscle myosin IIA

Activity of NMMIIA is regulated through reversible phosphorylation of the RLC and globular domain of the bipolar NMMIIA. Primary and secondary phosphorylation sites of RLC were located at Ser 19 and Thr 18 amino acid residues respectively. RLC can be mono- and di-phosphorylated to enhance ATPase activity of the globular head which allow the association/dissociation of NMMII head with actin filaments (Vicente-Manzanares and Horwitz, 2010). Reversible phosphorylation resulted in alteration of NMMII conformation hence generating actomyosin contraction. In the presence of calcium, phosphorylation of RLC is catalysed by myosin light chain kinase (MLCK) which is activated through calmodulin. In the absence of calcium, phosphorylation of RLC at Ser 19 can be mediated by Rho kinase or by myosin binding subunit (MBS) (which dephosphorylate RLC at Ser 19) of myosin protein phosphatase 1 (PP1M) (Kawano et al., 1999). Beside phosphorylation at Thr 18 and Ser 19, RLC can be phosphorylated at 3 different sites by protein kinase C (PKC) at Ser 1, Ser 2 and Thr 9 which lower the affinity of MLCK to RLC, promoting reorganisation of actin filaments (Nishikawa et al., 1984).

On the other hand, NMMHCII can be phosphorylated by PKC (at Ser 1917 (rat) or Ser 1916 (human)) or casein kinase II (CKII) (at Ser 1943 (rat) or Ser 1944 (human)) (Conti et al., 1991). Phosphorylation of NMMHCII resulted in dissociation of myosin from actin filaments or prevents its assembly.

1.2.3 Actomyosin contraction

As its name suggests, actomyosin contraction requires the association of actin filaments and myosin which results in generation of powerstroke (Figure 1.3). Actin exists as a globular monomer known as G-actin and in the presence of magnesium, potassium and sodium ions, ATP-bound G-actin subunits will polymerise into linear actin filaments known as F-actin from the barbed (+) end. Binding of ATP-bound G-actin at (+) end of F-actin resulted in loss of phosphate ion through hydrolysis resulting in linear chain of ADP-bound F-actin. The ADP-bound F-actin will dissociate from the pointed (-) end which results in a process known as actin filament treadmilling (Oda et al., 2009). This constant polymerisation/depolymerisation process of actin results in actin dynamicity which is an important feature of cell polarisation and migration. Actin crosslinker such as fascin, α -actinin, myosin and filamin will bundle the F-actins into thicker filaments to generate different structures. It has been demonstrated that crosslinking action of fascin results in the formation of filopodia (parallel alignment), a protrusive plasma membrane structure, whereas filamin results in formation of actin meshwork (Machesky and Li, 2010, Wang et al., 1975)

Alternating crosslinking action of NMMII and α -actinin result in stress fibers formation, which is essential for maintaining cell shape and regulating cell migration (Pellegrin and Mellor, 2007). Approximately 20 to 28 molecules of bipolar NMMII

homodimer bind to actin through its globular head domains and the ATPase activities of the heads enables conformational change which move actin filaments in anti parallel manner to facilitate locomotion or maintaining cell integrity (Verkhovsky and Borisy, 1993, Dominguez and Holmes, 2011). When RLC is phosphorylated, ATPase activity of globular domain of NMMII is increased. ATP-bound globular head of myosin resulted in dissociation of NMMII head domain from actin. During hydrolysis, 'cocking' of NMMII head occurs. When inorganic phosphate is released, weak association of NMMII head to actin occurs. Release of ADP results in powerstroke as NMMII head binds tightly to actin. The cycle continues when ATP is bound to NMMII head again which relieve actin-myosin association (Figure 1.4) (Malnasi-Csizmadia and Kovacs, 2010, Takács et al., 2010, Vicente-Manzanares et al., 2009b).

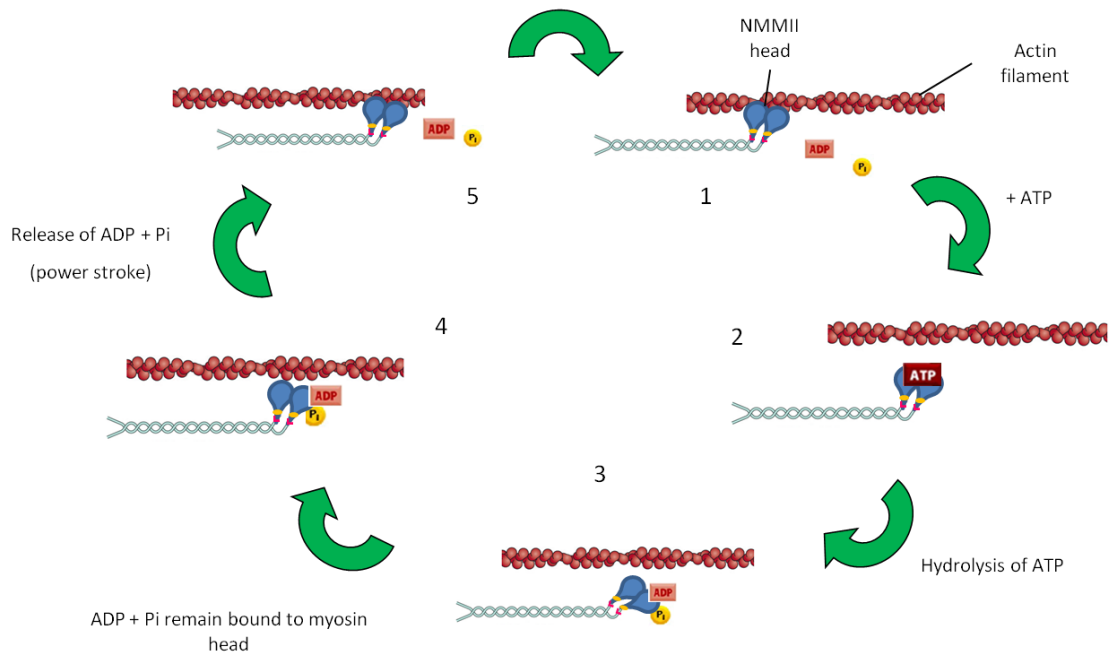


Figure 1.4 Actomyosin contraction. 1) Globular NMMII is attached to actin filament. 2) Addition of ATP resulted in dissociation of NMMII globular head from actin filament. 3) During hydrolysis, NMMII acquired 'cocking' conformation. 4) ADP and P_i resulted from hydrolysis of ATP restore weak affinity of globular head of NMMII to actin filament. 5) Release of ADP and P_i resulted in tight association of NMMII head with actin filament generating powerstroke which moved actin in anti parallel manner.

1.2.4 Myosin and S100A4

Binding of both NMMIIA and NMMIIB to S100A4 has been shown to occur at approximate stoichiometry of 3 moles of S100A4 per mole of NMHC II in a calcium dependent manner (Ford et al., 1997, Kriajevska et al., 1994). However, recent study of high resolution crystallography revealed that one dimer of S100A4 is sufficient to bind to one NMMIIA peptide to promote its conformational change to release actin (Kiss et al.,

2012). Although NMMIIA and NMMIIB shares 85% of amino acid identity in the globular domain and 72% in the helical rod, S100A4 has a 9-fold higher affinity for NMMIIA filaments than for NMMIIB filaments (Bresnick, 1999, Li et al., 2003). It was demonstrated that the NMMIIA binding site of S100A4 dimer is located at the C terminus region of amino acid residues at 1909 – 1924 where NMMIIB shares only 34% of sequence homology (Figure 1.5)(Li et al., 2003, Kriajevska et al., 2000). The low homology within this region could be the reason behind the lower affinity of S100A4 to NMMIIB than NMMIIA. Although the binding site on NMMIIA overlapped protein kinase C (PKC) phosphorylation site at Ser-1917, it was shown that the binding of S100A4 was not affected by PKC phosphorylation (Dulyaninova et al., 2007). Instead, Ser 19 phosphorylation by casein kinase II (CKII) was shown to inhibit the binding of S100A4 (Kriajevska et al., 2000). It has been further demonstrated that C terminus of S100A4 is vital for NMMII binding as deletion of the last 2 amino acids of its sequence is sufficient to increase the dissociation constant (Kd) of S100A4 to NMMII from 91nM to 680nM (Ismail et al., 2008b). The binding of S100A4 to NMMIIA promotes the unassembled state of NMMIIA, as it inhibits the ATPase activity of myosin resulting in dissociation of whole myosin complex from actin (Ford et al., 1997). This interaction is presumed to be, at least one of its properties, allowing S100A4 to regulate cell polarisation and directed motility where cells protrusions at the leading edge are observed (Li and Bresnick, 2006).

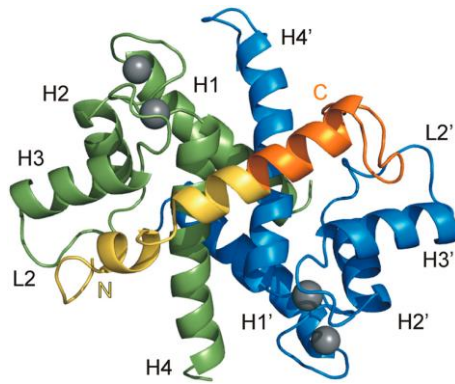


Figure 1.5 Interaction of S100A4 dimer with 45-residue long NMMIIA tail fragment. S100A4 dimers are shown in green and blue whereas NMMIIA peptide is in yellow (residues 1893-1913) and orange (residues 1914-1935) and calcium ions are in grey (Adapted from Kiss et al., 2012).

1.3 Migration

Cell migration is not only limited to metastasis process in malignant cancer, in fact, it is required in many biological processes such as tissue repair and regeneration, embryonic development as well as immune responses (Condeelis et al., 2005, Bailly and Condeelis, 2002, Yamaguchi et al., 2005). Following from a trauma or regeneration of lining of epithelial tissues, new cells will migrate up from the basal layer. During embryogenesis, groups of cells migrate to form trilaminar known as gastrula, an essential early phase of gastrulation. As for immune responses, leukocytes migrate to the site of inflammation to engulf microorganisms. In order for cell migration to take place, morphological as well as molecular changes played an important role in regulating this process. Mechanism of migration can be divided into four chronological steps; 1) cell polarisation, 2) stabilisation of extended leading edge, 3) contraction of cell body and 4) retraction of trailing end and disintegration of focal complexes, four events that will be reviewed independently in the following section.

1.3.1 Cell polarisation

Generally, in stably adhered cell, its morphology usually appeared somewhat symmetrical or out-spread. However, in order for migration to arise, the cell has to break its symmetrical shape to form a front and rear, termed as polarisation (Cramer, 2010). However, it remains unclear whether cell front or cell rear formed first or both at the same time during breaking of cell symmetry. In experiments conducted with human neutrophils, it was observed that in the presence of uniformly distributed chemoattractants, protusion signalling occurred first, subsequently by cell rear (Zigmond and Sullivan, 1979, Wong et al., 2006). Contrastingly, fibroblast and keratocytes has been shown to initiate formation of cell rear in the absence of chemoattractant (Mseka et al.,

2007, Yam et al., 2007). Nonetheless, cell polarisation is agreed universally as the first step to cell migration (Diz-Muñoz et al., 2010, Yamaguchi et al., 2005, Le Clainche and Carlier, 2008).

Cell polarisation occurred due to extracellular cues such as growth factors, cytokines and cell adhesion receptors, in combination with intracellular responses, which consists of numerous signalling proteins (Vicente-Manzanares et al., 2009a, Ridley et al., 2003). During cell polarisation, the cell front could extend into, at least, four different plasma membrane protrusions, known as lamellipodia, filopodia, invadopodia or blebs whereas the rear end usually consist of retraction fibers (Diz-Muñoz et al., 2010, Yamaguchi et al., 2005). These four protrusions are distinguished through their structures and shapes. In the following sections, only lamellipodia and filopodia and their relevance in 2D culture will be discussed due to the nature of this project.

1.3.1.1 Lamellipodia

The term 'lamellipodium' was first used in the 1970s to describe a sheet-like cytoplasmic region with a thickness of around 2µm located at the leading edge of the cell (Abercrombie et al., 1970). While bleb is formed on or within elastic substrate, lamellipodium is formed on rigid substrate. The former structure occurs due to destabilisation of actin filaments whereas lamellipodium occurs due to polymerisation of actin filaments to enhance protrusions. Other than acting as protrusive structure, lamellipodium are also involved in formation and maturation of focal adhesions. Numerous signalling proteins such as Rac, RhoA, Cdc42, Arp2/3 (Actin related protein 2 and Actin related protein 3) complex, formin and Spire families have been shown to contribute to lamellipodium extension. Rac, a member of the Rho family proteins,

stimulates actin polymerisation via Arp 2/3 complex which binds directly to existing actin filaments to form branches. However, stimulation of Arp 2/3 complex by Rac consists of multi-interaction steps which involve various proteins. First, Rac binds to insulin receptor tyrosine kinase substrate p53 (IRSp53) and the carboxy-terminal Src-homology 3 domain of IRSp53 binds to Wiskott-Aldrich syndrome protein (WASP) family verprolin-homologous protein (WAVEs) to form a trimolecular complex (Miki et al., 2000). This trimolecular complex is capable of binding to both G-actin monomer and Arp2/3 complex and this affinity brings the two substrates into close proximity, hence increasing F-actin polymerisation rate. Branching caused by nucleation of actin filaments by Arp2/3 complex causes spreading of cytoplasm termed lamellipodium.

Also, Rac is capable of inducing actin polymerisation by uncapping the actin filament at the barbed (+) end via interaction with phosphatidylinositol 4-phosphate 5-kinase (PIP 5-kinase) which stimulate the formation of phosphatidylinositol 4,5-bisphosphate (PIP₂), a complex responsible to remove capping protein (CP). As its name suggests, CP is responsible for capping the (+) end of F-actin filaments to prevent polymerisation and loss of actin subunits from (-) end (Wear et al., 2003). After removal of CP, formin prevents re-capping of the actin filaments and promotes monomeric elongation which produces unbranched actin filaments. Besides Arp2/3, a member of Spire family known as Cordon-Bleu, has been shown to localise to lamellipodia and overexpression of this protein promotes lamellipodia formation in cells (Campellone and Welch, 2010). Although lamellipodial persistence is important for cell migration, its termination is just as important. Indeed, when cells lamellipodia come in contact with each other, a process known as contact inhibition will retract to avoid collision of cells (Carmona-Fontaine et al., 2008, Groeger and Nobes, 2007).



Figure 1.6. Formation of lamellipodia through various signalling proteins. (A) Signalling proteins involved in lamellipodia regulation; 1) Rac stimulate the formation of PIP2 which remove capping protein on existing actin filaments, allowing Arp 2/3 complex to mediate branching. 2) Arp 2/3 complex is activated by trimolecular complex consisting of WAVE, IRSp53 and RAC. Polymerisation of G-actin monomer by formins through recruitment of profiling at Arp 2/3 branch point resulted in extension of branched actin filament network. 3) Formation of lamellipodia through actin nucleation independent of Arp 2/3 complex by formins (adapted from Ridley, 2011). (B) R37 S100A4 WT cell stained for fascin (FITC) and actin (rhodamine). Methods are fully detailed in Chapter 2.6.

1.3.1.2 Filopodia

Filopodia are needle-like extensions where their roles as sensory structures to probe the microenvironment and act as sites for signal transduction have been well documented (Amieva and Furthmayr, 1995). However, the roles of filopodia remained incompletely understood. While actin and fascin are positioned along the shaft to stabilise the extended filopodia, integrins are located at the tip of the filopodia to serve as extracellular cues transducer to initiate formation of focal adhesions and facilitate cell

migration (Mattila and Lappalainen, 2008). Similar to lamellipodia, formation of filopodia is regulated by Cdc42, but with different downstream effectors as it has been reported that fibroblasts devoid of N-WASP are capable of forming filopodia but incapable of forming lamellipodia (Lommel et al., 2001, Snapper et al., 2001, Mattila and Lappalainen, 2008). It has been demonstrated that Cdc42 interacts with the partial CRIB motif of the IRSp53 relieving IRSp53 from autoinhibitory conformation, thus allowing it to form complex with mammalian-enabled (MENA), a member of ENA/VASP family. Although this interacting pathway remains elusive, localisation of MENA to the tip of filopodia and focal adhesion sites through EVH1 (ENA/VASP homology) domain indicated its role in filopodia formation mediated by Cdc42 (Krugmann et al., 2001, Pichot et al., 2010). Beside Cdc42, another GTPase family protein known as Rho in filopodia (RIF) has been demonstrated to stimulate filopodia formation independent of Cdc42 (Pellegrin and Mellor, 2005). RIF is thought to regulate filopodia formation through activation of mammalian Diaphanous – related formins (formin mDia2) by promoting polymerisation of actin monomer subsequently stabilising actin cortex (Ellis and Mellor, 2000, Pellegrin and Mellor, 2005). Termination of filopodia is thought to be a consequence of direct binding of Dia interacting protein (DIP) to formin mDia2 as this interaction has been demonstrated to inhibit formin mDia2-dependent F-actin assembly and bundling (Eisenmann et al., 2007).



Figure 1.7 Formation of filopodium. (A) Signalling proteins involved in regulating filopodia formation; 1) IRSp53 and MENA (ENA/VASP family) form complex through formin mDia2 to recruit Cdc42 to stimulate actin polymerisation. 2) Myosin X clusters actin filaments containing Arp 2/3 complex which may initiates filopodia extensions. 3) Extension of filopodia mediated by fascin resulted in parallel alignment of actin filaments. 4) RIF or Formin homology of mDia2 associate with WASP which mediate actin polymerisation through recruitment of G-actin by profiling (adapted from Ridley, 2011). **(B)** Rama 37 control cells stained for fascin (FITC) and actin (Rhodamine). Immunofluorescence staining was carried out as described in Chapter 2.6.

1.3.2 Stabilisation of extended leading edge

After cell polarisation through membrane extension, the extended structures have to be stabilised for migration persistency. There are many receptors involved in the migration of different cell types, but integrins are the major receptors in transducing extracellular cues into the cell to forming nascent and transient adhesions which are distinguished by its small size and short-lived adhesive properties respectively. Recruitment of adaptor proteins to nascent adhesions stabilises the adhesions site into a structure known as focal complex. These focal complexes then matured into focal

adhesions through further recruitment of adaptor proteins and associating these adhesions to stress fibers which allow the extended structures to 'clamp' onto the extracellular matrix to prevent retraction and serve as traction points to facilitate cell locomotion (Small and Kaverina, 2003, Shemesh et al., 2009, Vicente-Manzanares and Horwitz, 2011b) (Figure 1.10).

1.3.2.1 Integrins and downstream signalling

As mentioned earlier, the extended structures consist of heterodimeric cell surface receptors known as integrins. Integrins are made up of two covalently linked transmembrane glycoprotein α and β subunit, each comprises of an extracellular domain to interact with extracellular matrix, such as fibronectin (FN), collagen and laminin, and a cytoplasmic domain interacting with intracellular signalling proteins (Guan, 1997, Kumar, 1998, Wiesner et al., 2006). Up to date, 18 α subunits and 8 β subunits to produce 24 different $\alpha\beta$ -integrins combinations have been identified in mammalian genomes (Humphries et al., 2006). Role of integrins is not only limited as transducer for cell migrations, they are also important for cell proliferation, survival and differentiation (Schwartz and Assoian, 2001, Cruet-Hennequart et al., 2003). As integrins do not themselves possess a kinase domain or enzymatic activity, these cytoplasmic domains will bind to adaptor proteins such as α -actinin, talin, filamin, vinculin and paxillin which will be organised around activated integrin clusters (Figure 1.8). Organisation of these adaptor proteins is known as focal complexes which will then mature into focal adhesions and linking integrins to the actin filaments either directly or indirectly (Wiesner et al., 2005). Clustering of integrins at the extended structures resulted in activation of focal adhesions

kinase (FAK) which further enhances nearby integrins activations (Mitra et al., 2005, Michael et al., 2009).

FAK is a 125 kDa autoinhibited, non-receptor cytoplasmic tyrosine kinase containing five major domains, namely, kinase domain, FERM (protein 4.1, ezrin, radixin and moesin homology) domain, focal adhesion targeting (FAT) domain and two proline rich domains. This cytoplasmic kinase has been implicated in cell proliferation, motility and survival (Zhao et al., 1998, Ilic et al., 1995, Renshaw et al., 1999). When FERM domain interacts with the FAK kinase domain, the resulting activated protein binds strongly to the Arp2/3 complex to facilitate nucleation of actin filaments. Activated FAK via integrins clusterings or binding of proteins to FAK-FERM domain led to autophosphorylation at tyrosine (Y) 397 which enable phosphorylated FAK to associate with Src family kinases (SFKs) at the SH2 domain. This newly formed complex will then interact with phosphorylate linker protein p130 Cas with both of its proline-rich domains causing it to release its association with Arp2/3 complex. Through p130 Cas protein, paxillin is phosphorylated by FAK to interact with actin cytoskeleton. The released Arp2/3 complex will be recruited to the extended leading edge to assist actin filament nucleation.

Paxillin, a 70 kDa phosphotyrosine-containing protein, is phosphorylated by binding to FAK at residue Tyrosine 397 located at the C terminal, which is also known as focal adhesion targeting (FAT) domain. Activation of paxillin via FAK results in subsequent activation of extracellular signal-regulated kinase (ERK) and p21-GTPase-activated kinase (PAK) which serves to activate myosin light chain kinase (MLCK) (Klemke et al., 1997). Besides, paxillin can also be phosphorylated by the Src family of the tyrosine kinases at the LIM domain and phosphorylated paxillin permits recruitment of CT10 regulator of kinase (CRK) adapter protein to protein linker p130 Cas and Rac GTP-exchange factor (GEF) DOCK

180 (Cote and Vuori, 2007). This trimolecular complex, in turn, activates Rac while inactivating Rho. Rac activation further enhances p130 Cas phosphorylation which led to increase Crk-Cas association which in turn activates integrins, suggesting a positive feedback mechanism (Wozniak et al., 2004).

Talin, an antiparallel homodimer with head and tail in each 270 kDa subunits, binds to FAK and cytoplasmic domain of integrins with its globular head subunits (Calderwood, 2004). Binding of talin to integrins resulted in unwinding of talin rod domain which allows binding of vinculin and α -actinin (Tomar and Schlaepfer, 2009). The antiparallel dimerisation of α -actinin results in exposure of two calponin homology (CH) domains which serves as actin binding domains (Ciobanasu et al., 2012). In an alternating arrangement, NMMIIA and α -actinin crosslinked actin filaments to form stress fibers, a structure responsible for the next mechanistic step. It was found that vinculin is capable of binding to FAK, paxillin and directly to actin filaments, suggesting the cross talk between adaptor proteins (Mierke et al., 2008). Vinculin binds to the N-terminal of paxillin at 3 different sites known as paxillin binding sequence and any mutations within this sequence has been shown to completely abolish the interaction (Schaller, 2001). Similar to FAK, vinculin exists in inactive conformation due to intramolecular associations between the head and the tail domains and will subsequently be activated upon binding to talin, actin or PIP₂ (Humphries et al., 2007). Due to low binding affinity of vinculin to talin, inactivated vinculin will form nascent focal adhesions with high turnover rate. However, if vinculin is activated, binding affinity of vinculin to talin will increase leading to low turnover rate and stabilisation of integrins and ultimately growth of focal adhesion (Chen et al., 2006, Humphries et al., 2007).

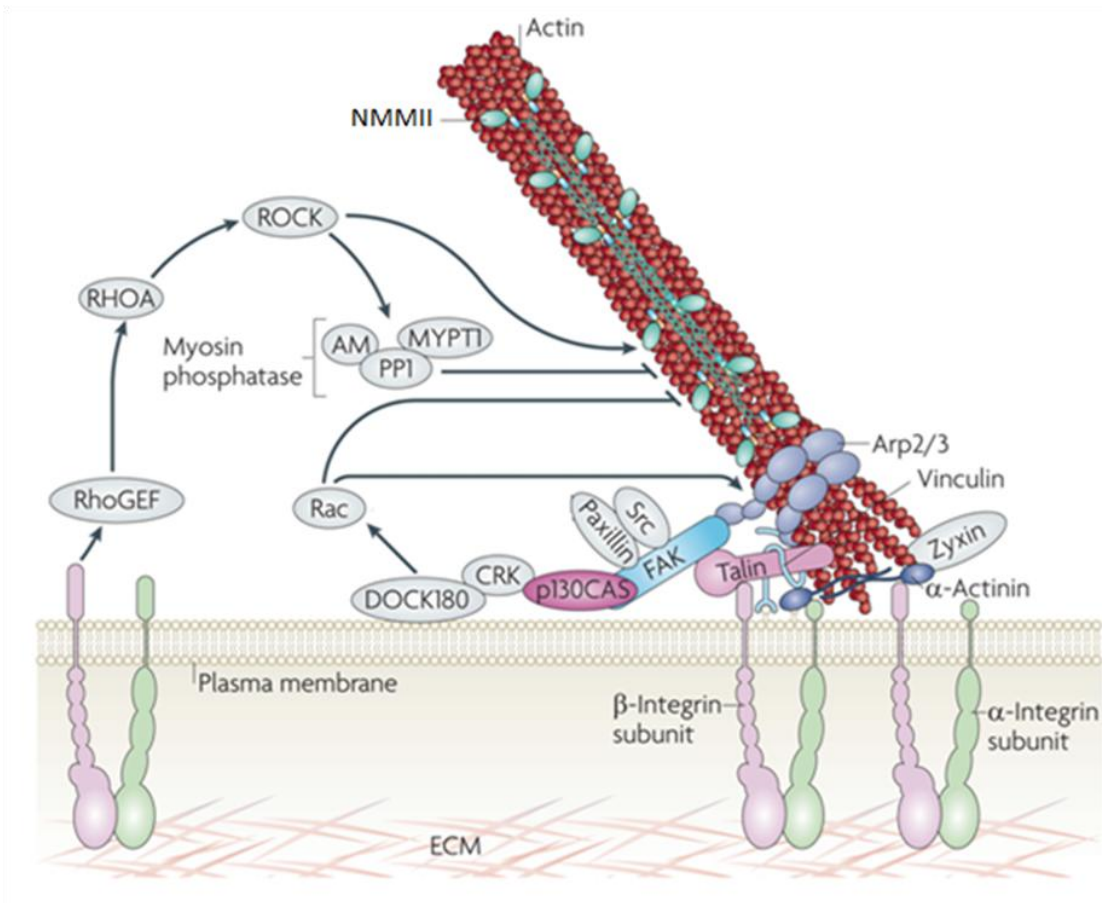


Figure 1. 8 Integrin transducing extracellular cues which led to recruitment of cytoplasmic protein signalling. Extracellular domains of integrins bind to extracellular ligands which activate the intracellular domains. Talin or vinculin (which can be activated by PIP₂) can bind directly to intracellular domains of integrins and actin filaments. Clustering of integrins also activate FAK which binds p130Cas to release Arp 2/3 complex as well as phosphorylating paxillin which led to activation of Rac via the Rac GTP-exchange factor (CRK) of DOCK 180. Activated Rac induces actin polymerisation through Arp 2/3 complex. Activation of RhoGEF by integrins led to activation of Rho kinases which subsequently phosphorylate RLC of NMMII to increase ATPase activity and inactivating myosin protein phosphatase (adapted from Vicente-Manzanares and Horwitz, 2011b).

1.3.3 Contraction of cell body

After stabilisation of leading edge via recruitment of adaptor proteins into matured focal adhesions, the cell has to proceed by 'pulling' its body forward in a process known as actomyosin contractility. In order for actomyosin contractility to occur, matured focal adhesions have to be interconnected to bundled actin filaments, known as stress fibers to exert traction force. Localisation of Ena/VASP at focal adhesion sites at leading edge stimulated actin polymerisation where this polymerisation serves to link focal adhesions to existing actin cytoskeleton or to adjacent focal adhesions to form different subtypes of stress fibers, owing to its two important domains; 1) N-terminal EVH1 domain which binds to FPPPP motifs of zyxin and resulted in localisation of Ena/VASP to focal adhesions, 2) C-terminus EVH2 domain which regulates both polymerisation of actin monomer and binding to F-actin (Reinhard et al., 1992)(Bachmann et al., 1999, Bear and Gertler, 2009, Rottner et al., 2001).

There are three types of stress fibers characterised by its association to focal adhesions; 1) ventral stress fibers, 2) dorsal stress fibers and 3) transverse arcs (Figure 1.9). Ventral stress fibers and transverse arcs are made up of 10-30 actin filaments crosslinked by α -actinin in which NMMIIs were integrated in the regions where α -actinin was depleted resulting in a α -actinin-NMMII alternating structure (Cramer et al., 1997). Ventral stress fibers are usually responsible for tail retraction as it is characterised by having focal adhesions located at both ends. Transverse arcs are not directly connected to focal adhesions, but their contractile force can be transmitted through dorsal stress fibers as it appeared to be localised parallel to lamellipodium in a crescent, connected to dorsal stress fibers. Dorsal stress fibers are characterised by having one end connected to focal adhesions and the other serving to polymerise actin monomer towards the cell center

linking this structure to the existing cytoskeletal network and/or transverse arcs. Also, as the trunks of dorsal stress fibers do not contain NMMII, it was presumed that this structure does not generate traction force (Tojkander et al., 2012). Dorsal stress fibers are thought to be the precursor to ventral stress fibers as it has been demonstrated that contractility generated by dorsal stress fibers-transverse arcs structures led to dissociation of region of transverse arcs that are not associated to the two dorsal stress fibers leading to formation of ventral stress fibers. Organisation of these stress fibers allows interaction of focal adhesions to NMMII to generate actomyosin contractility through reversible phosphorylation of myosin light chain (MLC) at Thr 18 and Ser 19.

MLC can be phosphorylated either by MLCK (calcium dependent process) or Rho-associated protein kinase (ROCK) (calcium independent process) and recently, it has been proposed that MLCK phosphorylate MLC located at the cell periphery whereas phosphorylation by ROCK appears to be in the center of the cell. As mentioned previously, MLCK is activated by matured focal adhesions via activation of MAP kinases (ERK) and P21 activated kinase (PAK). Phosphorylation of MLC by ROCK promotes the release of myosin II heavy chain (MHC) tail, allowing association of myosin head with the F-actin, resulting in pulling action or simply known as actomyosin contractility (refer to Section 1.2.3) (Olson and Sahai, 2009). Besides, ROCK also inhibit ADF/cofilin, an actin filament severing protein via activation of LIM-domain kinase 1 (LIMK1), promoting actin filaments maintenance (Sumi et al., 2001). Beside capable of directly phosphorylating MLC, ROCK is also capable of increasing phosphorylation of MLC via inhibition activity of myosin protein phosphatase 1 (PP1M), whose role is to dephosphorylate MLC.

In the presence of calcium, MLCK is activated through interaction with calmodulin and calcium. Activated MLCK resulted in subsequent phosphorylation of MLC and

generation of actomyosin contractility (Katoh et al., 2001a). It has been proposed that although both ROCK and MLCK are capable of phosphorylating MLC to generate actomyosin contraction, the calcium dependent pathway via calmodulin produces rapid and local response whereas calcium independent pathway via ROCK produces more sustained response (Tojkander et al., 2012).

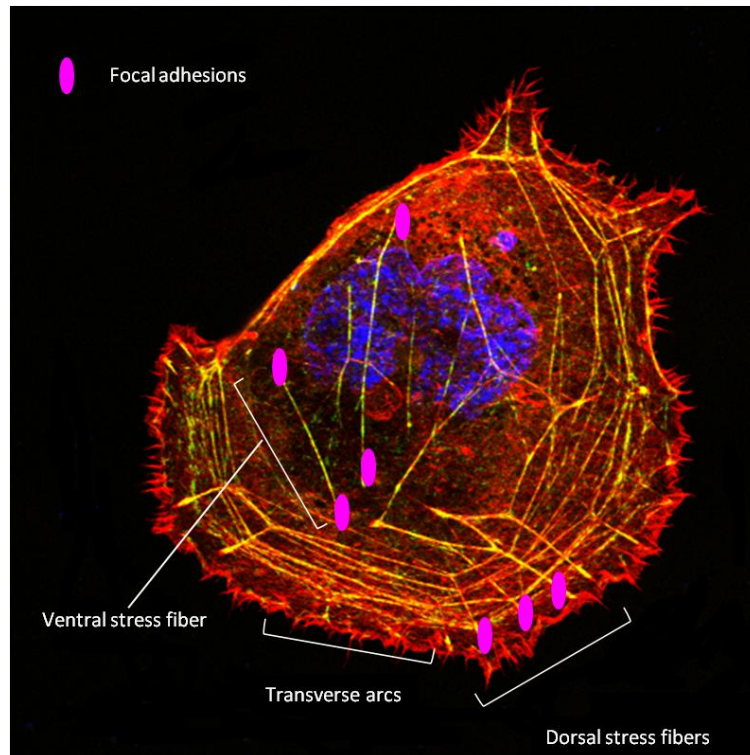


Figure 1.9 Different types of stress fibers distinguished by focal adhesions. Ventral stress fibers are characterised by having a focal adhesion located at each end of the fiber, dorsal stress fibers having one focal adhesion at either end and transverse arcs void of focal adhesions. Cos 7 cells seeded on coverslip pre-coated with fibronectin were transfected with PeGFP NMMIIA (FITC) encoding plasmid using Jetpei. After 48 hours the cells were fixed, blocked, stained for actin (Rhodamine) washed and mounted with DAPI (blue) before viewing with confocal microscope. Fully detailed method is described in Chapter 2.5 and 2.6.

1.3.4 Tail retraction and disintegration of focal complexes

In order for cell body to move forward through actomyosin contraction, new protrusions will be extended with formation of new adhesions. However, if existing adhesions do not disassemble, it is impossible for the cell to move forward. Therefore, as new protrusions are formed, some of the existing adhesions will disintegrate while the remaining ones will further mature for cell adherence and will be positioned underneath the cell center as the cell moves forward. The mechanism underlying focal adhesions disintegration remains elusive, but it has been proposed that extensions of microtubules to focal adhesions promote its disintegration by inducing FAK dephosphorylation (Ezratty et al., 2005, Watanabe et al., 2005, Small and Kaverina, 2003). FAK dephosphorylation can be induced by phosphatases such as PTP-PEST and SHP-2. Activation of ERK by Ras causes phosphorylation of FAK at Ser 910, exposing Pro 910 residue to peptidyl-prolyl cis/trans isomerase (PIN1). PIN1 brings FAK to close proximity with PTP-PEST hence dephosphorylating FAK. SHP-2, another FAK phosphatase, exists in autoinhibitory conformation due to interaction of two SH-domains at the N terminal. This autoinhibitory conformation is relieved through association pleckstrin homology (PH) domain of Gab1 (Nagano et al., 2012). Besides, in a calcium dependent manner, m-Calpain, a member of calpain family of proteases has been shown to be capable of cleaving talin, FAK and paxillin. Although little is known about the cleaving mechanism of m-Calpain, it was proposed that cleaving of these adaptor proteins led to disruption of crosstalk within the focal adhesion sites (Sieg et al., 2000, Franco and Huttenlocher, 2005, Nagano et al., 2012).

Therefore, as cell moves forward through actomyosin contraction, disintegration of focal adhesion at the trailing end of the cell led to retraction of tail.

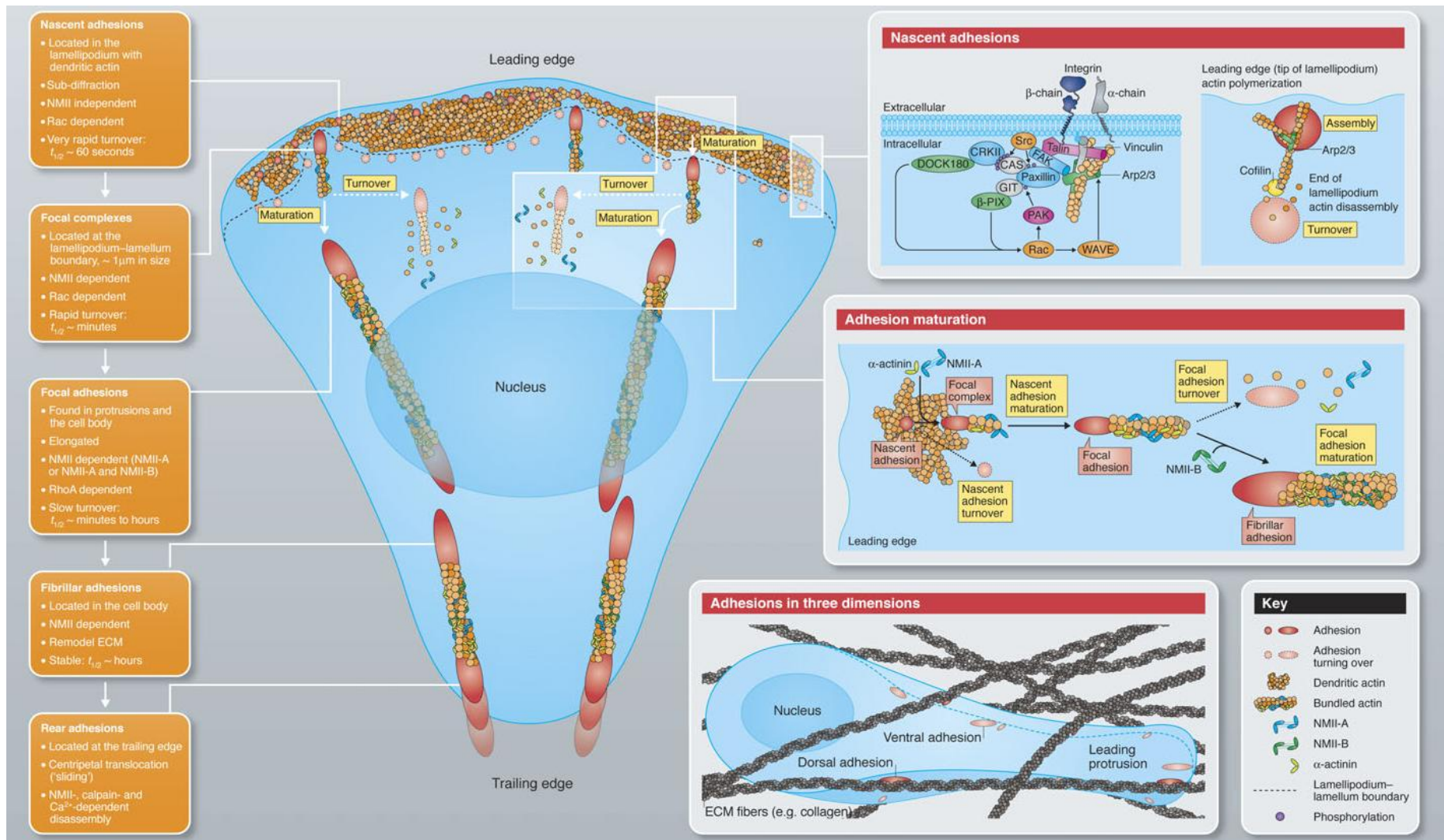


Figure 1.10 Signalling proteins involved in regulating focal adhesion dynamicity through actin filaments to facilitate cell migration. (Adapted from Vicente-Manzanares and Horwitz, 2011a).

1.4 Aims

In the first part of the work, we aimed to demonstrate the consequences of S100A4 overexpression on cell morphology, focal adhesions, as well as importance of C-terminus of S100A4 in mediating cell motility.

Following that, we set out to investigate the link between S100A4 and NMMIIA on cell migration and morphology using three approaches; 1) inhibition of NMMIIA with chemical compound, 2) knockdown of NMMIIA using SiRNA transfection and 3) using cellular system where NMMIIA is completely ablated.

Finally, utilising High Content Imaging (HCI) assay, we tested numerous chemical compounds for their ability to affect S100A4-induced migration through wound healing assay to provide more insight on the S100A4 activity.

Chapter 2:

Materials and Methods

Chapter 2: Materials and Method

2.1 Materials

2.1.1 Equipments (and softwares)..... 61

2.1.2 Reagents 62

2.2 Methods..... 65

2.2.1 Cell Culture 65

2.2.1.1 Culture of Rat mammary benign tumour (Rama 37)..... 67

2.2.1.2 Culture of African green monkey kidney cells (Cos 7)..... 67

2.2.1.3 Passage of cells 67

2.2.1.4 Cryopreservation of Cells..... 68

2.2.1.5 Cell Thawing..... 68

2.2.2 Cell Counting..... 68

2.2.3 Cell Viability Determination..... 69

2.2.4 CellIQ Scratch Assay 71

2.2.4.1 Determining Mitotic Index with CellIQ 72

2.2.5 Layout of Rama 37 cell lines seeding in 24 well plate for screening 72

2.2.5.1 Calculation of wound closure rate ($\mu\text{m}^2 \text{min}^{-1}$) 73

2.2.6 Transient Transfection 74

2.2.6.1 Transfection efficiency 76

2.2.7 SiRNA transfection 76

2.2.8	Immunofluorescence Staining	77
2.2.9	Live cell analysis.....	79
2.2.10	Quantification of focal adhesion clusters and filopodia of fixed cells.....	79
2.2.11	Quantification of focal adhesion clusters and filopodia of live cells.....	80
2.2.12	Cell force analysis.....	80
2.2.13	Preparation of chemically competent <i>E.coli</i>	81
2.2.14	<i>E.coli</i> Transformation for plasmid production.....	82
2.2.15	Mini-prep (Plasmid extraction)	83
2.2.16	Agarose gel electrophoresis.....	83
2.2.17	Preparation of total cell lysate	85
2.2.18	Protein Quantification (Lowry method).....	85
2.2.19	Polyacrylamide Gel Electrophoresis (PAGE).....	86
2.2.20	Western Blot.....	88
2.2.20.1	Blots Stripping	90
2.2.20.2	Quantification of bands intensity.....	91
2.2.21	Statistical analysis	91

2.1 Materials

2.1.1 Equipments (and Softwares)

BioRad, Hemel Hempstead, UK :

Bio-Rad mini-Protean II gel system , Mini Trans-Blot Cell, PowerPac™ Basic Power Supply

BioTek Potton, Bedfordshire,UK:

Plate Reader EL800

Beckam Coulter Ltd., High Wycombe, UK:

Avanti J-E centrifuge

Carl Zeiss Microscopy GmbH, Oberkochen, Germany:

Confocal microscope (LSM710) -EC Plan-Neofluar 40x/1.30 Oil Ph3 objective (immunofluorescence staining), Cell Observer system with CCD camera (AxioCam MRm)-40x/1.3 Ph3 plan neofluar oil objective (Cell force measurements- Matlab software)

Chip-Man Technologies Oy, Tampere, Finland:

Cell-IQ MLF-(Imagen™ Software, Analyser™ Software-Machine Vision Technology)

DJB Labcare Ltd, Buckinghamshire, UK:

Eppendorf Centrifuge 5810R

Geneflow, Staffordshire, UK:

DNA Gel Cast

Leica Microsystems Ltd, Milton Keynes, UK:

Inverted epifluorescence microscope (DM14000B) (AxioVision Version 4.7 software)- N-Plan 10x /0.25 PH1 objective (immunofluorescence staining), confocal microscope (TCS SP5 II Confocal) (AxioVision Version 4.7 software)- HCX PL APO 63x/1.4-0.6 oilCS objective (immunofluorescence staining)

Sigma-Aldrich, Poole, UK:

Sigma 2-6E centrifuge (83/L rotor)

Syngene, Cambridge, UK:

G:Box-UV transilluminator

Themoscientific, Loughborough,UK:

ThermoScientific NanoDrop™ 1000 UV/VIS Spectrophotometer (NanoDrop Software)

2.1.2 Reagents

Abcam, Cambridge, UK:

Polyclonal Goat anti-Mouse Immunoglobulins/FITC, Polyclonal Goat anti-Mouse Immunoglobulins/TRITC, Polyclonal Goat anti-Rabbit Immunoglobulins/FITC

Addgene, Cambridge, USA:

Human CMV-GFP non muscle myosin II A heavy chain (Plasmid 11347)

Appleton Woods, Birmingham, UK:

Tissue culture flasks and plates (Corning), Latex gloves, autoclave tapes, 200 µl pipette tips, 50 ml centrifuge tubes

Bioline, London, UK:

Molecular Grade Agarose

BioRad, Hemel Hempstead, UK :

Ethidium bromide, DC™ Protein Assay (Lowry method), Gel Loading Tips

Biosera, East Sussex, UK:

L-glutamine (100X)

Carl Zeiss Ltd, Hertfordshire, UK:

Immersion oil

CEAC, Aston University, UK:

Ethanol, Methanol, Propanol

Covance Inc., Leeds, UK:

Polyclonal affinity purified non muscle myosin heavy chain II-A antibody anti-rabbit, polyclonal affinity purified non muscle myosin heavy chain II-B antibody anti-rabbit

Dako, Ely, UK:

Polyclonal Rabbit Anti-Human S100A4

Enzo Life Sciences, Exeter, UK:

Blebbistatin

Expedeon, Cambridgeshire, UK:

Bradfordultra™

Fisher Scientific, Loughborough, UK:

2 units of individual tube of SiRNA non muscle myosin IIA heavy chain-Rat (1-GGUCAUCUCUGGCGUCCUU, 2-GCAGAUCCGACCAAUAAAC), SiRNA Buffer (5X), Fermentas mini-prep kit, PageRuler Plus Prestained Protein Ladder, Whatman Filter Paper Grade 1573 Roll Cellulose Fast, Microscope slide, Gerhard Menzel, SuperFrost® Plus, Acetic acid glacial (HPLC grade), Sodium chloride, Tris Base Ultra Pure, microcentrifuge tubes (0.5 ml, 1.5 ml, 2.0 ml), Bottle Borosilicate Screw cap (250 ml, 500 ml, 1000 ml), Plastipak Syringe disposable (10 ml, 20 ml),

syringe filter 33mm Millex PES Pore Size 0.22µm, Parafilm, Aluminium foil, Cling Film, Weighing boat polystyrene square (250ml), Virkon®

Geneflow, Staffordshire, UK:

EZ-PCR Mycoplasma test kit, DNA Gel Cast

Greiner, Stonehouse, UK:

Skirted, internal thread, blue cap, sterile cryovial (2.0 ml), Individual Wrapped Cell scraper

Invitrogen, Paisley, UK:

Alexa Fluor® 568 phalloidin, Monoclonal anti-paxillin antibody (mouse) Opti-MEM® Reduced Serum Medium (no phenol red)

Melford Laboratories Ltd, Suffolk, UK:

Glycine, Acrylamide/bis-acrylamide (40% w/v), MTT, Nuclease free water

Merck Chemicals Ltd, Nottingham, UK:

G 418 Sulfate (cell culture tested)

Milipore, Watford, UK:

Monoclonal anti-fascin antibody (mouse), Polyclonal anti-VASP antibody (rabbit)

New England Biolabs Ltd, Herts, UK:

1-10kb DNA ladder

PAA Laboratories Ltd., Somerset, UK:

High Glucose DMEM (4.5g/l) liquid without L-Glutamine, MEM Non Essential Amino Acids (100X), Goat Serum, Penicillin (500,000U/ml-1) /streptomycin (500,000µg/ml-1), Trypsin (10X), Fetal Bovine Serum (FBS)

Sarstedt Ltd, Leicester, UK:

Individually wrapped sterile serological pipette (5ml, 10 ml, 25 ml), 1000 µl blue tips, petri dish, Tissue culture dish (60x15mm)

SLS Ltd, Nottingham, UK:

High Clarity polypropylene centrifuge tubes (15ml), round coverslips (12mm and 13mm)

Starlab Ltd, Milton Keynes, UK:

Cordless pipette controller, 10 µl graduated tips

Sigma-Aldrich, Poole, UK:

Monoclonal anti-vinculin antibody (mouse), BDM, Fibronectin (human plasma), Dimethyl sulfoxide, Phosphate buffered saline tablets, Triton X-100, Kodak® GBX developer, Kodak® GBX fixer, Kodak® BioMax® light film, Hydrocortisone-Water Soluble, Insulin solution (human), Peroxidase-conjugated goat anti-rabbit immunoglobulins (whole molecule) polyclonal antibody, Peroxidase-conjugated goat anti-mouse immunoglobulins (whole molecule) polyclonal antibody, Ethylenediaminetetraacetic acid (EDTA), Kanamycin, Ampicillin, Ammonium persulphate (APS),

N,N,N',N'-Tetramethylethylenediamine (TEMED), Paraformaldehyde (PFA), sodium dodecyl sulphate (SDS), Sodium hydroxide (NaOH)

Tocris Bioscience, Bristol, UK:

Y-27632

Vector Laboratories Ltd, Peterborough, UK:

Vectashield hard set mounting medium containing 4'-6-diamidino-2-phenylindole (DAPI)

VWR International, Leicestershire, UK:

jetPEI® HTS DNA transfection reagent, INTERFERin® siRNA transfection reagent

All reagents were purchased from Sigma (Poole, UK), unless stated otherwise. Marvel dried milk powder was purchased from domestic outlets. And all solutions, reagents and utensils were sterilised by autoclaving at 121°C or by filtering through 0.22µm Millex PES Pore syringe filter.

2.2 Methods

2.2.1 Cell Culture

2.2.1.1 Culture of Rat mammary benign tumour (Rama 37)

The rat mammary (Rama 37) non-metastatic benign tumour derived cell line 37 expresses barely detectable levels of S100A4 mRNA and protein (Dunnington et al., 1983, Davies et al., 1994, Lloyd et al., 1998). The four cell lines used during this work were: a) the control cells transfected with the empty pBKCMV vector (Rama 37 Control), b) the cell line transfected with the human full length S100A4 wild type open reading frame inserted in the pBKCMV expression plasmid (R37 S100A4WT), c) R37 S100A4Δ2 cell line and d) R37 S100A4Δ6 cell line which were obtained by transfection of the expression vectors for S100A4 protein with C-terminal truncations lacking amino acids 100-101 or 96-101 respectively (Figure 2.2.1) (Ismail et al., 2008b, Ismail et al., 2010). These cell lines were kindly supplied by Prof. Philip Rudland and Dr. Roger Barraclough (University of Liverpool, UK) and level of S100A4 expressions were reconfirmed with western blot analysis (Figure 2.2.2).

The cells were routinely cultured in a humidified atmosphere at 37°C, 5% (v/v) CO₂ in Dulbecco minimal Eagle's medium (DMEM) supplemented with 4500mg/L glucose, sodium pyruvate (< 1%), sodium bicarbonate (< 0.37%), 2mM L-glutamine, 1% (v/v) non essential amino acids, penicillin/streptomycin (50 U/ml), 10% (v/v) fetal bovine serum (heat inactivated), 5ng/ml insulin, 5ng/ml hydrocortisone and 400µg/ml geneticin (G418).

R37 S100A4 WT – 82 IAMMCNEFFEGFPDKQPRKK 101

R37 S100A4 Δ2 – 82 IAMMCNEFFEGFPDKQPR 99

R37 S100A4 Δ6 – 82 IAMMCNEFFEGFPD 95

Figure 2.2.1 Illustration of C terminus region of S100A4 protein. A) C terminus of wild type S100A4 protein, B) truncation of the last two amino acids from C terminus of S100A4 protein and C) truncation of the last six amino acids from the C terminus of S100A4 protein.

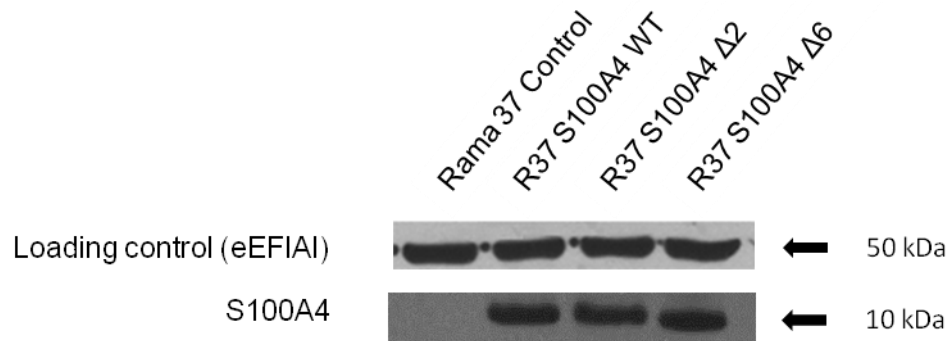


Figure 2.2.2 Western blot reconfirming level of S100A4 expression. Rama 37 cell lines with a density of 1.5×10^6 were seeded into 60mm tissue culture dish 24 hours prior to harvesting. Total protein for all cell lines were quantified and equal amount of total protein (80µg eEF1A1 and 150µg S100A4) loaded onto SDS Page gels (10% (w/v) and 15% (w/v) respectively). Resolved proteins were transferred onto nitrocellulose membrane before incubating with primary antibodies (eEF1A1 and S100A4) and then followed by secondary HRP conjugated antibody. Detection was undertaken using the customised detection system (Table 2.11). Methods are fully detailed in Chapter 2.2.11 to 2.2.15.

2.2.1.2 Culture of African green monkey kidney cells (Cos 7)

The wild type Cos 7 cells were a kind gift from Dr. Eric Hill (Aston University, UK). This cell line originates from African green monkey kidney and derives from the CV-1 cell line by transformation with an origin defective mutant of SV40 which codes for wild type antigen T. It has a fibroblast-like morphology and naturally lack of non muscle myosin IIA which is a vital part of this project. In this work, this cell line is transfected with four different plasmids: a) the control cells transfected with the empty PeGFP C3 plasmid (PeGFP C3), b) transfected with human PeGFP full length non muscle myosin IIA (NMIIA) (Addgene, USA) c) transfected with PeCFP C1 plasmid (PeCFP C1) and d) transfected with human PeCFP full length S100A4 protein (PeCFP S100A4 WT). The PeCFP plasmid encoding full length of S100A4 WT protein is a kind gift from Dr. Roger Barraclough (University of Liverpool, UK)

The wild type Cos 7 cells were cultured DMEM supplemented with 4500mg/L glucose, 2 mM L-glutamine, 1% (v/v) non essential amino acids, penicillin/streptomycin (50 U/ml) and 10% (v/v) fetal bovine serum (heat inactivated). Transfected Cos 7 cells were cultured as wild type Cos 7 but with additional 300 µg/ml geneticin (G418) for selection purposes. All cell lines were left for incubation in a humidified atmosphere at 37°C, 5% (v/v) CO₂, 95% (v/v) air.

2.2.1.3 Passage of cells

Cells were grown until they reach 80% confluency in any sized flask before passaging. The used media were pipette out and the cells were rinsed with serum free DMEM. The cells were then trypsinised by adding appropriate amount of trypsin (1 ml per 25 cm²) containing 2mM EDTA dissolved in PBS at pH7.4. The flask is then placed in the incubator for 5 minutes and the dislodged cells were determined by visualising under light microscope. The trypsin action was

inhibited by adding complete media which amount is twice of the amount of trypsin that has been added beforehand. The cells suspensions were centrifuged at 2000 rpm using 2-6E Sigma centrifuge for 5 minutes. The supernatants were discarded and the cell pellets were resuspended in fresh complete media and appropriate amount of cells were reseeded. If necessary, cell counting will be performed with a double chamber (refer to Section 2.2.2).

2.2.1.4 Cryopreservation of Cells

Centrifuged cells obtained while passaging cells (refer to Section 2.2.1.3) were resuspended in freezing mixture made up of 10% (v/v) DMSO and 90% (v/v) of fetal bovine serum. Cells were stored in pre-labelled cryovials and left in -20°C freezer for an hour before transferring them to -80°C freezer. The cells were transferred into liquid nitrogen the next day.

2.2.1.5 Cell Thawing

Frozen cells were quickly thawed in 37°C water bath. Cells were removed from the cryovial and placed into a T25 flask. Immediately, pre-warmed medium is added drop-wise into the cell suspension and gently mixing them at the same time. After 12-16 hours, depending on the rate of cell attachment, the used media is replaced with fresh ones.

2.2.2 Cell Counting

Numbers of cells were determined prior to every experiment conducted. After trypsinisation, centrifugation, and resuspension in fresh medium (refer to Section 2.2.1), 10 µl of cell suspension was applied to double chamber haemocytometer (Haemocytometer Improved

Neubauers double ruled, Fisher,UK). Cells in the four quadrants were counted and the average numbers of cells were multiplied by 10^4 to give the final number of cells per ml.

2.2.3 Cell Viability Determination

Viability of cells is determined by (3-(4,5-dimethylthiazol-2-yl)-2,5-diphenyl tetrazolium bromide) MTT assay. This technique is based on the colour formation caused by respiratory chain activity of proliferating or living cells (Mosmann, 1983). Tetrazolium salts measure the dehydrogenase enzyme activities, which is cleavage of tetrazolium ring in active mitochondria. This results in reduction of yellow MTT solution insoluble purple formazan (1-(4,5-dimethylthiazol-2-yl)-3,5-diphenylformazan) by succinate-tetrazolium reductase (Bernhard et al., 2003). With the addition of dimethylsulphoxide (DMSO) solution, the insoluble purple formazan is solubilised into coloured solution and the intensity of product's colour can be measured using a spectrophotometer where higher intensity indicates higher cells viability or cell number or mitochondrial activity.

The cell numbers to be seeded into a 24 well plate were determined by seeding different initial cell numbers into each well and the one which reaches confluency at day 7 will be used. The rationale behind this selection is that cells that were over-confluent will reduce cell growth rate hence interfering MTT determination. In some of the experiments, where cells viability was measured for 72 hours, it is important to ensure that the wells will not be over-confluent by 72 hours. For these cell lines, the optimum number of cells to be seeded into each well of 24 well plate is 10,000. The freshly seeded cells were left for 24 hours incubation prior to addition of inhibitors or other compounds. 40 μ l of MTT (5mg/ml in PBS) is added to 400 μ L of media and the cells were incubated at 37°C with MTT for 1 hour. The media were then pipette out and the cells were washed with PBS and solubilised with 400 μ l of DMSO. The solubilised MTT were then

transferred to 96 well plate before reading at 550nm with a plate reader. Any reading exceed the value of 1.1 is diluted with DMSO to obtain a more accurate reading.

2.2.4. CellIQ Scratch Assay

Cells were counted (refer to Section 2.2.6) and seeded into 24 well plate and left to incubate for 48 hours until it reaches 100% of confluency (refer below for specific cell types density). The used media were discarded and one scratch was done per well with a yellow tip. The scratched wells were then washed with serum free media to remove cell debris. Fresh media, with or without drugs, were then added into each well. The scored plates were left in the incubator for about 30 minutes with CellIQ customised lids prior to sealing them with sealing tape. Then, the plates were attached to the gas pipes within the CellIQ machine 37°C incubator where it serves to maintain constant gas flow. Three positions in different regions of each well were set with the CellIQ imaging software and images were taken for 24 hours. Then, images were processed with CellIQ analyser software.

Cell types	Number of cells to be seeded in each well of 24 well plate
Rama 37 control	150,000
R37 S100A4 WT cells	200,000
Cos 7 cells	100,000

Table 2.1 Densities of different cell lines to be seeded in each well of 24 well plate for scratch assay.

2.2.4.1 Determining Mitotic Index with CellIQ

Images of cells taken with CellIQ were browsed carefully using CellIQ software and morphology in different phases was assigned into respective classes as described in manufacturer's guide ; a) dividing cells, b) stable cells, c) dead cells and d) debris (Figure 2.2.2). Mitotic index were obtained by calculating the ratio between dividing cells and the total number of cells.

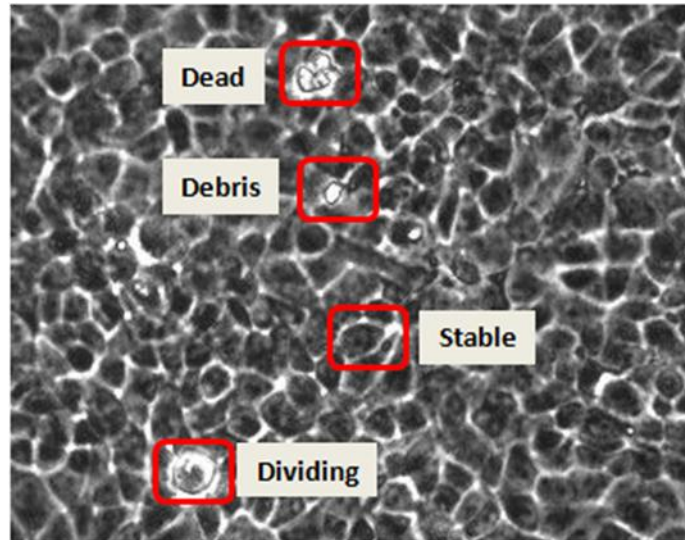


Figure 2.2.3. Representative image of Rama 37 control cells assigned into respective class using CellIQ imaging system.

2.2.5 Layout of Rama 37 cell lines seeding in 24 well plate for screening

Rama 37 cell lines (150,000 for Rama 37 control cells and 100,000 R37 S100A4 WT cells) were seeded in each well of 24 wells plate for 48 hours to obtain a confluent monolayer of cells (Figure 5.2.1 and 5.2.2). Cells were then wounded with a 200 μ L pipette tip and washed with PBS prior to adding 800 μ L of fresh media along with 5 μ M of chemical compounds to be tested. The plate was swirled gently to provide an even mixture before incubation for a maximum of 24 hours. The rest of the method is as mentioned in Chapter 2.2.4.

	1	2	3	4	5	6
A	○	◆	◆	◆	◆	◆
B	○	◆	◆	◆	◆	◆
C	◇	◆	◆	◆	◆	◆
D	◇	◆	◆	◆	◆	◆

Legend:

- Rama 37 Control Cells (untreated)
- ◇ R37 S100A4 WT Cells (untreated)
- ◆ R37 S100A4 WT Cells (treated)

Figure 2.2.4 Layout of cell types seeded on 24 well plate for preliminary screening

	1	2	3	4	5	6
A	○	◇	○	◇	●	◆
B	●	◆	●	◆	●	◆
C	●	◆	●	◆	●	◆
D	●	◆	●	◆	●	◆

Legend:

- Rama 37 Control Cells (untreated)
- Rama 37 Control Cells (treated)
- ◇ R37 S100A4 WT Cells (untreated)
- ◆ R37 S100A4 WT Cells (treated)

Figure 2.2.5 Layout of cell types seeded on 24 well plate for secondary and tertiary screening

2.2.5.1 Calculation of wound closure rate ($\mu\text{m}^2 \text{min}^{-1}$)

Images taken during wound healing process were analysed using CellIQ Analyser Software. This software will provide information about time when the images were taken, total wound area, total wound closure area and percentage of wound area closure. From this information, wound healing curves were obtained where percentage of wound closure is plotted against time (Figure 2.2.2).

From the raw data, the gradient of the curve is obtained as shown below:

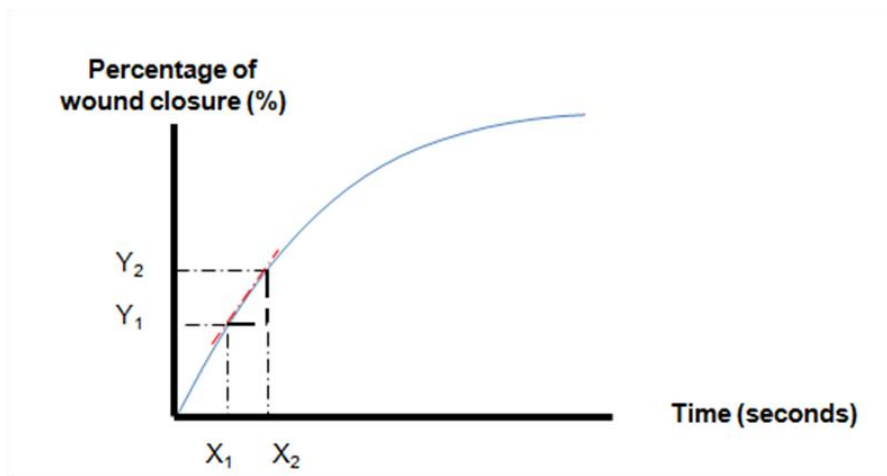


Figure 2.2.6 Illustration showing how a wound area closure rate is calculated from raw data obtained.

In the calculation of wound area closure rate, the gradient of the curve, m , is obtained using the formula:

$$Y = mX + C$$

where $Y = y_2 - y_1$ (Wound area in pixel²)

$X = x_2 - x_1$ (time in second)

The gradient of the wound healing curve was taken close to the mid section (50 %) with the following assumptions:

- 1) Wound healing curve at T = 0 is ignored as compound used may have slower effect on cells
- 2) Wound healing curve plateaus as it reaches 80 % of total closure

It is worth noting that the wound width is taken as pixel instead of μm and the time is taken as second. Hence, the area calculated correlates to pixel^2 . Since 10X objective was used in the entire screen, it is given that:

$$1 \text{ pixel} = 0.7 \mu\text{m}$$

Therefore, the **rate of wound area closure** is in $\mu\text{m}^2\text{min}^{-1}$:

$$\text{Rate} = m \times 0.49 (\mu\text{m}^2) \div 60 (\text{min})$$

2.2.6 Transient Transfection

Plasmid DNA or siRNA can be transfected into cells depending on manufacturer's protocol. Throughout this work, Polyplus Jetpei transfection reagent was used unless mentioned otherwise. Depending on nature of experiment and cell types, different number of cells will be seeded into either 24 well plate, 6 well plates or 60mm tissue culture dishes (refer below for specific cell types in different wells). The seeded cells were then left to attach for 24 hours before the used media were discarded, washed with serum free DMEM and replaced with fresh media void of antibiotics 1 hour prior to transfection. In two different eppendorf tubes, 100 μL NaCl (150mM) were added into each tube. Then, the transfection reagent (JetPei[®], VWR International, UK) and plasmid DNA were added into each tube respectively. The ratio of Jetpei to plasmid DNA should be determined beforehand to get optimum transfection efficiency. Both the tubes were vortexed for 10 seconds

and then centrifuged briefly. Then, the tube containing transfection reagent was added gently (dropwise) to the tube containing plasmid DNA. Again, the content were mixed thoroughly by 10 second vortexing and then briefly centrifuged to bring the solution down. The solution was left to incubate for 15 to 30 minutes at room temperature. The solution was added dropwise to the cells and the plate (flask or dish) were gently mixed by swirling action. After 24 to 48 hours, the cells should be transfected and ready for fixing or treatment.

In each well of 24 well plate		
Cell types	Number of cells to be seeded (wound healing assay-CellIQ)	Number of cells to be seeded (immunofluorescence staining)
Rama 37 control	80,000	10,000
R37 S100A4 WT cells	80,000	10,000
Cos 7 cells	80,000	10,000

Table 2.2 Density of respective cells to be seeded in each well of 24 well plate for transfection.

In each well of 60 mm culture dish (western blot)	
Cell types	Number of cells to be seeded
Rama 37 control	500,000
R37 S100A4 WT cells	500,000
Cos 7 cells	400,000

Table 2.3 Density of respective cells to be seeded in 60 mm culture dish for transfection prior to conducting western blot.

2.2.6.1 Transfection efficiency

Round glass coverslips measured at 13mm in diameter were placed into each well of 24 well plate. The plate was then exposed to UV for 10 minutes before coating the coverslips with 4µg of fibronectin per well in sterilised PBS. The plate was left for incubation for 1 hour in 37°C. Unbound fibronectin was washed with PBS for three times and the counted cells were seeded in 400 µl of complete media and left for 24 hours. The media were discarded and replaced with fresh media void of antibiotics 1 hour prior to transfection. Different transfections were done according to their customised protocols. After 24 hours, cells were washed and fixed with 3.7% (w/v) PFA for 20 minutes. Then, PFA was replaced with 30mM of glycine (solubilised in PBS) for 10 minutes to counter left over PFA activity. Cells were then mounted with Hardset mounting medium, DAPI (Vector Laboratories Ltd, UK). Images of cells were taken with inverted epifluorescence microscope (DM14000B, Leica) using a N-Plan 20x /0.25 PH1 objective (AxioVision Version 4.7 software). Total cell count (number of nucleus stained with DAPI) against transfectants (GFP/CFP expressing cells) were calculated and plotted as transfection efficiency.

2.2.7 SiRNA transfection

Respective cell lines were seeded into individual culture vessel (either 24 or 6 well plate) 24 hours prior to transfection. Used medium was replaced with Z Opti-MEM® and left for 4 hours prior to adding transfection mixture. The transfection mixture was obtained by adding W µL of SiRNA to X µL of serum free DMEM before being gently mixed by pipetting motion. Then, Y µL of INTERFERin® and the mixture were vortexed for 10 seconds and briefly centrifuged before being incubated for 10 minutes at room temperature. The mixture was added to the cells and incubated for 72 hours prior to further analysis.

Culture vessel	W (μL) volume of SiRNA added (20 μM stock concentration)	X (μL) volume of serum free DMEM	Y (μL) volume of INTERFERin [®] reagent	Z (μL) volume of Opti-MEM [®]
24 well	1	100	3	1000
6 well	3	200	9	2000

Table 2.4 Ratios of different reagents to be added in either 24 well or 6 well transfection.

2.2.8 Immunofluorescence Staining

Round glass coverslips (SLS Ltd, UK) measured at 13mm in diameter were placed into each well of 24 well plate. The plate was then exposed to UV for 10 minutes before coating the coverslips with 4 μg of fibronectin (Sigma, UK) per well in sterilised PBS. The plate was left for incubation for 1 hour in 37°C. Unbound fibronectin was washed with PBS for three times and the counted cells were seeded in 400 μl of complete media and left for 48 hours. Cells were washed with cytoskeleton buffer (CB buffer) (refer to Table 2.5) twice before fixing them with 3.7% (w/v) PFA in CB buffer at 37°C for 20 minutes. Then, cells were incubated with 30mM Glycine in CB buffer at room temperature for 10 minutes. Following this, 5% (v/v) Triton X-100 in CB buffer was added to the cells and left for 2 minutes to permeabilise and solubilise them. The cells were then washed 3 times for 5 minutes with CB buffer at room temperature. Blocking of cells was performed using 10% (v/v) goat serum in CB buffer for 30 minutes. Primary antibody incubation (refer to Table 2.4) in 1% (v/v) goat serum in CB buffer was done at 37°C for 45 minutes. The excess primary antibody is washed off with 1% (v/v) goat serum at room temperature for three times and 5 minutes for each wash. Then, the cells were incubated with secondary antibody (refer to Table 2.4) in 1% (v/v) goat serum in CB buffer at 37°C for 45 minutes. Cells were washed again with 1% (v/v) goat serum in CB buffer for three times and twice with distilled water to remove salt.

The coverslips were carefully mounted onto slides with hardest mounting medium, DAPI before viewing under a microscope. To avoid samples from drying out, nail varnish was applied around the edge of the coverslips and kept in 4°C.

Types of antibody	Dilution in CB buffer (1% Goat serum)
Monoclonal anti-Vinculin antibody (mouse)	1:60
Monoclonal anti-Paxillin antibody (mouse)	1:100
Polyclonal anti-NMMIIA (rabbit)	1:2000
Monoclonal anti-Fascin antibody (mouse)	1:500
Polyclonal anti- VASP antibody (rabbit)	1:200
Alexa Fluor® 568 phalloidin	1:40
FITC/ TRITC secondary conjugate (mouse and rabbit each respectively)	1:300

Table 2.5 Dilutions of antibodies used for immunofluorescence staining.

Making of 1 Litre of cytoskeleton buffer (CB buffer)	
Chemical compound	Weight (grams)
Sodium Chloride (NaCl)	8.766
Magnesium Chloride (MgCl₂)	0.476
Ethylene Glycol Tetraacetic Acid (EGTA)	1.901
Glucose	0.900
MES (2-n-morpholino ethansulfon acid)	2.130

Table 2.6 Formulations used for making 1L of cytoskeleton buffer (1x).

2.2.9 Live cell analysis

For live cell analysis, the different cell lines were seeded with density of 500,000 cells in a 50mm Petri dish and grown for 24 hours prior to pGZ21 GFP-vinculin expressing plasmid transfection with jetPei™ (a kind gift from Benjamin Geiger, Weizmann Institute of Science, Rehovot, Israel). The transfectants were trypsinised and reseeded at a density of 5,000 cells into a customised 170µm-thickness glass bottom Petri dish, pre-coated with 2.5 µm/cm² of fibronectin (BD Biosciences, Palo Alto, CA) for 30 minutes at 37°C. The analyses were carried out 24 hours post seeding with confocal microscope (LSM710, Zeiss) using EC Plan-Neofluar 40x/1.30 Oil Ph3 objective (Zeiss) at 37°C and 5% (v/v) CO₂. The duration for single cell analysis was set to 20 minutes per cell with 10 seconds intervals. Phase contrast and GFP imaging were taken with argon ion laser line with a wavelength of 488nm and 2.4 - 2.8% of laser intensity. All the parameters were kept constant throughout the analyses. Images obtained were optimised (background subtraction and contrast adjustment) with ImageJ for better visualisation.

2.2.10 Quantification of focal adhesion clusters and filopodia of fixed cells

Immunofluorescence staining images were taken as mentioned in Chapter 2.2.6. Single cell images were selected and open with ImageJ. Quantifications were done by manually counting the filopodia or clusters with multipoint selection tool.

2.2.11 Quantification of focal adhesion clusters and filopodia of live cells

Time-lapse images taken as mentioned in Chapter 2.2.7 were used. Time frames were frozen to quantify newly formed focal adhesions or filopodia. Using this method, the retracting fibers were distinguished from the filopodia by determining the rear and leading edge of the migrating cell.

2.2.12 Cell force analysis

Silicon wafer were cleaned in acetone, washed with methanol and then blow dried before being baked for 20 minutes at 120°C. The wafers were then silanised with trichloro(1H, 1H, 2H, 2H-perfluorooctyl)silane (Sigma). The elastic silicone rubber substrates were made with two-component silicone rubber (PDMS) formulation (*Sylgard 184*, Dow Corning GmbH, Wiesbaden, Germany) of either 55:1 or 50:1 (w/w) ratio of base material and cross-linker (with a Young's modulus of 8 kPa or 15kPa respectively). For micropatterning, red fluorescence beads (FluoSpheres, 0.2 µm, Crimson, Invitrogen, Karlsruhe, Germany) were mixed with one part of the silicone substrate and spread on the micro-structured silanised silicon dioxide wafer surface. Excess substrate on wafer was removed by wiping it off with lint-free tissue. Then, two glass spacers (80-100 µm) were placed on each side of the wafer and the remaining substrates without microbeads were added onto the wafer, in between the spacers. A coverslip was placed on top of the substrate even the surface. The sandwiched substrate was cross-linked by overnight baking at 60°C and glued to the bottom of a 35mm Petri dish which has been predrilled with 15mm holes (Cesa et al., 2007, Claudia Schäfer, 2010).

A density of 5000 cells (either Rama 37 control, R37 S100A4 WT, R37 S100A4 Δ2 or R37 S100A4 Δ6) per dish were seeded respectively onto the customised Petri dish and left for

overnight incubation. The attached cells in respective dish were removed with a micro manipulator and the phase contrast image of the cells and the deformation of microbeads patterns were taken with 40x/1.3 Ph3 plan neofluar oil objective (Carl Zeiss) on a Cell Observer system (Carl Zeiss) equipped with a CCD camera (AxioCam, MRm, Carl Zeiss). Complete removal of cell was demonstrated by taking a phase contrast image after cell removal. Microbeads patterns were visualised with DsRed filter.

The deformations of the beads caused by contraction force of the cells were calculated with Cellforce analysis software where the shifts of the beads before and after removal of the cells were calculated.

2.2.13 Preparation of chemically competent *E.coli*

E.coli (Dh5-Alpha strain) were grown overnight on an agar plate. Then, using a yellow tip, a single colony was picked and inoculated in 5 ml of Lennox Broth (LB) (refer to Table 2.6) in a shaker incubator at 37°C for overnight. Culture was diluted with a ratio of 1:1000 with fresh LB and left in the same incubator until the the absorbance at 600 nm was approximately 0.300. The culture was then left on ice for 15 minutes before adding equal volume (5 ml) of 2X Transformation and Storage Solution (TSS) (refer to Table 2.6). The culture was mixed gently and left on ice for a further 20 minutes. The mixture was centrifuged at 1000g at 4°C and the supernatant is carefully decanted. The pellet is resuspended in 1 ml of 1X TSS mixture (0.5 ml of 2X TSS and 0.5 ml of LB). The cells were then aliquoted and stored in -80°C for future use.

Chemical compound	Amount
Making of 1 Litre of Lennox Broth (LB)	
Tryptone	10.000 (g)
Yeast extract	5.000 (g)
Sodium Chloride (NaCl)	10.000 (g)
Distilled water	Top up to 1000 (ml)
Making of 100 ml of 2X-Transformation and Storage Solution (TSS) (pH 6.5)	
Polyethylene Glycol 3350 (PEG3350) (20% w/v)	20.000 (g)
Magnesium Chloride (MgCl₂) (100 mM)	9.521 (g)
LB Broth	Top up to 100 (ml)

Table 2.7 Formulations to prepare 1L of Lennox Broth and 100ml of Transformation and Storage Solutions (1X).

2.2.14 *E.coli* Transformation for plasmid production

To make transformants, 10ng of plasmid DNA was aliquoted into an eppendorf tube and left on ice. Then, competent bacteria previously prepared and stored in -80°C were rapidly thawed. To the aliquoted plasmid DNA, 40-50µl of competent bacteria was added. The mixture was left on ice for 30 minutes and shaking the tube at every 10 minutes interval. The tube was then placed in water bath at 42°C for 45 seconds and immediately kept on ice for 2 to 3 minutes. To the mixture, 800µl of pre-warmed LB liquid were added and left in shaker incubator for approximately 1 hour at 37°C. Then, 50 to 100 µl of suspension was spread onto an agar plate containing suitable antibiotic and left for overnight culture at 37°C. With a yellow tip, 1 colony was picked from the plate and dipped into 5ml LB containing antibiotic and again, left in shaker incubator (250 rpm) at 37°C overnight culture. To store the transformants, 1ml of cell suspension

was placed in a labelled cryovial and gently mixed with 500µl of 60% (v/v) glycerol and store in -80°C.

2.2.15 Mini-prep (Plasmid extraction)

Mini-prep can be done from overnight growth in 5 ml of LB containing antibiotic selection and cultured for 16 hours at 37°C while shaking at 250 rpm. Grown cultures were centrifuged at 3000 rpm for 5 minutes (Sigma 2-6E centrifuge). The supernatant was then discarded and continued using Fermentas mini-prep kit according to manufacturer's protocol (Fisher Scientific, UK). Briefly, the pellets were resuspended with 250 µl of Suspension Buffer each and equal volumes of Lysis Buffer were added before inverting the tubes a few times. 350 µl of Neutralisation Buffer was added to each tube and mixed carefully by repetitive pipetting. Mixtures were transferred to eppendorfs and spun at 13000 rpm for 5 minutes. The pellets were discarded and the supernatant were transferred into the column-eppendorfs and centrifuged at 13000 rpm for 2 minutes. The flowthroughs were discarded and 700 µl of Washing Buffer were added to each column and centrifuged again at 13000 rpm for 1 minute. The columns were removed and inserted into new eppendorfs before adding 50 µl of distilled water and incubated for 5 minutes before centrifuging at 13000 rpm for 1 minute. The purified plasmid DNA obtained was then stored at -20°C after running 5 µl on DNA electrophoresis for analysis.

2.2.16 Agarose gel electrophoresis

For different size of DNA fragment, different percentage of agarose gel should be used. For larger DNA fragments (5-10kb), gel of 0.7% (w/v) to 1% (w/v) should be used. For smaller fragments (0.2-1kb), gel as high as 2% (w/v) should be used. In this work, 1% (w/v) gel was made

by weighing 0.6 g of agarose powder and dissolving in 60 ml of 1X-Tris-Acetate-EDTA (TAE)(refer to Table 2.7) in a conical flask. Following heating up of the solution in a microwave until a clear solution was formed, the solution was allowed to cool and 10 µg of ethidium bromide (Bio-Rad, UK) was added. The solution was mixed by swirling the flask gently and the content was poured into the DNA Gel cast (Geneflow, UK). After the gel was set, it was placed in the chamber filled with 1X TAE buffer, followed by loading of samples and run for approximately 20 minutes or until the tracking dye (refer below for details) reach the bottom of the gel. The DNA sample was visualised with UV transilluminator (G: Box, SynGene, UK) using GeneSnap software.

Chemical compound	Amount
Making of 1 Litre of 1-X Tris-Acetate-EDTA (TAE)	
Tris Base	4.840 (g)
Glacial acetic acid	1.142 (ml)
0.5M EDTA (pH8.0)	2.000 (ml)
Distilled water	Top up to 1000 (ml)
Making of 10 ml of DNA Tracking Dye	
Bromophenol Blue	0.025 (g)
Sucrose	4.000 (g)
Distilled water	Top up to 10 (ml)

Table 2.8 Formulations of 1L of Tris-Acetate-EDTA (1X) and 10ml of DNA tracking dye.

2.2.17 Preparation of total cell lysate

Cells were collected either by scraping or trypsinising. After being grown in a 60mm tissue culture dish until 90% confluency, the used media were discarded and the cells were placed on ice which washing with ice cold PBS 3 times. Then, 150 μ l of homogenising buffer (0.25M sucrose, 5mM Tris-HCl pH7.4, 2mM EDTA, 200mM PMSF) were added and scrapped. Scrapped cells were transferred into eppendorf tubes and sonicated at 20 kHz (approximately 20% of power) for 10 seconds with an interval of 30 seconds for 3 times. The samples were spun down to remove cell debris and the clear supernatants were then split into two groups, one for protein quantification (proceed to Section 2.12) and the other to be added with 4x Laemmli loading buffer (refer to Table 2.10) and boiled for 2minutes prior to gel electrophoresis (proceed to Section 2.2.13).

2.2.18 Protein Quantification (Lowry method)

This Bio-Rad commercial kit is based on Lowry method (Lowry et al., 1951) where the total protein concentration is proportional to the colour change of the sample solution. In this method, 5 μ l of BSA standard solution ranging from 0.1 to 1.5 mg/ml was used and 5 μ l of samples were added to 96 well plate (in triplicate), followed by 25 μ l of reagent A and 250 μ l of reagent B. The samples were mixed by careful repetitive pipetting to avoid air bubbles and left for incubation for 10 minutes before being read at 750nm using an BioTek- EL808 Elisa plate reader (BioTek Potton, UK) to produce calibration graph.

2.2.19 Polyacrylamide Gel Electrophoresis (PAGE)

In this work, Glycine-SDS-PAGE (Sodium Dodecyl Sulphate PolyAcrylamide Gel Electrophoresis) was used where acrylamide forms linear polymers and bisacrylamide forms linkage between the linear polyacrylamide chains. The polymerisation process is promoted by both ammonium persulphate (APS) and N,N,N',N'-Tetramethylethylenediamine (TEMED).

The components used in assembling the gel are the Bio-Rad mini-Protean II gel system. Two different sizes of resolving gel casts were used in this work (80x60x0.75mm and 80x60x1.5mm) depending on volume and number of samples used. Glass plates and combs were cleaned with distilled water and ethanol and air dry before use. Depending on the size of protein to be separated (refer to Table 2.8), acrylamide resolving gel prepared were mixed thoroughly to prevent gel channelling. The resolving gel (refer to Table 2.9) was pipetted into the space between the glass plates, leaving approximately 0.5cm from the bottom of the comb. Water-saturated isopropanol was overlaid on top of the mixture immediately to ensure an even top surface and avoid meniscus formation. After the gel was completely polymerised, the layer of isopropanol was removed and the 3% stacking gel mixture (refer to Table 2.9) was poured over the polymerised resolving gel and the appropriate comb was inserted into the unpolymerised stacking gel.

Quantified samples (Section 2.11 and 2.12) were loaded into respective wells of polymerised gels and run at 90V for the first 15 minutes (with running buffer (Table 2.10)) to introduce the protein samples through the stacking gels. Then, the samples were run at 120V through the resolving gels for 60 minutes or until the Bromophenol Blue tracking dye reached the bottom of the gel.

Protein Size (kDa)	Gel Percentage (%)
4-40	20
12-45	15
10-70	12.5
15-100	10
25-200	8

Table 2.9 Appropriate percentage of gels to be used to separate different protein size.

Reagents	8% Resolving gel (ml)	10% Resolving gel (ml)	15% Resolving gel (ml)	3% Stacking gel (ml)
40% acrylamide	2.000	2.700	4.050	0.375
1.5M Tris-Base pH 8.8	1.700	1.700	1.700	-
0.5M Tris-Base pH 6.8	-	-	-	0.800
10% (w/v) SDS	0.067	0.067	0.067	0.033
Distilled water	6.200	5.500	4.150	1.725
10% (w/v) APS	0.050	0.050	0.050	0.020
TEMED	0.0033	0.0033	0.0033	0.0033

Table 2.10 Appropriate amount of different reagents to make up specific gel percentage.

Chemical compound	Amount
1 Litre of 1X-running buffer (pH 8.5)	
Tris Base	3.0
Glycine	14.4
SDS	1.0
Making of 50 ml of 4X-Laemmli buffer	
Tris Base (pH 6.8)	20.00 (ml)
Glycerol	20.00 (ml)
β-mercaptoethanol	2.00 (ml)
SDS	2.00 (g)
Bromophenol Blue	0.02 (g)

Table 2.11 Formulations to prepare 1L of running buffer (1X) and 50ml Laemmli buffer (4X).

2.2.20 Western Blot

The gel obtained from gel electrophoresis was placed on 0.45 μm nitrocellulose membrane (Bio-Rad, UK) and sandwiched in between six layers of Whatman filter papers (Fisher Scientific, UK) and two foams and secured with a cassette. The cassette along with an ice gasket were then inserted into Mini Trans-Blot Cell (Bio-Rad, UK) kit and filled with transfer buffer (refer to Table 2.11). The kit was placed in a chamber filled with ice and left for transfer at 200mA for 2 hours. The membrane was removed and the transfer was stained with Ponceau red which was removed with TBS tween via repetitive washing. The membrane was blocked with 5% (w/v) of dried milk (Marvel) in TBS tween for 30 minutes before incubating primary antibody solution overnight at 4°C on a shaker. Following this incubation, the membrane was washed with TBS tween 4 times for 10 minutes each prior to incubation with secondary antibody solution (HRP-conjugate antibodies polyclonal rabbit/mouse 1:1000 dilution in 1% (w/v) milk in PBS) for 2 hours at room temperature prior to another 45 minutes of washing with TBS tween. Custom made Horseradish peroxidase (HRP) detection reagent (refer to Table 2.11) was added onto the membrane (2.5ml for each blot) and incubated for a minute before being wrapped with cling film and developed in the dark room by exposing of blots with Kodak BioMax light film of varying lengths of time will produce different band intensities. Films were developed in Carestream Kodak developer (Sigma) and then rinsed with warm water followed by fixing with Carestream Kodak fixer (Sigma) for a few minutes. The fixed film was washed intensively before air drying.

Chemical compound	Amount
1 Litre of 1X-Transfer buffer (pH 8.3)	
Tris Base	3.025 (g)
Glycine	14.400 (g)
Methanol	200 (ml)
Distilled water	Top up to 1000 (ml)
100 ml of 1X-Ponceau Red	
Ponceau S Stain	0.200 (g)
Trichloroacetic acid (TCA)	0.400 (ml)
Distilled water	Top up to 100 (ml)
1 Litre of 1X-TBS Tween	
Tris Base	1.210 (g)
Sodium Chloride (NaCl)	8.770 (g)
Distilled water	Top up to 1000 (ml)
5 ml of 1X- Detection Reagent	
Tris Base (pH 8.5)	0.500 (ml)
50 mM Coumaric acid (Sigma-ready made)	0.011 (ml)
250 mM Luminol (Sigma-ready made)	0.025 (ml)
37% (v/v) Hydrogen Peroxidase (H₂O₂)	0.0015 (ml)
Distilled water	Top up to 5 (ml)

Table 2.12 Formulations for preparing different buffers used in Western Blot.

Types of antibody	Dilution in CB buffer (1% Goat serum)
Monoclonal anti-Vinculin antibody (mouse)	1:1000
Monoclonal anti-Paxillin antibody (mouse)	1:1000
Polyclonal anti-NMMIIA (rabbit)	1:5000
Polyclonal Anti-S100A4 (rabbit)	1:1000

Table 2.13 Dilutions of different primary antibodies used in Western Blot.

2.2.20.1 Blots Stripping

A nitrocellulose blot that has been probed and developed can be reused by removing all the antibodies so that the same blot can be reprobe with different antibodies. To conduct this, the used blots were submerged in stripping buffer (refer to Table 2.13) and incubated for 30 minutes at 50°C with occasional agitation. The blots were washed with PBS twice to remove any remaining stripping buffer. Finally, the blots were blocked with PBS containing 5% (w/v) dried milk product for 30 minutes at room temperature. The stripped blot is ready for reprobing.

Chemical compound	Amount
Making of 100 ml of Stripping Buffer	
10% (w/v) SDS	20.000 (ml)
0.5M Tris HCl (pH6.8)	12.500 (ml)
Distilled water	67.500 (ml)
B-mercaptoethanol (added in fumehood)	0.800 (ml)

Table 2.13 Preparation of stripping buffer.

2.2.20.2 Quantification of bands intensity

Intensities of the protein bands were quantified with ImageJ. Intensities of bands of interest were normalised with intensities of the respective loading controls. Percentage of protein expression reduction and knockdown, when applicable, were calculated after normalisation.

2.2.21 Statistical analysis

Data presented in this study are listed as mean \pm standard error (s.e.). The data sets were compared using Kolmogorov–Smirnov test or student t-Test (or ANOVA) (Analyse-it software or Excel statistical analysis programme respectively) and evaluated at 95% confidence level ($P < 0.05$) where the data set would be considered statistically significant and represented with * on the bars. $P < 0.01$ represented as ** whereas $P < 0.001$ represented as *** on the bars.

Chapter 3:

Upregulation of S100A4 promotes cell migration and filopodia instability

Chapter 3: Upregulation of S100A4 promotes cell migration and filopodia instability

3.1 Introduction	94
3.2 Results	
3.2.1 Overexpression of S100A4 increases cell motility	97
3.2.2 High level of S100A4 leads to reduction in focal adhesion formation	99
3.2.3 S100A4 reduces filopodia formation	105
3.2.3 Increment of expressions of adapter protein (vinculin and paxillin) in cells expressing high level of wild type S100A4 protein	111
3.2.4 Dynamicity of focal adhesion is linked to high expression of wild type S100A4 protein.....	113
3.2.5 S100A4 expressing cell generates weaker contraction force	120
3.3 Discussion	123

3.1 Introduction

Migrating cells are often distinguished by having a polarised structure which consists of a protruding leading edge and a retracting rear end; where the leading edge is characterised by four types of plasma membrane protusion known as filopodia, lamellipodia, blebs, and invadopodia in 2 and 3D organisation (Le Clainche and Carlier, 2008, Ridley et al., 2003, Mack and Marshall, 2010, Diz-Muñoz et al., 2010). Due to the relevancy of the work, only lamellipodia and filopodia in 2D organisation are highlighted in this chapter. Both of these structures are driven by polymerisation of polarised actin filaments, while lamellipodia consists of highly branched actin filaments which are woven across one another, filopodia, on the other hand is an unbranched protusions linearly polymerised by fascin (Nobes and Hall, 1995, Claudia Schäfer, 2010).

Filopodia is a thin spiky extension which functions as an extracellular sensor, consisting of tightly packed bundles of actin filaments cross-linked by fascin (Machesky and Li, 2010). Fascin is a 55 kDa actin bundling protein containing two actin monomer binding sites located in between amino acids 29 and 42 as well as 277 and 493 respectively, and phosphorylation by PKC α at residue Ser39 serves to inhibit its activity (Yamashiro et al., 1998). Pivotal role of fascin in filopodia formation was further established using monospecific anti-fascin immunoglobulins which resulted in reduction of spike formation and cell motility as binding of fascin to actin was inhibited (Adams and Schwartz, 2000). Although other actin bundling proteins such as α -actinin, filamin and ezrin have been discovered, none of these proteins were found in filopodia; proposing fascin as the most appropriate filopodia marker as it is directly linked to filopodia (DeRosier and Edds, 1980, Vignjevic et al., 2006).

On the other hand, lamellipodia is a thin sheets-like region with microfilaments localised diagonally where its force for locomotion is generated laterally as actin polymerisation takes place (Ridley, 2011). The large agglomeration of short branched actin filament is regulated by numerous

actin binding proteins coordinating the nucleation, polymerisation, severing and capping of actin filaments by Arp 2/3 complex, Ena/VASP, gelsolin and capping protein respectively. In vertebrates, there are three Ena-related genes known as mammalian Enabled (Mena), Ena-VASP-like (EVL) and Enabled/vasodilator-stimulated phosphoprotein (Ena/VASP) and Ena/VASP was found to be concentrated at the anterior tip of lamellipodia at leading edge of the cell periphery but not in the trailing end (Rottner et al., 1999, Rottner et al., 2001). Besides mediating actin polymerisation, Ena/VASP also acts as anti-capping protein which prevents capping of barbed end actin so polymerisation can take place (Bear et al., 2002, Bear and Gertler, 2009). Due to this, Ena/VASP is considered as lamellipodium marker. There are two Ena/VASP homology domains in this protein, each known as EVH1 domain and EVH2 domain located at N terminal and C terminal respectively (Ball et al., 2000). EVH1 domain acts as vinculin and zyxin binding site while EVH2 serves as binding site to G-actin and F-actin to facilitate actin polymerisation (Rottner et al., 2001). Ena/VASP also contains a central poly-proline region (PPR) which interacts with profilin. Profilin is a G-actin binding protein which mediates polymerisation of actin monomer to barbed ends of actin filaments via adding ATP to actin monomers (Bachmann et al., 1999, Benz et al., 2008). Immediately behind this dynamic structure is a more stable structure known as lamella where the actin network is coupled to NMMII to assist the formation of focal adhesion.

Focal adhesion, found preliminary near the leading edge of the cell, is another important structure that drives cell migration (Cramer, 2010). Two types of preliminary focal complexes formed are nascent and transient focal complexes. Nascent focal complex refers to its small size whereas transient focal complex refers to short-lived focal adhesion which disassembles fairly quickly. Nascent focal complex will undergo maturation as lamellipodium persist forward localising it to its rear. Maturation of focal adhesion requires actin polymerisation, contractility of NMMII and numerous signalling proteins such as integrin, vinculin, talin, and focal adhesion kinase

(Vicente-Manzanares et al., 2009a, Pasapera et al., 2010, Mitra et al., 2005, Vicente-Manzanares and Horwitz, 2011a) . As mature focal adhesion forms, they slow down the retrograde flow of lamella caused by the contractility force generated by NMMII and promote persistence in cell forward protrusion (Kuo et al., 2011, Wolfenson et al., 2009). The retrograde flow will then merge with anterograde flow of actin filaments in a region known as convergence zone which is located at the base of lamella. As cell body pushes forward, the focal adhesions were stationed to the rear of the cell where it moves centripetally and then disassemble, leaving trails of integrin on the substratum (Ezratty et al., 2005, Lim et al., 2010).

The role of the S100A4 protein as a metastasis promoter is well described, due to its correlative expression during carcinogenesis of different tissues (as mentioned in Chapter 1) and in benign tumour of rat mammary epithelial cells where its overexpression induces metastatic characteristics (Davies et al., 1994). Ability of S100A4 to promote metastasis has been linked to its calcium (Ca^{2+}) dependent interaction with non muscle myosin II (NMMII) (Badyal et al., 2011, Elliott et al., 2012, Kiss et al., 2012) where S100A4 is capable of binding to both NMMIIA and NMMIIB; with higher affinity to NMMIIA (9 fold) than NMMIIB (Bresnick, 1999, Li et al., 2003). Interaction of S100A4 with NMMIIA at C terminal amino acid residues 1909 -1924 causes unwinding of NMMIIA α helical tail, preventing its assembly, subsequently disassemble actin stress fibers (Kriajevska et al., 1994, Li et al., 2003).

In this chapter, we aimed to show at molecular level, the consequences of S100A4 overexpression on cell morphology, focal adhesions, as well as importance of C-terminus of S100A4 in mediating cell motility.

3.2 Results

3.2.1 Overexpression of S100A4 increases cell motility

In this work, scratch assays were used to determine whether the overexpression of S100A4 protein in cells has potential effect on wound healing motility. Expression of S100A4 protein was reconfirmed with Western blot analysis (Figure 2.2.2) and wound healing assays were conducted with CellIQ machine (Figure 3.2.1).

To establish whether C terminus of S100A4 protein is important for promoting migration, wound healing assay with R37 S100A4 $\Delta 2$ and R37 S100A4 $\Delta 6$ cell lines were done in conjunction with R37 S100A4 WT and Rama 37 control cell lines. Overexpression of wild type S100A4 protein showed elevation in cell migratory rate with initiation of gap closure starting 2 hours post scratching (Figure 3.2.1). Quantification of wound closure 8 hours post scratching shows that R37 S100A4 WT has an average of 98.7 ± 2.1 % of wound closed whereas Rama 37 control, R37 S100A4 $\Delta 2$ and R37 S100A4 $\Delta 6$ show $61.8 \pm 18.2\%$, $66.6 \pm 8.4\%$ and $57.9 \pm 7.3\%$ respectively (Figure 3.2.1 B). While there is no significant difference between the percentage of wound closure amongst Rama 37 control, R37 S100A4 $\Delta 2$ and R37 S100A4 $\Delta 6$, drastic enhancement of migration ($P < 0.001$) were observed when they were individually compared to R37 S100A4 WT.

To show that the effect seen on wound healing properties were not due to cell proliferation, mitotic index with 6 hour intervals for 24 hours were calculated alongside with wound healing assay (Figure 3.2.2). The mitotic indexes for all the four cell lines did not show significant differences among the different cell lines. With the highest mitotic index being less than 0.15, as calculated in R37 S100A4 WT cells, this indicate that at most, only 15% of total cell population were undergoing mitosis at any time. Since wound healing assays were conducted less

than 18 hours with wound healing percentage taken at 8 hours post initial wounding, it is unlikely that the observed wound closure rate is due to cell proliferation.

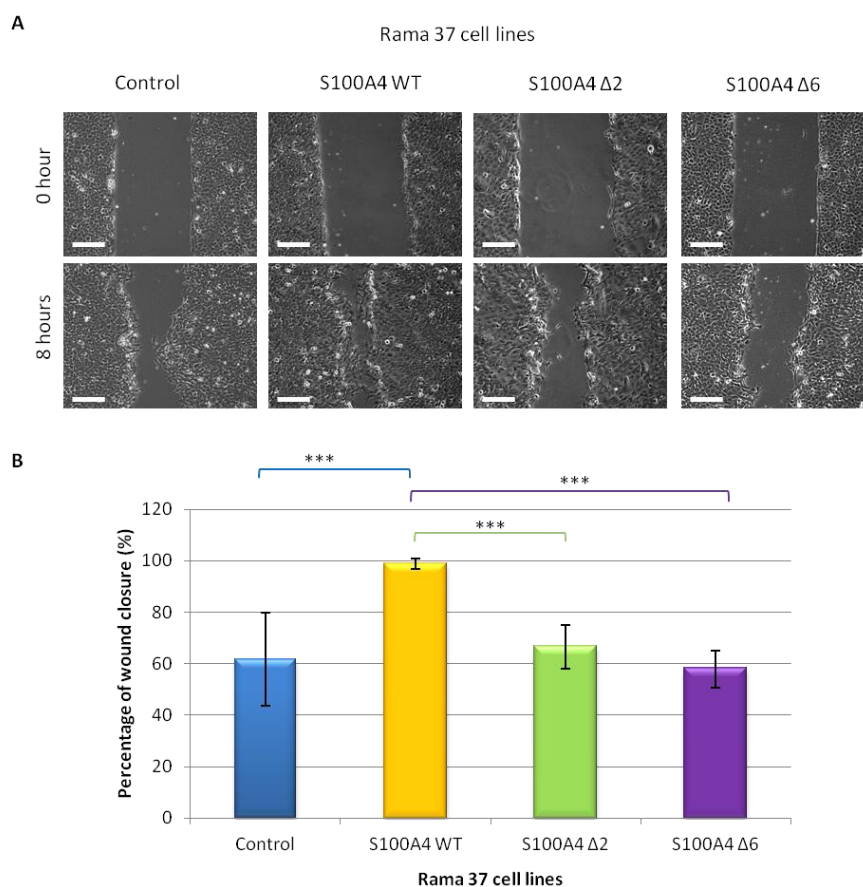


Figure 3.2.1. Wild type S100A4 protein expression promotes cellular migration in wound healing assay. Rama 37 control cells, cells expressing wild type S100A4, and cells truncated forms (S100A4 Δ2 and S100A4 Δ6) were grown for 24 hours in 24 well plate to confluency prior to scratching and monitoring of wound healing using CellIQ. A) Representative time-lapse images of Rama 37 cells scratch assays immediately after the scratches had been made and then after 8 hours. Scale bar = 200μm. B) Quantification of percentage of wound closure 8 hours post scratching. Results are mean values ± s.e. from 3 independent experiments. Student t-Test were done by comparing Rama 37 control cells, R37 S100A4 Δ2 and R37 S100A4 Δ6 respectively to R37 S100A4 WT *** $p < 0.001$. Methods are fully detailed in Chapter 2.2.4.

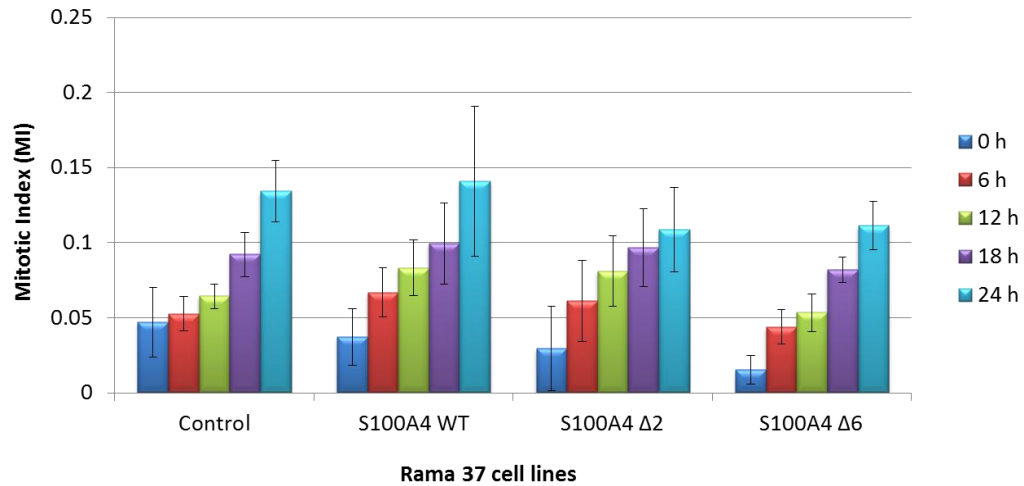


Figure 3.2.2. Low mitotic index during wound healing assay. Respective cells were seeded in a density of 150,000 into each well of 24 well plate. Using the CellIQ imaging system, cells morphologies at different cell cycle phase were selected manually and then analysed with CellIQ software where cell were assigned into respective phases. Mitotic index (MI) values obtained are mean \pm s.d. obtained from 3 different wells from one experiment. Methods are fully detailed in Chapter 2.2.4.1

3.2.2 High level of S100A4 leads to reduction in focal adhesion formation

As impacts of S100A4 overexpression at cellular level remained elusive, we sought to analyse S100A4 effects on specific cell structures via immunofluorescence. Here, we used vinculin and paxillin as focal adhesion markers since they are recruited to activated integrins to form focal complexes which later mature into focal adhesions during cell adhesion and migration (Humphries et al., 2007, Schaller, 2001, Hynes, 1992). Cells were seeded on coverslips pre coated with fibronectin for 48 hours prior to fixation, permeabilisation and staining. Overexpression of S100A4 was found to dramatically reduce the number of adapter protein clusters, vinculin, hence minimising focal contacts at the leading edge (Figure 3.2.3). It was observed that in the Rama 37 control cells, distinct localisation of vinculin clusters were exhibited at the cell periphery with non-polarised morphology and much pronounced actin stress fibers surrounding the cell stroma

(Figure 3.2.4 A-A'). Elevation of S100A4 protein level in R37 S100A4 WT cell line caused abolishment of foci formation around the cells (Figure 3.2.3 B-B'). In S100A4 overexpressing cells, actin network was less organised and displayed more prominent polarisation with a define leading edge (Fig 3.2.3 B). The expression of either S100A4 $\Delta 2$ or S100A4 $\Delta 6$ in Rama 37 cells (Figure 3.2.3 C and Figure 3.2.3 D respectively) displayed similar phenotype to that of the Rama 37 control cells where vinculin clusters and actin organisation were more pronounced.

As interaction between actin cytoskeleton and transmembrane protein of the integrin type is not only facilitated by vinculin (other adapter proteins such as paxillin, talin or FAK could also connect such bridges), we further confirm the effects of S100A4 on micro colocalisation of vinculin with paxillin. Similarly, cells were seeded onto coverslips pre coated with fibronectin and left for 48 hours before proceeding to fixing, permeabilising and staining for paxillin localisation. The stainings of paxillin revealed similar trait as those of vinculin where total loss of focal contacts were observed in cells expressing high level of S100A4 (Figure 3.2.4). In Rama 37 control, R37 S100A4 $\Delta 2$ and R37 S100A4 $\Delta 6$, paxillin were localised in similar manner as vinculin where prominent paxillin clusters were found in cell periphery (Figure 3.2.4 A – A', C – C' and D – D').

Quantification of each adapter protein clusters, vinculin and paxillin, were done for statistical analysis (Table 3.2.1 and Table 3.2.2 respectively). The quantification of both adapter proteins clustering at the periphery of individuals cells revealed similar trend where R37 S100A4 WT cells displayed a significant reduction in both vinculin (2.8 ± 0.8) and paxillin (5.4 ± 3.6) clusters when compared to either of the other three cell lines. Rama 37 control cells (27.4 ± 2.9 and 16.4 ± 4.1), R37 S100A4 $\Delta 2$ (27.8 ± 1.6 and 16.5 ± 3.5) and S100A4 $\Delta 6$ (28.2 ± 4.7 and 15.2 ± 3.0) show no significant differences in either vinculin or paxillin clusters respectively.

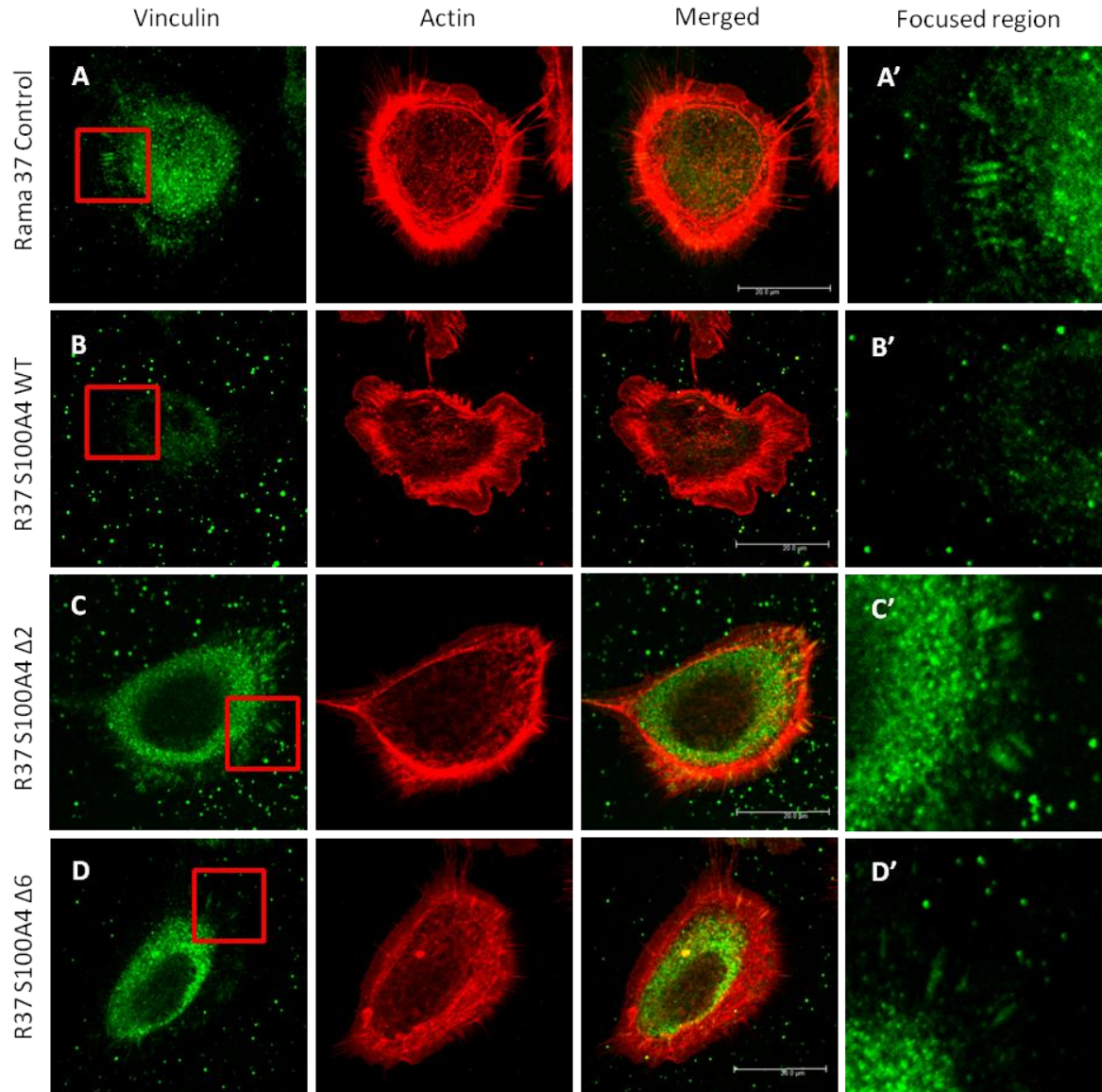


Figure 3.2.3 Overexpression of wild type S100A4 but not the C-terminal truncated forms of $\Delta 2$ and $\Delta 6$ prevents the formation of mature vinculin clusters. Respective cells were seeded onto coverslips pre-coated with fibronectin and incubate for 48 hours before fixing, permeabilising and incubating with vinculin (FITC). Then, the cells were incubated with FITC-conjugate secondary antibody along with phalloidin for actin staining (rhodamine) and mounted with DAPI prior to viewing with confocal microscope. Rama 37 control cells were labelled as A – A', R37 S100A4 WT cells as B – B', R37 S100A4 $\Delta 2$ as C – C' and R37 S100A4 $\Delta 6$ as D – D'. Panels A', B', C' and D' correspond to focused regions of the cell. Scale bar = 20 μ m. Images displayed for each cell line were representative image obtained from 3 independent experiments. Methods are fully detailed in Chapter 2.2.8.

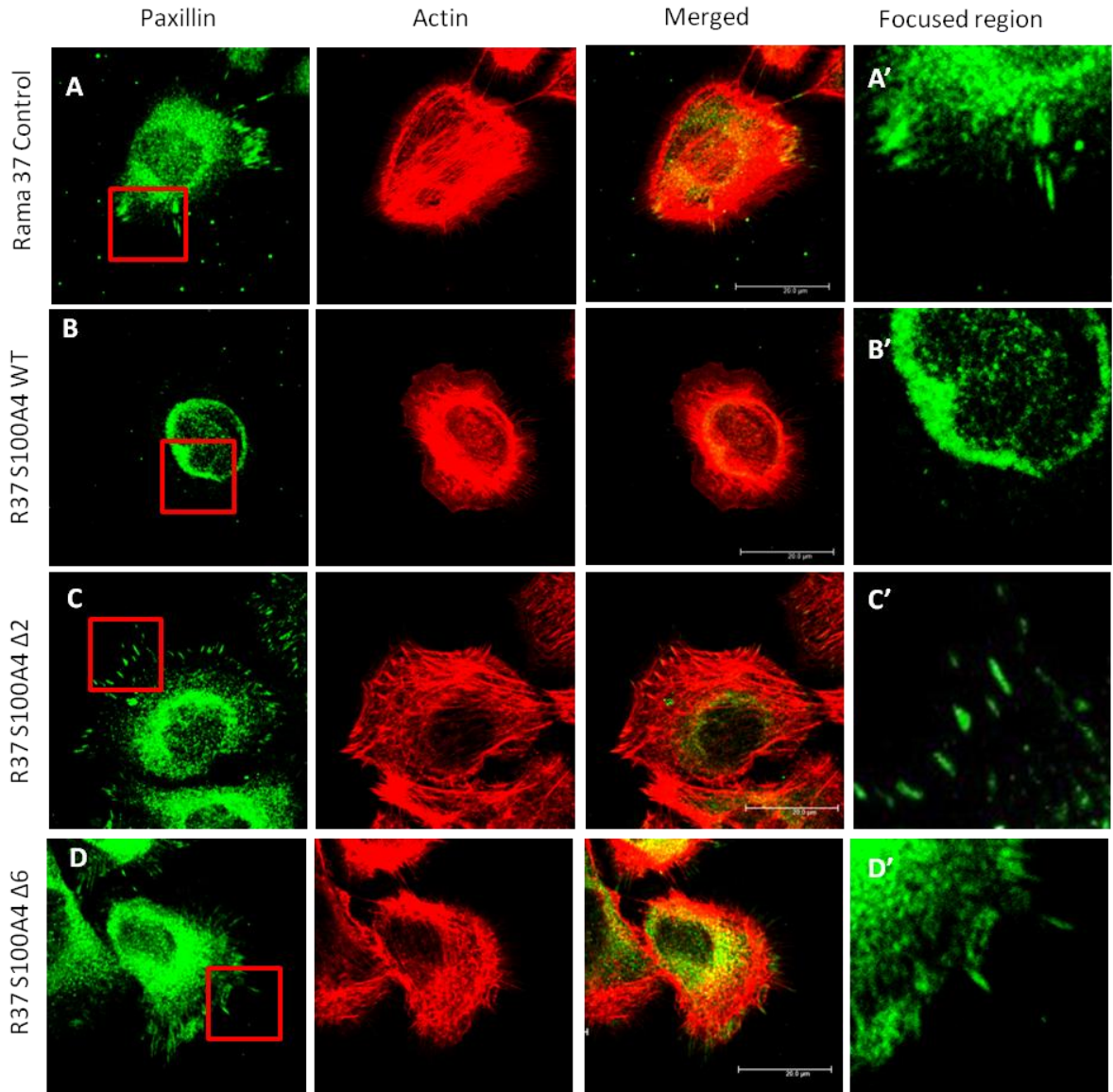


Figure 3.2.4 Maturation of paxillin clusters was observed in Rama 37 control, R37 S100A4 Δ 2 and R37 S100A4 Δ 6. Immunofluorescence stainings were conducted as described in figure 3.2.3 but incubated with paxillin antibody (FITC) instead of vinculin. Rama 37 control cells were labelled as A – A', R37 S100A4 WT cells as B – B', R37 S100A4 Δ 2 as C – C' and R37 S100A4 Δ 6 as D – D'. Panels A', B', C' and D' correspond to focused regions of the cell. Scale bar = 20 μ m. Images displayed for each cell line were representative image obtained from 3 independent experiments. Methods are fully detailed in Chapter 2.2.8.

Rama 37 cell lines	Number of focal adhesions (vinculin) per cell \pm s.e. (n=36)	P-value ^a	P-value ^b	P-value ^c
Control	27.4 \pm 2.9	8.055E-08		
S100A4 WT	2.8 \pm 0.8			
S100A4 Δ 2	27.8 \pm 1.6	1.521E-09	0.794	
S100A4 Δ 6	28.2 \pm 4.7	2.143E-06	0.752	0.861

Table 3.2.1 Overexpression of S100A4 protein resulted in loss of vinculin clusters.

Immunofluorescence stainings were conducted as described in Figure 3.2.3. Images obtained were quantified manually by counting the number of clusters localised at the periphery of each cell. Results are the mean values \pm s.e. from 5 independent experiments.

^a P-value obtain from Student t-Test where number of focal adhesions (vinculin) per cell present in R37 S100A4 WT were compared to Rama 37 control, R37 S100A4 Δ 2 and R37 S100A4 Δ 6.

^b P-value obtain from Student t-Test where number of focal adhesions (vinculin) per cell present in Rama 37 control were compared to R37 S100A4 Δ 2 and R37 S100A4 Δ 6.

^c P-value obtain from Student t-Test where number of focal adhesions (vinculin)per cell present in R37 S100A4 Δ 2 were compared to R37 S100A4 Δ 6.

Methods are fully detailed in Chapter 2.2.10.

Rama 37 cell lines	Number of focal adhesions (paxillin) per cell \pm s.e. (n=36)	P-value ^a	P-value ^b	P-value ^c
Control	16.4 \pm 4.1	1.255E-16		
S100A4 WT	5.4 \pm 3.6			
S100A4 Δ 2	16.5 \pm 3.5	1.282E-18	0.935	
S100A4 Δ 6	15.2 \pm 3.0	1.170E-16	0.186	0.119

Table 3.2.2 Significant reduction of number of paxillin clusters in cells expressing full length of S100A4 protein. Immunofluorescence stainings were conducted as described in Figure 3.2.4.

Images obtained were quantified manually by counting number of clusters localised at the periphery of each cell. Results are the mean values \pm s.e. from 5 independent experiments.

^a P-value obtain from Student t-Test where number of focal adhesions (paxillin) per cell present in R37 S100A4 WT were compared to Rama 37 control, R37 S100A4 Δ 2 and R37 S100A4 Δ 6.

^b P-value obtain from Student t-Test where number of focal adhesions (paxillin) per cell present in Rama 37 control were compared to R37 S100A4 Δ 2 and R37 S100A4 Δ 6.

^c P-value obtain from Student t-Test where number of focal adhesions (paxillin)per cell present in R37 S100A4 Δ 2 were compared to R37 S100A4 Δ 6.

Methods are fully detailed in Chapter 2.2.10.

3.2.3 S100A4 reduces filopodia formation

Actin counterstaining in the previous experiments indicate noticeable modifications of cell morphology in S100A4 overexpressing cells (Figure 3.2.3 and Figure 3.2.4). Indeed, cells expressing higher level of S100A4 protein presented polarised morphology with more pronounced lamellipodium at the leading edge, replacing filopodium projections observed around the peripheries of the less polarised three cell lines (Rama 37 control, S100A4 $\Delta 2$ and S100A4 $\Delta 6$). To show the significance of filopodia reduction induced by S100A4 overexpression, the number of filopodia present in individual cell ($n=14$ for each cell line) was quantified by manually counting filopodia extended around the cell periphery. From the quantification, it was shown that S100A4 expressing cells demonstrated drastically reduced filopodia projections (39.1 ± 9.4) compared to Rama 37 control cells (105.2 ± 8.3), R37 S100A4 $\Delta 2$ (100.3 ± 13.5) and S100A4 $\Delta 6$ (113.2 ± 15.6) respectively (Table 3.2.3). Rama 37 control cells, R37 S100A4 $\Delta 2$ and S100A4 $\Delta 6$ showed no significant differences in filopodia projections amongst themselves.

Since filopodia extension is attributed to actin-bundling properties of fascin, the cellular localisations of fascin for the four cell lines were analysed. Immunofluorescence staining performed against fascin depicted the localisation of fascin throughout the length of the filopodium projections with an accumulation at the tip in Rama 37 control cells and Rama 37 cells expressing the truncated forms of S100A4 $\Delta 2$ or S100A4 $\Delta 6$ (Figure 3.2.5). R37 S100A4 WT cells, on the other hand, show little amount of fascin-mediated filopodial protrusions present at the cell periphery. For each cell line, 14 images were randomly selected from 3 independent immunofluorescence stainings of fascin (counterstained with actin), quantitative analysis of the number of those stably adhered projections were carried out (Table 3.2.4). S100A4 expressing cells demonstrated significantly lower protrusions containing fascin (3.80 ± 1.5) compared to Rama 37 control, R37 S100A4 $\Delta 2$ and R37 S100A4 $\Delta 6$ (41.2 ± 8.6 , 35.4 ± 9.3 and 22.6 ± 8.8 respectively).

In order to further characterise the differences in cell polarisation and leading edge formation observed when S100A4 is overexpressed, further immunofluorescence analysis were performed with VASP, a marker for lamellipodium. VASP immunofluorescence staining revealed its localisation at the tip of lamellipodium of R37 S100A4 WT cells. However, in Rama 37 control cells, VASP was localised behind the filopodia projections which indicates that VASP is not found within filopodia shaft (Figure 3.2.6 A – A'). In both R37 S100A4 $\Delta 2$ and $\Delta 6$, similar observation where no VASP were found to localised within the filopodia shaft (Figure 3.2.6 C –C' and D – D'). This indicates that lamellipodia is a prominent structure in the leading edge of R37 S100A4 WT cells rather than filopodia as observed in the rest of the three cell lines.

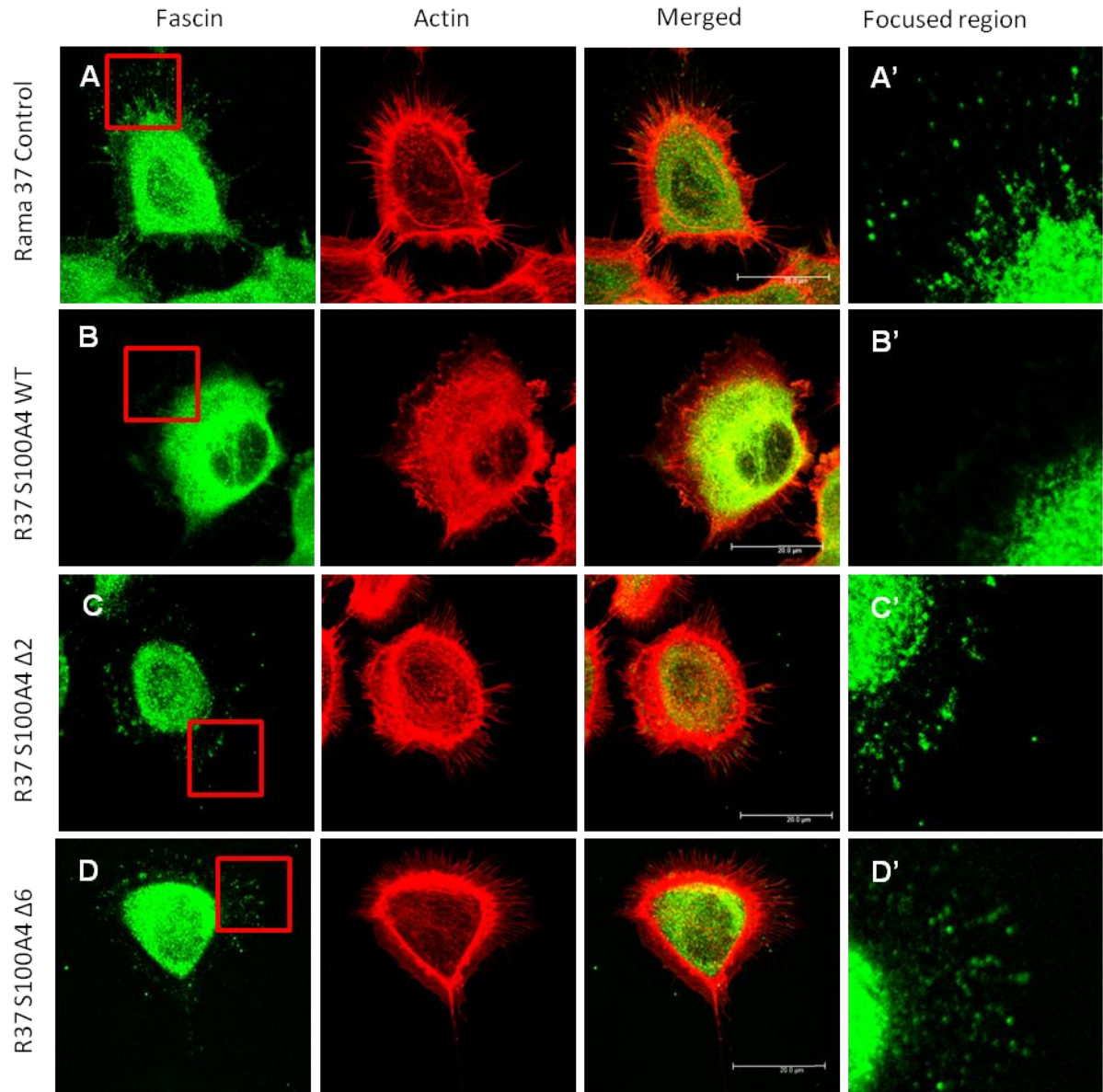


Figure 3.2.5 Truncated forms of S100A4 protein (S100A4 Δ2 and Δ6) did not affect the localisation of fascin within filopodia as observed in Rama 37 control cells. Immunofluorescence stainings were conducted as before but incubated with fascin antibody. Rama 37 control cells were labelled as A – A', R37 S100A4 WT cells as B – B', R37 S100A4 Δ2 as C – C' and R37 S100A4 Δ6 as D – D'. Panels A', B', C' and D' correspond to focused regions of the cell. Scale bar = 20µm. Images displayed for each cell line were representative image obtained from 3 independent experiments. Methods are fully detailed in Chapter 2.2.8.

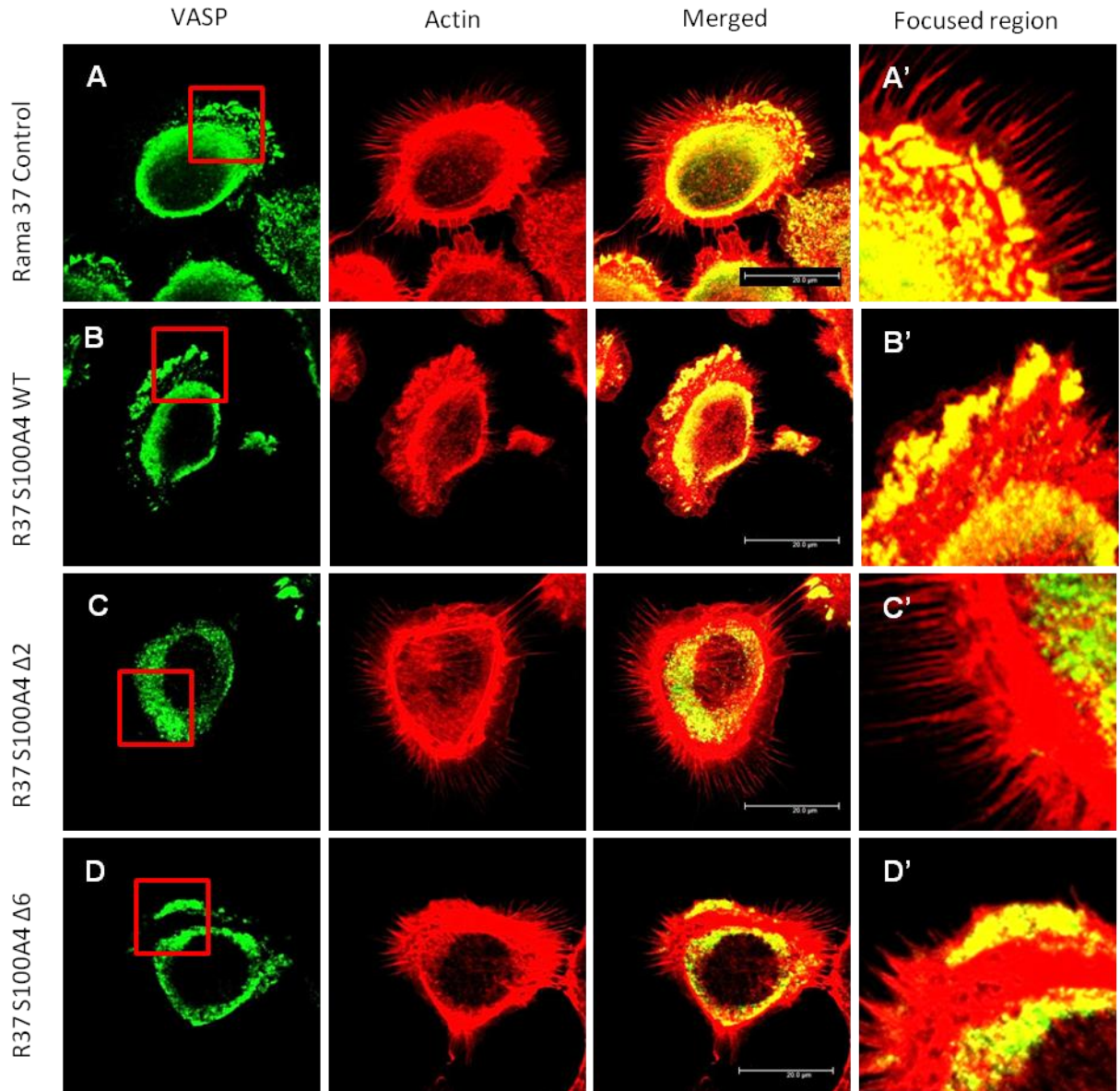


Figure 3.2.6 Cells expressing full length of S100A4 protein display prominent lamellipodium structure.

Immunofluorescence stainings were conducted as before but incubated with VASP antibody. Rama 37 control cells were labelled as A – A', R37 S100A4 WT cells as B – B', R37 S100A4 Δ2 as C – C' and R37 S100A4 Δ6 as D – D'. Panels A', B', C' and D' correspond to focused regions of the cell. Scale bar = 20μm. Images displayed for each cell line were representative image obtained from 3 independent experiments. Methods are fully detailed in Chapter 2.2.8.

Rama 37 cell lines	Number of filopodia per cell \pm s.e. (n=14)	P-value ^a	P-value ^b	P-value ^c
Control	105.2 \pm 8.3	1.440E-13		
S100A4 WT	39.1 \pm 9.4			
S100A4 Δ 2	100.3 \pm 13.5	8.206E-11	0.316	
S100A4 Δ 6	113.2 \pm 15.6	1.630E-11	0.148	0.051

Table 3.2.3 Number of filopodia protusions was significantly lowered in R37 S100A4 WT cells.

Cells were seeded, fixed, permeabilised and stained as described in Chapter 2.2.8. Quantification of filopodia was done manually by counting the number of protusions around the periphery of cells after staining with phalloidin. Results are the mean values \pm s.e. from 7 independent experiments.

^a P-value obtain from Student t-Test where number of filopodia per cell present in R37 S100A4WT were compared to Rama 37 control, R37 S100A4 Δ 2 and R37 S100A4 Δ 6.

^b P-value obtain from Student t-Test where number of filopodia per cell present in Rama 37 control were compared to R37 S100A4 Δ 2 and R37 S100A4 Δ 6.

^c P-value obtain from Student t-Test where number of filopodia per cell present in R37 S100A4 Δ 2 were compared to R37 S100A4 Δ 6.

Methods are fully detailed in Chapter 2.2.10.

Rama 37 cell lines	Number of fascin-mediated filopodia projections per cell \pm s.e. (n=14)	P-value ^a	P-value ^b	P-value ^c
Control	41.2 \pm 8.6	1.151E-05		
S100A4 WT	3.80 \pm 1.5			
S100A4 Δ 2	35.4 \pm 9.3	7.135E-05	0.337	
S100A4 Δ 6	22.6 \pm 8.8	0.001	0.009	0.056

Table 3.2.4 Overexpression of S100A4 protein reduced the number of fascin-mediated filopodia projections. Cells were seeded, fixed, permeabilised and stained as described in Chapter 2.2.8. Quantification of fascin projections was done manually by counting the number of fascin localised within the filopodia around the periphery of cells after co-staining with fascin and phalloidin. Results are the mean values \pm s.e. from 3 independent experiments.

^a P-value obtain from Student t-Test where number of fascin projections per cell present in were R37 S100A4 WT compared to Rama 37 Control, R37 S100A4 Δ 2 and R37 S100A4 Δ 6.

^b P-value obtain from Student t-Test where number of fascin projections per cell present in Rama 37 control were compared to R37 S100A4 Δ 2 and R37 S100A4 Δ 6.

^c P-value obtain from Student t-Test where number of fascin projections per cell present in R37 S100A4 Δ 2 were compared to R37 S100A4 Δ 6.

Methods are fully detailed in Chapter 2.2.10.

3.2.3 Increment of expressions of adapter protein (vinculin and paxillin) in cells expressing high level of wild type S100A4 protein

From the immunofluorescence stainings, it was observed that the number of focal adhesion is influenced by the expression of wild type S100A4 protein. Since paxillin and vinculin clusters were reduced specifically in S100A4 expressing cells, western blotting were performed on these cell lines to determine if the reduction of clusters were due to S100A4 affecting their localisation and/or expressions. From the blots obtained, the level of vinculin and paxillin were quantified with densitometry. The protein level expressed in R37 S100A4 WT cells were taken as 100% while the level expressed in the three other cell lines were normalised from it. It was found that although the level of vinculin expression is slightly higher in R37 S100A4 WT cells ($100.0 \pm 0.0\%$) when compared to Rama 37 control ($89.2 \pm 7.7\%$), R37 S100A4 $\Delta 2$ ($90.9 \pm 5.5\%$) and R37 S100A4 $\Delta 6$ ($88.2 \pm 8.2\%$), no significant difference were observed ($P = 0.138$, $P = 0.103$ and $P = 0.131$ respectively) (Figure 3.2.7 B). However, quantification on paxillin expression level, revealed significant increment of paxillin expression in R37 S100A4 WT ($100.0 \pm 0.0\%$) as opposed to Rama 37 control ($82.9 \pm 4.3\%$), R37 S100A4 $\Delta 2$ ($76.3 \pm 5.4\%$) and R37 S100A4 $\Delta 6$ ($80.9 \pm 5.0\%$) ($P = 0.020$, $P = 0.017$ and $P = 0.021$ respectively) (Figure 3.2.7 B).

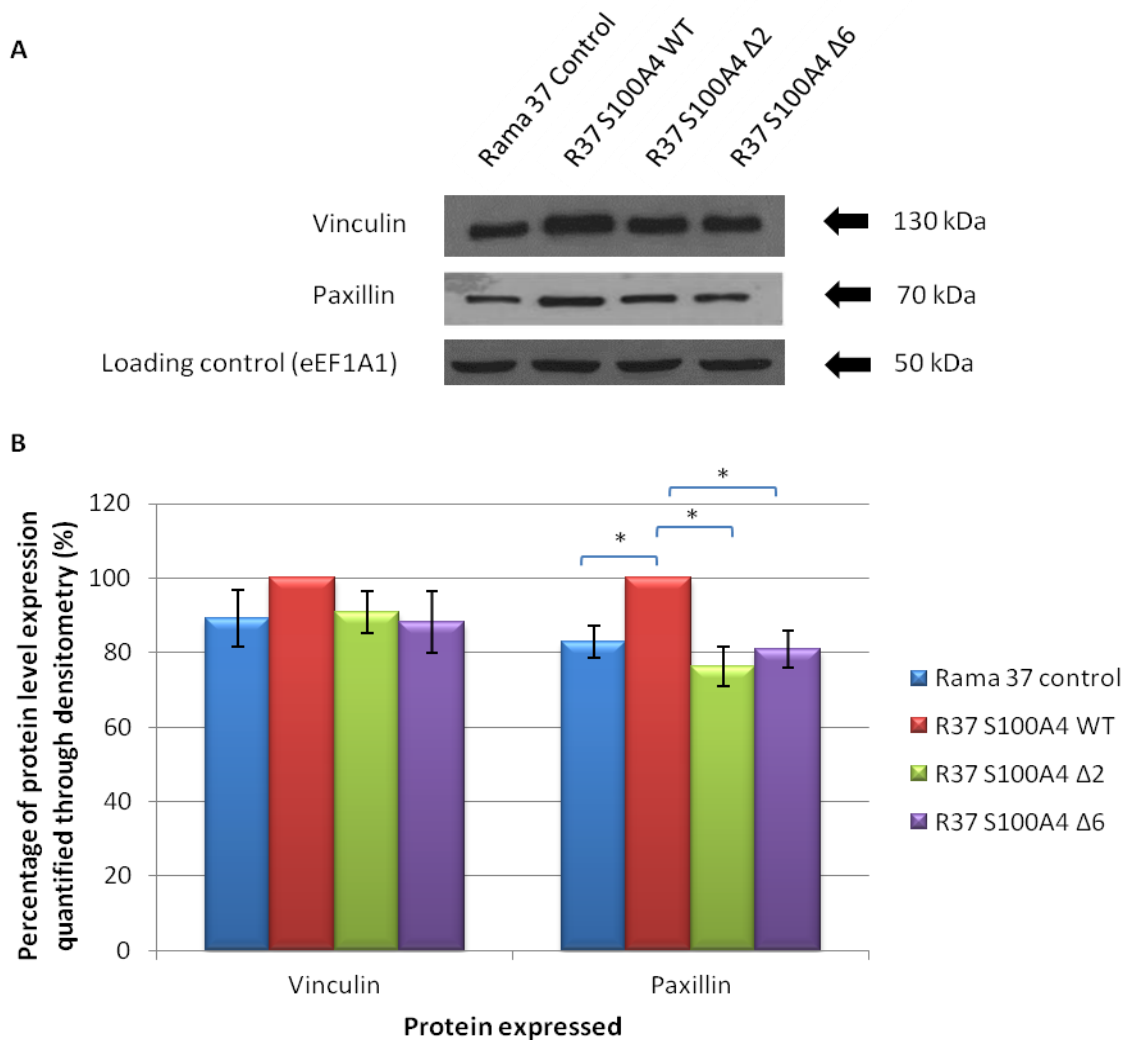


Figure 3.2.7 Elevation of vinculin and paxillin expressions in R37 S100A4 WT cells. Rama 37 cell lines with a density of 1.5×10^6 were seeded into 60mm tissue culture dish 24 hours prior to harvesting (as described in Chapter 2.2.17 to 2.2.20). Total protein for all cell lines were quantified and equal amount of total protein (150 μ g vinculin and 80 μ g paxillin and eEF1A1) loaded onto 10% SDS Page gels. Resolved proteins were transferred onto nitrocellulose membrane before detection for specific protein required. A) Blots shown are representative data obtained from 3 independent experiments. B) Densitometry showing level of vinculin and paxillin expressed in respective Rama 37 cell lines quantified with ImageJ. Results obtained are mean values \pm s.e from 3 independent experiments. Student t-Tests were done by comparing normalised value of R37 S100A4 WT cells to Rama 37 control cells, R37 S100A4 Δ 2 and R37 S100A4 Δ 6 respectively. *P < 0.05.

3.2.4 Dynamicity of focal adhesion is linked to high expression of wild type S100A4 protein

Following the previous experiments, elevation of S100A4 protein resulted in diminishing localisation of vinculin and paxillin clusters at the foci around the cell periphery. Hence, experiments were conducted in live cells to further validate this observation in real time and along with determining the dynamicity of these clusters. To confirm this, all cell lines were transfected with GFP-vinculin expressing plasmid and analysed over time using confocal microscopy. In Figure 3.2.8, a representative image of Rama 37 cell were frozen in different time frames to allow quantification of focal adhesions formation over time. From the 20 minutes time-lapse video collected for each transfected cell lines, newly formed focal contacts (black arrows) were distinguished from those that were already present. It was clearly observed that formation of focal adhesion was initiated by stably adhered filopodium and subsequently overgrown by lamellipodium (Figure 3.2.8 B).

The quantification of focal adhesions from live cells showed that Rama 37 control cells, R37 S100A4 $\Delta 2$ and R37 S100A4 $\Delta 6$ (Supplementary video 1, 3 and 4 respectively) exhibited similarities in overall number of focal adhesion present over the duration of 20 minutes (89.4 ± 13.4 , 93.6 ± 6.3 and 83.6 ± 12.1 respectively) (Table 3.2.5). However, when S100A4 protein was overexpressed, remarkable reduction of number of GFP-vinculin were incorporated into focal adhesion (50.2 ± 11.5) (Supplementary video 2). This observation is consistent with the data obtained from immunofluorescence staining, highlighting the loss of overall vinculin clusters in the presence of high level of S100A4.

However, the above quantification only demonstrated the overall number of vinculin clusters present during the 20 minutes duration, but not considering the number of vinculin clusters formed within the 20 minutes period. To assess more specifically the rates of focal adhesion assembly, the number of focal adhesions formed over the duration of 20 minutes was

quantified (Table 3.2.6). This analysis showed that the rate of focal adhesion formation of R37 S100A4 WT cells (11.4 ± 3.5), was significantly lower than cell lines expressing either S100A4 $\Delta 2$ or S100A4 $\Delta 6$ proteins (28.2 ± 6.9 and 23.6 ± 6.6 respectively). Conversely, Rama 37 control cells did not show significant difference in focal adhesion formation (14.4 ± 2.1) when compared to R37 S100A4 WT cells ($P=0.071$). However, the overall mean value of focal adhesions observed in Rama 37 control cells, R37 S100A4 $\Delta 2$ and R37 S100A4 $\Delta 6$ were still higher than that of R37 S100A4 WT cells (Table 3.2.6).

So far, we have shown that S100A4 overexpressing cells has lower focal adhesions formation rate which is consistent with the overall reduction of focal adhesions observed in immunofluorescence stainings of paxillin and vinculin. Since maturation of focal adhesion is dependent upon tension produced via myosin-generated force and filopodia adherent to extracellular matrix, it is important to investigate whether reduction of focal adhesions is due to inability of S100A4 expressing cells to form filopodia or stabilisation of filopodia is inhibited. To assess this, the quantification of filopodia on live cells was carried out by randomly halting images at a single time point as shown in Figure 3.2.9. Through this analysis, it is possible to monitor the dynamicity of filopodia, distinguishing retraction fibers from filopodia (Figure 3.2.9 B) as well as discriminate nascent (Figure 3.2.9 C) from stable filopodium (Figure 3.2.9 A). Surprisingly, this analysis showed that the wild type S100A4 expressing cells have higher formation of filopodia (17.3 ± 7.2) within the 20 minutes as opposed to Rama 37 control cells (10.9 ± 2.71 , $P=0.027$) and R37 S100A4 $\Delta 6$ cells (10.9 ± 4.5 , $P=0.031$) (Table 3.2.7). Although the filopodia quantified in S100A4 $\Delta 2$ shows no significant difference ($P=0.546$), the mean value is still lower than those of the R37 S100A4 WT cells.

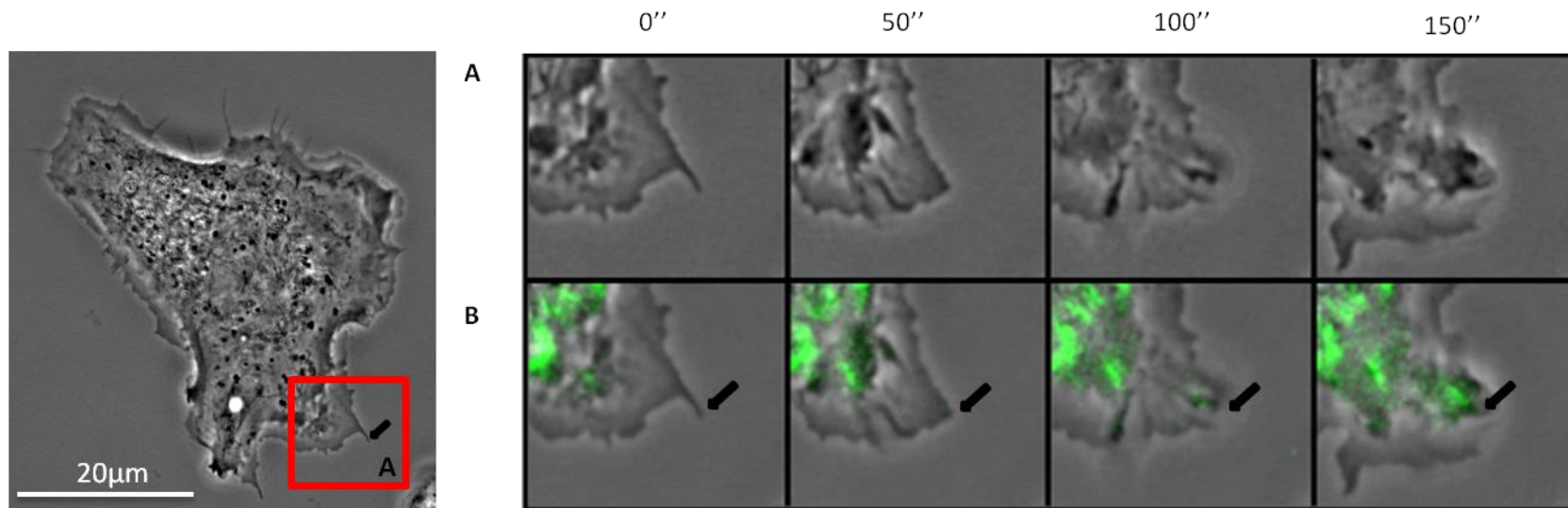


Figure 3.2.8 Distinguishing matured from nascent focal adhesion in Rama 37 cells. Control Rama 37 cells transfected with pGZ21 GFP-vinculin expressing plasmid were seeded on fibronectin coated coverslips for 24 hours before analysis. Cells were analysed over the duration of 20 minutes in (A) phase contrast and in (B) fluorescence. Red box in the overview indicates the zoomed area shown in the time series. Time points are recorded in seconds. The black arrow highlights the same filopodium position over time. For better visualisation, phase contrast images were sharpened and GFP-images were background-subtracted and the contrast was adjusted before overlaying the images. Scale bar = 20µm. Time lapse image shown is a representative image of a Rama 37 control cell used to distinguish nascent from stable filopodia. Five time-lapsed images were done on each individual cell lines in 2 independent transfection experiments. Methods are fully detailed in Chapter 2.2.9.

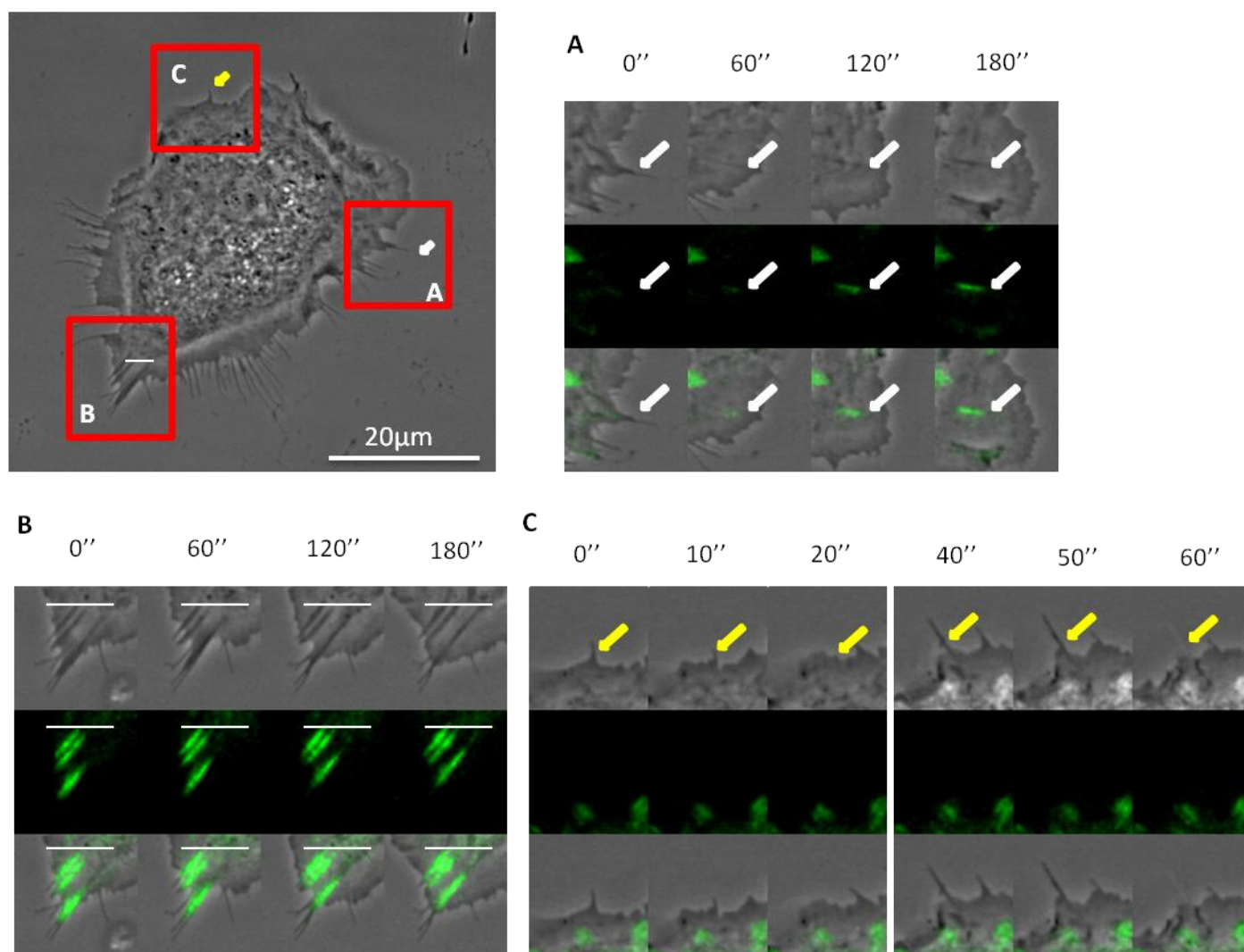


Figure 3.2.9 Establishment of stably adhered filopodia, retraction fibers and unstable filopodia in Rama 37 cells. Rama 37 cells transfected as described in figure 3.2.8. Cells were analysed over the duration of 20 minutes in phase contrast and in fluorescence to quantify **(A)** stably adhered filopodia (white arrow), **(B)** retraction fibres and **(C)** unstable filopodia (yellow arrow). Area **A** was enlarged to show the formation of stable filopodia (top panel), the subsequent maturation of FA (middle panel) and the overlay of both time lapse images (bottom panel) over time **(A)**. Area **B** was enlarged with a white line drawn above to show the retracting FA right behind the retraction fibers over time **(B)**. Area C was enlarged to show the unstable formation of filopodia over time **(C)**. For **A**, **B** and **C**, the top panel is shown in phase contrast, the middle panel in fluorescence and the bottom panel as overlays of both images. Time points are given in seconds. Note that the time

lapse has shorter intervals for **C** whereas **A** and **B** have a similar time lapse. First image of all analysis corresponds to the main figure (time zero) and then subsequent time lapse images are shown. For better visualisation, phase contrast images were sharpened and GFP-images were background-subtracted and enhanced in contrast before overlaying the images. Scale bar = 20 μ m. Time lapse image shown is a representative image of a Rama 37 control cell used to distinguish nascent from stable filopodia. Five time-lapsed images were done on each individual cell lines in 2 independent transfection experiments.

Methods are fully detailed in Chapter 2.2.9.

Rama 37 cell lines	Number of focal adhesions present per cell (over 20 minutes) \pm s.e. (n=5)	P-value ^a	P-value ^b	P-value ^c
Control	89.4 \pm 13.4	0.003		
S100A4 WT	50.2 \pm 11.5			
S100A4 Δ 2	93.6 \pm 6.3	0.002	0.629	
S100A4 Δ 6	83.6 \pm 12.1	0.033	0.606	0.153

Table 3.2.5 Significantly lower count of focal adhesions observed in live cell analysis of R37

S100A4 WT cells. Respective cell lines were transfected with pGZ21 GFP-vinculin expressing plasmid were seeded on customized glass bottom dish, pre-coated with fibronectin for 24 hours. Cells were then analysed over the duration of 20 minutes with both phase contrast and fluorescence. Results are the mean values \pm s.e. from 5 individual cells from each cell lines in single experiment.

^a P-value obtain from Student t-Test where number of total focal adhesions present over 20 minutes in R37 S100A4 WT were compared to Rama 37 Control, R37 S100A4 Δ 2 and R37 S100A4 Δ 6.

^b P-value obtain from Student t-Test where number of total focal adhesions present over 20 minutes in Rama 37 control were compared to R37 S100A4 Δ 2 and R37 S100A4 Δ 6.

^c P-value obtain from Student t-Test where number of total focal adhesions present over 20 minutes in R37 S100A4 Δ 2 were compared to R37 S100A4 Δ 6.

Methods are fully detailed in Chapter 2.2.9 and 2.2.11.

Rama 37 cell lines	Number of newly formed focal adhesions per cell (within 20 minutes) \pm s.e. (n=5)	P-value ^a	P-value ^b	P-value ^c
Control	14.4 \pm 2.1	0.071		
S100A4 WT	11.4 \pm 3.5			
S100A4 Δ 2	28.2 \pm 6.9	0.011	0.009	
S100A4 Δ 6	23.6 \pm 6.6	0.004	0.000	0.216

Table 3.2.6 R37 S100A4 WT displays lower focal adhesion formation. Respective cell lines were transfected with pGZ21 GFP-vinculin expressing plasmid were seeded on customised glass bottom dish, pre coated with fibronectin and left for incubation for 24 hours. Cells were then analysed over the duration of 20 minutes with both phase contrast and fluorescence. Results are the mean values \pm s.e. from 5 individual cells from each cell lines in single experiment.

^a P-value obtain from Student t-Test where number of newly formed focal adhesions within 20 minutes in R37 S100A4 WT were compared to Rama 37 Control, R37 S100A4 Δ 2 and R37 S100A4 Δ 6.

^b P-value obtain from Student t-Test where number number of newly formed focal adhesions within 20 minutes in Rama 37 control were compared to R37 S100A4 Δ 2 and R37 S100A4 Δ 6.

^c P-value obtain from Student t-Test where number of newly formed focal adhesions within 20 minutes in R37 S100A4 Δ 2 were compared to R37 S100A4 Δ 6.

Methods are fully detailed in Chapter 2.2.9 and 2.2.11.

Rama 37 cell lines	Number of filopodia present per cell (at any given time) \pm s.e. (n=9)	P-value ^a	P-value ^b	P-value ^c
Control	10.9 \pm 2.71	0.027		
S100A4 WT	17.3 \pm 7.2			
S100A4 Δ 2	14.6 \pm 6.9	0.546	0.168	
S100A4 Δ 6	10.9 \pm 4.5	0.031	1.000	0.204

Table 3.2.7 Cells overexpressing full length of S100A4 protein show higher filopodia dynamics.

Live cells videos taken over the duration of 20 minutes with both phase contrast and fluorescence were halted at random intervals and the filopodia present at that particular time frame was quantified. Results are the mean values \pm s.e. from 9 individual cells from each cell lines in 3 independent live cell experiment.

^a P-value obtain from Student t-Test where number of filopodia present per live cell at any given time in R37 S100A4 WT were compared to Rama 37 Control, R37 S100A4 Δ 2 and R37 S100A4 Δ 6.

^b P-value obtain from Student t-Test where number of filopodia present per live cell at any given time in Rama 37 control were compared to R37 S100A4 Δ 2 and R37 S100A4 Δ 6.

^c P-value obtain from Student t-Test where number of filopodia present per live cell at any given time in R37 S100A4 Δ 2 were compared to R37 S100A4 Δ 6.

Methods are fully detailed in Chapter 2.2.9 and 2.2.11.

3.2.5 S100A4 expressing cell has lower generation of cell force

So far, all the data indicated the possibility of S100A4 protein affecting the localisation and maturation of focal adhesions as well as stabilisation of filopodia. One of the possible explanations at molecular level for the low focal adhesion could be due to interaction of S100A4 protein with NMMIIA which resulted in disassembly of stress fibers and ultimately affecting focal adhesions formation and maturation. Indeed, myosin-generated tension has been shown to promote focal adhesion maturation and the disassembly by S100A4 could possibly reduce this tension.

To demonstrate the connection between myosin generated tensions and focal adhesions, all the four cell lines were seeded on both 8kPa and 15kPa custom-made micropatterned silicone elastomer respectively. In the 8kPa micropatterned elastomer, it was observed that there was no significant difference between the forces generated by the four cell lines tested (data not shown). However, on 15kPa micropatterned elastomer, it was observed that R37 S100A4 WT cells exhibited significantly lower contractile force ($17.5 \pm 6.02\text{nN}$) when compared to either of Rama 37 control cells ($63.6 \pm 32.0\text{nN}$, $P < 0.001$), R37 S100A4 $\Delta 2$ cells ($49.4 \pm 32.5\text{nN}$, $P = 0.002$) or R37 S100A4 $\Delta 6$ cells ($50.2 \pm 24.1\text{nN}$, $P < 0.001$) (Table 3.2.8). This results correlates with the lack of matured focal adhesions observed in either live cell analysis or immunofluorescence stainings of R37 S100A4 WT cell lines.

Next, we proceeded to investigate if the level of NMMIIA expressed in the four cell lines differs using western blot and densitometry analysis (Figure 3.2.10 A). It was found that the level of NMMIIA expressed in R37 S100A4 WT cell lines was lower than other three cell lines. Quantification of NMMIIA expression level showed that Rama 37 control cells, R37 S100A4 $\Delta 2$ and R37 S100A4 $\Delta 6$ exhibited higher level of NMMIIA ($232.5 \pm 16.5\%$, $234.2 \pm 25.4\%$ and $224.0 \pm 37.7\%$ respectively) when compared to R37 S100A4 WT cells (100%) (Figure 3.2.10 B).

Rama 37 cell lines	Average contractile force exerted per cell (nN) \pm s.e. on 15kPa elastomer (n= 15)	P-value ^a	P-value ^b	P-value ^c
Control	63.6 \pm 32.0	0.000		
S100A4 WT	17.5 \pm 6.02			
S100A4 Δ 2	49.4 \pm 32.5	0.002	0.240	
S100A4 Δ 6	50.2 \pm 24.1	0.000	0.209	0.940

Table 3.2.8 R37 S100A4 WT cells exerts significantly lower contractile force. Cells were seeded onto micropatterned silicone elastomer and left to incubate for 24 hours prior to detaching each cell with needles under fluorescence microscope (to capture the position of fluorescent beads embedded within elastomer) as well as phase contrast (to capture the shape of the cells). Results are mean values \pm s.e of 15 cells obtained form 4 independent experiment.

^a P-value obtain from Student t-Test where total for contractile force per cell in R37 S100A4 WT were compared to those of Rama 37 Control, R37 S100A4 Δ 2 and R37 S100A4 Δ 6.

^b P-value obtain from Student t- Test where total for contractile force per cell in Rama 37 control were compared to those of R37 S100A4 Δ 2 and R37 S100A4 Δ 6.

^c P-value obtain from Student t-Test where total for contractile force per cell in R37 S100A4 Δ 2 were compared to those of R37 S100A4 Δ 6.

Methods are fully detailed in Chapter 2.2.12.

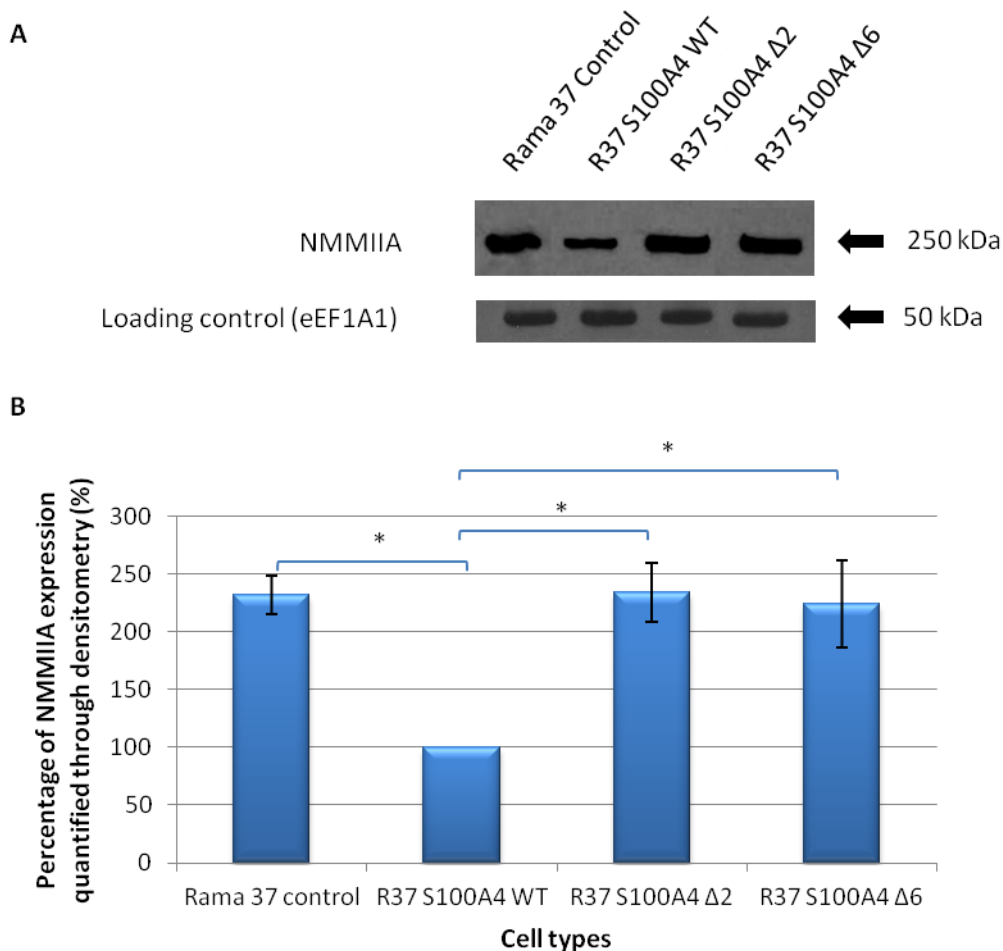


Figure 3.2.10. Reduction of NMMIIA expressions in wild type S100A4 expressing cells. Rama 37 cell lines were seeded 24 hours prior to harvesting. Total protein for all four cell lines were quantified and equal amount of total protein (80µg NMMIIA and eEF1A1) loaded onto 10% SDS Page gels. Resolved proteins were transferred onto nitrocellulose membrane before detection for specific protein required. **A)** Blots shown are representative data obtained from 3 independent experiments. **B)** Densitometry showing level of NMMIIA expressed in respective Rama 37 cell lines quantified with ImageJ (Chapter 2.15.2). Results obtained are mean values \pm s.e from 3 independent experiments. Student t-Tests were done by comparing normalised value of R37 S100A4 WT cells to Rama 37 control cells, R37 S100A4 Δ2 and R37 S100A4 Δ6 respectively. *P < 0.05. Methods are fully detailed in Chapter 2.2.17 – 2.2.20.

3.3 Discussion

Malignancies of cancer ranging from melanoma to non-small cell lung carcinoma and cancers of oral, breast and stomach due to overexpression of S100A4 protein has been demonstrated in various reports (Andersen et al., 2004, Rudland et al., 2000, Yonemura et al., 2000b, Moriyama-Kita et al., 2005). Furthermore, down-regulation of cellular motility through reduction in S100A4 protein expression in tumour cells has also been demonstrated (Takenaga et al., 1997a, Bjornland et al., 1999). There is, therefore, a clear link between overexpression of S100A4, cell motility and metastasis. Yet, at molecular level, the biological consequences of S100A4 elevation remain vague. Here, we aimed to provide further evidences correlating overexpression of S100A4 protein and modification of intracellular structures such as actin and focal adhesions to facilitate cell motility.

The effect of S100A4 protein on cell motility was first identified through wound healing assay (Figure 3.2.1). Using the truncated C-terminus versions of S100A4 proteins in the same cells, we demonstrated that the S100A4-induced motility was abolished. This indicated that C-terminus of S100A4 protein is an essential part of the protein which could possibly hold the key to modify intracellular structures to facilitate migration. Previous work done by Ismail *et al.* in 2008, has demonstrated that deletion of C-terminus in S100A4 increases dissociation constant (K_d) of S100A4 with rNMMHC-IIA, hence may indirectly regulates cytoskeletal structures. Through their work, the authors demonstrated that wild type S100A4 protein has higher affinity for rNMMHC-IIA (K_d 100nM) compared to S100A4 $\Delta 2$ and S100A4 $\Delta 6$ (K_d 680nM and K_d 6.2 μ M respectively). Due to this reduced affinity, it is speculated that inability of truncated versions of S100A4 protein to modify actin via NMMHC-IIA interaction resulted in appearance of highly organised actin filaments observed in the immunofluorescence staining performed which was not observed in cell expressing full length S100A4 protein (Figure 3.2.3, 3.2.4, 3.2.5 and 3.2.6). It is unclear whether

truncation of 2 or 6 amino acids from the C terminus of S100A4 protein could affect the ability of the protein to dimerise, a conformation proved to be essential for regulating NMMIIA since single mutations at any one of the two calcium binding motifs reduce its calcium binding properties by 30 to 60 fold. Thus, we could not rule out the possibility of the effect observed were due to inability of S100A4 protein to dimerise. While dimerisation of S100A4 has been shown to induce invasiveness, S100A4 monomers did not exert such effect (House et al., 2011). However, it has been shown that dimerisation of S100A4 in vitro is only affected when amino acid residues between 72 to 91 were mutated whereas in vivo, only Phe72, Tyr75, Phe78 and Leu79 were essential for S100A4 dimerisation (Tarabykina et al., 2001, Ismail et al., 2010). Due to this, it is possible that truncation of 2 or 6 amino acids from C terminus of S100A4 protein did not affect dimerisation, but may possibly limits its target protein range or reduces its affinities to certain proteins, thereby reducing its effects on cell motility.

In order to facilitate cell migration, cytoskeletal structures undergo modification at their leading edges in 3 chronological steps; projections of filopodia and/or lamellipodia, followed by attachment of leading lamella to extracellular cues and formation of focal contacts that matured through production of tensile forces (Vicente-Manzanares and Horwitz, 2011a). Immunofluorescence stainings of S100A4 expressing cells showed significant reduction of filopodia; replaced by out-spread lamellipodium (Figure 3.2.3). Minimal matured focal contacts formed via paxillin and vinculin were exhibited by R37 S100A4 WT cells and lost of distinct stress fibers were observed (Figure 3.2.4). All of these modifications were consistent with enhancement of cell motility, where S100A4 has been shown to induce forward protusions during chemotaxis and disassembly of NMMIIA filaments by S100A4 led to recruitment of S100A4-NMMIIA complex to the leading edge of polarised cells (Li and Bresnick, 2006, Kim and Helfman, 2003).

In the fixed cells analysis, it was observed that Rama37 control, R37 S100A4Δ2 and R37 S100A4Δ6 cells displayed higher number of filopodia protrusions when compared to R37 S100A4 WT cells (Table 3.2.3). Co-staining of actin with fascin, a well-known actin cross-linking protein that localises to filopodia revealed that filopodia projections in Rama37 control, R37 S100A4Δ2 and R37 S100A4Δ6 cells consist of fascin co-localising with actin throughout the filopodia shaft with accumulation at the tip of microspike and the quantification of this localisation was consistent with the observation where higher level of filopodia containing fascin was found in Rama37 control, R37 S100A4Δ2 and R37 S100A4Δ6 cells (Table 3.2.4). The higher number of paxillin and vinculin clusters in cell lines that exert higher number of filopodia is within expectation as formation of focal contacts were initiated by adherence of filopodia where is it overgrown by lamellipodium and its maturations is assisted by the tensile strength exerted through actomyosin contraction (Geiger et al., 2009, Vicente-Manzanares and Horwitz, 2011a). Interestingly, the expression levels of adapter protein, vinculin and paxillin are higher in R37 S100A4 WT cells but focal adhesions clusters containing these proteins were significantly reduced in the immunofluorescence stainings (Figure 3.2.3, 3.2.4 and 3.2.7). This indicates that although expression levels of the proteins were increased, the proteins failed to be recruited or activated to the adhesion sites. Although there are no studies done on effects of S100A4 on focal adhesion reduction, it was demonstrated that overexpression of S100P in Rama 37 cells, could led to reduced focal adhesion, as demonstrated in this work, via an unknown mechanism (Du et al., 2012).

Through live cell analysis, contrasting results showing formation of filopodia extensions in R37 S100A4 WT was higher than Rama37 control, R37 S100A4Δ2 and R37 S100A4Δ6 cells. It is possible that during the fixation procedure, the usage of detergent resulted in the loss of nascent and unstable filopodia, but not the stably adhered ones. This contrasting filopodia quantification

of live and fixed cells suggested that the S100A4 protein somehow prevents adherence of filopodia rather than inhibiting its formation. It has been demonstrated that myosin X is involved in formation of filopodia where upon dimerisation, it acts as actin bundling protein to initiate filopodia protrusion (Watanabe et al., 2010). Although interaction of S100A4 with myosin X has not been demonstrated in any studies, its interaction with NMMIIA and NMMIIB suggests the possibility of S100A4 interaction with myosin X to regulate filopodia formation (Li et al., 2003, Ford et al., 1997). Furthermore, through blastp protein alignment, it was found that NMMIIA and myosin X shared 36% of amino acid identity which spans between 3 regions; 1) 32 to 820, 2) 1444 to 1504 and 3) 1033 to 1117. However, these regions were not found to be identical to the binding sequence of S100A4 on NMMIIA which spans from 1909 to 1924 amino acids which led to speculations of S100A4 interacting with other target proteins to promote filopodia instability.

Through cell force analysis where 15 kPa elastomer substrates were used, it was found that R37 S100A4 WT cells generated lower contractile force when compared to those exerted by the control or those expressing truncated versions of S100A4 protein (Table 3.2.8). As contractile force is aroused from tension generated by NMMII coupling with actin, the lower overall contractile force in S100A4 expressing cells suggested that the capability of S100A4 to disassemble NMMIIA could directly weaken the contractile force or indirectly by inhibiting organisation of stress fibers through NMMIIA disassembly which weakens the actomyosin force, hence preventing the maturation of focal adhesions, ultimately leading to lower overall contractile force exerted (Hotulainen and Lappalainen, 2006, Bershadsky et al., 2006, Shutova et al., 2012, Grosheva et al., 2006). Since mature focal adhesions are essential to slow down retrograde flow to prevent filopodial retraction while persisting protrusion, this could be the underlying reason as of why S100A4 overexpressing cells lack of stable filopodia. Also, acceleration of filopodia formation in

R37 S100A4 WT cells indicated that actin polymerisation rate is not affected (Figure 3.2.9) (Cai et al., 2006, Parsons et al., 2010).

However, it remained uncertain if the lower contractile forces generated by S100A4 overexpressing cells were due to reduced NMMIIA expression or reduced focal adhesion (Figure 3.2.10). We speculated that the reduction of NMMIIA expression level could be S100A4-mediated as numerous reports have demonstrated that overexpression of S100A4 through transfection resulted in down-regulation of E-cadherin and tissue inhibitor of metalloproteinases (TIMPs) and up-regulations of matrix metalloproteinases (MMPs) (Andersen et al., 2004, Kimura et al., 2000, Moriyama-Kita et al., 2005, Yonemura et al., 2000b, Andersen et al., 2011, Bjornland et al., 1999, Lu et al., 2004, Yammani et al., 2006, Zhang et al., 2011). However, the mechanism regarding expression regulation by S100A4 remained to be investigated.

In another independent work which utilises Rama 37 cell system transfected with S100P protein, we demonstrated the consistency where S100P-induced motility correlates with reduced focal adhesion clusters along with disorganised actin filaments. S100P, a member of S100 superfamily, has been shown to interact with NMMIIA and its overexpression has been linked to poor survival of breast cancer patients in which S100A4 protein has shown similar correlations (Basu et al., 2008, Parkkila et al., 2008, Wang et al., 2006, Du et al., 2012). In the presence of calcium, S100P protein undergoes conformational changes, forming hydrophobic cleft which serves as an active site for target protein binding (Gribenko and Makhatadze, 1998, Koltzsch and Gerke, 2000). It has also been shown that transfection of S100P into Rama 37 cell system induces metastatic characteristics as displayed by S100A4 transfected Rama 37 cells (Wang et al., 2006). Due to the analogous characteristic exhibited by these proteins, similar experiments were done on Rama 37 cells, but transfected with plasmid encoding wild type S100P and also their C-terminus-

mutant counterparts (A-mutant, replacement of lysine residue to alanine and Stop-mutant, deletion of lysine residue).

Quantification of focal complexes (paxillin) and wound healing rates from these cell lines revealed that number of focal complexes correlates with wound healing rate where (as observed in the R37 S100A4 WT cell system); the lower the number of focal complexes, the faster the wound healing. In this experiment, it was observed that R37 S100P WT (Wound Closure (WC) = $37.5 \pm 4.9\%$, Focal complex (FC) = 3.1 ± 1.7) has the highest percentage of wound closure 6 hours post wounding but lowest focal contacts, followed by A-mutant (WC = 24.9 ± 10.4 , FC = 8.2 ± 3.4), Rama 37 control cells (WC = $28.6 \pm 8.0\%$, FC = 17.4 ± 3.6) and Stop-mutant (WC = 8.88 ± 3.28 , FC = 21.2 ± 2.8) (data not shown). In our collaborative work with Liverpool University, our observations also correlated with their affinities to NMMIIA using optical biosensor approach. In their work, it was shown that the binding affinities of S100P to NMMIIA was significantly increased (K_d 300 - 400 nM) when compared to Stop-mutant and A-mutant (K_d 6 μ M and K_d 4 μ M respectively) (in preparation data). These data obtained from S100P transfected Rama 37 cell system further strengthen the observation obtained using S100A4 transfected Rama 37 cell system where reduction of focal adhesions as well as disorganisation of stress fibers may lead to enhancement of cell motility.

Chapter 4:

Independency of non muscle myosin II pathway in S100A4-induced cell migration

Chapter 4 : Independency of non muscle myosin II pathway in S100A4-induced cell migration

4.1 Introduction	131
4.2 Results	
4.2.1 Determination of optimal blebbistatin, Y-27632 and BDM concentration in Rama 37 cell system	135
4.2.2 Inhibition of NMMII failed to prevent S100A4-induced migration	138
4.2.3 Inhibition of NMMII reduces focal adhesions	140
4.2.4 Knockdown of NMMIIA affects migration	148
4.2.5 Knockdown of NMMIIA reduces focal adhesions	152
4.2.6 Optimisation of Cos 7 cells transfections.....	155
4.3.6.1 Determination of efficiency of different transfection reagents.....	155
4.2.7 Restoration of NMMIIA in Cos 7 cells result in impediment of cell motility and reversible effect obtained using NMMII inhibitors	158
4.3.7.1 Rescue of NMMIIA reduces migration.....	158
4.3.7.2 Treatment with either blebbistatin or Y-27632 restore migrational ability of NMMIIA expressing Cos 7 cells.....	160
4.3.7.3 Inhibitory effects of blebbistatin and Y-27632 resulted in reduction of paxillin clusters and ventral stress fibers.....	162
4.2.8 Introduction of S100A4 enhance migration	167
4.2.9 Opposing effects of NMMIIA and S100A4 on focal adhesions of Cos 7 cells.....	169
4.3 Discussion	174

4.1 Introduction

Numerous studies have aimed to decipher the structural and mechanical roles of non muscle myosin II (NMMII). The NMMII complex comprised of three pairs of peptides; two heavy chains (230kDa), two regulatory light chain (RLC) (20kDa) and two essential light chains (ELC) (17kDa). The heavy chains, which contain the globular heads, bundle actin filaments via their C-terminal domains to generate actomyosin forces whereas the two regulatory light chains upon phosphorylations, result in alteration of the globular heads and ATPase activities of the 3 isoforms of NMMII; NMMIIA, -IIB and -IIC (Betapudi et al., 2006, Sandquist et al., 2006). Phosphorylation of RLC of NMMII at Thr 18 or Ser 19 promotes binding of ATP at the globular heads and results in its dissociation from actin. During hydrolysis, NMMII changes its conformation and releases ADP and inorganic phosphate which increases its affinity to actin. The reassociation of NMMII globular heads to actin complete a cycle of actomyosin contraction and the continuous cycle enable cells to drive forward locomotion. Although NMMIIA and NMMIIB shares 85% of amino acid identity in the globular domain and 72% in the helical rod and have been shown to be simultaneously expressed in variety of vertebrate cells, its distinct but overlapping distributions suggested different roles for these complexes (Lo et al., 2004, Kolega, 2006, Cai et al., 2006, Togo and Steinhardt, 2004). NMMIIA is found localised to the front of migrating cells and knockdown via SiRNA resulted in loss of stress fibers and focal adhesion maturation and size (Cai et al., 2006, Bresnick, 1999). NMMIIB, on the other hand, is found to be concentrated at the rear and important for maintaining stress fibers integrity (Cai et al., 2006, Kolega, 1998).

In stable stress fibers, dissociation and association of NMMII with actin is in equilibrium due to intermediate level of ATPase activity. Consequently, activation of ATPase activity of NMMIIA resulted in increased association with actin filaments to form stress fibers whilst dissociation of NMMII from actin is dominant when ATPase activity is low (Watanabe et al., 2007,

Iwasaki et al., 2001). In the studies to demonstrate the importance of NMMII ATPase activity to regulate its activity, two common NMMII inhibitors have been used; blebbistatin and Y-27632. Blebbistatin is a selective membrane permeable NMMII ATPase inhibitor which exists in two forms (+)-blebbistatin and (-)-blebbsitatin where (-) enantiomer is found to be the active form (Limouze et al., 2004). This inhibitor interacts with the actin-bound NMMII, slowing the phosphate release (Pi) and indirectly foiling the formation of actomyosin complex (Takács et al., 2010, Ramamurthy et al., 2004, Limouze et al., 2004). Such properties are not due to blebbistatin competing with ATP binding to NMMII, but rather affecting the inorganic phosphate release. (Ramamurthy et al., 2004, Kovács et al., 2004). Consequently, treatment with blebbistatin has been shown to induce dramatic changes at the cellular levels, resulting in severe reduction in stress fibers as well as focal adhesions (Liu et al., 2010, Lucas-Lopez et al., 2008, Pasapera et al., 2010).

Y-27632 is a ROCK kinase inhibitor, inhibiting both the two isoforms ROCKI and ROCKII, sharing approximately 90% identity. Y-27632 has also been shown to inhibit other kinases such as protein kinase C (PKC), cAMP-dependent kinase and myosin light chain kinase (MLCK) with however, a 100 fold lower efficiency, suggesting that its primarily target in cell is the ROCK proteins (Uehata et al., 1997). Phosphorylation status of RLC (at location Ser-19 and Thr-18) has been shown to result in significant increase of ATPase activity (Ikebe and Hartshorne, 1985, Ikebe et al., 1988, Asano et al., 2009, Kondo et al., 2011, Vicente-Manzanares and Horwitz, 2010, Kanda et al., 1985). It is therefore thought that ROCK can equally contribute to myosin ATPase activities through regulating phosphorylation of RLC (Amano et al., 1996, Kureishi et al., 1997, Kimura et al., 1996). Accordingly, inhibition of ROCK by Y-27632 results in loss of stress fibers and modifications in focal adhesions size (Kawano et al., 1999, Amano et al., 2010), suggesting a direct link between ROCK, RLC phosphorylation and NMMII activities. It has also been shown that prolong incubation of Swiss 3T3 cell lines with Y-27632 induces a long neurite or dendritic morphology in

concentration dependent manner and enhancement of wound healing properties by 67% was observed after inhibitor treatment (Ishizaki et al., 2000).

Another common myosin inhibitor, with myosin phosphatase-like activity is the cell permeable compound 2,3-Butanedione monoxime (BDM). BDM has been shown to inhibit the ATPase activity of muscle myosin II, resulting in the reduction contraction force by promoting the formation of myosin-ADP complex or myosin-ADP-Pi complex (McKillop et al., 1994). It is, however unclear whether this inhibitor can similarly regulate the activities of NMMII and therefore demonstrate myosin contractibility effects in other cells (Ostap, 2002, Cramer and Mitchison, 1995). For instance, BDM has been shown not to inhibit the ATPase activity of NMMII in Swiss 3T3 and BS-C1 cells instead preventing the localisation of actin and other partners (VASP, Arp 2/3 complex and WAVE) at their leading edge whereas in other cases, it has been shown to specifically inhibit NMMII activities in Walker carcinosarcoma resulting in reduced cell motility and polarity (Yarrow et al., 2003, Cheung et al., 2002, Keller et al., 2002).

Over the years, NMMII has been established as one of the main binding partner for S100A4, possibly linking their association towards changes in cell motility (Li et al., 2003, Li and Bresnick, 2006, Ismail et al., 2008b). Although NMMIIA and NMMIIB displayed high sequence homology, S100A4's affinity for the two complexes are very different; with 9-fold higher binding capacity for NMMIIA filaments than for NMMIIB filaments (Bresnick, 1999, Li et al., 2003). The binding site on NMMIIA for S100A4 has been shown to lie within the amino acid residues stretch from 1909 to 1924, at C terminus end of NMMIIA, a region that is approximately 34% conserved between the two isoforms. This interaction appears to be regulated in a calcium dependent manner (Li et al., 2003, Kriajevska et al., 2000), resulting in the inhibition of NMMIIA ATPase activity and the dissociation of the actomyosin network, at least in vitro (Ford et al., 1997).

In this section, we aimed to investigate the link between S100A4 protein and NMMIIA protein on cell migration and morphology. For this purpose, different strategies were adopted, using either NMMII inhibitors or cellular systems where NMMIIA had been knocked down or completely ablated.

4.2 Results

4.2.1 Determination of optimal blebbistatin, Y-27632 and BDM concentration in Rama 37 cell system

To investigate the roles of S100A4 protein and its independency of NMMII in cell migration, three different NMMII inhibitors were used; (1) Blebbistatin, (2) Y-27632 and (3) 2,3-Butanedione monoxide (BDM).

Viability of Rama 37 control cells after 24 hours pre-treatment with blebbistatin (0 μ M to 125 μ M), Y-27632 (0 μ M to 100 μ M) and BDM (0 mM to 20 mM) was determined using MTT assay (Figure 4.2.1). While treatment with blebbistatin and BDM resulted in concentration dependent reduction of cell viabilities, Y-27632 did not show any effects. It was found that reduction of cell viability after blebbistatin treatment started from 25 μ M ($74.6 \pm 15.2\%$) while BDM effects started from 10 mM ($78.1 \pm 0.2\%$) (Figure 4.2.1 A and 4.2.1 B respectively). As the standard error for MTT assay of 25 μ M of blebbistatin is high, this concentration is repeated with 10 μ M of blebbistatin. Further viability assay carried out over 24 hours with an interval of 2 hours using 10 μ M or 25 μ M blebbistatin treatments showed that cell viabilities for both concentrations were not affected (Figure 4.2.1 D). The lower increment of cell viability in 25 μ M treated cells compared to 10 μ M and untreated cells could possibly be due to lower cell number as blebbistatin has been shown to affect cytokinesis where multinucleated cells were observed. Due to incapability of MTT assay to determine optimal concentration for Y-27632 on Rama 37 control cells, changes in cell morphology as well as actin organisation through immunofluorescence staining against actin were used. It was observed that 50 μ M of Y-27632 treatment and onwards resulted in changes in cell morphology as well as disorganisation of actin filaments (Figure 4.2.2). Also, similar stainings were done on blebbistatin (10 μ M and 25 μ M) and BDM (5mM and 10 mM) treated Rama 37 control cells (Figure 4.2.2) where was found that 10 μ M of blebbistatin and both 5mM and 10 mM of BDM

did not cause any significant changes in actin filaments and cell morphology. Thus, the established concentrations of blebbistatin and Y-27632 are 25 μ M and 50 μ M respectively. As BDM did not cause any effects on cell morphology but significantly reduce cell viability, this inhibitor was not used in proceeding experiments.

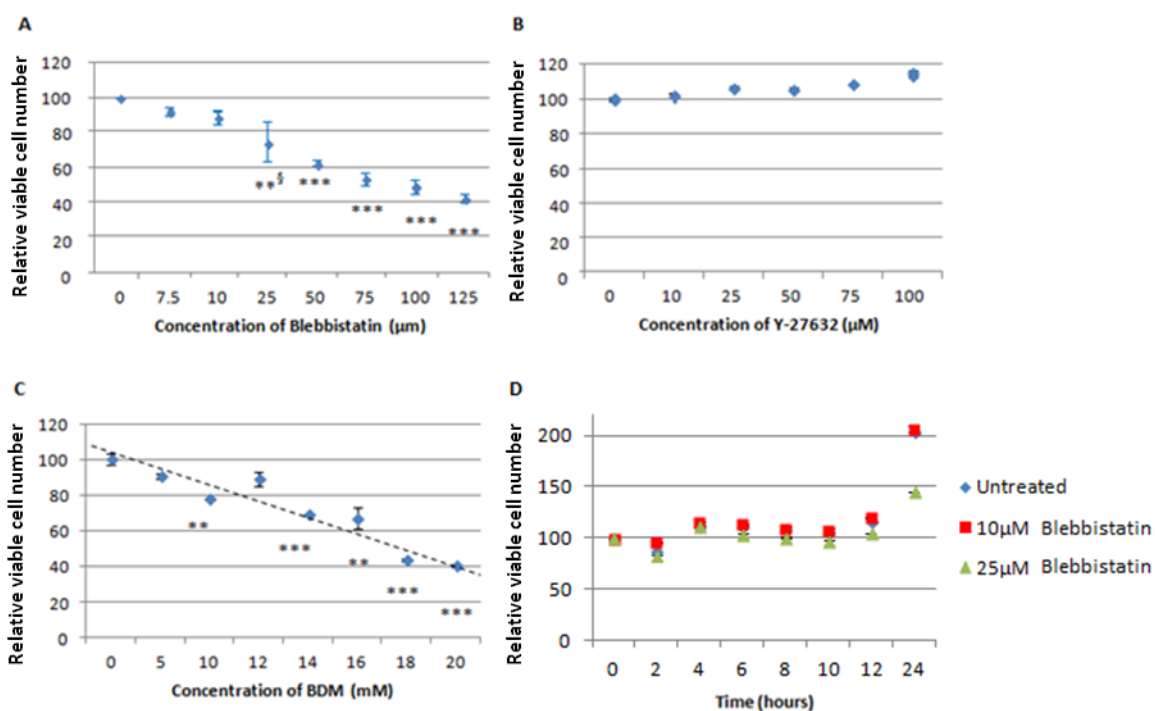


Figure 4.2.1 Blebbistatin and BDM, but not Y-27632 post 24 hours treatment on Rama 37 control cells reduces cell viability. Rama 37 control cells were seeded into 24 well plates and left to grow for 24 hours before treatment with different concentration of respective inhibitors; (A) Blebbistatin, (B) Y-27632 and (C) BDM into each well. After 24 hours, 4 μ L of MTT (5mg/ml) dissolved in PBS were added into each well and incubated for one hour before solubilising the precipitate in 400 μ L DMSO. (D) Either 10 μ M or 25 μ M of blebbistatin were added into each well and at every 2 hours interval and 4 μ L MTT were added and solubilised as mentioned before. The absorbances were read at 550 nm wavelength and the untreated readings were taken at 100% viable. The absorbance value were converted to percentage and plotted against respective inhibitors concentration used. Results are mean \pm s.e taken from 3 individual wells.

Methods are fully detailed in Chapter 2.2.3.

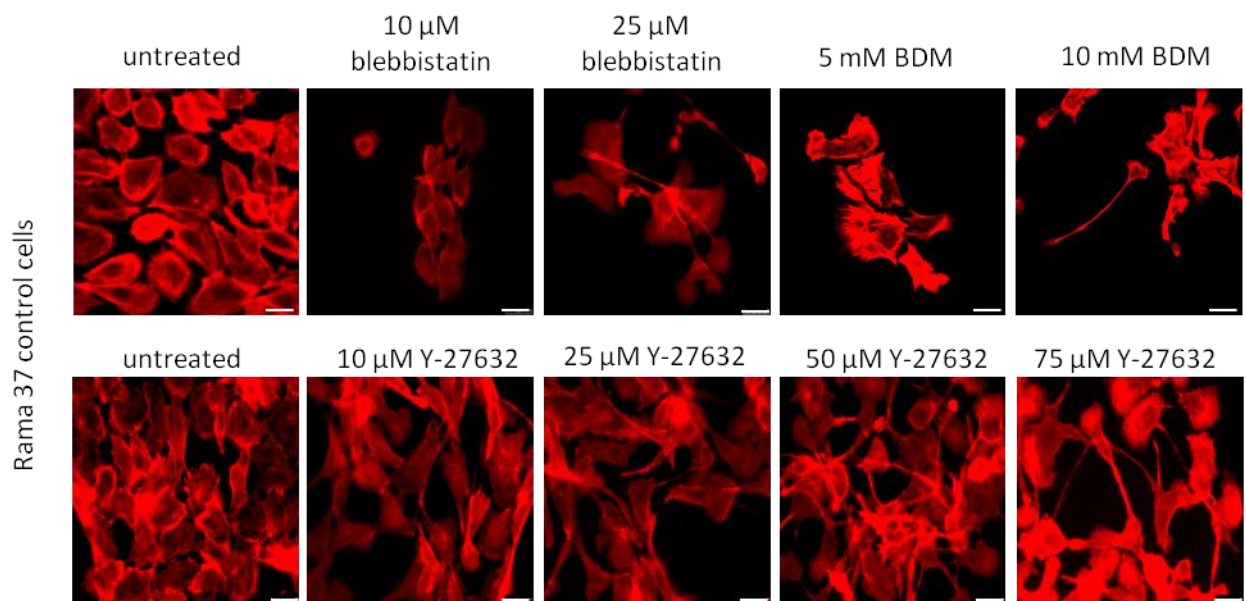


Figure 4.2.2. Blebbistatin (25 μ M) and Y-27632 (50 μ M) resulted in alteration of cell morphology and actin filaments disorganisation. Rama 37 control cells were seeded onto coverslips pre coated with fibronectin and left to incubate for 24 hours prior to addition of blebbistatin. Cells were fixed, stained with phalloidin and mounted with DAPI 24 hours post blebbistatin treatment. Cells were then view with immunofluorescence microscope. Images displayed for each cell line were representative images obtained form 3 independent experiments. Scale bar = 25 μ m. Methods are fully detailed in Chapter 2.2.8.

4.2.2 Inhibition of NMMII failed to prevent S100A4-induced migration

After establishing the optimum concentration for blebbistatin and Y-27632 (25 and 50 μ M respectively), the cells were pre-treated before performing scratch assay using CellIQ machine (Figure 4.2.3 A). Images obtained were analysed and depicted in corresponding histograms shown in Figure 4.2.3 B which demonstrated that untreated R37 S100A4 WT cells closed wound significantly faster ($68 \pm 13.0\%$) than untreated Rama 37 control cells ($55 \pm 6.3\%$, $P = 0.033$), as previously shown in Chapter 3 (Figure 4.2.3 B). However, after treatment with blebbistatin and Y-27632 the percentage of wound closure of Rama 37 control cells significantly increases to $91 \pm 4.6\%$ ($P < 0.001$) and $85 \pm 12.2\%$ ($P < 0.001$) respectively as opposed to $55 \pm 6.3\%$ of the untreated cells. On the other hand, the similar treatment also increased wound closure percentage of R37 S100A4 WT cells to $96.6 \pm 3.7\%$ ($P < 0.001$) and $99.4 \pm 0.7\%$ ($P < 0.001$) which were significantly faster than its untreated controls; $68 \pm 13.0\%$.

Improvement of cell motility after treatment with NMMII inhibitors to demolish NMMII-actin integrity highlighted the dispensable acto-myosin contraction in promoting cell motility. In fact, the improvement in motility suggested that NMMII may be more important in cell adhesion and acceleration of wound closure in S100A4 overexpressing cells after treatment suggested that NMMII may not be the only target protein of S100A4 in promoting cell motility.

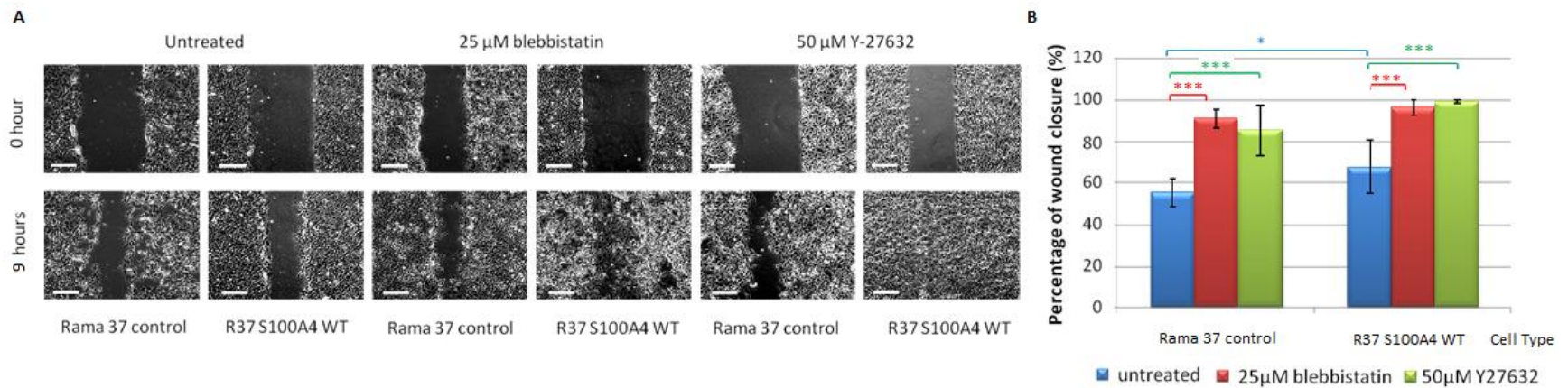


Figure 4.2.3. Inhibition of NMMII with blebbistatin or Y-27632 promotes wound healing in both Rama 37 control cells and R37 S100A4 WT cells. Equal numbers of cell were seeded into 24 well plate and left for 48 hours of incubation to create a confluent monolayer of cells. The cells were scratched, washed and fresh medium containing either 25 μM of blebbistatin or 50 μM of Y-27632 were added into the respective wells. The plates were placed in CellIQ machine and time lapse images were taken until the gap closes. **(A)** The time lapse images on the indicated time point were chosen. Scale bar = 200 μm. Images obtained are representative images from 3 independent experiments. **(B)** Time lapse images were analysed with CellIQ Analyser software and percentage of wound closure after 9 hours post scratching for each cell lines and its treatments were calculated and plotted as above. Data shown in each treatment are mean values ± s.e. of 3 regions of triplicates and is representative data from 3 independent experiments. Student t-Tests were done by comparing the treatment of each cell line to its respective untreated controls and also between the untreated samples of both cell lines. * $p < 0.05$, ** $p < 0.01$, *** $p < 0.001$. Methods are fully detailed in Chapter 2.2.4.

4.2.3 Inhibition of NMMII reduces focal adhesions

From immunostaining of paxillin, actin and NMMIIA conducted in the previous chapter, it was demonstrated that promotion of cell migration by S100A4 protein resulted in reduction of focal adhesions and actin filaments disassembly. Therefore, we sought to determine if treatment with either blebbistatin or Y-27632 poses similar effects.

Immunofluorescence staining of paxillin in Figure 4.2.4 demonstrated that treatment with 25 μ M of blebbistatin resulted in changes of cell morphology. After treatment with 25 μ M of blebbistatin Rama 37 control cells displayed polarised morphologies with a prominent lamellipodium found at the leading edge of the cells along with significant reduction of paxillin clusters. This treatment also causes disassembly of dorsal stress fibers, but transverse arcs remained intact around the perinuclear of the cells (Figure 4.2.4 A – A' and B – B'). On the other hand, R37 S100A4 WT cells treated with blebbistatin demonstrated less prominent transverse arcs, thinner actin filaments and actin residues were dispersed throughout the cytoplasm (Figure 4.2.4 C – C' and D – D').

Consistent with the results following treatment with blebbistatin, addition of Y-27632 also resulted in overall loss of focal adhesions (paxillin) in Rama 37 cells (Figure 4.2.5). Treatment of Rama 37 control cells with 50 μ M of Y-27632 resulted in the loss of dorsal stress fibers, but transverse arcs were still visible (Figure 4.2.5 A – A' and B – B'). Unlike inhibition with blebbistatin, there were no prominent lamellipodium present but projections of filopodia were clearly visible (Figure 4.2.10 B – B'). Under similar treatment, prominent lamellipodium present in the untreated R37 S100A4 WT cells were replaced by numerous projections of filopodia around the cells (Figure 4.2.10 C – C' and D – D') with speckles of actin filaments dispersed throughout the cytoplasm of the treated cells.

This noticeable reduction of paxillin clusters were quantified in Table 4.2.1. When compared to untreated Rama 37 control cells (16.4 ± 4.1), cells that were treated with blebbistatin (2.3 ± 1.6) and Y-27632 (1.6 ± 1.4) show significant paxillin clusters reduction ($P < 0.001$). Similarly, paxillin clusters in untreated R37 S100A4 WT cells (5.4 ± 3.6) reduced to 0.2 ± 0.4 and 0.6 ± 1.1 after treatment with blebbistatin and Y-27632 respectively ($P < 0.001$).

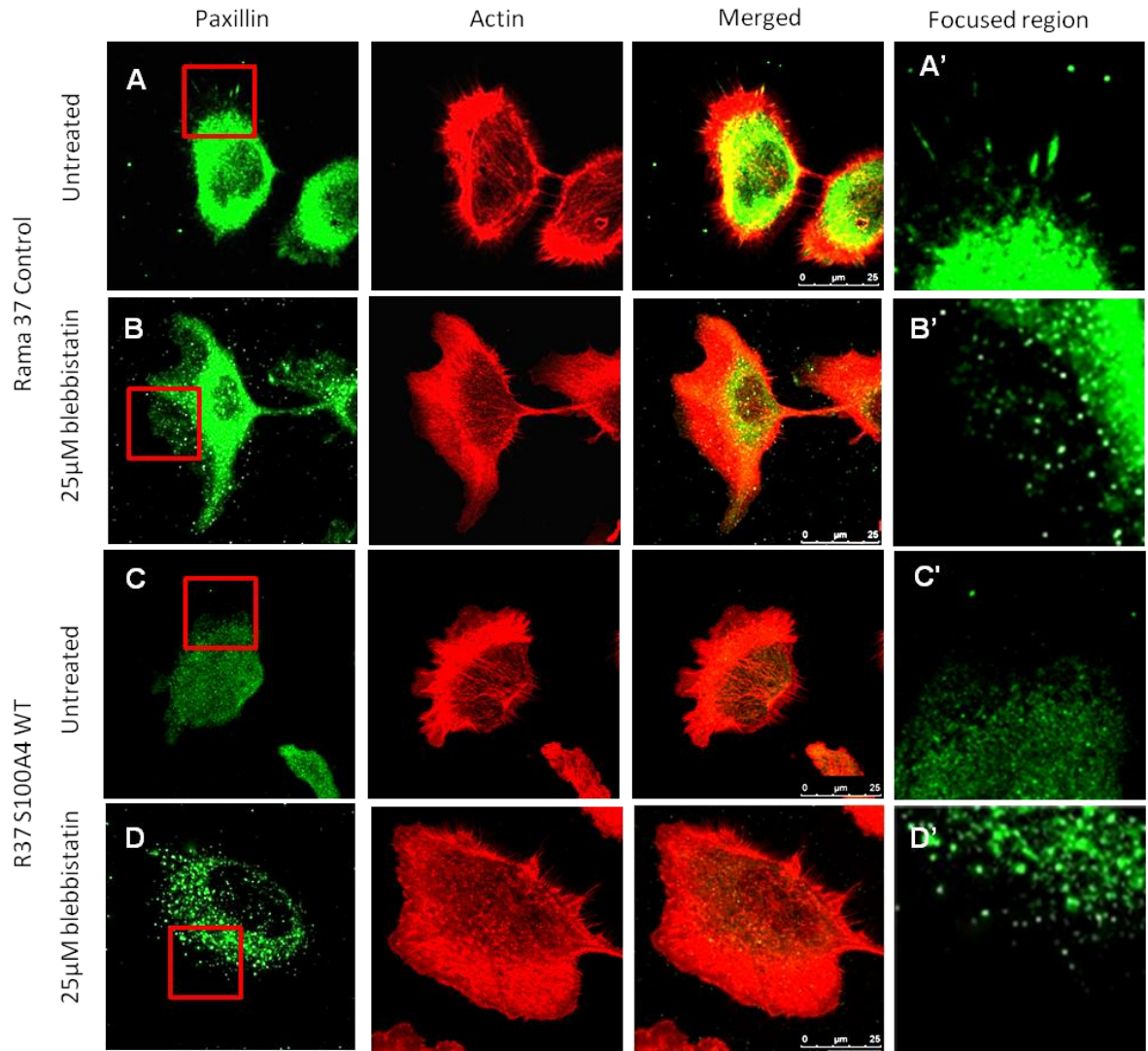


Figure 4.2.4 Reduction of paxillin clusters and disassembly of actin stress fibers in Rama 37 cells as a consequence of NMMII inhibition by blebbistatin. Rama 37 cells were seeded onto coverslips pre coated with fibronectin and left for 48 hours before further incubation with 25 μ M of blebbistatin. After 4 hours, the cells were fixed, blocked, incubated with primary antibody (paxillin), and followed by secondary antibody (FITC) along with phalloidin incubation. Then, the cells were washed and mounted with DAPI before viewing with confocal microscope. Untreated Rama 37 control cells were labeled as A - A' whereas treated cells were labeled as B - B'. Untreated R37 S100A4 WT cells were labeled as C - C' and those treated were labeled as D - D'. Panels A', B', C' and D' correspond to focused regions of the cell. Scale bar = 25 μ m. Images displayed for each cell line were representative image obtained from 3 independent experiments. Methods are fully detailed in Chapter 2.2.8.

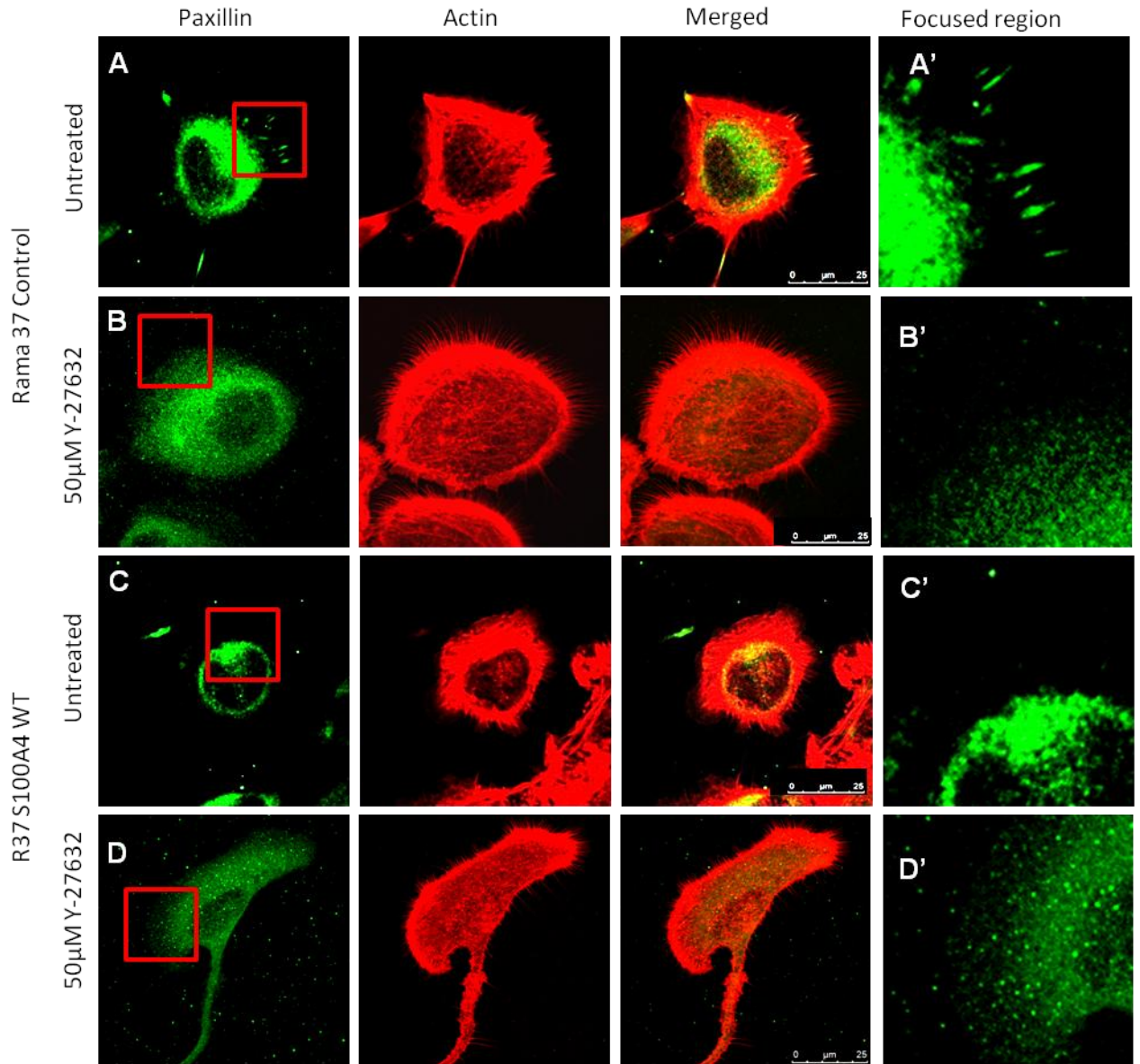


Figure 4.2.5 Reduction of paxillin clusters and disassembly of actin stress fibers in Rama 37 cells as a consequence of NMMII inhibition by Y-27632. Cells were prepared as mentioned in figure 4.2.4 but treated with 50 μM of Y-27632. Untreated Rama 37 control cells were labeled as A - A' whereas 50 μM Y-27632 treated cells were labeled as B – B'. Untreated R37 S100A4 WT cells were labeled as C – C' and those treated with 50 μM of Y-27632 were labeled as D – D'. Panels A', B', C' and D' correspond to focused regions of the cell. Scale bar = 25μm. Images displayed for each cell line were representative image obtained from 3 independent experiments. Methods are fully detailed in Chapter 2.2.8.

Treatment	Cell Lines	Number of focal adhesions (paxillin) per cell \pm s.e.	P-value
Untreated	Rama 37 control	17.8 \pm 5.1	
	R37 S100A4 WT	4.5 \pm 3.2	
25 μ M Blebbistatin	Rama 37 control	2.3 \pm 1.6	4.3377E-13
	R37 S100A4 WT	0.2 \pm 0.4	5.88905E-05
50 μ M Y-27632	Rama 37 control	1.6 \pm 1.4	8.6876E-14
	R37 S100A4 WT	0.6 \pm 1.1	0.000195951

Table 4.2.1 Inhibition of NMMII resulted in loss of paxillin clusters. Cells were seeded and stained as described in figure 4.2.5. Images obtained were quantified manually by counting the number of clusters localised at the periphery of each cell. Results are mean values \pm s.d. from 3 independent experiments (n=10).

P-values were obtained from Student t-Test where number of focal adhesions (paxillin) per respective treated cell line was compared to its untreated control.

Methods are fully detailed in Chapter 2.2.10.

To establish the effects of blebbistatin and Y-27632 on localisation and structures of NMMIIA, immunofluorescence stainings of NMMIIA with actin were done on both Rama 37 controls and R37 S100A4 WT cells.

Immunofluorescence staining demonstrated that untreated Rama 37 control cells showed NMMIIA colocalised with the actin filaments found across the cytoplasm, but after treatment with blebbistatin, this localisation of NMMIIA was lost and appeared to be dispersed throughout the cytoplasm of the cells (Figure 4.2.6 A – A' and B – B'). The treated cells also acquire polarised morphology with prominent lamellipodium found at the leading edge of the cells. Similar traits were observed in Rama 37 control cells after Y-27632 treatment (Figure 4.2.7).

In the untreated R37 S100A4 WT cells, NMMIIA were found to be concentrated at the transverse arcs where actin was most concentrated (Figure 4.2.6 C – C'). After blebbistatin treatment, R37 S100A4 WT cells displayed loss of transverse actin arcs and NMMIIA were found to be localised throughout the cytoplasm of the cells (Figure 4.2.6 D – D'). Treatment with Y-27632 displayed similar traits (Figure 4.2.7 D – D').

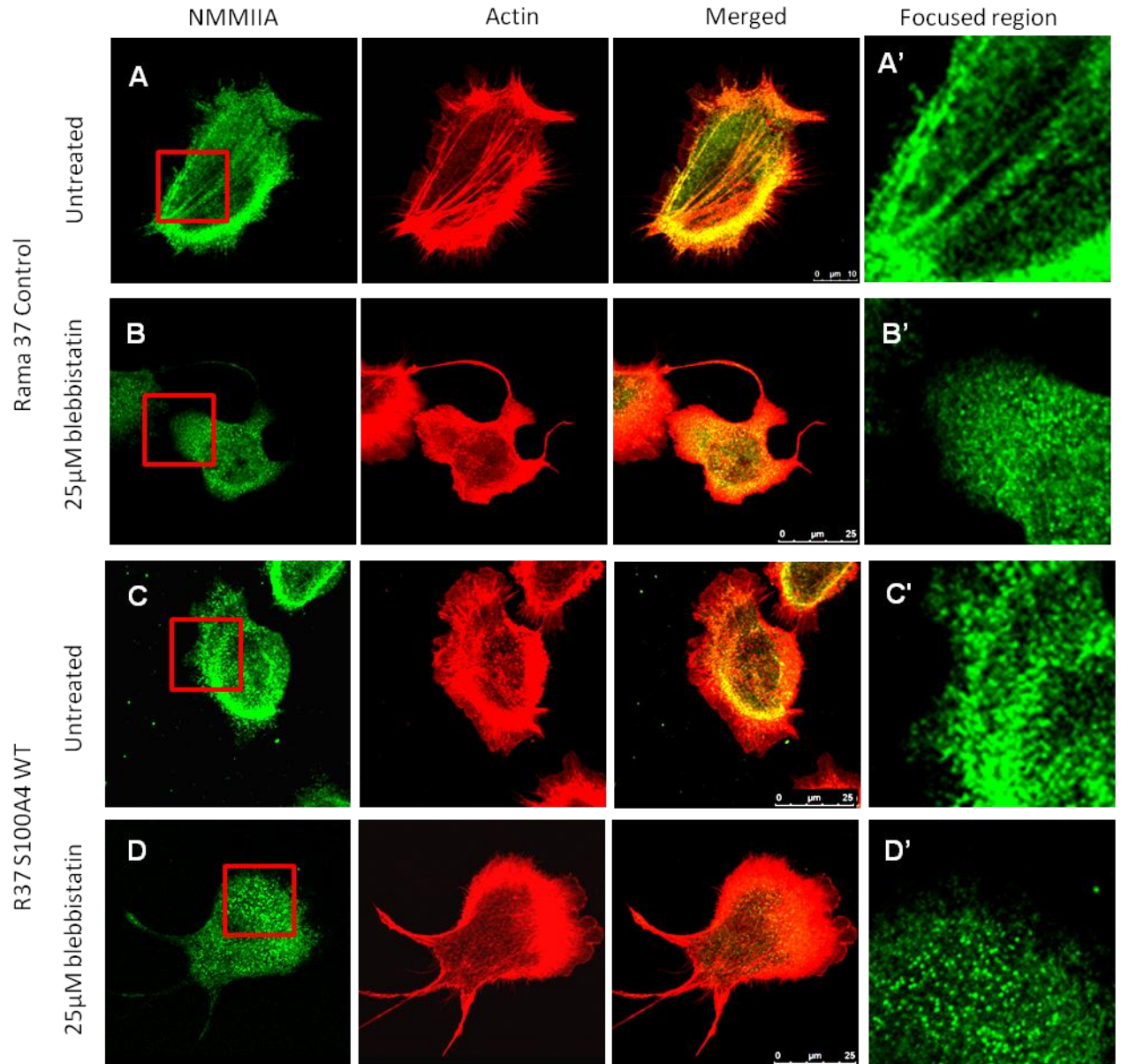


Figure 4.2.6 Treatment with 25 μM of blebbistatin resulted in loss of transverse arcs and distribution of NMMIIA throughout the cytoplasm of the cells. Cells were seeded and stained as described in figure 4.2.4 but incubated with NMMIIA primary antibody. Untreated Rama 37 control cells were labeled as A - A' whereas 25 μM blebbistatin treated cells were labeled as B - B'. Untreated R37 S100A4 WT cells were labeled as C - C' and those treated with 25 μM of blebbistatin were labeled as D - D'. Panels A', B', C' and D' correspond to focused regions of the cell. Scale bar = 25μm. Images displayed for each cell line were representative image obtained from 3 independent experiments. Methods are fully detailed in Chapter 2.2.8.

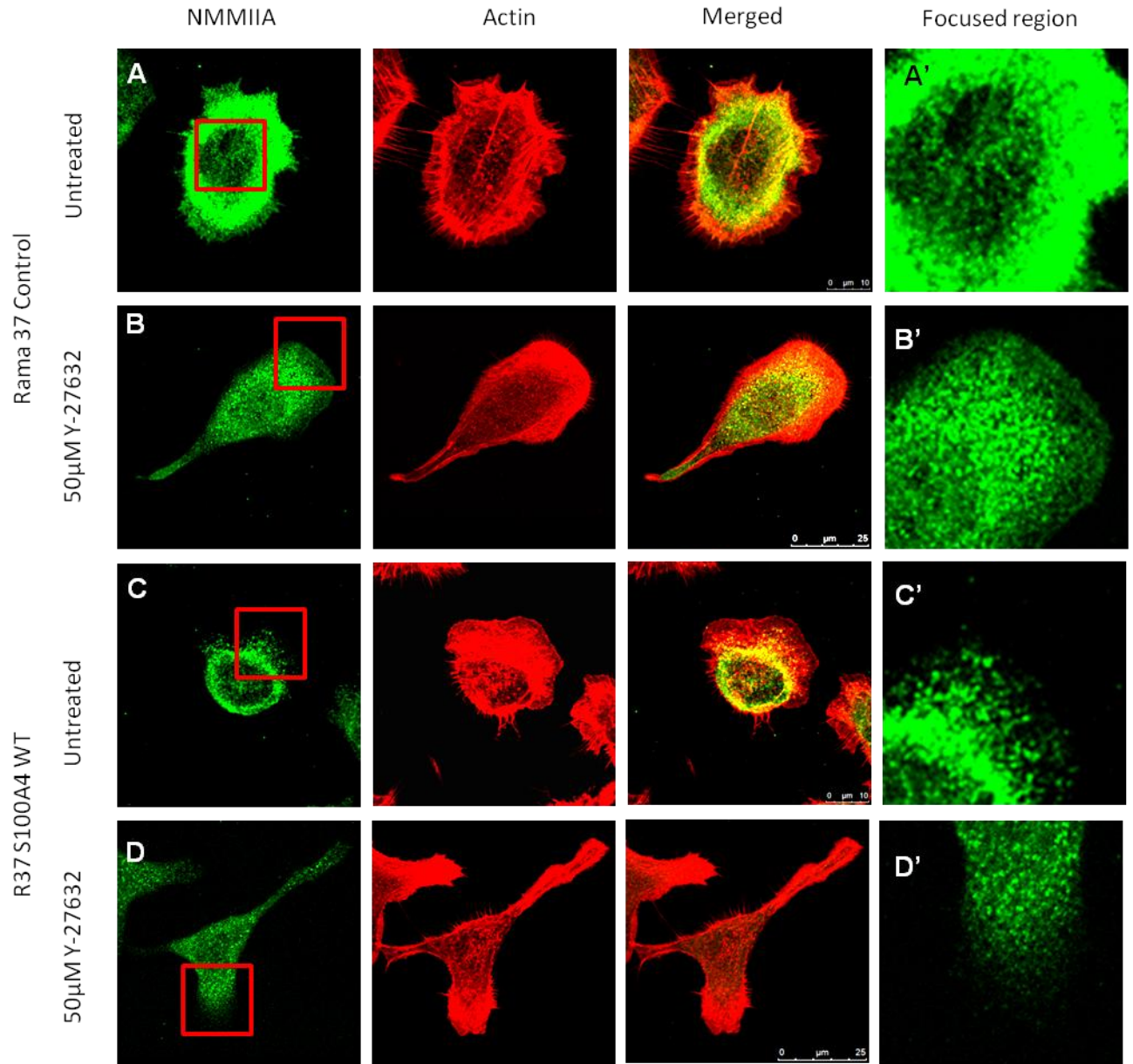


Figure 4.2.7 NMMII inhibition by Y-27632 resulted in loss of actin stress fibers and distribution of NMMIIA throughout the cytoplasm of the cells. Cells were seeded as described in figure 4.2.4 but treated with 50 μ M Y-27632 and stained for NMMIIA. Untreated Rama 37 control cells were labeled as A - A' whereas 50 μ M Y-27632 treated cells were labeled as B – B'. Untreated R37 S100A4 WT cells were labeled as C – C' and those treated with 50 μ M of Y-27632 were labeled as D – D'. Panels A', B', C' and D' correspond to focused regions of the cell. Scale bar = 25 μ m. Images displayed for each cell line were representative image obtained from 3 independent experiments. Methods are fully detailed in Chapter 2.2.8.

4.2.4 Knockdown of NMMIIA affects migration

Due to the further reduction of focal adhesion clusters (paxillin) (Table 4.2.1) and enhancement of wound healing in both Rama 37 control cells and R37 S100A4 WT cells (Figure 4.2.3) after treatment with blebbistatin or Y-27632, we speculated that S100A4-induced migration may not be NMMIIA dependent. To justify this speculation, we opted to perform wound healing assay along with immunofluorescence with NMMIIA-knocked down Rama 37 cell lines.

Before conducting any experiments, NMMIIA SiRNA transfections on Rama 37 cells were optimised. It was shown that SiRNA2 is more efficient in knockdown of NMMIIA expression than SiRNA1 and NMMIIA expression corresponding to the blot presented shows reduction of NMMIIA expressed in Rama 37 control cells after transfection with SiRNA1 (18.2%) and SiRNA2 (1.11%)(Figure 4.2.8). On the other hand, NMMIIA expression in R37 S100A4 WT cells were reduced to 71.6% and 4.2% when transfected with SiRNA1 and SiRNA2 respectively (Figure 4.2.8 B).

After demonstrating the reduction of NMMIIA expression level in both cell lines, wound healing assay was carried out (Figure 4.2.9). In Rama 37 control cells, the percentage of wound closure is $44.9 \pm 5.8\%$ whereas after inhibition with SiRNA1, it was demonstrated that there was insignificant increase in the wound closure percentage ($50.8 \pm 10.7\%$, $P = 0.171$). However, as level of NMMIIA expression decreases using SiRNA2 knockdown, significant increase in wound closure percentage was observed (57.2 ± 9.2 , $P = 0.004$). It was demonstrated that SiRNA1 is less effective in inhibiting the expression of NMMIIA when compared to SiRNA2, this data is consistent with the wound healing data where gradual improvement of cell migration was observed in cell expressing lower level of NMMIIA (Figure 4.2.8 and 4.2.9).

An inverse correlation between level of NMMIIA and percentage of wound closure was observed in R37 S100A4 WT cells. Significant reduction of percentage of wound closure was observed in SiRNA2 ($73 \pm 12.0\%$, $P = 0.012$) and insignificant reduction with SiRNA1 treatment ($81.3 \pm 16.0\%$, $P = 0.280$) when compared to untreated R37 S100A4 WT ($84.1 \pm 21.5\%$) (Figure 4.2.9).

Since there is an alteration in migratory level after NMMIIA knockdown, it is important to investigate if there are any modifications in focal adhesion (paxillin) and cellular structure (NMMIIA and actin) using immunofluorescence staining, if any.

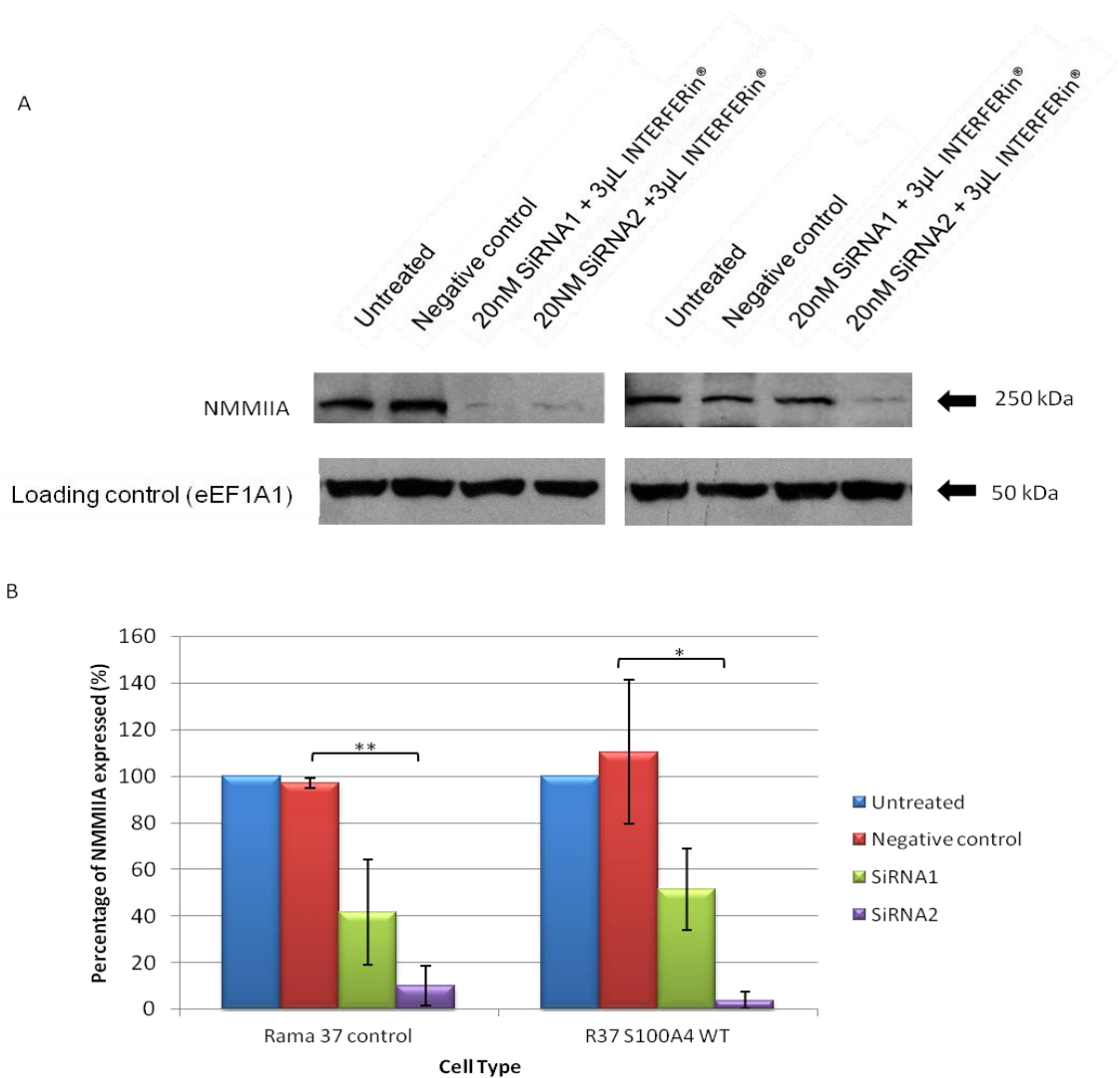


Figure 4.2.8 Level of NMMIIA expression is significantly reduced after knockdown with SiRNA2.

Cells were seeded into 6 well plate and left to incubate for 24 hours. Cells were washed and used media were replaced with Opti-MEM® and left for 4 hours before adding the transfection mixture prepared. After 72 hours, cells were harvested and total proteins were quantified and 150 µg of total protein were loaded for each sample into 8% (w/v) SDS-PAGE gel and the resolved proteins were transferred onto nitrocellulose membrane before incubating the membrane with primary antibody (NMMIIA) and then followed by secondary HRP conjugated antibody. Detection was undertaken using the customized detection system (Table 2.12). A) Blots shown are representative data obtained from 3 independent experiments. B) Percentage of NMMIIA expressed corresponds to presented blot using ImageJ after scanning the blots and normalising them with its respective controls. Methods are fully detailed in Chapter 2.2.17 to 2.2.20.

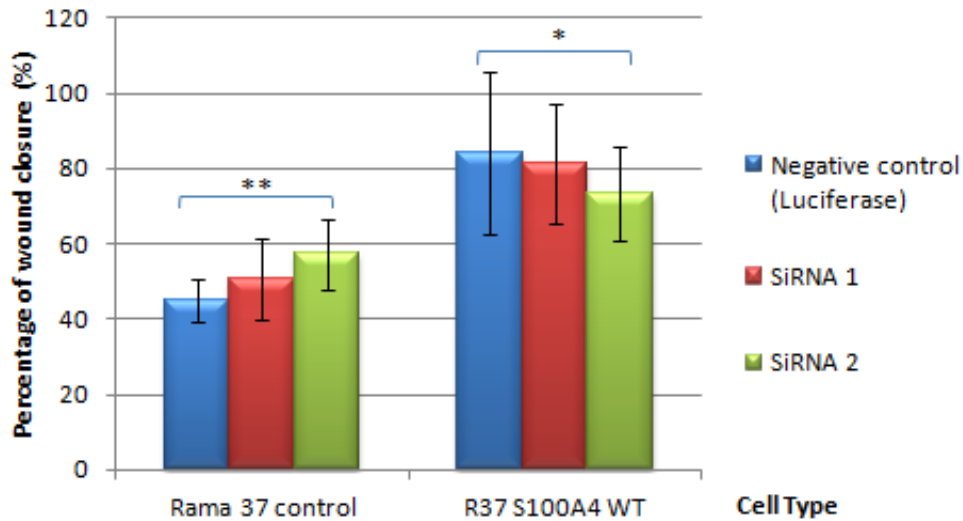


Figure 4.2.9 Knockdown of NMMIIA has opposing motility effects in Rama 37 control cells and R37 S100A4 WT cells. Cells were seeded into 24 well plates and left to incubate for 24 hours. Cells were washed and used media were replaced with Opti-MEM® and left for 4 hours before adding the transfection mixture prepared. After 72 hours, the confluent monolayer of cells were scratched, washed and fresh medium were added into the respective wells. The plates were then place in CellIQ machine to run until the gap closes and the raw data were analysed with CellIQ Analyser software. Percentage of wound closure after 8.2 hours post scratching were calculated and plotted as above. Data shown are mean values \pm s.e. of 3 regions of triplicates and a representative data from 3 independent experiments. Student t-Tests were done by comparing the treated samples to untreated controls. * $p < 0.05$, ** $p < 0.01$, *** $p < 0.001$. Methods are fully detailed in Chapter 2.2.4 and Chapter 2.2.7.

4.2.5 Knockdown of NMMIIA reduces focal adhesions

Since reduction of focal adhesions has been shown to correlate with increased motility of Rama 37 cells, immunofluorescence stainings for paxillin and NMMIIA of the cells after SiRNA transfection were performed. The reduced expression of NMMIIA in Rama 37 control cells correlated with the loss of paxillin clusters and filopodia projections were replaced by wide-spread lamellipodium when compared to untreated control (Figure 4.2.10 A – A' and B – B'). Also, treated cells acquired polarised morphology with loss of dorsal stress fibers, but retaining the transverse stress fibers. The knockdown of NMMIIA in R37 S100A4 WT cells resulted in further loss of paxillin clusters and multiple pseudopodia projected around the cells' periphery instead of lamellipodia as observed in its untreated counterpart (Figure 4.2.10 C – C' and D – D').

Immunofluorescence stainings of Rama 37 cells against NMMIIA and actin after SiRNA transfection were done. In untreated Rama 37 control cells, it was observed that NMMIIA were colocalised along the actin filaments (Figure 4.2.11 A – A'). Knockdown of NMMIIA in Rama 37 control cells led to cells acquiring polarised morphology and relocalisation of remaining NMMIIA towards the nuclear of the cells (Figure 4.2.11 B – B'). Cells expressing S100A4 WT protein showed some colocalisation of NMMIIA along the actin stress fibers with higher NMMIIA intensities within the nucleus of the cells (Figure 4.2.11 C – C'). After NMMIIA SiRNA transfection, the polarisation of the S100A4 WT expressing cells was slightly altered where multiple pseudopodia were observed (Figure 4.2.11 C – C' and D – D'). Also, the localisation of the NMMIIA concentrated within the nucleus of the cells and the previously observed elongated strands of actin stress fibers in the untransfected R37 S100A4 WT cells were replaced with speckles of actin entities throughout the cell cytoplasmic region (Figure 4.2.11 C – C' and D – D').

Since such a trait is observed, similar experiments were conducted with Cos 7 cells, which naturally void of NMMIIA to show if the consistent observations are attainable.

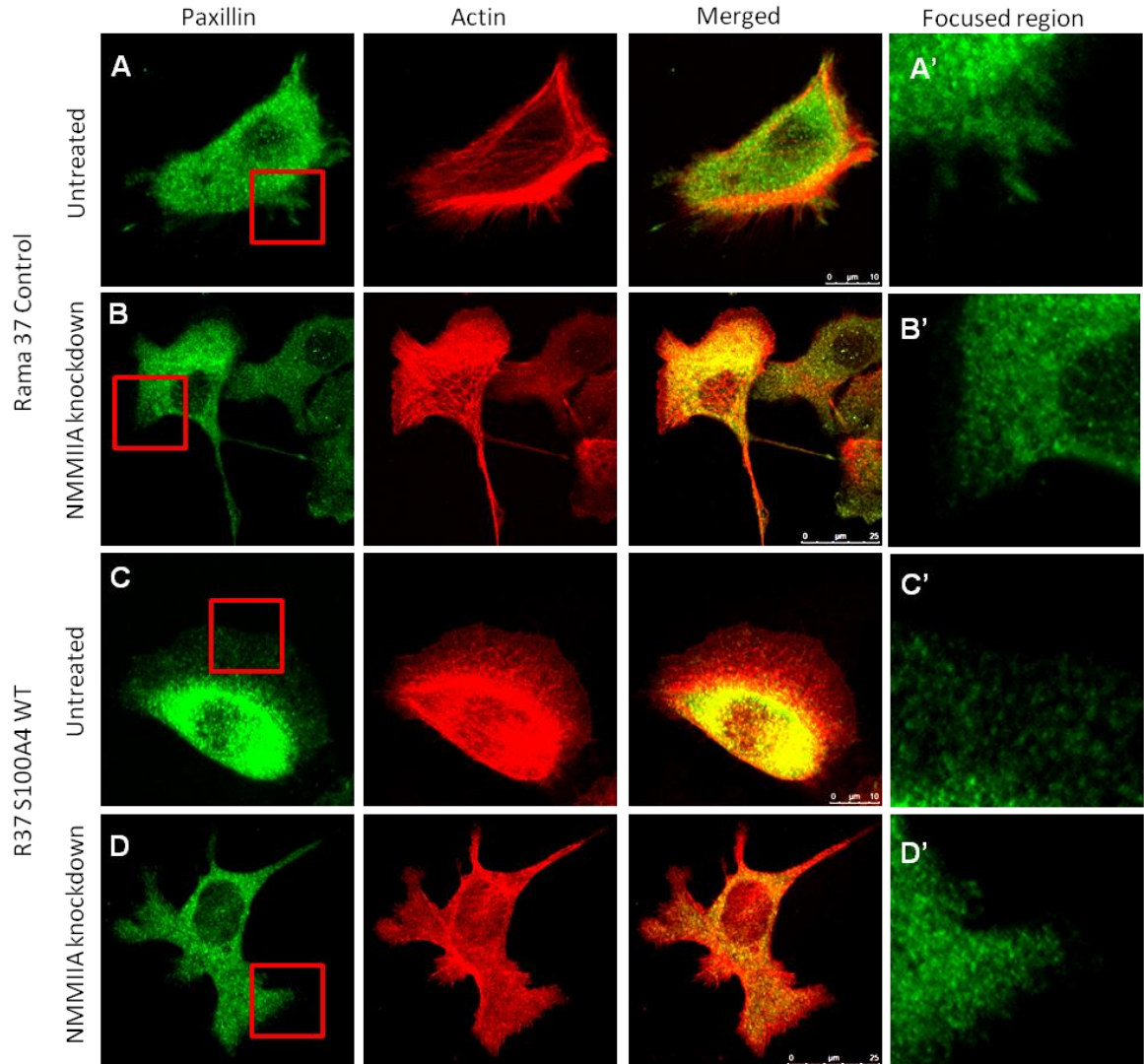


Figure 4.2.10 Inhibition of NMMIIA resulted in overall loss of paxillin clusters while promoting polarisation of Rama 37 cells. Cells were seeded into 24 well plates and left to incubate for 24 hours. Cells were washed and used media were replaced with Opti-MEM® and left for 4 hours before adding the transfection mixture prepare. After 72 hours, the cells were fixed, blocked, incubate with primary antibody (paxillin), and then with secondary antibody (FITC) along with phalloidin. Then, the cells were washed and mounted with DAPI before viewing with confocal microscope. Untreated Rama 37 control cells were labeled as A - A' whereas SiRNA transfected cells were labeled as B – B'. Untreated R37 S100A4 WT cells were labeled as C – C' and those transfected with SiRNA were labeled as D – D'. Panels A', B', C' and D' correspond to focused regions of the cell. Scale bar = 25μm. Images displayed for each cell line were representative image obtained from 3 independent experiments. Methods are fully detailed in Chapter 2.2.8.

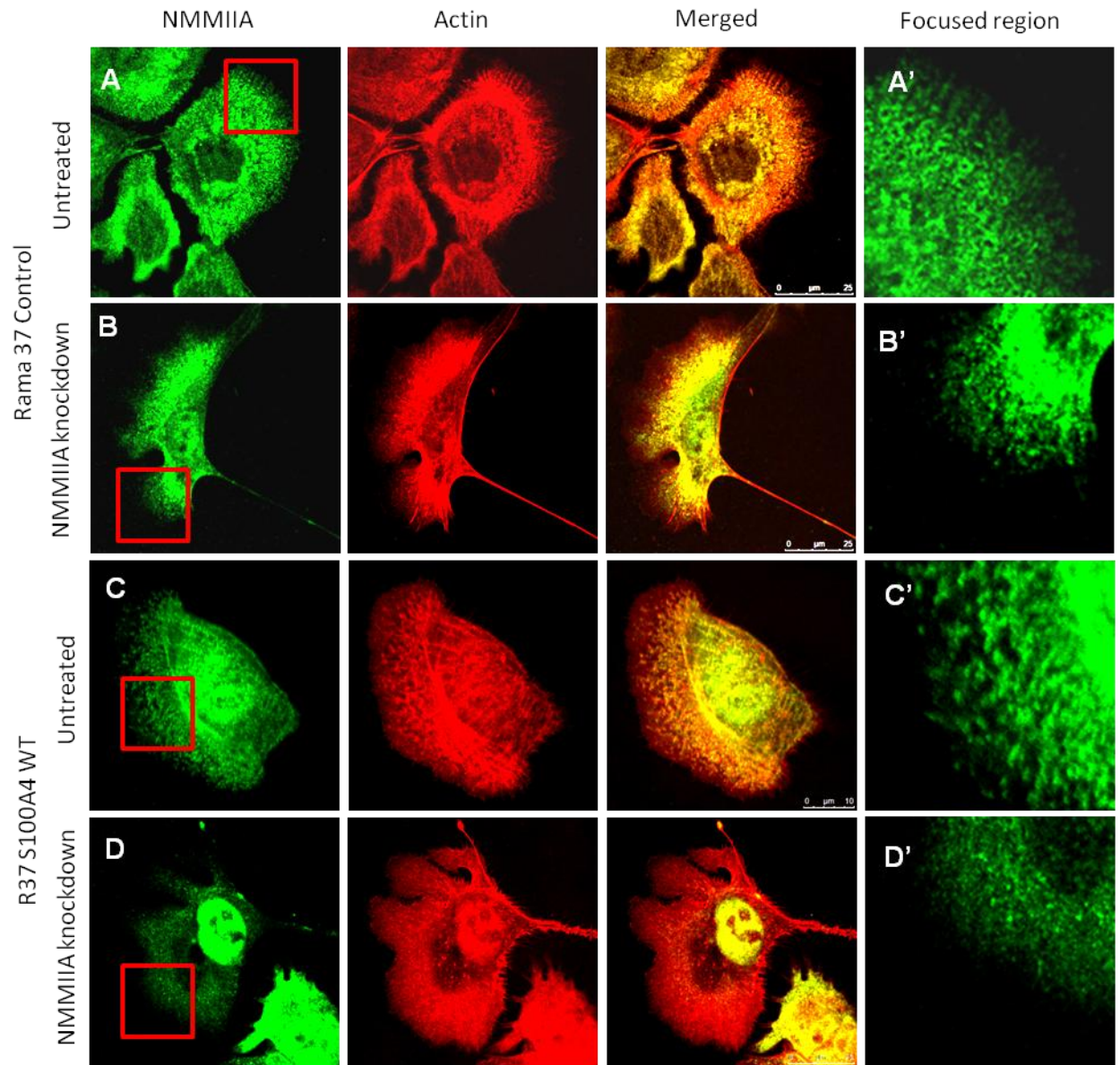


Figure 4.2.11 Inhibition of NMMIIA resulted in loss of colocalisation of NMMIIA with actin stress fibers. Cells were seeded and stained for NMMIIA using similar methodology as described in figure 4.3.10. Untreated Rama 37 control cells were labeled as A - A' whereas SiRNA transfected cells were labeled as B - B'. Untreated R37 S100A4 WT cells were labeled as C - C' and those transfected with SiRNA were labeled as D - D'. Panels A', B', C' and D' correspond to focused regions of the cell. Scale bar = 25 μ m. Images displayed for each cell line were representative image obtained from 3 independent experiments. Methods are fully detailed in Chapter 2.2.8.

4.2.6 Optimisation of Cos 7 cells transfections

Cos 7 cells are of fibroblastic origin and found to be naturally lacked of NMMIIA, hence this cell system is used to investigate the effect of S100A4 in cell migration in either absence or presence of NMMIIA. To achieve this, Cos 7 cells were transfected with either NMMIIA-GFP expressing plasmid or S100A4 WT-GFP expressing plasmid to demonstrate the independency effect of both proteins. Before proceeding into detailed experiments, the efficiency of different transfection reagents was determined.

4.2.6.1 Determination of efficiency of different transfection reagents

Five different transfection reagents were used to transfected PeCFP plasmid into Cos 7 cells. Jetpei produced the highest transfection efficiency ($36.3 \pm 1.0\%$), followed by Lipofectamine ($28.5 \pm 2.2\%$) gene HP ($26.3 \pm 5.6\%$), Trans 293 ($15.1 \pm 7.0\%$), Gene 9 ($4.1 \pm 0.9\%$) and finally, Trans TI ($3.1 \pm 3.1\%$) (Figure 4.2.12 A). Since the ratio of transfectants to plasmid DNA may affect transfection efficiency, the optimum ratio using Jetpei transfectant is established (Figure 4.2.12 B). It was demonstrated that with the density of 80,000 cells, the ratio of 0.8 μg of DNA plasmid to 2 μL of Jetpei gives a transfection efficiency of $42.2 \pm 4.8\%$, whereas 2 μg of DNA plasmid to 4 μL of Jetpei produce an efficiency of $38.3 \pm 10.7\%$. Finally, the ratio of 1 μg of DNA plasmid to 1.5 μg of Jetpei gives an efficiency of $37.3 \pm 10.1\%$. Using Jetpei A ratio, expression of PeGFP NMMIIA plasmid and PeCFP S100A4 plasmid in transfected Cos 7 cells were confirmed using western blot (Figure 4.2.13).

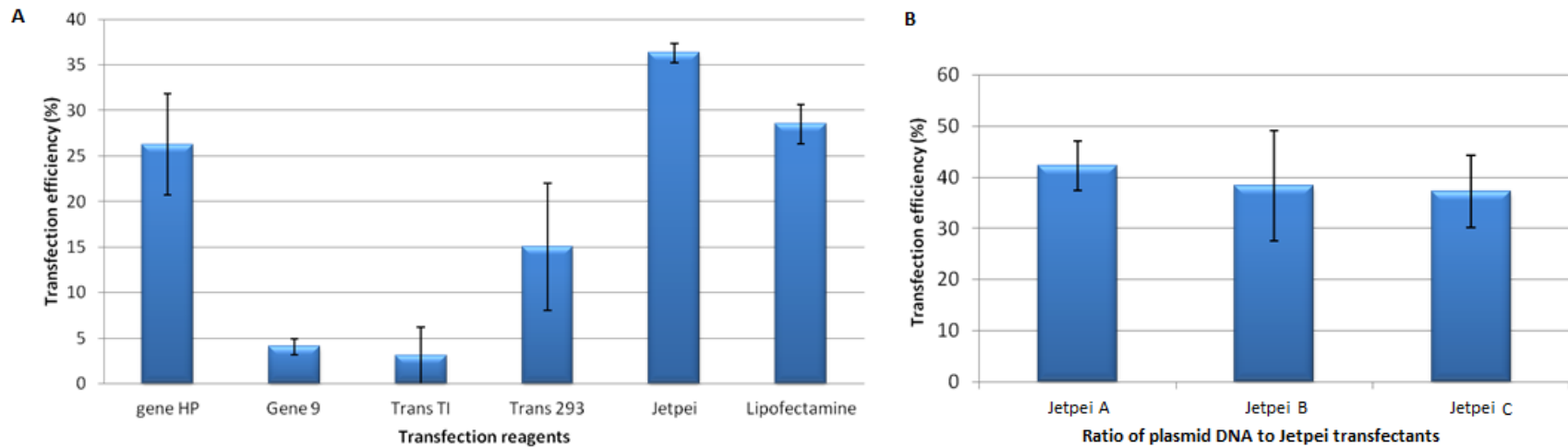


Figure 4.2.12 Jetpei transfection reagents gives the highest transfection efficiency in Cos 7 cells. **A)** Equal numbers of cell were seeded into 24 well plate and left to incubate for 24 hours. The cells were then wash and fresh medium without antibiotics were added into each well 4 hours prior to adding transfection reagents. Then, cells were left to incubate for 24 hours before being fixed and stained with DAPI. Images were taken with immunofluorescence microscope and GFP transfected cells were manually quantified against the total number of cell present which is stained with DAPI. **B)** Transfections were carried out as mentioned in A but with respective ratios; Jetpei A : 0.8 μ g plasmid DNA and 2 μ L Jetpei; Jetpei B : 2 μ g plasmid DNA and 4 μ L Jetpei and Jetpei C: 1 μ g plasmid DNA and 1.5 μ L Jetpei. Both results are mean values \pm s.e from 3 independent experiments ($n > 100$). Methods are fully detailed in Chapter 2.2.5.

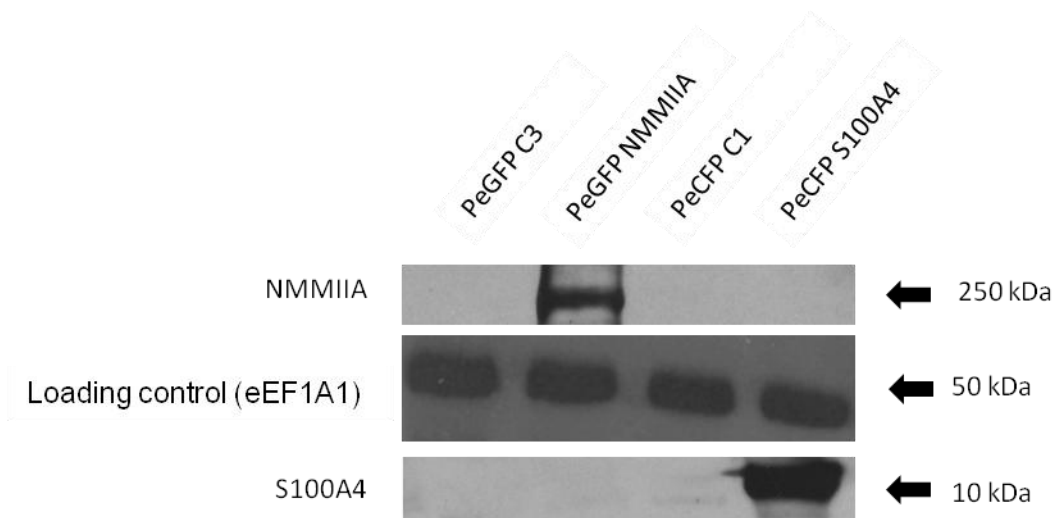


Figure 4.2.13 High level of NMMIIA and S100A4 protein expression in Cos 7 cells transfected with PeGFP NMMIIA and PeCFP S100A4 WT. Cos 7 cells were seeded in 60mm petri dishes 24 hours prior to transfection procedure. The cells were washed and fresh medium without antibiotics were added into each dish 4 hours prior to adding transfection mixture containing either PeGFP C3, PeGFP NMMIIA, PeCFP C1 or PeCFP S100A4 WT with Jetpei. Cells were left to incubate for 48 hours before harvesting. Total proteins for all four cell lines were quantified and equal amount of total protein (80µg) loaded onto 8% (v/v) (for NMMIIA blot) and 10% (v/v) (for S100A4 and eEF1A1 blot) SDS Page gels. Resolved proteins were transferred onto nitrocellulose membrane before incubating with primary antibody followed by secondary antibody and finally, detection with customised detection system (Table 2.12). Image shown are representative data obtained from 3 independent experiments. Methods are fully detailed in Chapter 2.2.17 to 2.2.20.

4.2.7 Restoration of NMMIIA in Cos 7 cells results in impediment of cell motility and reversible effects obtained using NMMII inhibitors

From the previous sections, we have shown that treatments of Rama 37 cells with blebbistatin or Y-27632 resulted in improvement of migration whether or not S100A4 is overexpressed. Here, to show that the changes in phenotype were purely caused by NMMIIA introduction in Cos 7 cells, we used myosin inhibitors (blebbistatin and Y-27632) to reinstate its original phenotype.

4.3.7.1 Rescue of NMMIIA reduces Cos 7 cells migration

Cos 7 cells transfected with either control plasmid (PeGFP C3) or PeGFP NMMIIA expressing plasmid were succumbed to wound healing assay using CellIQ system. Wound healing images were continuously taken up to 18 hours for data analysis (Figure 4.2.14 A). Quantification of wound closure 18 hours post scratching shows that Cos 7 cells transfected with PeGFP NMMIIA has significantly lower percentage of wound closure ($23.5 \pm 4.5 \%$) compared to those transfected with control plasmid, PeGFP C3 ($43.0 \pm 7.1 \%$, $P < 0.001$)(Figure 4.2.14 B).

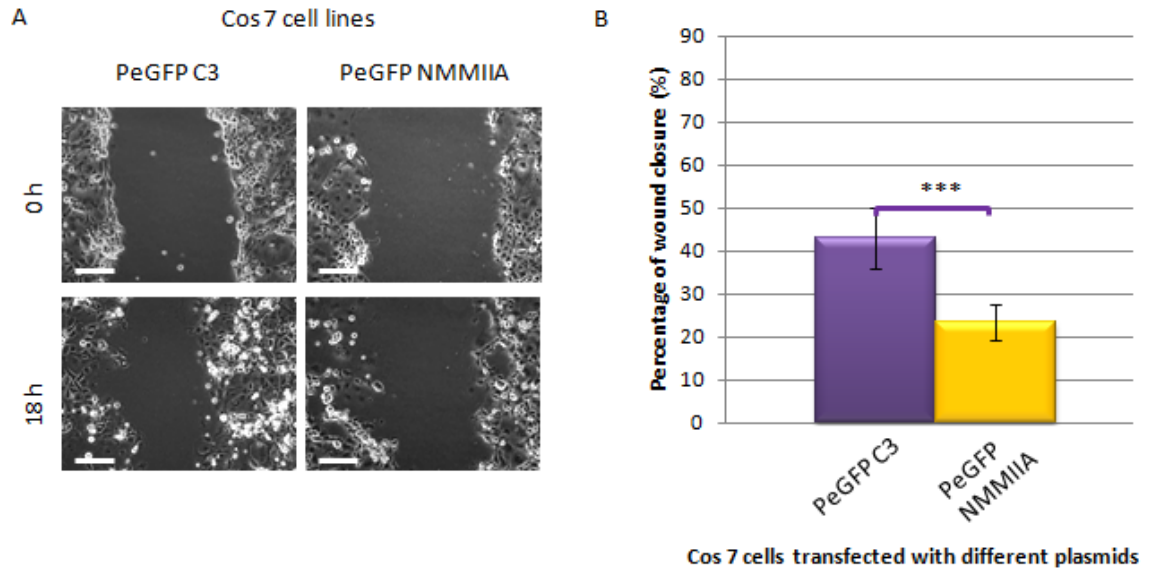


Figure 4.2.14 Rescue of NMMIIA in Cos 7 reduces migration. Cos 7 cells were seeded into 24 well plates and left to incubate for 24 hours. Cells were washed and fresh medium without antibiotics were added into each well 4 hours prior to adding transfection mixture containing either PeGFP C3, PeGFP NMMIIA, PeCFP C1 or PeCFP S100A4 WT with Jetpei. After 48 hours, the confluent monolayers of cells were scratched. The plates were then place in CellIQ machine to run until the gap closes and the raw data were analysed with CellIQ Analyser software. **A)** Representative time-laspe images of Cos 7 cells scratch assays immediately after the scratches had been made and then after 18 hours. Scale bar = 200µm. **B)** Percentage of wound closure after 18 hours post scratching were calculated and plotted as above. Data shown are mean values \pm s.e. of 3 regions of triplicates and a representative data from 3 independent experiments. Student t-Tests were done by comparing the treated samples to untreated controls. * $p < 0.05$, ** $p < 0.01$, *** $p < 0.001$. Methods are fully detailed in 2.2.4.

4.2.7.2 Treatment with either blebbistatin or Y-27632 restore migrational ability of NMMIIA expressing Cos 7 cells

To verify the specificity of blebbistatin and Y-27632, Cos 7 cells transfected with either PeGFP C3 control plasmid or PeGFP NMMIIA plasmid were treated with 25 μ M of blebbistatin or 50 μ M of Y-27632. Acceleration of Cos 7 PeGFP NMMIIA cells were observed after treatment with blebbistatin or Y-27632 (Figure 4.2.15). Quantification of time-lapsed images of Cos 7 PeGFP C3 showed insignificant changes in wound healing either treated with blebbistatin, Y-27632 or untreated (91.8 ± 3.2 %, 79.0 ± 15.3 % and 85.3 ± 8.8 %; $P = 0.055$ and $P = 0.207$ respectively when compared to untreated control). However, when Cos 7 PeGFP NMMIIA cells were treated with blebbistatin or Y-27632, enhancement of percentage of wound closure is observed (69.7 ± 8.7 %, $P = 0.010$ and 76.9 ± 8.4 %, $P < 0.001$ respectively) (Figure 4.2.15).

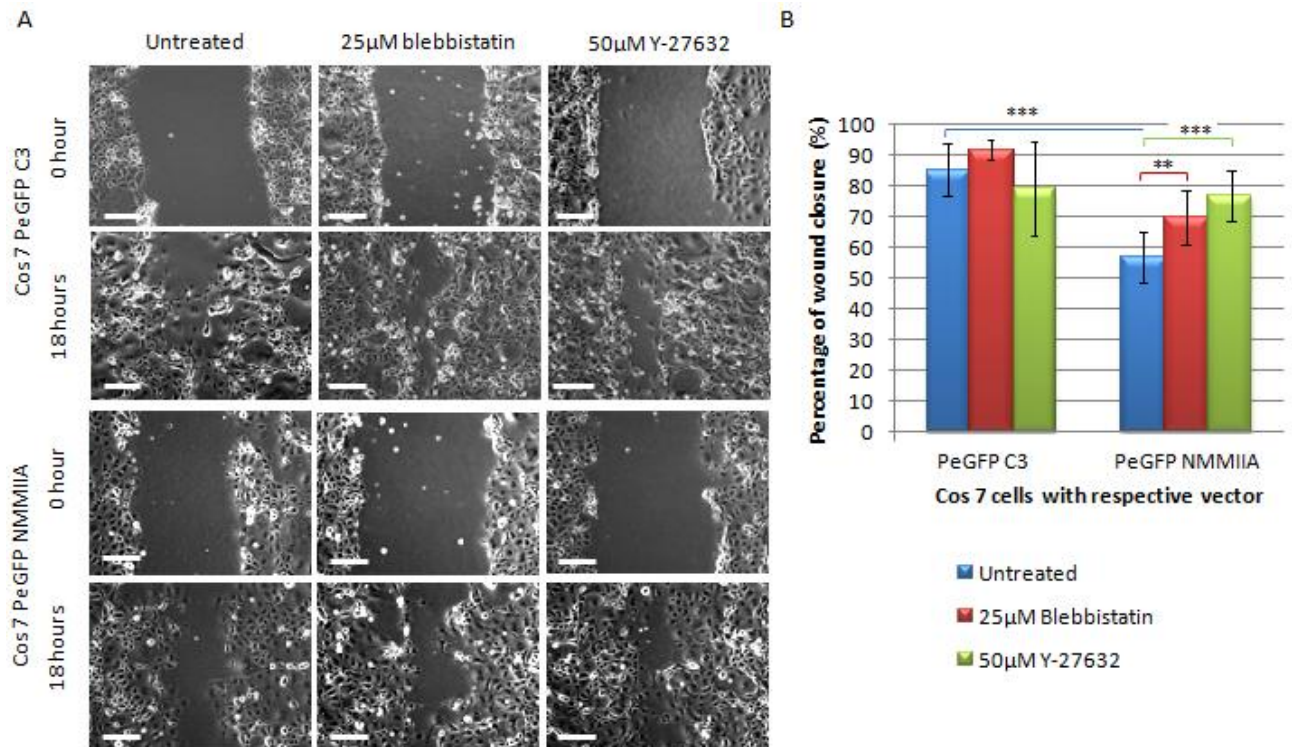


Figure 4.2.15 Inhibition of NMMIIA in Cos 7 PeGFP NMMIIA restored its original phenotype. Cos 7 cells were seeded into 24 well plates and left to incubate for 24 hours. Cells were washed and fresh medium without antibiotics were added into each well 4 hours prior to adding transfection mixture containing either PeGFP C3 or PeGFP NMMIIA with Jetpei. After 48 hours, the confluent monolayer of cells was scratched, washed and fresh medium containing 0.6mg/ml G418 either with or without addition of blebbistatin or Y-27632 was added. The plates were then place in CellIQ machine to run until the gap closes and the raw data were analysed with CellIQ Analyser software. A) Representative time-laspe images of Cos 7 cells scratch assays immediately after the scratches had been made and then after 18 hours. Scale bar = 200μm. B) Percentage of wound closure after 18 hours post scratching were calculated and plotted as above. Data shown are mean values \pm s.e. of 3 regions of triplicates and a representative data from 3 independent experiments. Student t-Tests were done by comparing the treated samples to untreated controls. * $p < 0.05$, ** $p < 0.01$, *** $p < 0.001$. Methods are fully detailed in Chapter 2.2.4.

4.2.7.3 Inhibitory effect of blebbistatin or Y-27632 resulted in reduction of paxillin clusters and ventral stress fibers

To verify the restoration of migrational ability after treatment with NMMII inhibitors is related to number of focal adhesions (paxillin) and reorganisation of actin cytoskeleton, immunofluorescence staining were done on Cos 7 cells treated with either blebbistatin or Y-27632. In Cos 7 PeGFP C3 cells, no significant difference was observed in localisation of plasmid fused with GFP and stress fibers were still visible (Figure 4.2.16 A – A' and B – B'). On the other hand, drastic changes were observed in Cos 7 PeGFP NMMIIA treated with blebbistatin. Inhibitory effect of blebbistatin on NMMIIA localisation was clearly noticeable as cells acquired polarised morphology with speckles of NMMIIA dispersed throughout the cell cytoplasm and loss of actin arcs were observed in blebbistatin treated Cos 7 PeGFP NMMIIA (Figure 4.2.16 C – C' and D – D'). Immunofluorescence staining of paxillin demonstrated that inhibition of NMMIIA expressed in Cos 7 transfectants resulted in reduction of paxillin clusters along with ventral stress fibers when compared to its untreated control (Figure 4.2.17).

Inhibitory effect of Y-27632 produced similar effect as observed blebbistatin-treated Cos 7 cells. Y-27632 has no significant effect on the morphology of Cos 7 PeGFP C3 cells. However, in Y-27632 treated-Cos 7 PeGFP NMMIIA cells, reduction of paxillin clusters (Figure 4.2.19 C – C' and D – D') were observed along with disassembly of NMMIIA and dissolution of actin filaments (Figure 4.2.18 C – C' and D – D').

All these modifications in cells were consistent with the alteration of wound healing properties, suggesting that there may be a strong correlation between cell migration, focal adhesions and NMMIIA assisted stress fibers.

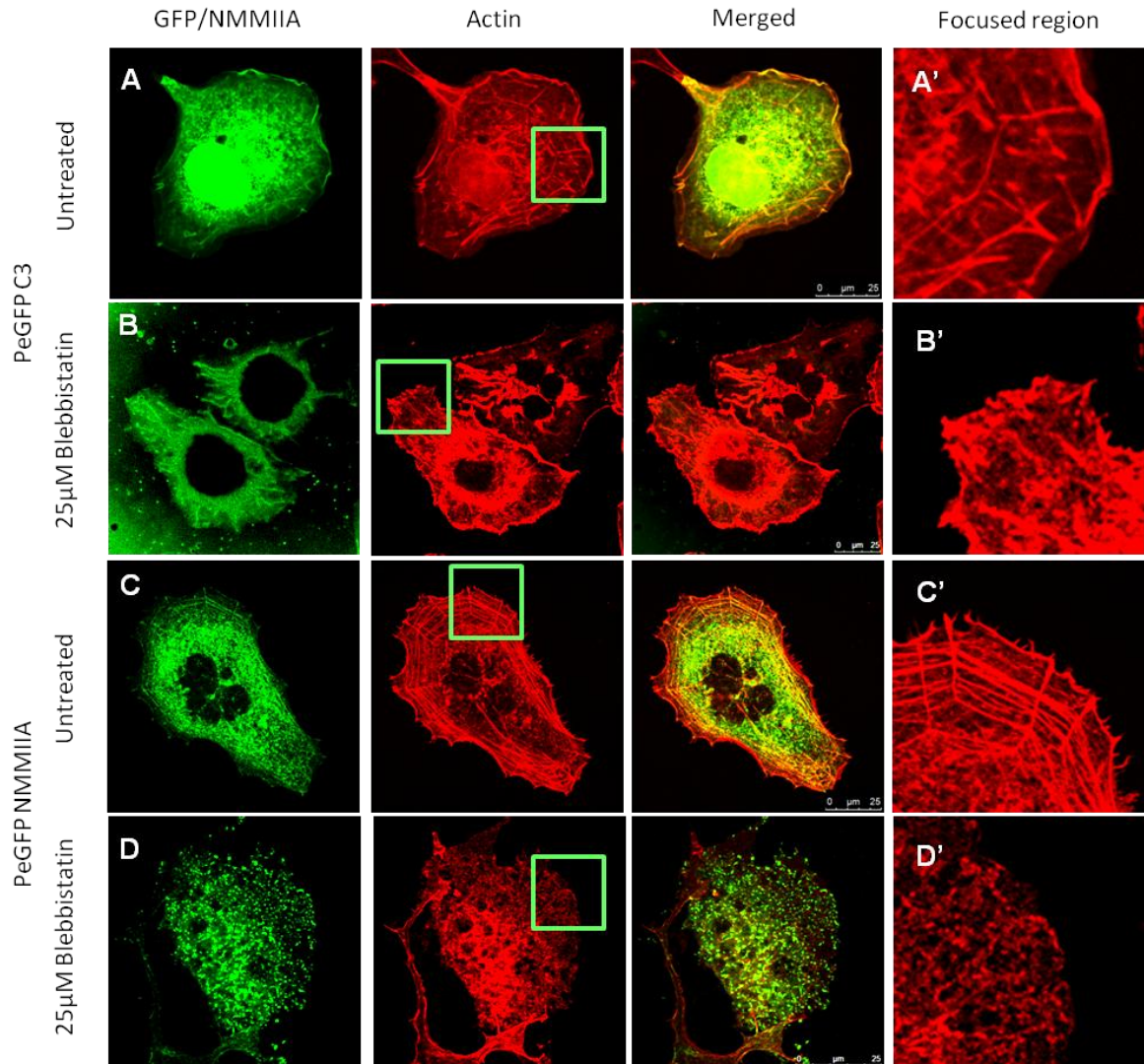


Figure 4.2.16 Blebbistatin inhibition causes disassembly of NMMIIA localisation along actin stress fibers. Cells were seeded onto coverslips pre-coated with fibronectin and left for 24 hours. Fresh medium were added 4 hours prior to adding transfection mixture (either PeGFP C3 or PeGFP NMMIIA with Jetpei). After 48 hours and 4 hours prior to fixing, 25 µM of blebbistatin were added into respective wells. The treated cells were fixed, blocked, incubate with phalloidin washed and mounted with DAPI before viewing with confocal microscope. Cos 7 cells transfected with PeGFP C3 under untreated condition were labeled as A - A' whereas blebbistatin treated were labeled as B - B'. Untreated Cos 7 cells transfected with PeGFP NMMIIA were labeled as C - C' and those treated with blebbistatin were labeled as D - D'. Panels A', B', C' and D' correspond to focused regions of the cell. Scale bar = 25µm. Images displayed for each cell line were representative image obtained from 3 independent experiments. Methods are fully detailed in Chapter 2.2.8.

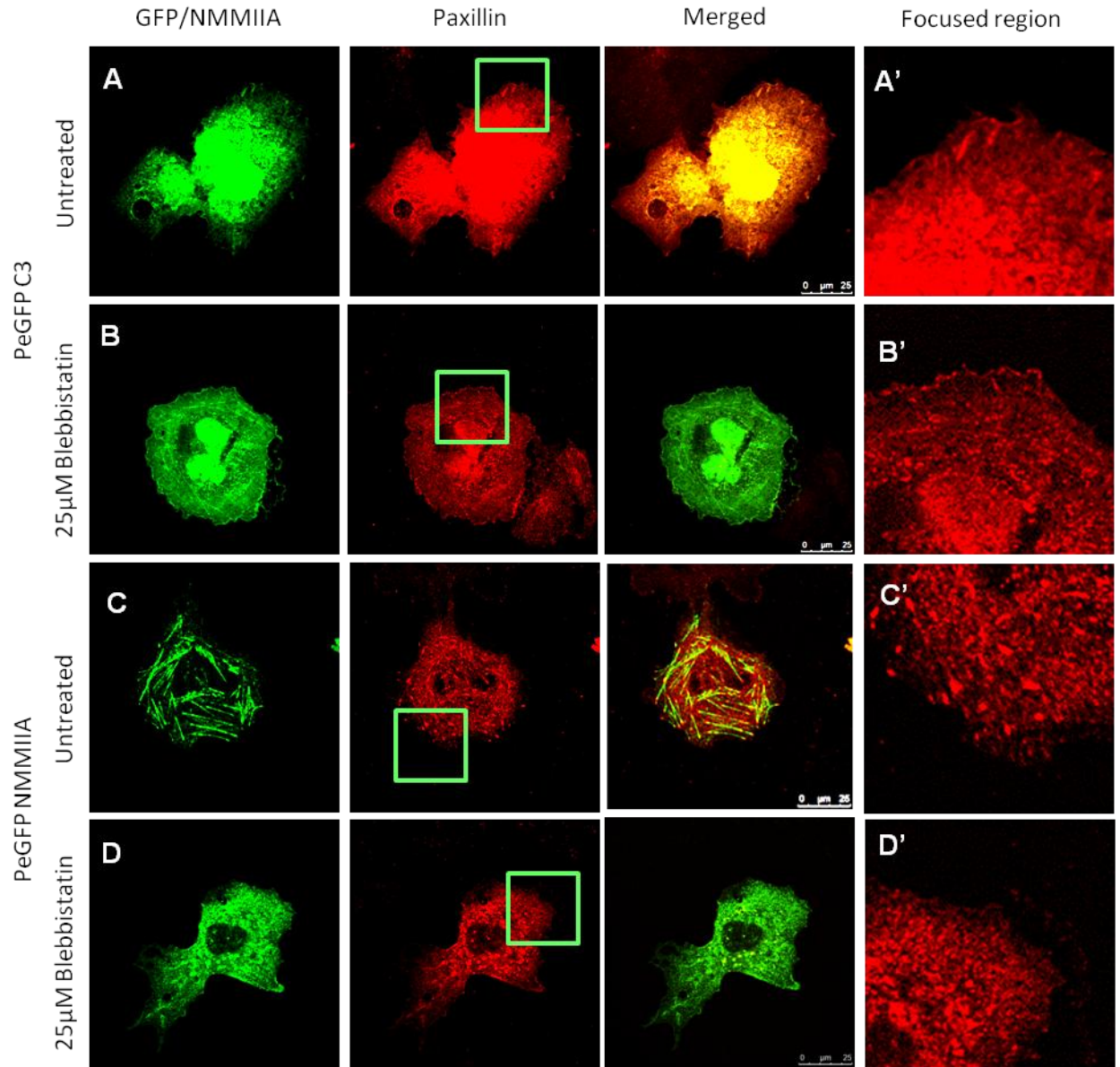


Figure 4.2.17 Blebbistatin inhibition causes reduction of paxillin clusters in NMMIIA transfected Cos 7 cells. Cells were seeded and transfected as described in figure 4.2.15 but stained for paxillin. Cos 7 cells transfected with control vector, PeGFP C3 under untreated condition were labeled as A - A' whereas blebbistatin treated were labeled as B - B'. Untreated Cos 7 cells transfected with PeGFP NMMIIA were labeled as C - C' and those treated with blebbistatin were labeled as D - D'. Panels A', B', C' and D' correspond to focused regions of the cell. Scale bar = 25µm. Images displayed for each cell line were representative image obtained from 3 independent experiments. Methods are fully detailed in Chapter 2.2.8.

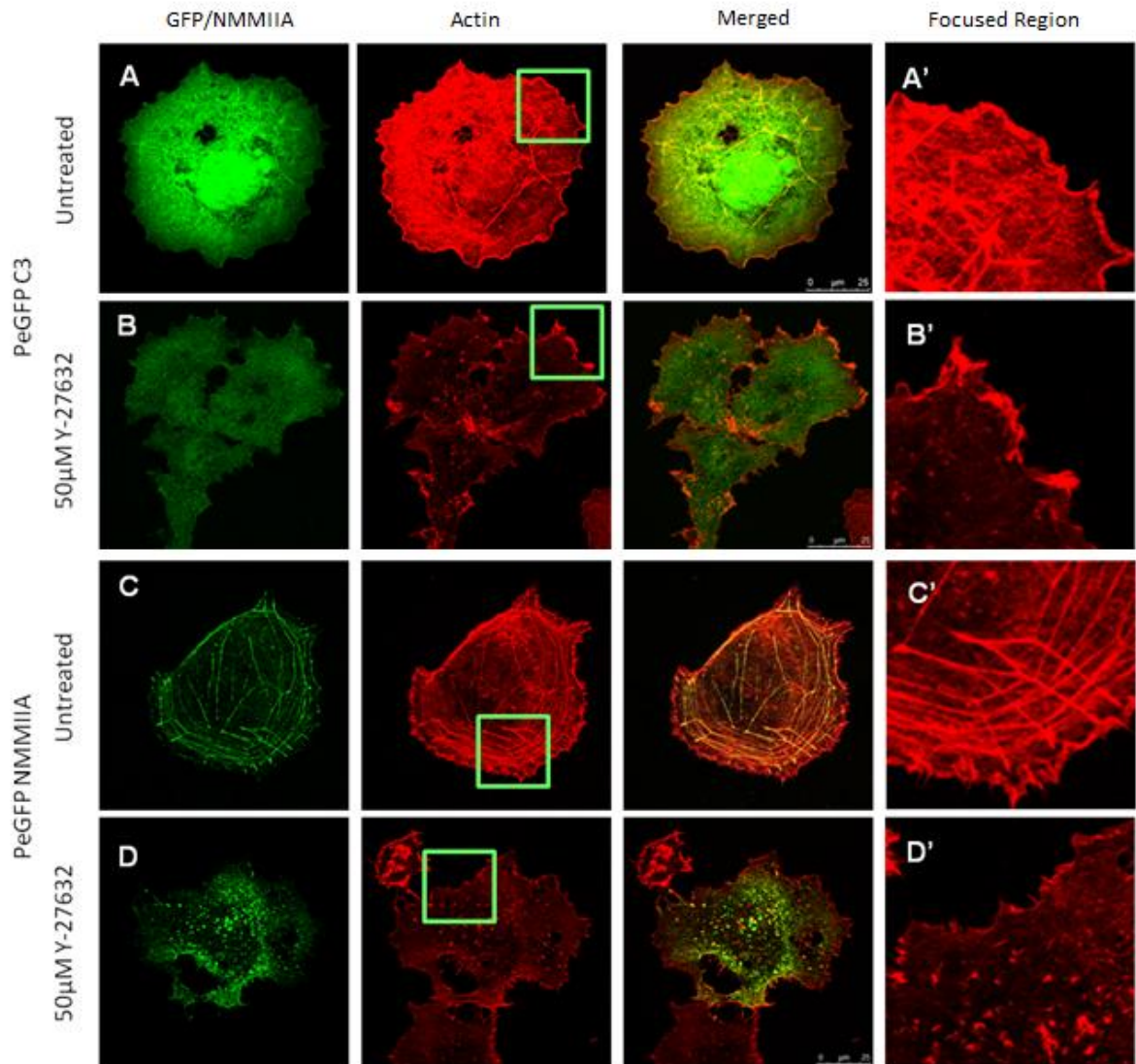


Figure 4.2.18 Y-27632 inhibition disassembly of NMMIIA along actin stress fibers in Cos 7 cells transfected with NMMIIA. Cells were seeded, transfected and treated (with 50 μ M Y-27632 instead of blebbistatin) as described in figure 4.2.15. Cos 7 cells transfected with control vector, PeGFP C3 under untreated condition were labeled as A - A' whereas Y-27632 treated were labeled as B - B'. Untreated Cos 7 cells transfected with PeGFP NMMIIA were labeled as C - C' and those treated with Y-27632 were labeled as D - D'. Panels A', B', C' and D' correspond to focused regions of the cell. Scale bar = 25 μ m. Images displayed for each cell line were representative image obtained from 3 independent experiments. Methods are fully detailed in Chapter 2.2.8.

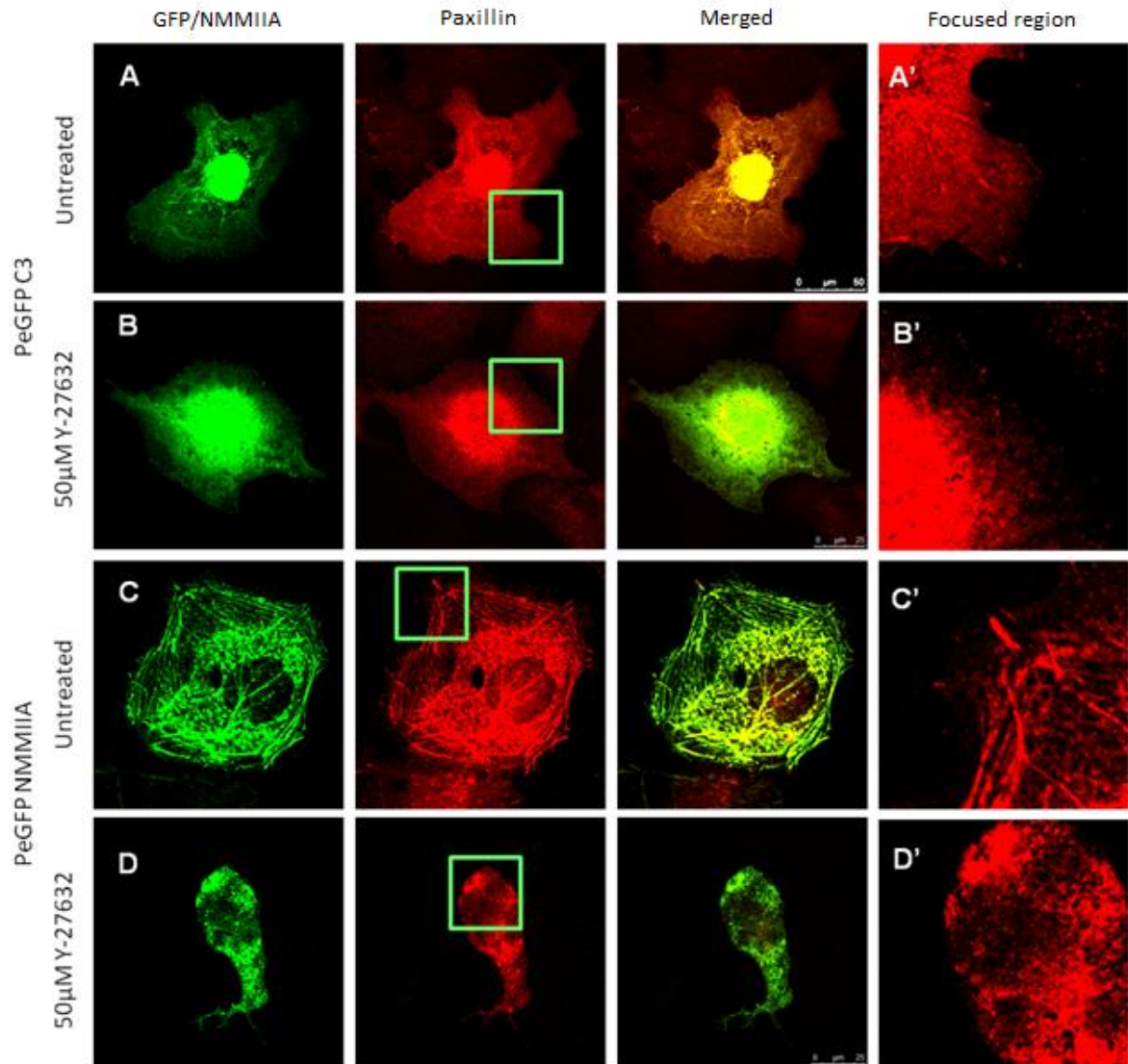


Figure 4.2.19 Y-27632 inhibition resulted in reduction of paxillin clusters in Cos 7 cells transfected with NMMIIA. Cells were seeded, transfected and treated (with 50 μ M Y-27632 instead of blebbistatin) as described in figure 4.2.15 but stained for paxillin. Cos 7 cells transfected with control vector, PeGFP C3 under untreated condition were labeled as A - A' whereas Y-27632 treated were labeled as B - B'. Untreated Cos 7 cells transfected with PeGFP NMMIIA were labeled as C - C' and those treated with Y-27632 were labeled as D - D'. Panels A', B', C' and D' correspond to focused regions of the cell. Scale bar = 25 μ m. Images displayed for each cell line were representative image obtained from 3 independent experiments. Methods are fully detailed in Chapter 2.2.8.

4.2.8 Introduction of S100A4 enhance migration

In this section, Cos 7 cells naturally lacked of NMMIIA were transfected with plasmid encoding the fusion protein S100A4 WT-CFP to demonstrate the effect of S100A4 protein independent on NMMIIA existence.

Wound healing images at 0 hours and 18 hours post scratching depicted in Figure 4.2.20 A showed that PeCFP S100A4 WT expressing cells were more motile. Quantified data corresponding to the images were portrayed as histogram in Figure 4.2.20 B. Cos 7 cells expressing empty vector PeCFP C1 had significantly lower wound closure percentage ($36.4 \pm 9.7 \%$) as opposed to those expressing PeCFP S100A4 WT plasmids ($65.9 \pm 15.0 \%$, $P < 0.0001$). Also, it was found that Cos 7 cells transfected with control plasmids (PeGFP C3 and PeGFP C1) showed similar percentage of wound closure after 18 hours ($P = 0.157$) whereas PeGFP NMMIIA expressing cells exhibited significantly lower percentage of wound closure ($P < 0.001$)(Figure 4.2.14 and Figure 4.2.20). From this, it was demonstrated there is a possibility where S100A4 protein orchestrated cell motility independently of NMMIIA protein.

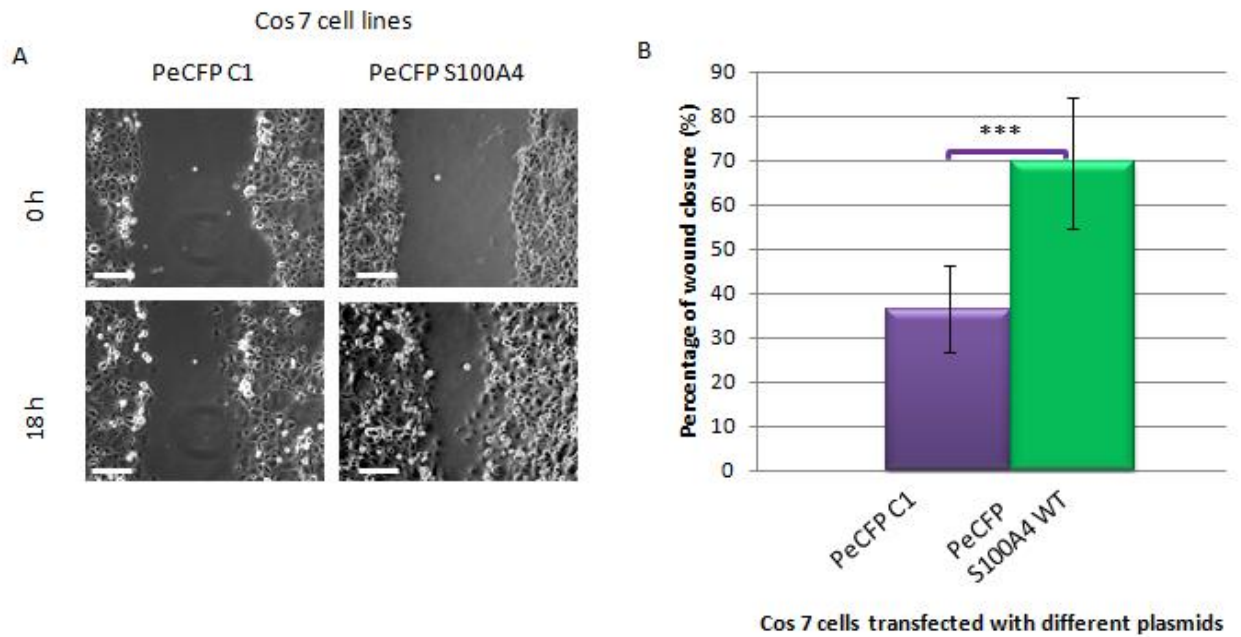


Figure 4.2.20 Introduction of S100A4 enhance migration. Cos 7 cells were seeded and transfected as described in figure 4.2.14. The plates were then place in CellIQ machine to run until the gap closes and the raw data were analysed with CellIQ Analyser software. **A)** Representative time lapse images of Cos 7 cells scratch assays immediately after the scratches had been made and then after 18 hours. Scale bar = 200 μ m. **B)** Percentage of wound closure after 18 hours post scratching were calculated and plotted as above. Data shown are mean values \pm s.e. of 3 regions of triplicates and a representative data from 3 independent experiments. Student t-Tests were done by comparing the treated samples to untreated controls. * $p < 0.05$, ** $p < 0.01$, *** $p < 0.001$. Methods are fully detailed in Chapter 2.2.4.

4.2.9 Opposing focal adhesions affect of NMMIIA and S100A4 in Cos 7 cells

Since restoration of NMMIIA protein or introduction of S100A4 protein into Cos 7 cells caused significant effect on migration via wound healing assay, we sought to investigate these effect on actin cytoskeleton and focal adhesion using immunofluorescence assay.

In Cos 7 PeGFP C3 and PeCFP C1 cells, it was observed that stress fibers were found across the cytoplasm of the cells and the GFP/CFP plasmid were localised throughout the cytoplasm, concentrated within the nucleus (Figure 4.2.21 A – A' and C – C'). When NMMIIA was restored, it was observed that NMMIIA were found colocalised along the actin stress fibers (Figure 4.2.21 B – B'). Cos 7 cells transfected with S100A4 WT-CFP acquired polarised morphology with actin arcs localised around the periphery (Figure 4.2.21 D – D'). Also, it was observed that S100A4 WT-CFP were localised throughout the cytoplasm, concentrating at the nucleus and at the edge of the cell cytoplasmic membrane.

Next, we proceeded to investigate if there are any modifications on focal adhesions by conducting immunofluorescence staining for paxillin. It was found that in Cos 7 cells transfected with control vectors, PeGFP C3 and PeCFP C1, some paxillin clusters were found around the periphery of the cells where the dorsal stress fibers were located (Figure 4.2.22 A – A' and C – C'). Also, the control vector transfected cells appeared to have more wide spread cytoplasm. In cells transfected with PeGFP NMMIIA, there is a significant increase of paxillin clusters with prominent appearance of dorsal and ventral stress fibers (Figure 4.2.22 B – B'). On the other hand, the Cos 7 cells transfected with PeCFP S100A4 WT has some paxillin clusters within the nucleus and also at the edge of the cytoplasm membrane (Figure 4.2.22 D – D'). Also, Cos 7 cell expressing S100A4 WT protein acquired polarised morphology which has not been exhibited by the rest of the cells. Quantification of paxillin clusters of the respective transfected Cos 7 cells, demonstrated that Cos 7 cells that expressed NMMIIA protein showed the higher paxillin clusters (25.4 ± 3.9) when

compared to its control counterpart, Cos 7 PeGFP C3 (13.2 ± 2.5 , $P < 0.001$) (Table 4.2.2). Conversely, Cos 7 cells expressing S100A4 WT protein demonstrated significant decrease of number of paxillin clusters when compared to its control, PeCFP C1 (1.0 ± 1.6 and 14.5 ± 3.4 respectively, $P < 0.001$). The student t-Test done on the both controls showed that there were no significant difference in paxillin clusters ($P = 0.344$) whereas the comparison between Cos 7 PeGFP NMMIIA and Cos 7 PeCFP S100A4 WT demonstrated significant difference ($P < 0.001$) (Table 4.2.2).

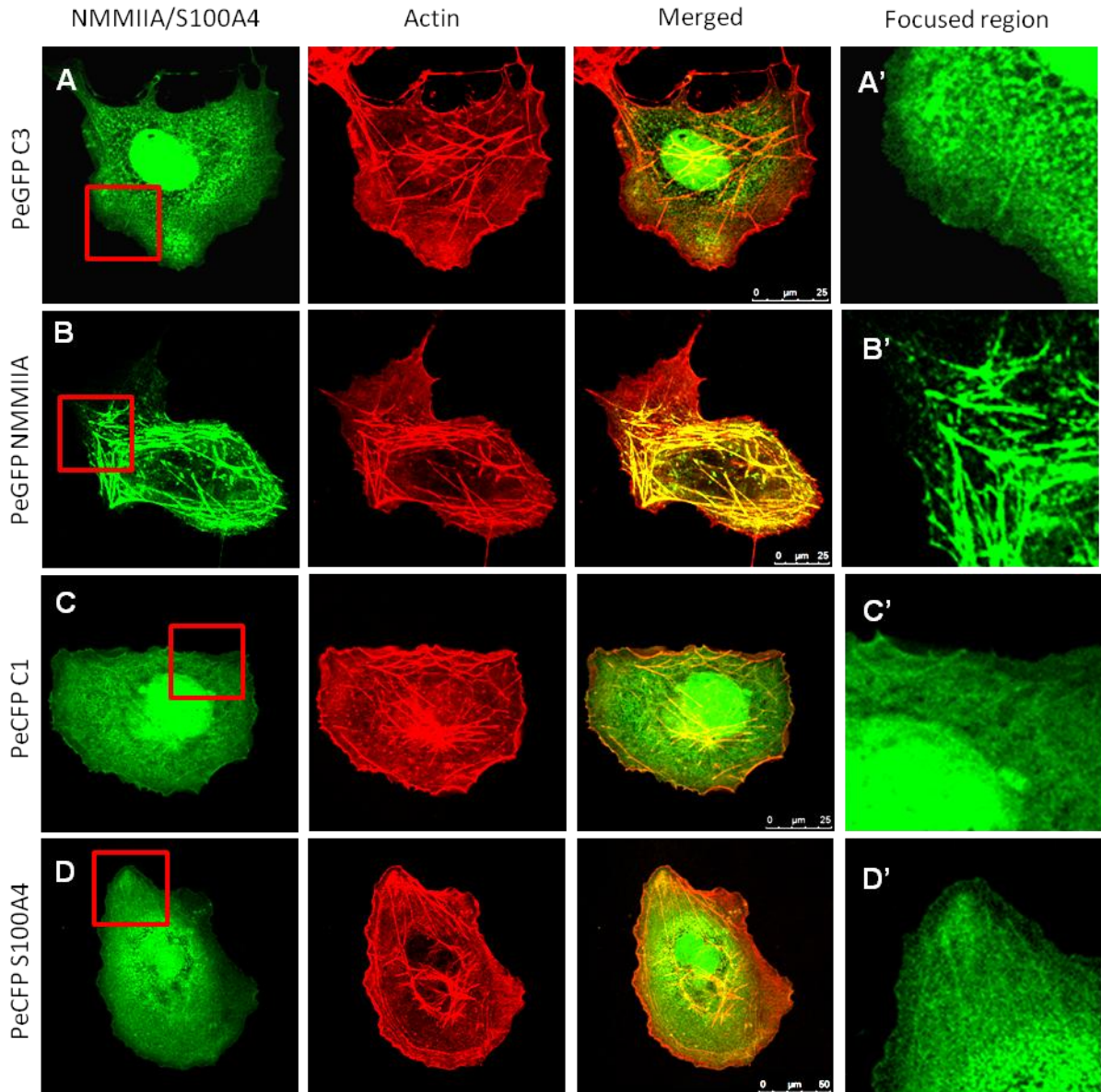


Figure 4.2.21 Restoration of NMMIIA in Cos 7 cells leads to increment of stress fibers whereas introduction of S100A4 resulted in polarisation. Cells were seeded, transfected and stained as described in figure 4.2.14 but without any inhibitor treatment. Cos 7 cells transfected with control vector, PeGFP C3 were labeled as A - A' whereas PeGFP NMMIIA transfected cells were labeled as B - B'. Cos 7 cells transfected with control for PeCFP S100A4 (PeCFP C1) were labeled as C - C' and those transfected with PeCFP S100A4 WT were labeled as D - D'. Panels A', B', C' and D' correspond to focused regions of the cell. Scale bar = 25μm. Images displayed for each cell line were representative image obtained from 3 independent experiments. Methods are fully detailed in Chapter 2.2.8.

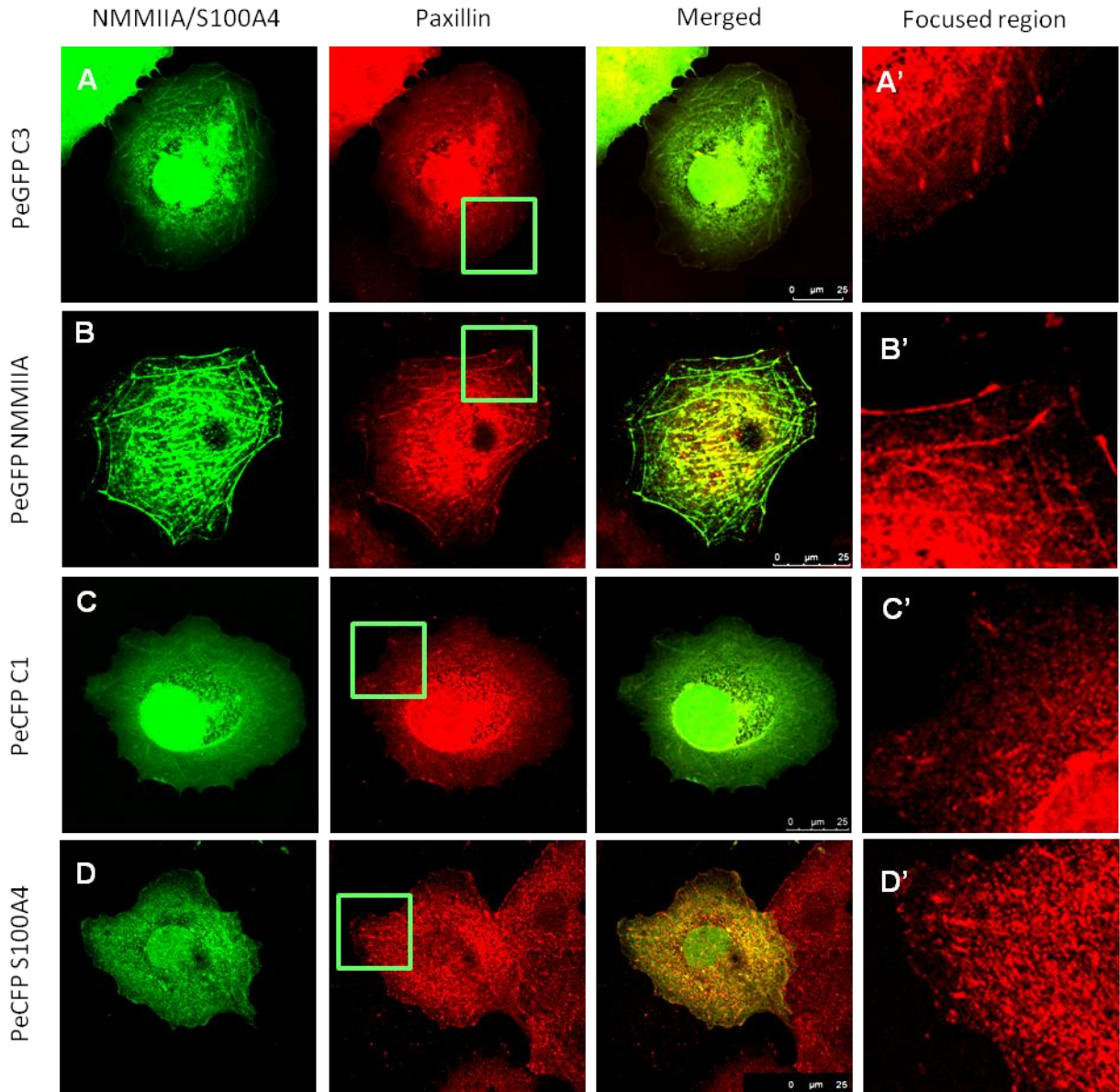


Figure 4.2.22 Introduction of S100A4 protein into Cos 7 cells leads to polarisation while significant increase of paxillin clusters were observed in NMMIIA expressing Cos 7 cells. Cells were seeded and transfected as described in figure 4.2.14 but without any inhibitor treatment and stained for paxillin. Cos 7 cells transfected with control vector, PeGFP C3 were labeled as A - A' whereas PeGFP NMMIIA transfected cells were labeled as B - B'. Cos 7 cells transfected with control for PeCFP S100A4 (PeCFP C1) were labeled as C - C' and those transfected with PeCFP S100A4 WT were labeled as D - D'. Panels A', B', C' and D' correspond to focused regions of the cell. Scale bar = 25 μ m. Images displayed for each cell line were representative image obtained from 3 independent experiments. Methods are fully detailed in Chapter 2.2.8.

Cos 7 cells	Number of focal adhesions (paxillin) per cell \pm s.e. (n=10)	P-value ^a	P-value ^b
PeGFP C3 Plasmid	13.2 \pm 2.5		
PeGFP NMMIIA Plasmid	25.4 \pm 3.9	3.64786E-08	
PeCFP C1 Plasmid	14.5 \pm 3.4		
PeCFP S100A4 WT Plasmid	1 \pm 1.6	7.94897E-11	4.07187E-13

Table 4.2.2 Introduction of NMMIIA and S100A4 into Cos 7 cells causes opposing effect on focal adhesion clusters. Images for quantification were obtained as described in figure 4.2.21 and random images were selected and quantified manually by counting the number of clusters localised at the periphery of each cell. Results are mean values \pm s.e. from 3 independent experiments (n=10).

^a P-value obtain from Student t-Test where number of paxillin clusters quantified in Cos 7 PeGFP NMMIIA and Cos 7 PeCFP S100A4 WT were compared to their respective controls (Cos 7 PeGFP C3 and Cos 7 PeCFP S100A4 WT).

^b P-value obtain from Student t-Test where number of paxillin clusters quantified in Cos 7 PeGFP NMMIIA were compared to Cos 7 PeCFP S100A4 WT.

Methods are fully detailed in Chapter 2.2.10.

4.3 Discussion

In depth studies has been conducted to demonstrate the roles of actin and NMMIIA in cell migration. It is generally accepted that the dynamic process of polymerisation and depolymerisation of actin is the critical steps in persistence of directive cell migration. Here, we focus on two protrusion structures results from polymerisation of actin at periphery of the cells; (1) lamellipodial actin network where Arp 2/3 complex mediating branching of actin filament; or (2) filopodial (lateral extension) or microvillus (dorsal extension) projections where Formin homology mediate monomeric polymerisation of linear F-actin (Pellegrin and Mellor, 2007, Olson and Sahai, 2009).

In the Rama 37 cell model used in this study, the control cells exhibited higher stress fibers along with focal adhesions clusters (paxillin), but lower wound healing properties whereas the S100A4 expressing cells were found to be more motile with low levels of focal adhesion clusters. As numerous studies had demonstrated the ability of S100A4 to interact with and disassemble NMMIIA, loss of dorsal stress fibers observed in the R37 S100A4 WT cell line may be a consequence of this interaction. Actin monomers are polymerised by actin-crosslinking proteins such as α -actinin, fascin, espin and filamin into linear polymerised structure known as actin filaments (Chen et al., 1999, Wang et al., 1975, Lazarides and Burridge, 1975). Around 10 to 30 of these linear actin filaments bundled alternately by NMMIIA and α -actinin into stress fibers. Upon phosphorylation, NMMIIA changes its conformation which resulted in acto-myosin contractility (Hotulainen and Lappalainen, 2006). Although this contraction is needed for migration, higher stress fibers are often associated with stationary cells and stress fibers are not required in migration (Deguchi and Sato, 2009, Burridge, 1981, Hall and Nobes, 2000). Here, we further strengthen this observation where the less motile cells exhibited thicker and more organised stress fibers across the cytoplasm (Rama 37 control cells when compared to R37 S100A4

WT cells and untreated cells to blebbistatin/Y-27632-treated Rama 37/ Cos 7 cells) (Figure 4.2.3, 4.2.6, 4.2.7, 4.2.14, 4.2.15, 4.2.19 and 4.2.20).

The treatment of Rama 37 control cells with blebbistatin or Y-27632 resulted in the Rama 37 control cell line acquiring similar phenotype as those expressing S100A4 proteins; such as loss of focal adhesions and stress fibers, increase of cell migration and long trailing ends morphology. Interestingly, increment of filopodia around the cells after Y-27632 treatment was not observed in blebbistatin treated cells (Figure 4.2.5 and 4.2.4 respectively). The increase of filopodia is consistent with other studies demonstrating the specificity roles of RhoA, Cdc42 and Rac. It was shown that RhoA is specific for formation of stress fibers and focal adhesion, Cdc42 regulates the formation of filopodia whereas Rac induces the formation of lamellipodia and membrane ruffles (Nobes and Hall, 1995, Hall, 1998). Since Y-27632 is specific for Rho kinase inhibition, it will only affect RhoA, but not Cdc42 or Rac, thus, the increase of filopodia in this case further demonstrate the specificity of Y-27632 inhibitory activity (Routhier et al., 2010, Chen et al., 2012, Wheeler and Ridley, 2004).

However, when R37 S100A4 WT cells were treated with blebbistatin or Y-27632, further increment of wound healing properties was observed (Figure 4.2.3). This enhancement was supported by the quantification of focal adhesion clusters where significant reduction was observed, along with loss of most existing transverse stress fibers when compared to the untreated controls (Figure 4.2.4). These results proposed two possibilities; (1) S100A4 protein may have similar affect as blebbistatin and Y-27632 where the disassembly of NMMIIA by S100A4 had not reached its saturation point in R37 S100A4 WT cells, hence addition of blebbistatin or Y-27632 resulted in extreme disruption of NMMIIA; or (2) S100A4 acts synergistically with the inhibitors to promote migration where NMMIIA disassembly is a consequence of S100A4 direct/indirect interactions with other signaling proteins such as CD44V6, E-cadherin, tissue inhibitor of

metalloproteinases 2 (TIMP-2) and matrix metalloproteinases (MMPs) (Lakshmi et al., 1997, Ma et al., 2010, Sherbet and Lakshmi, 1998, Zhang et al., 2011).

S100A4 has been shown to cause relocalisation of CD44V6, an isoform of the CD44 cell-surface glycoprotein which plays an important role in regulating cell-cell and cell-extracellular matrix adhesion. It has been demonstrated that up-regulation of S100A4 in ML8 cell lines resulted in clustering of CD44V6 as opposed to uniform distribution in control cells, suggesting the possibility of S100A4 regulating localisation of CD44V6 to facilitate cell motility (Lakshmi et al., 1997). Recently, specificity of CD44V6 regulation on cell motility has been demonstrated using anti-CD44V6 monoclonal antibody where general anti-CD44s antibody resulted in inhibition of cell adhesion, motility and invasion indirectly suggesting the possibility of S100A4-induced motility could be CD44V6 related (Afify et al., 2009). Besides, up-regulation of S100A4 were found to be inversely regulated with E-cadherin and TIMP2, a type 1 transmembrane protein which takes part in cell –cell adhesion and a natural inhibitor of MMPs, matricellular proteins important for matrix remodeling respectively. As TIMP2 was found to be down-regulated in the presence of high level of S100A4, increased expressions of MMPs, a group of extracellular matrix degrading protein, were detected. In another study, it has been demonstrated in a pull-down assay that S100A4 binds to Receptor for Advanced Glycation Endproducts (RAGE) leading to increased expression of MMP13 in chondrocytes which led to speculations if S100A4-RAGE interaction is responsible for other MMPs regulations (Yammani et al., 2006). Although the precise mechanisms of S100A4 regulating the expression of these proteins remained to be solved, these direct/indirect interactions highlighted the possibility of S100A4-induced motility may not be NMMIIA-specific.

In the immunofluorescence staining of actin in untreated R37 S100A4 WT cells, transverse arcs were still visible but dorsal and most ventral stress fibers were inhibited. It has been suggested that loss of focal adhesions causes disappearance of dorsal stress fibers as dorsal stress

fibers are formed from focal adhesion (Burrige and Wittchen, 2013, Tojkander et al., 2012). This observation indicated the possibility of S100A4 either capable of directly or indirectly inhibit focal adhesions, resulting in loss of dorsal stress fibers but leaving transverse arcs intact as arcs formation is strictly dependent on NMMII activity (Hotulainen and Lappalainen, 2006). In the experiment conducted with Cos 7 cells, it was observed that transverse arcs were still perceptible even in the cells overexpressing S100A4-CFP fusion protein. However, its focal adhesion clusters were significantly lower than Cos 7 cells that either expresses NMMIIA-GFP fusion protein or its control which devoid of NMMIIA. These observations proposed that S100A4 may have higher affinity to other signaling proteins which directly or indirectly involved in focal adhesion formation rather than NMMIIB.

Wound healing experiment with Cos 7 cells transfected with plasmid encoding the fusion protein S100A4-CFP demonstrated that S100A4 protein was capable of enhancing migration independent of NMMIIA. Although NMMIIB is present in Cos 7 cells and S100A4 has been demonstrated to bind to NMMIIB at lower affinity than NMMIIA, its wound healing roles could be disregarded as studies has demonstrated that, in NMMIIB-null embryonic stem (ES) cells, there was no increment in cell migration whereas in the same study, NMMIIA-null ES cells resulted in enhancement of cell migration (Even-Ram et al., 2007). Also, in the same study, it was shown that long trailing ends were observed in NMMIIA-depleted cells and this observation is consistent with the morphology observed in our NMMIIA-depleted Rama 37 control cells (Figure 4.3.10 and 4.2.11). Similar morphology was observed in immunostaining when either Cos 7 or Rama 37 cells when treated with blebbistatin or Y-27632 inhibitor (Figure 4.2.15, 4.2.16, 4.2.17 and 4.2.18). It has been demonstrated that Y-27632, a Rho kinase inhibitor, prevents Rho-GTPase from interacting with the COOH terminal of coiled-coil domain of Rho kinase which resulted in deactivation of the phosphotransferase activity of Rho kinase and ultimately preventing signaling

of RhoA to Rho kinase to regulates the retraction of migrating monocytes which was depicted by the long trailing ends of our Y-27632-treated cell system (Worthylake and Burridge, 2003). Also, in Y-27632 treated cells, it was observed that the stress fibers localised at the center of the cells were affected, but stress fibers at the periphery of the cells were less affected which demonstrated the roles of Rho kinase in maintaining stress fibers and focal adhesions at the central of the cells (Katoh et al., 2001a, Katoh et al., 2001b, Totsukawa et al., 2000). Moreover, it was observed that in either blebbistatin or Y-27632 treated cells (Cos 7 or Rama 37 cells), significant reduction of focal adhesions were observed and pieces of motile cytoplasm were found (determined by no staining of nucleus with DAPI) which demonstrate the incapability of NMMII to retract its tail and acceleration of cells causes the pieces of motile cytoplasm to be left behind as cell migrate (Lo et al., 2004).

Fascinatingly, in R37 S100A4 WT cells, knockdown of NMMIIA did not result in increase of cell migration, instead, inhibition of cell migration was observed. Although there was a decrease in wound healing properties in NMMIIA-depleted R37 S100A4 WT cells, its overall motility was still higher than both NMMIIA-depleted Rama 37 control cells and Rama 37 control cells (+ NMMIIA). This showed that in extinction of NMMIIA, S100A4 still retained its ability to promote motility although not as efficient. This observation proposed that functionality of S100A4 is not dependent on NMMIIA, but availability of NMMIIA increased its potential to enhance cell motility. Studies have shown that deprivation of NMMIIA (as observed in NMMIIA knockdown Rama 37 cells system) resulted in destabilisation of microtubules at the edge of the cells and functional polymerised microtubules were associated with increase of velocity which is consistent with the trend observed with the exception of NMMIIA-knockdown R37 S100A4 WT cells where reduction of migration were observed (Even-Ram et al., 2007, Shutova et al., 2012). In the same studies, it was shown that blebbistatin treatments mimicked this destabilisation to enhance migration which

is also observed in the blebbistatin-treated cells in our experiments proposing that blebbistatin may be aiding S100A4 to enhance migration by localising NMMIIA monomer to close proximity with actin located at the leading edge as the actin binding affinity of blebbistatin-constricted NMMIIA monomer was not affected (Goeckeler et al., 2008).

It has been shown that inhibition of NMMIIA by blebbistatin resulted in enrichment of monomeric, MRLC phosphorylated form (pre-powerstroke state) of NMMIIA at the cell periphery but polymerisation was inhibited despite the ongoing MRLC phosphorylation where this conformation prevented its association but not binding affinity with actin filament (Takács et al., 2010, Goeckeler et al., 2008, Shutova et al., 2012). It was suggested that this unpolymerised but activated NMMIIA which initiates focal contacts should be a dominant but transient population in lamellipodia (Shutova et al., 2012). This study was supported by the findings that when cells are microinjected with a proteolytic fragment of myosin II containing the full motor head (HMM), but lacking the most of the rod-like tail and incapable of filament formation, the edge of cytoplasm of the cells were enriched with the HMM but little or no NMMIIA were present and this smaller fragment could localise to the leading edge of the cells more rapidly than the full length NMMIIA (Kolega, 2006). From this, it is likely that the disassembly of NMMIIA by blebbistatin resulted in more efficient localisation of NMMIIA to the leading edge to assist S100A4 to enhance migration. However, when NMMIIA level was depleted through SiRNA of R37 S100A4 WT cells, this assistance could be disrupted, resulting in less efficient migration.

As our data shown that both S100A4 overexpressing and non overexpressing cells exhibited enhanced migration after blebbistatin treatment, this may possibly suggest that S100A4-induced migration is independent of NMMIIA. This hypothesis is supported by the experiment using Cos 7 PeCFP S100A4 WT cells where improvement of cell migration in the absence of NMMIIA and further reduction of focal adhesions was demonstrated when compared

to Cos 7 PeCFP C1 control or Cos 7 PeGFP NMMIIA. This further reduction of focal adhesion via S100A4 overexpression suggested that S100A4 may be interacting with other target proteins to maneuver cell motility through reducing focal adhesion formations.

Chapter 5:

Targeting S100A4 protein in high throughput screen technology

Chapter 5: Targeting S100A4 protein in high throughput screen technology

5.1 Introduction.....	183
5.2 Results	
5.2.1 Preliminary screening of drugs effect on S100A4 with regards to wound healing.....	186
5.2.2 Secondary screening determining reproducibility and specificity of compound to S100A4 protein	191
5.2.3 Tertiary screening determining reproducibility and specificity of compound to S100A4 protein	197
5.2.4 Optimising working concentration of Apomorphine hydrochloride, 1S, 2R-phenylpropanolamine hydrochloride and Nylidrin hydrochloride	201
5.3 Discussion	204

5.1 Introduction

High throughput screening (HTS) is a process of screening and assaying a large number of effectors against specific target to accelerate drug discovery, especially in pharmaceutical industries. Effectors are usually chemical compounds whereas targets are usually cell membrane receptors which make up the largest group (45%), enzymes (28%), hormones (11%), unknowns (7%), ion channels (5%), nuclear receptors (2%), and finally target DNA (2%)(Martis et al., 2011).

HTS assays are categorised into 3 broad ranges; 1) biochemical assays, 2) ion-channel assays and 3) cell-based assay. In this report, we concentrate on cell-based assay which is further classified into 4 categories; 1) second messenger assay, 2) reporter gene assay, 3) cell proliferation assay, and 4) high content screening (HCS) (Hertzberg and Pope, 2000), or in our case, high content imaging (HCI) assay (sub category of HCS), where epifluorescence or light imaging platforms, combined with image analysis algorithms is utilised. In HCI assay, cells are bombarded with variety of chemical compounds and any phenotypic effects are captured. Effects that can be observed through this assay include cell cycle status, cell differentiation, nuclear and cell morphology, angiogenesis, metastasis and cell movement (Szymański et al., 2011, Yarrow et al., 2004).

As a rule of thumb, only 1% of the compounds tested in preliminary screening HTS will demonstrate antagonistic or agonistic effects which are referred to as 'hits'. Then, the hits will be validated again for reproducibility in secondary screening in which reproducible hits will be selected for optimisation. After optimisation of chemical compound concentration, modification will be done on the compound so that it is safe for human use. Modified chemical compound will then proceed to be tested in animal models for safety and effectiveness and finally to be tested in human.

Here, we concentrate on cell movement-based HCl assay where pre-treated monolayer of cell is wounded and the wound healing process is observed by taking time-lapse images over a specific period of time or until wound has completely healed. Depending on software, data such as migrational video, wound healing rate, mitotic index, cell polarisation, and matrix remodeling can be analysed. Screening of effects of drug-like compounds on wound healing has been successfully demonstrated with different effects such as inhibiting migration, affecting morphology, blocking completion of mitosis, and disrupting the cell monolayer has been observed through this assay (Yarrow et al., 2004).

As mentioned earlier, HTS assay requires effector against specific targets and here, the effectors used are numerous chemical compounds whereas the specific target is the S100A4 protein. *In vivo* studies have shown that the elevated expression of S100 proteins correlates with cancer progression and metastatic properties (Davies et al., 1994, Andersen et al., 2011, Andersen et al., 2004, Cabezón et al., 2007). In particular, the S100A4 protein which has been highlighted as metastatic promoter and regarded as potent marker for breast cancer prognosis where patient's mortality correlates with its elevation (Ismail et al., 2008a, Boye and Mælandsmo, 2010, Rudland et al., 2000). Recently, niclosamide, a drug initially developed to treat tapeworm infection, has been found to be effective against colon cancer via blocking the expression of S100A4 via reducing its mRNA expression (Sack et al., 2011, Helfman, 2011). Similarly, an anti-S100A4 blocking antibody has been found to suppress metastasis in mice lungs by binding to its recognition site which overlapped the target binding interface of S100A4 (Klingelhofer et al., 2012). Besides, in another study, a compound known as phenothiazines has been found to disrupt S100A4-NMMIIA interaction by inducing oligomerisation of S100A4 (Malashkevich et al., 2010). Therefore, using Rama 37 control and Rama 37 S100A4 WT cell lines combined with HCl-cell movement based-

assay, various chemical compounds were tested for their ability to affect S100A4-induced migration through wound healing assay to provide more insight of the protein activity.

5.2 Results

5.2.1 Preliminary screening of drugs effect on S100A4 with regards to wound healing

In collaboration with the Medical Research Council Technology, UK, more than 1400 different chemical compounds solubilised in 100% dimethyl sulfoxide (DMSO) were supplied to conduct initial screen. Before bombarding the Rama 37 cell lines with various chemical compounds, the effect of DMSO on cells viability were evaluated to establish the inhibitory prospects of the vehicle solution. This optimisation determined that the working concentration is 5 μ M per compound which accounts for 0.5% of DMSO.

In the primary screen, different effects on wound healing and cell behaviour were observed (Figure 5.2.1). The wound healing curves obtained in each 24 well plate were compared to their respective controls in the plate. First, the migrational curves of untreated R37 S100A4 WT cells were compared to those of the untreated Rama 37 control cells. The steeper curves displayed by untreated R37 S100A4 WT cells, indicate shorter time for wound closure. After comparing the untreated controls, the curves obtained from compound-treated R37 S100A4 WT cells were compared to the untreated counterparts (Figure 5.2.1 A). The effects observed were grouped into; slowing of migration, causing cell death, inhibition of migration, acceleration of migration and delayed of compound activity (Figure 5.2.1 B).

Out of all the chemical compounds screened, 30 hits were obtained (Table 5.2.1). These hits were classified into four groups; A) slowing migration, B) causing cell death, C) inhibiting migration, and D) accelerating migration. Chemical compounds that have delayed activity were classed into appropriate groups by observing the steepness of the curve after exerting its effects. It was observed that 19 of the chemical compounds slowed wound healing process (63.4 %), 4 compounds inhibit wound healing without causing cell death (13.3 %), 6 compounds caused cell

death (20.0 %) and finally, only one compound accelerates wound healing (3.3 %). Mefloquine, the only compound that accelerates wound healing, has no cross therapeutic properties when compared to the rest of the 29 hits. For the rest of the compounds, cross-therapeutic properties were observed between the 3 different groups. Compounds that have antibacterial property were shared among the groups that slow and inhibit migration, but not observed in the group that causes cell death whereas anti-inflammatory property were shared among the three groups. In the group where the compound causes cell death, pomiferin is the only compound that has antioxidant properties.

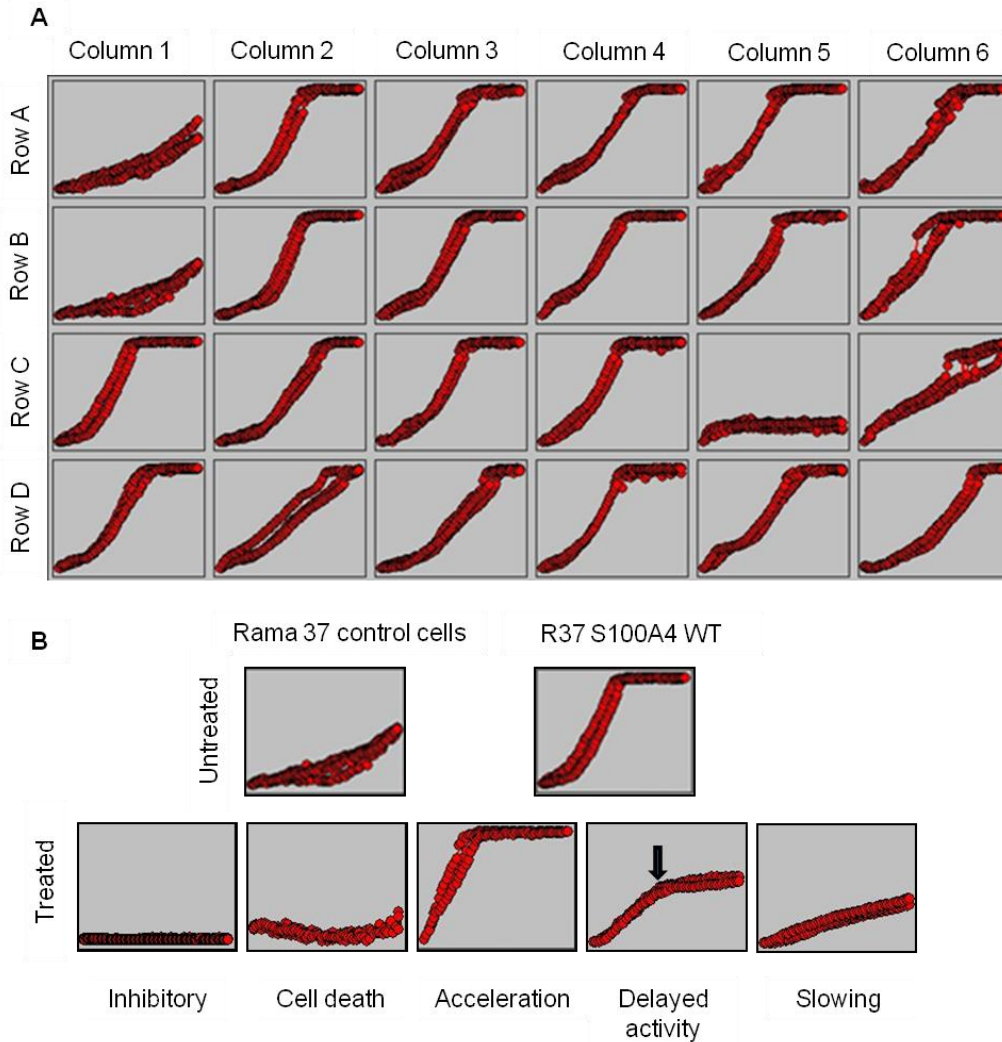


Figure 5.2.1 Preliminary screening showing different effects of chemical compounds on S100A4 protein through wound healing. Rama 37 cells (150,000 and 200,000 for Rama 37 control cells and R37 S100A4 WT cells respectively) were seeded in 24 well plate (as described in Figure 2.2.4) 48 hours prior to scratching and addition of 5 μ M compound. The process of wound healing was monitored by time-lapse imaging using CellIQ machine for 16 hours. The images were then analysed with CellIQ Analyser Software to obtain the curve table as shown. The different curves obtained were divided into different categories. A) Untreated controls are seeded in Column 1 whereas different chemical compounds were added in Column 2 - 6. B) Different wound healing effects caused by various chemical compounds were observed. Data shown is a representative image from the preliminary screen. Method is fully detailed in Chapter 2.2.4.

COMPOUND	THERAPEUTIC PROPERTIES
SLOWING MIGRATION GROUP	
CETYLPYRIDINIUM CHLORIDE	antiinfective (topical)
ANTIPYRINE	analgesic
APOMORPHINE HYDROCHLORIDE	emetic
CAFFEINE	CNS stimulant
ORPHENADRINE CITRATE	muscle relaxant (skeletal), antihistaminic
OXYBENZONE	ultraviolet screen
PHENINDIONE	Anticoagulant
NOVOBIOCIN SODIUM	Antibacterial
OXYTETRACYCLINE	Antibacterial
1S,2R-PHENYLPROPANOLAMINE HYDROCHLORIDE	decongestant, anorexic
NYLIDRIN HYDROCHLORIDE	vasodilator (peripheral)
PARACHLOROPHENOL	topical antibacterial (topical)
PHYSOSTIGMINE SALICYLATE	cholinergic, anticholinesterase, miotic
SALICYL ALCOHOL	anesthetic (local), antiinflammatory
TRIMEPRAZINE TARTRATE	Antipruritic
THIOGUANINE	antineoplastic, purine antimetabolite
PROTOVERATRINE B	antihypertensive, emetic; LD50(mouse) 0.21 mg/kg sc
3-AMINOPROPANESULPHONIC ACID	antibacterial; GABA agonist
NEROL	weak estrogen receptor blocker
CAUSING CELL DEATH GROUP	
COLCHICINE	antimitotic, antigout agent
SULOCTIDIL	peripheral vasodilator
CELASTROL	antineoplastic, antiinflammatory, NO synthesis inhibitor,

	chaperone stimulant
GAMBOGIC ACID	antiinflammatory, cytotoxic, inhibits HeLa cells in vitro
AMOXAPINE	antidepressant, inhibits norepinephrine uptake
PIROXICAM	antiinflammatory
INHIBITING MIGRATION GROUP	
MEPENZOLATE BROMIDE	Anticholinergic
FENBUFEN	antiinflammatory
FENOFIBRATE	antihyperlipidemic
CEFTIBUTEN	Antibacterial
ACCELERATING MIGRATION GROUP	
MEFLOQUINE	Antimalarial

Table 5.2.1 Out of 30 hits, compounds that slow migration occupy the largest group, followed by causing cell death, inhibition of wound healing and accelerate wound healing. Experiments were conducted as mentioned in figure 5.2.1 and different wound healing curves obtained through CellIQ Analyser Software were classified into respective groups.

5.2.2 Secondary screening to identify S100A4-specific cellular effects

Whilst the initial screen had identified differences in wound healing properties, it remained to be demonstrated if such phenotypic were cell or protein specific. We sought to establish the specificities of the compounds towards S100A4 protein. Hence, in the follow on screen, the specificity of the drug to S100A4 protein was determined by treating both Rama 37 control cells and R37 S100A4 cells with the same compound.

Figure 5.2.2 demonstrated that wound healing based-HCI is capable of distinguishing the effects of compound on S100A4 expressing and non-expressing cells. The Rama 37 control cells and R37 S100A4 WT cells, located adjacent to each other, were treated with the same compound and all the wound healing curves were compared to the untreated controls wells which were located in Row A, Column 1 – 4 (Figure 5.2.2 A). For instance, in figure 5.2.2 A, it was observed that the particular compound has effect only on Rama 37 control cells (Row B, Column 3), but not on R37 S100A4 WT cells (Row B, Column 4). Whereas in Row B Column 5 and 6 demonstrated that the compound affected both cell lines. Through this HCI-based wound healing analysis, the specificity of the compound against S100A4 protein can be discriminated. The distinctive curves were then classified into 3 groups as shown in figure 5.2.2 B; A) Affecting both cell lines B) Affecting only Rama 37 control cells and C) Affecting only R37 S100A4 WT cells, which only the latter is of interest as they correlates with the objectives of this chapter.

From the wound healing curves obtained, the steepness of the curve is calculated as wound closure rate ($\mu\text{m}^2\text{min}^{-1}$) and grouped in Table 5.2.2 which highlighted a good reproducibility when comparing the two screens. Since the specificity of the compound on S100A4 protein is of the main interest, those compounds that did not show any significant effect on wound healing properties of Rama 37 control cells but inhibit or slow down wound healing properties of cells

expressing S100A4 protein were selected for further analysis. Out of the 30 compounds, only 9 compounds met the requirement and were selected for tertiary screen. These compounds were apomorphine hydrochloride, novobiocin sodium, 1S, 2R-phenylpropanolamine hydrochloride, nylidrin hydrochloride, parachlorophenol, salicyl alcohol, trimeprazine tartrate, protoveratrine b and 3-aminopropanesulphonic acid. Mefloquine, the only compound that accelerates wound closure showed consistency in secondary screen, but the value obtained was not significant.

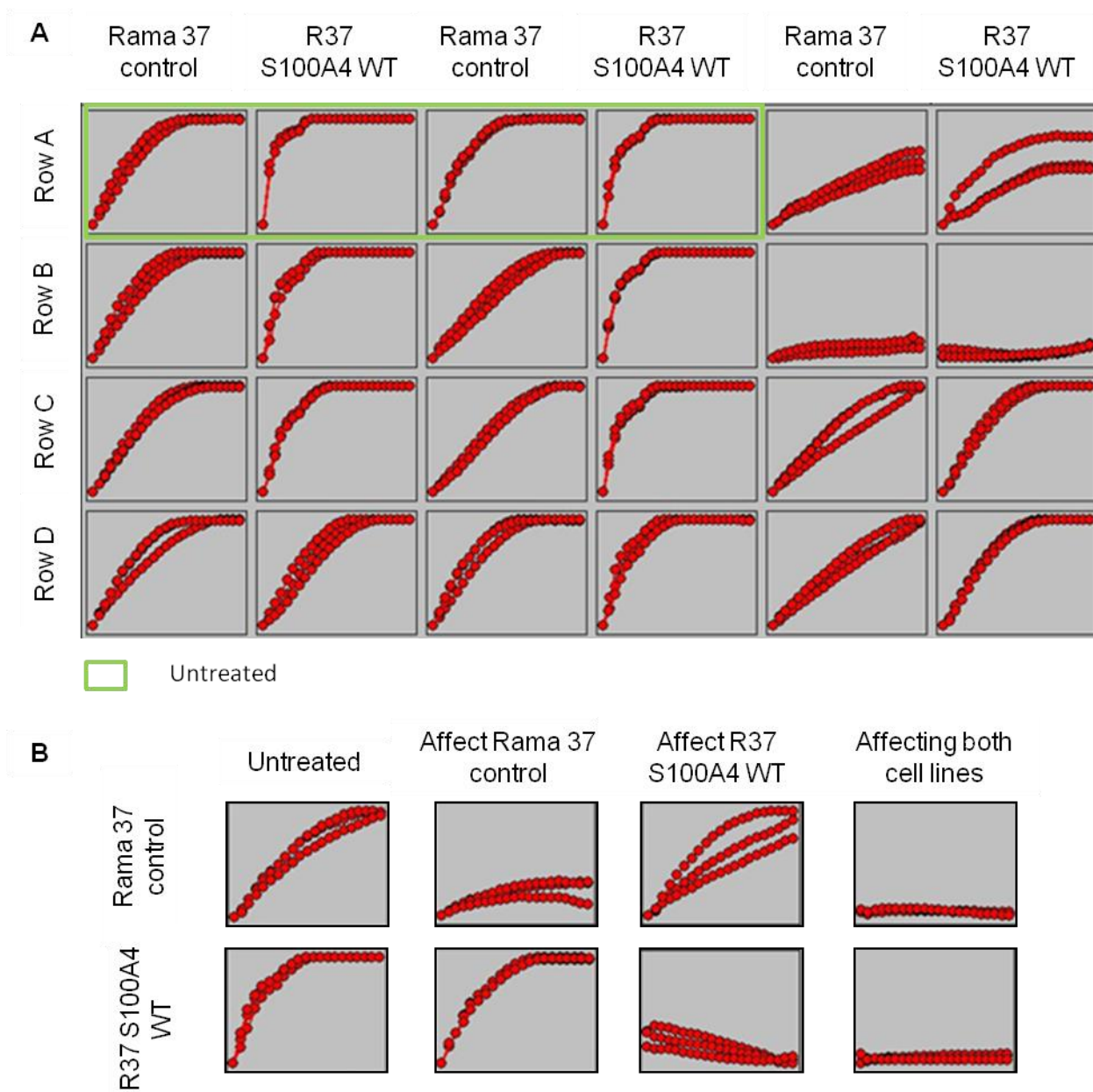


Figure 5.2.2 Specificity of compounds to S100A4 protein can be shown through wound healing based-HCI. The secondary screen is conducted as mentioned in figure 5.2.1 and the layout of the plate is as shown in figure 2.2.5. The different curves obtained were divided into different categories. A) Layout of 24 well plate as described in figure 2.2.4 showing wound closure curves. B) Different wound healing effects caused by various chemical compounds were observed. Data shown is a representative image from the secondary screen.

SLOWING MIGRATION GROUP				
UNTREATED	Rama 37 Control		R37 S100A4 WT	
	0.137 ± 0.02		0.213 ± 0.01	
COMPOUND (5µM)	Wound closure rate (µm²min⁻¹)	P-value^a	Wound closure rate (µm²min⁻¹)	P-value^b
CETILPYRIDINIUM CHLORIDE	death		0.059 ± 0.00	< 0.001
ANTIPYRINE	0.121 ± 0.01	0.259	0.258 ± 0.04	0.128
BUSULFAN	0.120 ± 0.02	0.300	0.154 ± 0.02	0.006
APOMORPHINE HYDROCHLORIDE	0.171 ± 0.03	0.194	0.144 ± 0.03	0.013
CAFFEINE	0.193 ± 0.04	0.077	0.250 ± 0.06	0.362
PHENINDIONE	0.141 ± 0.02	0.771	0.186 ± 0.04	0.428
NOVOBIOCIN SODIUM	0.120 ± 0.03	0.330	0.117 ± 0.01	0.015
OXYTETRACYCLINE	0.132 ± 0.04	0.832	0.165 ± 0.04	0.186
1S,2R-PHENYLPROPANOLAMINE HYDROCHLORIDE	0.104 ± 0.02	0.062	0.126 ± 0.02	0.025
NYLIDRIN HYDROCHLORIDE	0.135 ± 0.02	0.864	0.103 ± 0.03	0.016
PARACHLOROPHENOL	0.153 ± 0.06	0.605	0.151 ± 0.03	0.086
PHYSOSTIGMINE SALICYLATE	0.166 ± 0.01	0.004	0.183 ± 0.06	0.436
SALICYL ALCOHOL	0.131 ± 0.01	0.631	0.097 ± 0.03	0.003
TRIMEPRAZINE TARTRATE	0.148 ± 0.01	0.410	0.133 ± 0.01	0.001
THIOGUANINE	death		0.080 ± 0.01	<0.001
PROTOVERATRINE B	0.113 ± 0.02	0.148	0.141 ± 0.03	0.016
3-AMINOPROPANESULPHONIC ACID	0.157 ± 0.03	0.307	0.118 ± 0.02	0.002
NEROL	0.283 ± 0.01	0.012	0.268 ± 0.06	0.176

CAUSING CELL DEATH GROUP				
UNTREATED	Rama 37 Control		R37 S100A4 WT	
	0.137 ± 0.02		0.213 ± 0.01	
COMPOUND (5µM)	Wound closure rate (µm ² min ⁻¹)	P-value ^a	Wound closure rate (µm ² min ⁻¹)	P-value ^b
COLCHICINE	death		death	
SULOCTIDIL	<20 hours		<20 hours	
CELASTROL	death		death	
GAMBOGIC ACID	death		death	
AMOXAPINE	death		death	
PIROXICAM	death		death	

INHIBIT MIGRATION GROUP				
UNTREATED	Rama 37 Control		R37 S100A4 WT	
	0.137 ± 0.02		0.213 ± 0.01	
COMPOUND (5µM)	Wound closure rate (µm ² min ⁻¹)	P-value ^a	Wound closure rate (µm ² min ⁻¹)	P-value ^b
MEPENZOLATE BROMIDE	0.141 ± 0.04	0.855	0.173 ± 0.06	0.316
FENBUFEN	0.176 ± 0.02	0.053	0.180 ± 0.06	0.391
FENOFIBRATE	0.185 ± 0.04	0.104	0.156 ± 0.06	0.143
CEFTIBUTEN	0.145 ± 0.01	0.520	0.184 ± 0.02	0.066

ACCELERATING MIGRATION GROUP				
UNTREATED	Rama 37 Control		R37 S100A4 WT	
	0.137 ± 0.02		0.213 ± 0.01	
COMPOUND (5µM)	Wound closure rate (µm ² min ⁻¹)	P-value ^a	Wound closure rate (µm ² min ⁻¹)	P-value ^b
MEFLOQUINE	0.197 ± 0.02	0.028	0.229 ± 0.04	0.318

Table 5.2.2 High reproducibility of primary screen result is achieved and detailed calculation of wound area closure rate correlates with the wound healing curves. Experiment was conducted as mentioned in figure 5.2.1 and calculation of rate of wound area closure was as explained in Chapter 2.2.5.1. The calculated rate for each compound were organised in its respective group as shown in Table 5.2.1. Values obtained are mean ± s.e. from three different regions of the well in a single screen.

P-value^a obtain from Student t-Test where the rate of wound area closure of treated Rama 37 control cells were compared respectively to the untreated Rama 37 control cells.

P-value^b obtain from Student t-Test where the rate of wound area closure of treated R37 S100A4 WT were compared respectively to the untreated R37 S100A4 WT cells.

5.2.3 Tertiary screening determining reproducibility and specificity of compound to S100A4 protein

In the tertiary screen, the effect on the wound healing observed in both Rama 37 cell lines by the compound tested has to be reproducible. At the same time, the reproducible wound healing effect has to be specific to R37 S100A4 WT cells but not Rama 37 control cells so that the compound can be presumed to be explicitly targeting S100A4 protein, hence demonstrating the effect shown previously. As mentioned before, from the secondary screen, only 9 compounds were selected for tertiary screen. Out of the 9 compounds, 6 compounds did lower the rates of migration in R37 S100A4 WT cells, but the rates lowered were insignificant (Table 5.2.3). Interestingly, 3 compounds demonstrated high reproducibility and selectivity towards R37 S100A4 WT cells while having no significant effect on Rama 37 control cells motility (Figure 5.2.3 A).

The three compounds narrowed down were; 1) apomorphine hydrochloride, 2) 1S, 2R-phenylpropanolamine hydrochloride, and 3) nylidrin hydrochloride where they significantly inhibit migrational properties of R37 S100A4 WT cells ($P = 0.033$, $P = 0.009$, and $P = 0.006$ respectively), but not Rama 37 control cells ($P = 0.084$, $P = 0.385$, and $P = 0.564$ respectively) while not affecting the viabilities of both cell lines at $5\mu\text{M}$ of treatment (Figure 5.2.3 B).

To confirm this observation, the wound area healing rates from secondary screen for these three compounds were compared to the tertiary screen. Interestingly, similar trend were observed in all three compounds (data not depicted in histogram, refer to Table 5.2.2). It was found that when the untreated Rama 37 control cell were compared to those treated with apomorphine hydrochloride, 1S, 2R-phenylpropanolamine hydrochloride, and nylidrin hydrochloride, no significant difference were observed ($P = 0.194$, $P = 0.062$, and $P = 0.864$ respectively to untreated Rama 37 control) (Figure 5.2.3 A). However, significant difference were

observed when the same compounds were treated with R37 S100A4 WT cells ($P = 0.013$, $P = 0.025$, and $P = 0.016$ respectively) (Figure 5.2.3 A). To show that the inhibition of migration by the three compounds were not due to reduction of cell viability, MTT assays were performed. Except for Apomorphine hydrochloride, which reduced cell viability to 80% in Rama 37 control cells (as opposed to 100% of untreated Rama 37 control cells), but not in R37 S100A4 WT cells, the remaining compounds did not affect cell viability (Figure 5.2.3 B).

To further confirm this trend, the wound area closure rates for these three compounds from primary screen were calculated (data not shown). However, in the primary screen, the compounds were not treated on Rama 37 control cells (refer to Figure 2.2.4). Therefore, the treated R37 S100A4 WT cells were compared to both untreated R37 S100A4 WT cells and untreated Rama 37 control cells. The T-test comparison on either apomorphine hydrochloride, 1S, 2R-phenylpropanolamine hydrochloride or nylidrin hydrochloride treated R37 S100A4 WT cells to untreated Rama 37 control cells showed no significant difference in wound area closure rate ($P = 0.139$, $P = 0.064$, and $P = 0.574$ respectively). On the other hand, when the untreated R37 S100A4 WT cells were compared to treated R37 S100A4 WT cells, significantly lower wound closure rate were demonstrated ($P = 0.002$, $P = 0.001$, and $P = 0.021$ respectively).

9 DRUGS SELECTED FROM SECONDARY SCREEN				
UNTREATED	Rama 37 Control		R37 S100A4 WT	
	0.083 ± 0.03		0.229 ± 0.06	
COMPOUND (5µM)	Wound closure rate (µm ² min ⁻¹)	P-value ^a	Wound closure rate (µm ² min ⁻¹)	P-value ^b
APOMORPHINE HYDROCHLORIDE	0.110 ± 0.01	0.133	0.142 ± 0.04	0.054
NOVOBIOCIN SODIUM	0.104 ± 0.04	0.337	0.240 ± 0.07	0.813
1S,2R-PHENYLPROPANOLAMINE HYDROCHLORIDE	0.066 ± 0.02	0.360	0.130 ± 0.00	0.027
NYLIDRIN HYDROCHLORIDE	0.106 ± 0.05	0.408	0.122 ± 0.01	0.019
PARACHLOROPHENOL	0.094 ± 0.01	0.469	0.226 ± 0.10	0.963
SALICYL ALCOHOL	0.082 ± 0.03	0.950	0.191 ± 0.05	0.370
TRIMEPRAZINE TARTRATE	0.035 ± 0.01	0.084	0.225 ± 0.08	0.947
PROTOVERATRINE B	0.123 ± 0.01	0.147	0.189 ± 0.03	0.439
3-AMINOPROPANESULPHONIC ACID	0.060 ± 0.02	0.389	0.282 ± 0.12	0.456

Table 5.2.3 Tertiary screen showing 3 drugs having significant specificity towards R37 S100A4 WT cells but not Rama 37 control cells. Experiment was conducted as mentioned in figure 5.2.1 and calculation of rate of wound area closure was as explained in Chapter 2.2.5.1. Values obtained are mean ± s.e. from three different regions of the well in a single screen.

P-value^a obtain from Student t-Test where the rate of wound area closure of treated Rama 37 control cells were compared respectively to the untreated Rama 37 control cells.

P-value^b obtain from Student t-Test where the rate of wound area closure of treated R37 S100A4 WT were compared respectively to the untreated R37 S100A4 WT cells.

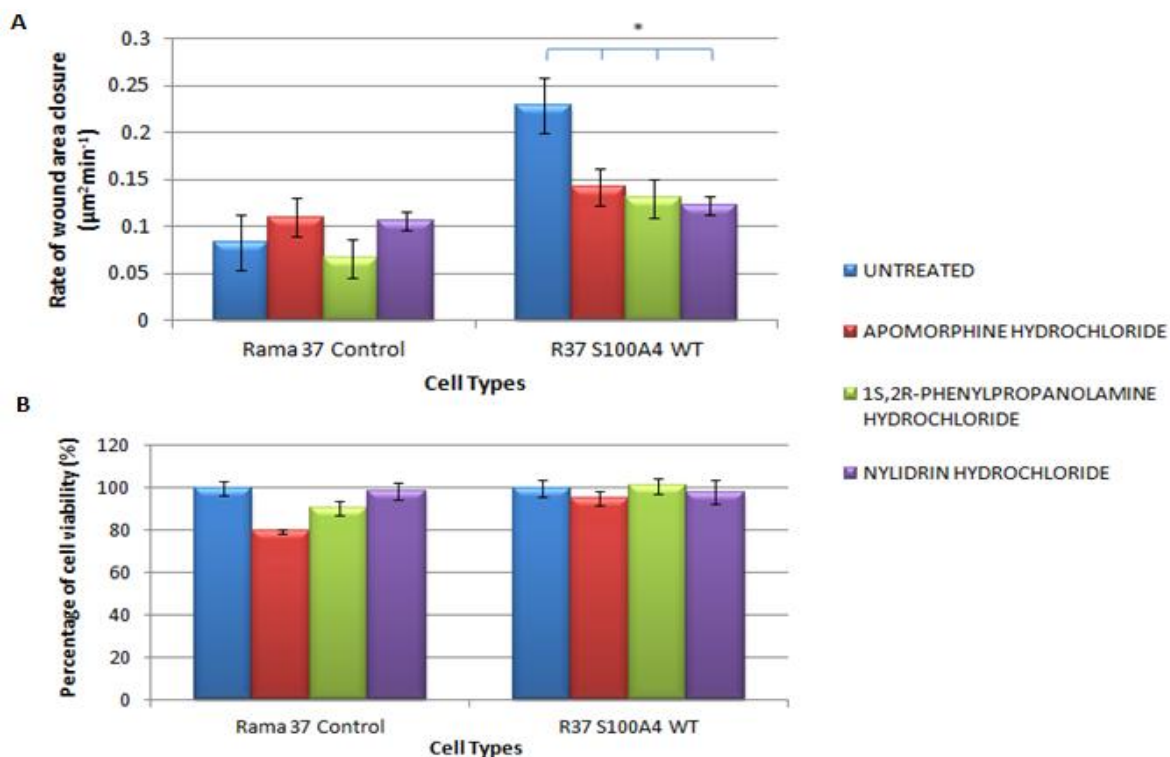


Figure 5.2.3 Compounds demonstrating reproducibility and specificity for S100A4 protein whilst not affecting cell viability. Experiment was conducted as mentioned in figure 5.2.1 and calculation of rate of wound area closure was as explained in Chapter 2.2.5.1. The wound closure rates for compounds that show reproducibility and specificity to S100A4 protein were depicted in histogram above. A) Rate of untreated, apomorphine hydrochloride, 1S, 2R-phenylpropanolamine hydrochloride and nyldrin hydrochloride treated Rama 37 cell lines from tertiary screening. Values obtained are mean \pm s.e. from three different regions of the well in a single screen. *P < 0.05. B) Percentage of cell viability 24 hour post treatment. Equal number of Rama 37 cells was seeded and left to incubate for 24 hours. Then, specific compounds were added to each well and 24 hours later, MTT assay were conducted as mentioned in Chapter 2.2.3. The first time points were taken at 100% viable and values were converted to percentages. Values obtained are mean \pm s.e. from three different wells form a single experiment.

5.2.4 Optimising working concentration of Apomorphine hydrochloride, 1S, 2R-phenylpropanolamine hydrochloride and Nylidrin hydrochloride

Having confirmed the effects of apomorphine hydrochloride, 1S, 2R-phenylpropanolamine hydrochloride and nylidrin hydrochloride on Rama 37 cell lines at 5 μ M, we proceeded to determine a dose-response curve using same assay. Concentration of the compound ranges from 0.04 to 25.00 μ M were tested in both Rama 37 cell lines.

This experiment demonstrated 5 μ M as the optimal working concentration to inhibit wound healing (apomorphine hydrochloride, 1S, 2R-phenylpropanolamine hydrochloride and nylidrin hydrochloride) (Figure 5.2.4). At 25 μ M, Rama 37 control cells were more susceptible to apomorphine hydrochloride and nylidrin hydrochloride as cell death were observed in wound healing assay whereas there is no significant difference in wound healing in 1S, 2R-phenylpropanolamine hydrochloride treatment (Figure 5.2.4 A). However, when R37 S100A4 WT were treated with similar concentration, significant reduction in migration were observed when compared to untreated sample, but not cell death (all compounds showed $P < 0.001$) (Figure 5.2.4B). Consistently, when the three compounds were added to Rama 37 control cells, no significant difference in wound area closure rate were observed in concentration of 5 μ M or less. On the other hand, treatment of R37 S100A4 WT with 5 μ M of apomorphine hydrochloride, 1S, 2R-phenylpropanolamine hydrochloride and nylidrin hydrochloride significantly affected wound healing properties as observed in all the previous screens ($P = 0.046$, $P = 0.002$, $P = 0.012$ respectively) and this concentration is the lowest active concentration as all the compounds showed no effect on R37 S100A4 WT migration below this concentration.

Also, R37 S100A4 WT cells treated with 1S, 2R-phenylpropanolamine hydrochloride and nylidrin hydrochloride showed significant difference within the group, indicating that higher

concentration of these drugs will affect its wound closure rate ($P = 0.003$ respectively). However, in Rama 37 control cells, only 1S, 2R-phenylpropanolamine hydrochloride treated cells showed significant concentration dependent response ($P = 0.004$), but not nylidrin hydrochloride-treated Rama 37 control cells ($P = 0.674$). From this, it showed that apomorphine hydrochloride is less likely to affect motility in higher concentration as there are no significant differences in both treated-Rama 37 control cells and -R37 S100A4 WT cells ($P = 0.968$ and $P = 0.173$ respectively).

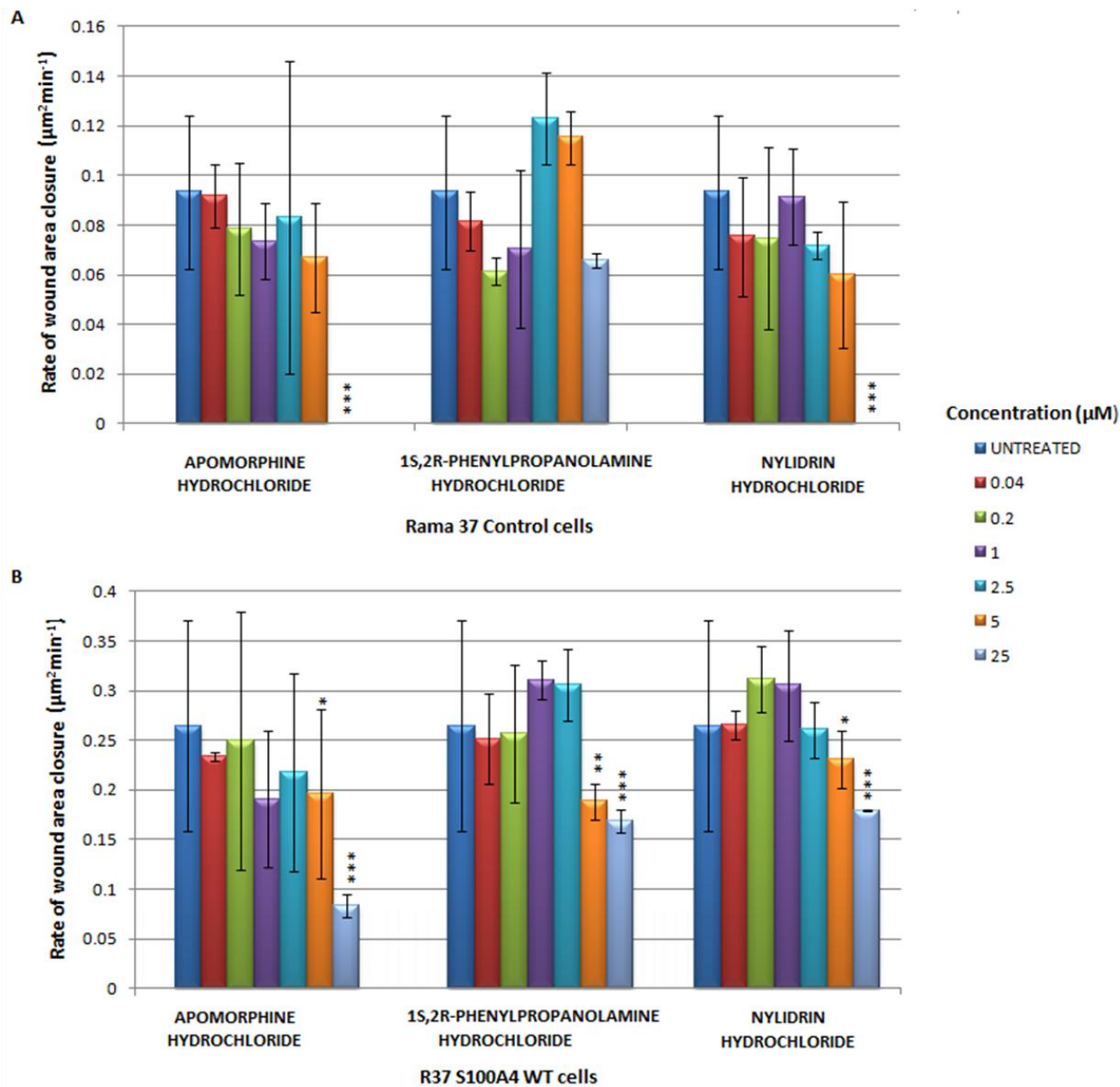


Figure 5.2.4 Optimisation of working concentration of the selected compounds through wound healing assay shows 5 μM as optimal. Experiment was conducted as mentioned in figure 5.2.1 with different concentrations (ranges from 0.04 to 25 μM) of apomorphine hydrochloride, 1S, 2R-phenylpropanolamine hydrochloride and nyldrin hydrochloride and calculation of rate of wound area closure was calculated as in Chapter 2.2.5.1. The wound closure rates of A) Rama 37 control cells and B) R37 S100A4 WT cell lines treated with different concentrations. Values obtained are mean \pm s.e. from three different regions of the well in a single screen. Statistical analyses were conducted using single factor ANOVA. *P < 0.05, ** P < 0.01 and *** P < 0.001.

5.3 Discussion

Since the development of high throughput screening (HTS), the major aim has been set to miniaturise samples to produce higher efficiency. Wound healing assay, one of the HTS, has routinely been used to study cell migration and its underlying mechanisms such as polarisation, matrix remodelling, and chemotaxis (Lampugnani, 1999, Fischer et al., 1990, Herren et al., 2001, Huang et al., 2003, Lu et al., 2004). As mentioned before, S100 proteins, especially S100A4, has a well established reputation as metastasis promoter in carcinoma ranges from oral, esophageal, lung, breast, gastric, colorectal, pancreatic to skin. Due to this, numerous work has been dedicated on this protein in an effort to provide more insights and ideally, to generate new avenues for therapeutic purposes.

Here, we set to investigate if wound healing could be used with our cell system to provide more insight about S100A4 proteins and its effect on cell migration. Using Rama 37 cell lines combined with HCI-based assay, specificity of chemical compounds to S100A4 protein can be tested. Surprisingly, given that the primary and secondary screen were conducted a year apart, relatively high reproducibility was demonstrated with this assay. From primary to tertiary screens, similar wound healing trends were exhibited by the 3 chemical compounds selected (apomorphine hydrochloride, 1S, 2R-phenylpropanolamine hydrochloride (also known as phenylpropanolamine) and nylidrin hydrochloride (also known as tolazoline). These three compounds were found to affect the migratory properties of S100A4 overexpressing cells but not its control counterpart. Therefore, this result suggests that these compounds affect S100A4-induced wound healing, although the mechanisms regulating such properties are currently unknown.

There were no therapeutic links found between these three compounds as they were prescribed as emetic (apomorphine hydrochloride), decongestant (1S, 2R-phenylpropanolamine

hydrochloride) and vasodilator (nylidrin hydrochloride) respectively. Their taxonomy substructures revealed that these three compounds shared 3 substructures among themselves; 1) Benzene and derivatives, 2) Phenethylamines and 3) Aromatic compounds and act as agonist to Class A of G-protein coupled receptors (GPCRs) (Zhu et al., 2012). GPCRs form the largest family of membrane proteins, characterised by the presence of seven transmembrane-helices separated by alternating intracellular and extracellular loops (Rosenbaum et al., 2009, Foord et al., 2005). Coincidentally, these three compounds act as agonist to Class A of GPCRs which is also known as rhodopsin-like class. Apomorphine hydrochloride was found to be exerting its agonist effect through D2, D3 and D4 dopamine receptors, α - (2C and 2B) and β -adrenergic receptors (Kvernmo et al., 2008, Kim et al., 2001, Millan et al., 2002). On the other hand, the other two compounds, were found to promote activity of α - (1A and 2A) adrenergic receptors (Imming et al., 2006, Wellman et al., 1997, Flavahan, 2005, Niemeyer et al., 1987, Santala et al., 1990).

Generally, GPCRs acts as a transducer where extracellular stimuli produced through binding of cell surface ligands is sent into the cell to secondary messengers known as heterotrimeric guanine nucleotide-binding protein (G-proteins), which consists of G_{α} , G_{β} , and G_{γ} subunits (Gong et al., 2010). The activation of GPCR by extracellular ligand causes conformational changes in the GPCR which in turn activate G-proteins by acting as guanine nucleotide exchange factor (GEF), where GDP is replaced by GTP. This causes the GTP bound- α subunit of the G-protein to dissociate from the $\beta\gamma$ -complex (Neer, 1994). The dissociated G_{α} subunit and $G_{\beta\gamma}$ -complex (combinations of 7 different β and 12 different γ subunits) can independently activate downstream effectors such as adenylyl cyclase, phosphodiesterases, phospholipase C, and ion channels (Svoboda et al., 2004). Although G_{α} subunit consists of more than 20 members that are divided into four main groups, there are only two main downstream pathways; 1) the cAMP signal pathway and 2) the phosphatidylinositol signal pathway (Figure 5.3.1).

Apomorphine hydrochloride is a dopamine 2 receptor (DR2) agonist prescribed to treat acute poisoning by inducing potent emetic as well as to treat alcoholism by suppressing craving for alcohol (Scherkl et al., 1990, Dent, 1949). Dopamine receptors are divided into two main groups according to their biochemical and pharmacological properties; 1) D1-like (comprises of D1 and D5) receptors release G_s subunit proteins which stimulate adenylyl cyclase while; 2) D2-like (comprises of D2, D3, and D4) receptors releases $G_{i/o}$ subunits which inhibit adenylyl cyclase (Prou et al., 2001) (Figure 5.4.1). DR2 has been shown to interact with FLN-A (non-muscle filamin or actin binding protein ABP280) which resulted in inhibition adenylyl cyclase activities and subsequently, modulating activities of potassium (K^+) and calcium (Ca^{2+}) channels (Li et al., 2000, Seabrook et al., 1994). Cross-talk between DR2 and intracellular Ca^{2+} concentrations, $[Ca^{2+}]_i$, was established in a study where it was demonstrated that influx of Ca^{2+} resulted in elevation of $[Ca^{2+}]_i$ which inhibit DR2 through interaction with calmodulin (Bofill-Cardona et al., 2000). Inhibition of adenylyl cyclase (ADC) by DR2 agonist (in this case, apomorphine hydrochloride) could possibly resulted in decrease of intracellular cAMP, which directly reduces protein kinase A (PKA) and ultimately causing reduction in intracellular $[Ca^{2+}]_i$ (Sontag et al., 1990, Bigornia et al., 1990). Interestingly, DR2 levels are usually low in normal mammary gland tissue, but this level were found to be aberrantly upregulated in malignant breast carcinoma (Carlo et al., 1986). Since the level of DR2 has never been assessed in these cell systems, but it would be worth to further investigate if this level is increased. However, in the current state of the work, the primary focus is on S100A4 induced motility.

On the other hand, the other two compounds (1S, 2R-phenylpropanolamine hydrochloride and nylidrin hydrochloride), are known to agonise α_{2a} adrenergic receptor (A2AR); member of G-protein-coupled family of transmembrane receptors (Zhu et al., 2012). Binding of A2AR agonists to such receptor has been shown to induce release of $G\alpha_i$ subunits leading to inhibition of adenylyl

cyclase and phospholipase C (PLC) activities and causes depletion of intracellular $[Ca^{2+}]$. PLC hydrolyses phospholipid phosphatidylinositol 4,5-bisphosphate (PIP_2) into diacyl glycerol (DAG) and inositol 1,4,5-triphosphate (IP_3). While DAG remained on the membrane to activate protein kinase C, IP_3 is released into the cytosol to bind with IP_3 receptors located on the smooth endoplasmic reticulum (ER). IP_3 receptors which is a Ca^{2+} channel, will therefore, release Ca^{2+} stored in the ER (Figure 5.4.1) (Teoh et al., 2012, Billington and Penn, 2003, Pohl et al., 1997). However, since PLC activity is inhibited by A2AR agonists, the level of $[Ca^{2+}]$ in the cytosolic region should be depleted (Haenisch et al., 2010, Ma et al., 2005).

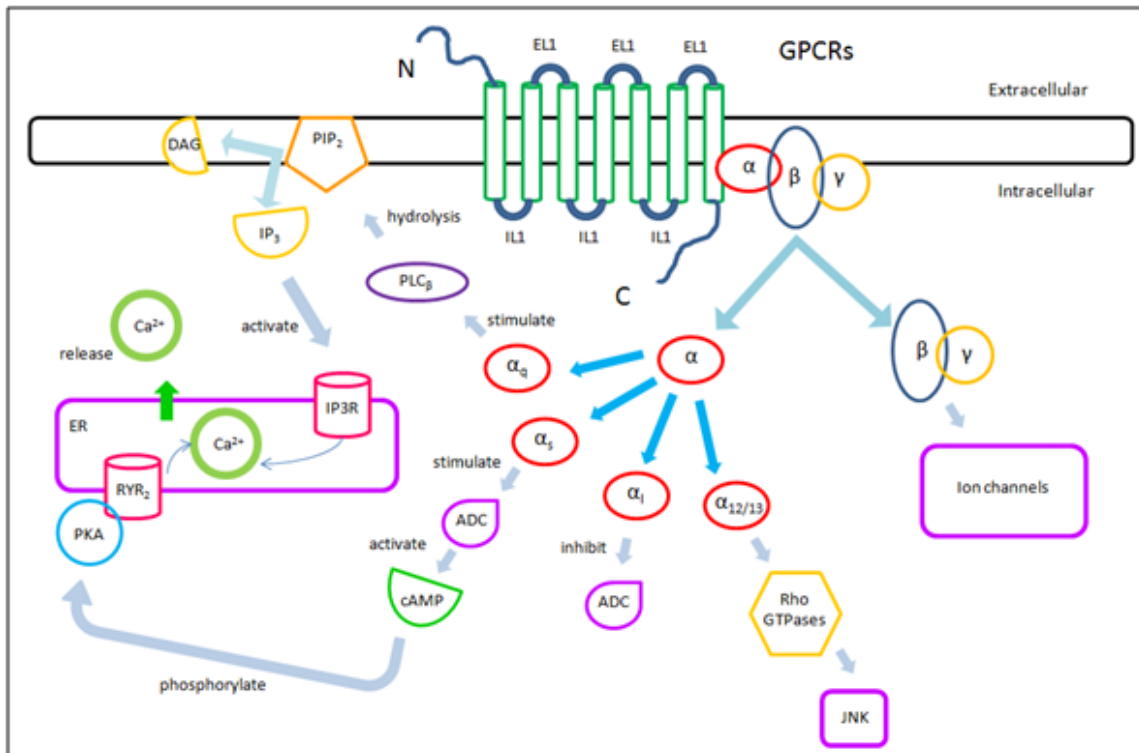


Figure 5.3.1. Mobilisation of calcium through GPCRs triggered pathway. Intracellular Ca²⁺ is released through multiple action of secondary messengers. Extracellular ligands bind to GPCRs causing the release of different isoforms of G-α subunits and βγ-complexes. Here, D2-like receptors (stimulated by apomorphine hydrochloride) as well as A2AR (stimulated by 1S, 2R-phenylpropanolamine hydrochloride and nylidrin hydrochloride) resulted in release of G_{αi} subunits which inhibit ADC. G_{αs} subunits, antagonist of G_{αi} subunits, released through dopamine 1-like receptors activate ADC which in turn produces cAMP to activate PKA. Activation of PKA phosphorylate RYR₂, a Ca²⁺ release channel. On the other hand, G_q subunits release are stimulated by M₁₋₃ receptors which activate PLC_β to cleave PIP₂ into DAG (which remain bound to the membrane) and IP₃ which diffuse into the cytosolic region and bind to IP₃R, another Ca²⁺ channel located on the ER. This activation release Ca²⁺ from ER into the cytosolic region. G_{α12/13} subunits released will bind to Rho GEFs which in turn activate small GTPases and finally activate Rho kinase. Depending on the isoforms of Gβγ subunit, it can either directly bind to ion channels or activate PLA. GPCR, G-protein coupled receptor; D2-like, Dopamine 2-like receptor; A2AR, α-2-adrenergic receptor; ADC, adenylyl cyclase; cAMP, cyclic adenosine monophosphate; PKA, protein kinase A; RYR₂, ryanodin receptor 2; M₁₋₃, muscarinic 1-3 receptor; PLC, phospholipase C; PIP₂, Phosphatidylinositol 4,5-bisphosphate; DAG, diacylglycerol; IP₃, phosphatidylinositol (3,4,5)-triphosphate; IP₃R, IP3 receptor; ER, endoplasmic reticulum; PLA, phospholipase A₂.

Through profiling the three compounds, depletion of $[Ca^{2+}]$ in the cytosolic region seemed to be their mutual effect. While it is highly unlikely that overall intracellular depletion of $[Ca^{2+}]$ could be the reason behind the inhibitory effect observed in R37 S100A4 WT cells, one cannot rule out the possibility that localised intracellular levels of Ca^{2+} may potentially play a role in regulating S100A4 activities. Relocalisation of S100A4 from the perinuclear towards the cell periphery upon $[Ca^{2+}]$ increase has been demonstrated in both MDA MB231 cells and HELA cells using 3 different approaches, but showing the same results; 1) ionophore A23187 which serves to transport Ca^{2+} through the plasma membrane, 2) cyclic ADP-ribose which induces the release of Ca^{2+} from IP_3 -insensitive ER stores and 3) thapsigargin (TG) which induces the release of Ca^{2+} from IP_3 -sensitive ER stores (Mueller et al., 1999). Therefore, it is possible that the depletion of intracellular $[Ca^{2+}]$ could potentially inhibit relocalisation of S100A4 which subsequently affected its interactions with target proteins located at the cell periphery.

Interestingly, it has been demonstrated that apomorphine can specifically reduce S100B secretion in three different rat brain preparations (hippocampal slices, cortical astrocytes and C6 glioma cells) (Nardin et al., 2011). Although the direct or indirect modulation of apomorphine on S100B remained unknown, it was proposed that this effect could possibly be regulated by dopamine receptor and/or serotonin receptors. Since S100A4 and S100B share 48% of identity, it is possible that apomorphine hydrochloride could affect S100A4 in similar manner. Similar to dopamine receptor, serotonin receptors (also known as 5-hydroxytryptamine (5-HT) receptors) belongs to Class A of GPCRs, consisting of 14 or more subtypes, where binding of 5-HT (substrate) to 5-HT receptor resulted in dissociation of G_α subunit and $G_{\beta\gamma}$ -complex as mentioned in figure 5.3.1.

Although there is no work relating S100A4 to dopamine receptors, it has been shown that S100A4 is regulated by both 5-HT receptor and serotonin reuptake transporter (SERT) (Lawrie et al., 2005). SERT are dependent on extracellular sodium and chloride ions, where it selectively binds a sodium ion followed by a chloride ion extracellularly resulting in the transporter flipping inside the cell, releasing 5-HT (serotonin) intracellularly. Then, a potassium ion binds to the transporter intracellularly which caused the transporter to flip outwards of the cell, continuing the cycle (Figure 5.3.2)(Stahl, 1998). In their study, it was found that addition of exogenous 5-HT to human artery pulmonary smooth muscle cells (hAP-SMC) resulted in stimulation of 5-HT receptors to secretion of S100A4 into media. It was found that inhibition of 5-HT 2A and 5-HT 2B receptors did not block S100A4 secretion, but inhibition of 5-HT 1B receptor resulted in inhibition of S100A4 secretion. In SERT SiRNA-transfected hAP-SMCs, addition of 5-HT did not induce S100A4 secretion, showing that both SERT and 5-HT receptors are essential in regulating secretion of S100A4 through an unknown mechanism (Lawrie et al., 2005). It was speculated that 5-HT 1B receptor mediates phosphorylation of extracellular signal-regulated kinases (ERKs) while 5-HT transporter allows translocation of phosphorylated ERK to the nucleus to stimulate S100A4 expression which led to its secretion. In the Rama 37 cell system used, extracellular S100A4 concentrations were not determined prior and post treatment with the 3 compounds, hence it is possible that these 3 compounds inhibit the expression and/or secretion of S100A4 into extracellular matrix mediated by 5-HT receptor in conjunction with SERT to induce migration.

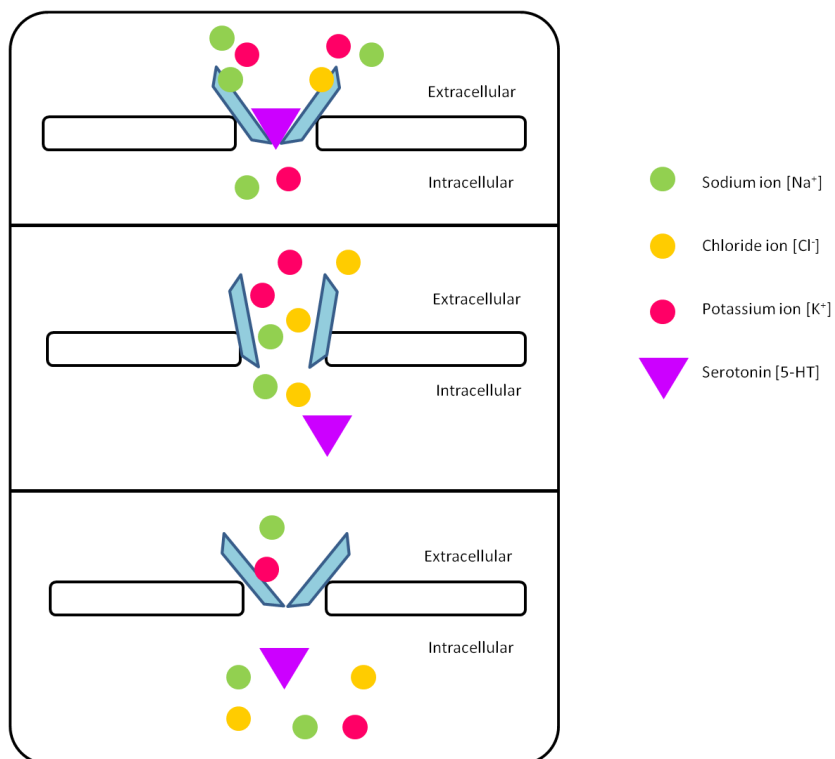


Figure 5.3.2 Mechanism of uptake of serotonin through SERT. Extracellularly, SERT is bound to one of each sodium and chloride ions resulting in opening of SERT transporter to recruit serotonin into the cytoplasm. Binding of a potassium ion upon release of bound sodium and chloride ions causes closing of transmembrane transporter.

If expression of S100A4 is lowered as speculated, the inhibitory effect observed in wound healing assay could be due to unavailability of S100A4 protein to exert its effect on intracellular targets such as NMMIIA, actin, TMs, liprin β 1 and yet to be identified proteins to induce cell motility. Besides, it has been demonstrated that expression of S100A4 is inversely correlated to the expression of E-cadherin and this similar trend has been repetitively exhibited by different carcinoma cell lines, such as skin, breast, lung, gastric, prostate, esophageal and thyroid (Keirsebilck et al., 1998, Perl et al., 1998, Yonemura et al., 2000b, Andersen et al., 2004, Moriyama-Kita et al., 2005). This correlation was further demonstrated with reduction of E-

cadherin expression after transfecting oral squamous cell carcinoma (OSCC) cell lines (expresses E-cadherin) with S100A4-expression vector (Moriyama-Kita et al., 2005). Down-regulation of E-cadherin has been linked to reduced cell-cell adhesion which led to mesenchymal morphology, increased cell migration, invasion as well as metastasis (reviewed by Rodriguez et al., 2012). Besides, suppression of S100A4 expression has also been linked to suppression of matrix metalloproteinase (MMP) 2, MMP 3 and MMP 9 (Zhang et al., 2011, Gao et al., 2005, Bjornland et al., 1999, Andersen et al., 2011, Saleem et al., 2006). As its name suggests, MMPs are proteinase that degrades extracellular matrix proteins to facilitate matrix remodeling (Nagase et al., 2006). If the chemical compound exerted their effect through suppression of S100A4 expression, it is possible that E-cadherin could be up-regulated whereas MMPs could be down-regulated.

Although the interactions between S100A4 and MMPs remained unresolved, it has been clearly demonstrated that addition of exogenous S100A4 induces MMP 3 expression whereas transfection of S100A4-expression vector increases MMP 2 and MMP 9 expressions (Andersen et al., 2011, Mathisen et al., 2003, Saleem et al., 2006). Interestingly, upregulation of these three MMPs has been shown to induce epithelial-mesenchymal transition (EMT) which led to carcinoma malignancy (Sternlicht et al., 1999, Tester et al., 2000). It remained elusive as to how exogenous S100A4 induce MMP 3 expression, nonetheless, this finding highlighted the role of extracellular S100A4 in inducing cell motility.

From all these observations, there is a possibility that the 3 compounds (apomorphine hydrochloride, 1S, 2R-phenylpropanolamine hydrochloride and nylidrin hydrochloride) inhibit expression and/or secretion of extracellular S100A4 mediated by 5-HT receptor in conjunction with SERT which resulted in overall reduced cell motility observed? Although these speculations remain vague, we have demonstrated that HCl-based assay as an effective drug discovery method

and in the future, these compounds could possibly be tested in animal models to demonstrate its efficacy in inhibiting metastasis cause by S100A4 overexpression.

Chapter 6:

General Discussion

Chapter 6: General Discussion

Due to diversity of S100 protein family's functions, they have been intensely studied in researches from all areas including neuroscience, cardiovascular, oncology, proteomic, immunology, histology, biochemistry, and even dermatology. Through these various areas of research, in depth understanding of these proteins have been exploited to realise their potentials in generating new therapeutic avenues. So far, S100A1 has been introduced in clinical trial for gene therapy to combat heart failure as diminishing level of S100A1 correlates with heart failure (Most et al., 2013). On the other hand, S100A4 is now regarded as a powerful palliating tool and an important marker of patient prognosis (Ismail et al., 2008a, Rudland et al., 2000, Andersen et al., 2011, Xue et al., 2003, Wang et al., 2010, Yonemura et al., 2000b, Ikenaga et al., 2009, Kimura et al., 2000, Zou et al., 2004). In an attempt to combat S100A4 promoted metastasis, an anti-S100A4 blocking antibody has been identified as a potential therapeutic avenue as animal models treated with this antibody has lower incidence of lung metastases. This antibody is generated in such a way that it binds to the recognition site which overlapped the target binding interface of S100A4 (Klingelhofer et al., 2012). Besides, another compound known as niclosamide has also been identified as a potential candidate where it has been found to be effective against S100A4-mediated colon cancer as it significantly reduce mRNA expression of S100A4 (Helfman, 2011, Sack et al., 2011).

To further diversify our therapeutic arsenal, first, we have to acquire more understanding of the proteins' structure and functions, including its different binding partners and subsequent downstream effects within cells. Therefore, we aimed to provide more insights on molecular mechanism of mediated by S100A4 to facilitate migration. While there are abundant reports demonstrating the potential role for NMMIIA in the S100A4-dependent migration, the direct link between the proteins in vivo remains elusive (Badyal et al., 2011, Elliott et al., 2012, House et al.,

2011, Ismail et al., 2008b, Kiss et al., 2012, Chen et al., 2001, Ford et al., 1997). No studies, for instance, have shown if S100A4 is capable of promoting migration in the absence of NMMIIA or when activity of NMMIIA is inhibited; both of which are the aims of this work.

Initially, we demonstrated that overexpression of wild type S100A4 in Rama 37 cells resulted in more efficient wound healing when compared to Rama 37 control cells. This is the first time, to our knowledge that S100A4 can promote wound healing in breast tumourigenic cells, providing yet another evidence for this protein to promote cellular migration. However, overexpressions of truncated versions of S100A4 ($\Delta 2$ and $\Delta 6$ from C terminus of S100A4 protein) did not improve migration, revealing the importance of the C terminus of this protein (Figure 3.2.1). Consistently, enhancement of migration due to overexpression of wild type S100A4 proteins was observed along with reduction of matured focal complexes (Figure 3.2.3 and 3.2.4), replacement of stable filopodia by out-spread lamellipodium (Figure 3.2.5 and 3.2.6) and loss of stress fibers. However, none of these traits were observed in the Rama 37 cells overexpressing truncated versions of S100A4 and the Rama 37 control cells. This observation suggested that only full length S100A4 could exert such effects and the truncation of C-terminus resulted in loss of S100A4 activity either by; 1) preventing the dimerisation of the protein, 2) preventing them from binding to NMMIIA or other target proteins, 3) calcium binding abilities and 4) other unknown functions.

So far, no work has been done to show if deletion of 2 or 6 amino acids from C-terminus of S100A4 protein will prevent dimerisation of the protein, but it has been demonstrated that this deletions led to reduced binding affinity of S100A4 to NMMIIA (Ismail et al., 2008b, Ismail et al., 2010). Two independent reports, has shown that only amino acids from region 72 – 91 contributed to the dimerisation in vitro whereas in vivo, only Phe 72, Tyr 75, Phe 78 and Leu 79 were essential (Tarabykina et al., 2001, Ismail et al., 2010). From this, we speculated that the

truncation of 2 or 6 amino acids from C-terminus of S100A4 protein should not prevent dimerisation, thus leaving three other possibilities. The EF hand motifs (helix E-loop-helixF) of S100A4 flanked from amino acids 12 – 47 and 50 – 84, proposing that deletions of 2 or 6 amino acids from the C terminus end should not inhibit its calcium binding capability (Kiss et al., 2012). However, we could not rule out the possibility that deletion of 2 or 6 amino acids could possibly alter the conformation of S100A4, thereby reducing its affinity for calcium or alternatively, limits its target proteins range or prevent its binding to NMMIIA. Following this, we aimed to demonstrate if inhibition of NMMIIA could result in reduced motility, as exhibited by truncated versions of S100A4 as it is impossible to demonstrate if the range of S100A4's target proteins is reduced, unless all of its binding partners have been identified.

As mentioned previously, overexpression of S100A4 led to modifications of several structures within the Rama 37 cells. It is unknown whether S100A4 directly resulted in the loss of stress fibers through NMMIIA disassembly or this loss is a consequence of reduction of matured focal complex by S100A4. Contradictory reports have demonstrated that loss of stress fibers could result in reduction of focal complex and vice versa. It has been demonstrated that dorsal stress fibers emerge from focal adhesions via actin polymerisation mediated by mDia formins where F-actins were crosslinked by α -actinin 1 (Cramer et al., 1997, Hotulainen and Lappalainen, 2006, Burridge and Wittchen, 2013, Kovac et al., 2013). Directly bonded behind the dorsal stress fibers are transverse arcs; generated via assembly of short actin bundles by Arp 2/3 complexes where NMMII and α -actinin are incorporated at the same time to produce a more regular structure and occasionally, extra NMMII may be added to generate a centripetal shape (Hotulainen and Lappalainen, 2006). It has been demonstrated that during contraction mediated by dorsal stress fibers-transverse arcs structure (having at least two focal adhesions from corresponding dorsal stress fibers), the transverse arcs regions that were not associated to the two dorsal stress fibers

began dissociating, leading to formation of ventral stress fiber; characterised by having focal adhesion at either end (Hotulainen and Lappalainen, 2006, Naumanen et al., 2008). Ambiguous to this, it has been reported that although dorsal stress fibers arose from focal adhesions, this structure served nothing more than a structural template as inhibition of actin polymerisation via mDia or knockdown of α -actinin prevented the maturation of focal adhesion even though tension exerted by NMMII in transverse arcs remained unaffected (Oakes et al., 2012). This work also demonstrated that reduction of tension by 80% did not prevent maturation of focal adhesion, proposing that maturation of focal adhesion could be a NMMII-independent process. Due to this contradiction, we could not conclude if overexpression of S100A4 inhibits maturation of focal adhesion which led to disassembly of stress fibers or vice versa. Following this, we set out to investigate if S100A4-induced motility is a NMMIIA-dependent process or a consequence of focal adhesion reduction.

Using live cell analysis, it was demonstrated that reduction of filopodia was not due to incapability of filopodia formation in R37 S100A4 WT cells, filopodia formation was, in fact, accelerated in this cell lines when compared to either Rama 37 control or the truncated versions (Table 3.2.9). Further investigation indicated that filopodia formed were not able to adhere stably to the extracellular matrix. This observation suggested the possibility of S100A4 preventing the adherence of filopodia rather than inhibiting its formation. Since NMMIIA is not present in filopodia, it may be possible that S100A4 is exerting this effect through other target proteins which may directly or indirectly facilitate filopodia formation (such as fascin, Arp 2/3 complex, Cdc42, IRSp53, Ena/VASP, actin, etc.) causing filopodia destabilisation. It has been demonstrated that stably adhered filopodia are essential for subsequent maturation of focal adhesion via recruitment of focal adhesion proteins such as talin, Paxillin, vinculin and focal adhesion kinase to activated integrins located at the tip of filopodia (Wiesner et al., 2005, Mitra et al., 2005, Calderwood, 2004,

Tomar and Schlaepfer, 2009, Schaller, 2001, Humphries et al., 2007). If S100A4 is regulating other target proteins, does this mean that NMMIIA disassembly is just a consequence of focal adhesion reduction in order to facilitate migration?

To address this, experiments were conducted to establish a direct link between NMMIIA and S100A4 in facilitating migration. First, it was observed that NMMIIA expression was reduced in S100A4 WT overexpressing cells and contractile forces exerted by these cells were significantly lower than those exerted by R37 S100A4 $\Delta 2$, R37 S100A4 $\Delta 6$ and Rama 37 control cells (Table 3.2.10). It is unclear whether this lower contractile force generated by R37 S100A4 WT cells is due to lower level of NMMIIA expression or inability of S100A4 WT overexpressing cells to generate contractile forces. As numerous reports have demonstrated that S100A4 is capable of regulating E-cadherin or MMPs expressions, we speculated that the down-regulation of NMMIIA could possibly be regulated through the same mechanism, which is yet to be solved. It has been demonstrated that expression of E-cadherin was reduced in oral squamous carcinoma cells (OSCCs) when transfected with S100A4 expressing vector whereas MMP 2 and MMP 9 were up-regulated, thus proposing that NMMIIA expression could be regulated in the same way (Moriyama-Kita et al., 2005, Mathisen et al., 2003, Saleem et al., 2006, Andersen et al., 2011). Moreover, as contractile force arose from tension generated by NMMII interacting with actin, disassembly of NMMII filaments by S100A4 could possibly be the culprit behind this observation (Chen et al., 2001, Ismail et al., 2010, Li and Bresnick, 2006, Badyal et al., 2011, Elliott et al., 2012, House et al., 2011). Overall, these observations remained consistent that expression of S100A4 resulted in lower contractile forces in cells possibly due to lower number of matured focal complexes and reduced NMMIIA expression.

Since it has been demonstrated that highly motile R37 S100A4 WT cells generate lower overall contractile forces, reduced focal adhesions as well as disorganised actin filaments, we set

to establish if such S100A4-induced effects were NMMIIA dependent. For this, two NMMII inhibitors were used; 1) blebbistatin, a NMMIIA specific ATPase inhibitor and 2) Y-27632, a Rho kinase inhibitor. Interestingly, we found that inhibition of NMMII led to increase of migration in Rama 37 cell systems with further enhancement of motility in S100A4 overexpressing cells (Figure 4.2.8). This, therefore, indicates that S100A4 could promote cellular motility even in an environment where NMMII contractibility is inhibited and such enhancement after inhibitors treatment could possibly be due to; 1) amount of NMMII surpasses that of S100A4, hence inhibitors facilitate S100A4 to disassemble NMMII or 2) S100A4 is regulating other target protein to facilitate cell motility and inhibition of NMMII by inhibitors synergistically facilitate this activity. It was also observed that the enhancement of motility in the R37 S100A4 WT cells treated with NMMII inhibitors, also present further reduction of focal adhesions (paxillin) through immunofluorescence staining (Figure 4.2.9 and 4.2.10). This observation appeared to be consistent with the previous experiments conducted where motility were found to be inversely correlated with number of focal adhesions.

However, these experiments could not directly establish whether enhancement of wound healing in cells overexpressing S100A4 protein is indeed NMMIIA dependent. Thus, we resorted to Cos 7 cell lines as alternative to provide more conclusive evidences. These cells have been widely used as they are the sole experimental system available where NMMIIA expression is ablated, whilst no changes are seen for NMMIIB and/or NMMIIC. In the wound healing assay conducted, the increase in S100A4 levels resulted in significant improvement in wound healing when compared to its control counterpart (Figure 4.2.25). This result therefore clearly demonstrated that S100A4 could promote cell migration in the absence of NMMIIA. At cellular level, Cos 7 overexpressing S100A4 protein showed significant reduction in focal adhesions number whereas restoration of NMMIIA in Cos 7 cells led to increment of focal adhesions and impediment of

wound healing (Table 4.2.2). Also, it was observed that in S100A4 expressing (Cos 7) cells retained its transverse arcs, but no dorsal or ventral stress fibers were observed. Contrasting effect were observed in NMMIIA expressing (Cos 7) cells; where visible dorsal and ventral stress fibers were observed along with numerous focal adhesions (Figure 4.2.26). Even though NMMIIA has been shown to be the dominator in transverse arcs, presence of NMMIIB were still detectable proposing that in the absence of NMMIIA, NMMIIB could be incorporated into actin filaments along with α -actinin to form transverse arcs observed in Cos 7 cells (Vallénus, 2013). It has been shown that S100A4 has 9-fold higher affinity for NMMIIA than NMMIIB, hence we hypothesised S100A4 can selectively bind to NMMIIB in the absence of NMMIIA in Cos 7 cells. However, the presence of transverse arcs in Cos 7 PeCFP S100A4 WT cells proposed there could be other target proteins in which S100A4 could interact with to regulate the maturation of focal adhesions and/or facilitate motility as it has been demonstrated that inhibition of NMMIIB in NMMIIA-null ES cells causes remaining stress fibers to disintegrate (Li et al., 2003, Zhang et al., 2005, Even-Ram et al., 2007). Furthermore, it has been demonstrated that ventral stress fibers are rich in NMMIIB but, the disappearance of ventral stress fibers (characterised by having focal complex located at either end) and retention of transverse arcs (characterised by having no association with focal complex) in S100A4 overexpressing Cos 7 cells indicated that S100A4 did not disassemble NMMIIB, but instead, the loss of focal adhesions leading to disappearance of ventral stress fibers deemed more appropriate.

To determine if this NMMIIA independent effect of motility was a cell-specific feature, we justify this effect using NMMIIA SiRNA technology in Rama 37 cell system. Knockdown of NMMIIA expression by over 80% resulted in increased cell migration along with reduction of focal adhesion (Figure 4.2.15 and 4.2.16). Consistent with our other findings in Cos 7 cells, this demonstrate that presence of NMMIIA in cells resulted in lower cellular migration and more mature focal adhesion

and similar observations have been demonstrated in the same cell line by Even-Ram et al. in 2007. Interestingly, it was observed that knockdown of NMMIIA causes reduction of cell motility in cell expressing high level of S100A4 but the rate of migration were still significantly faster than those of the control cells (Figure 4.2.15). This intermediate wound healing properties of R37 S100A4 WT (- NMMIIA) cells when compared to R37 S100A4 WT (+ NMMIIA) and Rama 37 control (+/- NMMIIA) cells proposed the possibility of NMMIIA providing assistance to S100A4 in regulating cell motility as R37 S100A4 WT (- NMMIIA) was slower than R37 S100A4 (+ NMMIIA) cells. However, as R37 S100A4 (- NMMIIA) cells exhibited faster wound healing rate than both Rama 37 control (+/- NMMIIA) cells we speculate that S100A4 could also regulate cell motility independent of NMMIIA as shown previously using Cos 7 cell lines. The inhibitory effect observed in wound healing assay conducted on R37 S100A4 WT (- NMMIIA) as opposed to R37 S100A4 WT (+ NMMIIA) as well as further enhancement in NMMIIA inhibitors-treated cells proposed that disassembly of NMMIIA could assist S100A4 in cell migration but is not essential. It has been demonstrated that treatment of cells with blebbistatin caused NMMII to be constricted in a pre-powerstroke monomeric conformation which was more efficiently localised to the periphery of the cell where it was proposed that this monomeric-unpolymerised NMMII conformation should be dominant but transient population in the lamellipodia to initiate focal adhesions (Takács et al., 2010, Goeckeler et al., 2008, Shutova et al., 2012, Kolega, 2006). Furthermore, NMMIIA has been found to directly interact with $\alpha_4\beta_3$ integrins and $\alpha_4\beta_1$ integrins where association of NMMIIA- $\alpha_4\beta_1$ integrin has been demonstrated to facilitate cell motility in CHO cells (Sajid et al., 2000, Rivera Rosado et al., 2011). Due to these associations, it was proposed that $\alpha_4\beta_3$ integrins and $\alpha_4\beta_1$ integrins may not be the only integrin isoforms that interacts with NMMIIA. On the other hand, blocking of $\alpha_5\beta_1$ integrins has been shown to reduce S100A4-mediated motility (Wang and Griffin, 2013) which led us to presume that the reduction of cell motility in R37 S100A4 WT (-NMMIIA) as

opposed to R37 S100A4 WT (+ NMMIIA) could be due to unavailability of NMMIIA to interact with integrins to further assist S100A4-mediated motility. As it has been shown that fragment of NMMII consisting only of the full motor head were more efficiently localised to the cell periphery than the full length of NMMIIA, the enhancement of motility post blebbistatin treatment in all Rama 37 cells seems befitting as monomeric NMMIIA should be more efficiently localised to associate with integrins to facilitate motility. However, the exact mechanism employed by S100A4 to facilitate migration remained elusive.

In the final chapter, Rama 37 cell system was used in HCI based assay to identify compound that may be capable of inhibiting cell migration induced by overexpression of S100A4. Interestingly, after rounds of selection and analysis, 3 independent compounds were found to be capable of affecting wound healing properties of R37 S100A4 WT cells but not Rama 37 control cells, highlighting their specificity for targeting S100A4-mediated motility. These compounds could possibly shed some light on how S100A4 regulate cell motility if not develop for in vivo treatment in animal model. One of the compounds, apomorphine hydrochloride, was found to regulate the secretion of S100B to extracellular matrix and these three compound were found to affect the GPCRs and this proposed that setting NMMIIA aside, there could be other S100A4 potential targets to regulate cell motility (Nardin et al., 2011, Carlo et al., 1986, Scherkl et al., 1990).

Although we have demonstrated that S100A4-induced motility is NMMIIA-independent, the exact mechanism utilised by S100A4 to maneuver motility remained elusive. In the future, the possible mechanisms should be explored. Therefore, we proposed that treatment of Rama 37 cells and Cos 7 cells with exogenous recombinant S100A4 protein and anti-S100A4 blocking antibody could shed some light if extracellular S100A4 is responsible for S100A4-induced motility. Also, using co-immunoprecipitation or pull down assay to investigate if S100A4 could be directly/

indirectly interacting with focal adhesion-related protein such as; 1) different integrin isoforms (especially $\alpha_5\beta_1$ integrin as it has been shown to be up-regulated when S100A4 is overexpressed with reduced motility when blocked), 2) fascin, as S100A4 has been shown to destabilise filopodia and fascin is present within the shaft, 3) Ena-VASP and Arp 2/3 complex, as these proteins has been shown to be the precursor to lamellipodium and filopodium formation, and 4) paxillin, vinculin, talin and FAK as they are primary proteins to be recruited to activated integrins to form focal complex. These approaches could further identify the binding partners of S100A4 as well as investigate the potential role of exogenous S100A4 in facilitating motility.

References

References

- ABERCROMBIE, M., HEAYSMAN, J. E. M. & PEGRUM, S. M. 1970. The locomotion of fibroblasts in culture. III. Movements of particles on the dorsal surface of the leading lamella. *Experimental Cell Research*, 62, 389-398.
- ADAMS, J. C. & SCHWARTZ, M. A. 2000. Stimulation of fascin spikes by thrombospondin-1 is mediated by the GTPases Rac and Cdc42. *J Cell Biol*, 150, 807-22.
- AFIFY, A., PURNELL, P. & NGUYEN, L. 2009. Role of CD44s and CD44v6 on human breast cancer cell adhesion, migration, and invasion. *Experimental and Molecular Pathology*, 86, 95-100.
- AMANO, M., ITO, M., KIMURA, K., FUKATA, Y., CHIHARA, K., NAKANO, T., MATSUURA, Y. & KAIBUCHI, K. 1996. Phosphorylation and Activation of Myosin by Rho-associated Kinase (Rho-kinase). *Journal of Biological Chemistry*, 271, 20246-20249.
- AMANO, M., NAKAYAMA, M. & KAIBUCHI, K. 2010. Rho-kinase/ROCK: A key regulator of the cytoskeleton and cell polarity. *Cytoskeleton (Hoboken)*, 67, 545-54.
- AMBARTSUMIAN, N., GRIGORIAN, M. & LUKANIDIN, E. 2005. Genetically modified mouse models to study the role of metastasis-promoting S100A4(mts1) protein in metastatic mammary cancer. *J Dairy Res*, 72 Spec No, 27-33.
- AMBARTSUMIAN, N., KLINGELHOFER, J., GRIGORIAN, M., CHRISTENSEN, C., KRIAJEVSKA, M., TULCHINSKY, E., GEORGIEV, G., BEREZIN, V., BOCK, E., RYGAARD, J., CAO, R., CAO, Y. & LUKANIDIN, E. 2001. The metastasis-associated Mts1(S100A4) protein could act as an angiogenic factor. *Oncogene*, 20, 4685-95.
- AMIEVA, M. R. & FURTHMAYR, H. 1995. Subcellular Localization of Moesin in Dynamic Filopodia, Retraction Fibers, and Other Structures Involved in Substrate Exploration, Attachment, and Cell-Cell Contacts. *Experimental Cell Research*, 219, 180-196.
- ANDERSEN, K., MORI, H., FATA, J., BASCOM, J., ØYJORD, T., MÆLANDSMO, G. M. & BISSELL, M. 2011. The metastasis-promoting protein S100A4 regulates mammary branching morphogenesis. *Developmental Biology*, 352, 181-190.

- ANDERSEN, K., NESLAND, J. M., HOLM, R., FLORENES, V. A., FODSTAD, O. & MALANDSMO, G. M. 2004. Expression of S100A4 combined with reduced E-cadherin expression predicts patient outcome in malignant melanoma. *Mod Pathol*, 17, 990-997.
- ASANO, S., HAMAOKA, K. & HOSOYA, H. 2009. Direct evidence for roles of phosphorylated regulatory light chain of myosin II in furrow ingression during cytokinesis in HeLa cells. *Genes to Cells*, 14, 555-568.
- BACHMANN, C., FISCHER, L., WALTER, U. & REINHARD, M. 1999. The EVH2 domain of the vasodilator-stimulated phosphoprotein mediates tetramerization, F-actin binding, and actin bundle formation. *J Biol Chem*, 274, 23549-57.
- BADYAL, S. K., BASRAN, J., BHANJI, N., KIM, J. H., CHAVDA, A. P., JUNG, H. S., CRAIG, R., ELLIOTT, P. R., IRVINE, A. F., BARSUKOV, I. L., KRIAJEVSKA, M. & BAGSHAW, C. R. 2011. Mechanism of the Ca²⁺-Dependent Interaction between S100A4 and Tail Fragments of Nonmuscle Myosin Heavy Chain IIA. *Journal of Molecular Biology*, 405, 1004-1026.
- BAILLY, M. & CONDEELIS, J. 2002. Cell motility: insights from the backstage. *Nat Cell Biol*, 4, E292-E294.
- BALL, L. J., KUHNE, R., HOFFMANN, B., HAFNER, A., SCHMIEDER, P., VOLKMER-ENGERT, R., HOF, M., WAHL, M., SCHNEIDER-MERGENER, J., WALTER, U., OSCHKINAT, H. & JARCHAU, T. 2000. Dual epitope recognition by the VASP EVH1 domain modulates polyproline ligand specificity and binding affinity. *EMBO J*, 19, 4903-14.
- BARRACLOUGH, R. 1998. Calcium-binding protein S100A4 in health and disease. *Biochimica et Biophysica Acta (BBA) - Molecular Cell Research*, 1448, 190-199.
- BARRACLOUGH, R., GIBBS, F., SMITH, J. A., HAYNES, G. A. & RUDLAND, P. S. 1990. Calcium-ion binding by the potential calcium-ion-binding protein, p9Ka. *Biochem Biophys Res Commun*, 169, 660-6.
- BARRACLOUGH, R., SAVIN, J., DUBE, S. K. & RUDLAND, P. S. 1987. Molecular cloning and sequence of the gene for p9Ka. A cultured myoepithelial cell protein with strong homology to S-100, a calcium-binding protein. *J Mol Biol*, 198, 13-20.

- BASU, G. D., AZORSA, D. O., KIEFER, J. A., ROJAS, A. M., TUZMEN, S., BARRETT, M. T., TRENT, J. M., KALLIONIEMI, O. & MOUSSES, S. 2008. Functional evidence implicating S100P in prostate cancer progression. *International Journal of Cancer*, 123, 330-339.
- BEAR, J. E. & GERTLER, F. B. 2009. Ena/VASP: towards resolving a pointed controversy at the barbed end. *Journal of Cell Science*, 122, 1947-1953.
- BEAR, J. E., SVITKINA, T. M., KRAUSE, M., SCHAFFER, D. A., LOUREIRO, J. J., STRASSER, G. A., MALY, I. V., CHAGA, O. Y., COOPER, J. A., BORISY, G. G. & GERTLER, F. B. 2002. Antagonism between Ena/VASP proteins and actin filament capping regulates fibroblast motility. *Cell*, 109, 509-21.
- BECCAFICO, S., RIUZZI, F., PUGLIELLI, C., MANCINELLI, R., FULLE, S., SORCI, G. & DONATO, R. 2011. Human muscle satellite cells show age-related differential expression of S100B protein and RAGE. *Age (Dordr)*, 33, 523-41.
- BELOT, N., POCHET, R., HEIZMANN, C. W., KISS, R. & DECAESTECKER, C. 2002. Extracellular S100A4 stimulates the migration rate of astrocytic tumor cells by modifying the organization of their actin cytoskeleton. *Biochimica et Biophysica Acta (BBA) - Proteins & Proteomics*, 1600, 74-83.
- BENZ, P. M., BLUME, C., MOEBIUS, J., OSCHATZ, C., SCHUH, K., SICKMANN, A., WALTER, U., FELLER, S. M. & RENNE, T. 2008. Cytoskeleton assembly at endothelial cell-cell contacts is regulated by alphaII-spectrin-VASP complexes. *J Cell Biol*, 180, 205-19.
- BERGE, G. & MÆLANDSMO, G. 2011. Evaluation of potential interactions between the metastasis-associated protein S100A4 and the tumor suppressor protein p53. *Amino Acids*, 41, 863-873.
- BERNHARD, D., SCHWAIGER, W., CRAZZOLARA, R., TINHOFER, I., KOFLER, R. & CSORDAS, A. 2003. Enhanced MTT-reducing activity under growth inhibition by resveratrol in CEM-C7H2 lymphocytic leukemia cells. *Cancer Letters*, 195, 193-199.
- BERNIER, S. G., TAGHIZADEH, N., THOMPSON, C. D., WESTLIN, W. F. & HANNIG, G. 2005. Methionine aminopeptidases type I and type II are essential to control cell proliferation. *Journal of Cellular Biochemistry*, 95, 1191-1203.
- BERSHADSKY, A., KOZLOV, M. & GEIGER, B. 2006. Adhesion-mediated mechanosensitivity: a time to experiment, and a time to theorize. *Current Opinion in Cell Biology*, 18, 472-481.

BETAPUDI, V. 2010. Myosin II Motor Proteins with Different Functions Determine the Fate of Lamellipodia Extension during Cell Spreading. *PLoS ONE*, 5, e8560.

BETAPUDI, V., LICATE, L. S. & EGELHOFF, T. T. 2006. Distinct Roles of Nonmuscle Myosin II Isoforms in the Regulation of MDA-MB-231 Breast Cancer Cell Spreading and Migration. *Cancer Research*, 66, 4725-4733.

BHARGAVA, P., MARSHALL, J. L., RIZVI, N., DAHUT, W., YOE, J., FIGUERA, M., PHIPPS, K., ONG, V. S., KATO, A. & HAWKINS, M. J. 1999. A Phase I and Pharmacokinetic Study of TNP-470 Administered Weekly to Patients with Advanced Cancer. *Clinical Cancer Research*, 5, 1989-1995.

BHATTACHARYA, S., BUNICK, C. G. & CHAZIN, W. J. 2004. Target selectivity in EF-hand calcium binding proteins. *Biochim Biophys Acta*, 1742, 69-79.

BIGORNIA, L., ALLEN, C. N., JAN, C. R., LYON, R. A., TITELER, M. & SCHNEIDER, A. S. 1990. D2 dopamine receptors modulate calcium channel currents and catecholamine secretion in bovine adrenal chromaffin cells. *J Pharmacol Exp Ther*, 252, 586-92.

BILLINGTON, C. K. & PENN, R. B. 2003. Signaling and regulation of G protein-coupled receptors in airway smooth muscle. *Respir Res*, 4, 2.

BJORNLAND, K., WINBERG, J. O., ODEGAARD, O. T., HOVIG, E., LOENNECHEN, T., AASEN, A. O., FODSTAD, O. & MALANDSMO, G. M. 1999. S100A4 Involvement in Metastasis: Deregulation of Matrix Metalloproteinases and Tissue Inhibitors of Matrix Metalloproteinases in Osteosarcoma Cells Transfected with an Anti-S100A4 Ribozyme. *Cancer Res*, 59, 4702-4708.

BOFILL-CARDONA, E., KUDLACEK, O., YANG, Q., AHORN, H., FREISSMUTH, M. & NANOFF, C. 2000. Binding of Calmodulin to the D2-Dopamine Receptor Reduces Receptor Signaling by Arresting the G Protein Activation Switch. *Journal of Biological Chemistry*, 275, 32672-32680.

BONI, R., BURG, G., DOGUOGLU, A., ILG, E. C., SCHAFFER, B. W., MULLER, B. & HEIZMANN, C. W. 1997. Immunohistochemical localization of the Ca²⁺ binding S100 proteins in normal human skin and melanocytic lesions. *Br J Dermatol*, 137, 39-43.

BOYE, K. & MÆLANDSMO, G. M. 2010. S100A4 and Metastasis: A Small Actor Playing Many Roles. *The American journal of pathology*, 176, 528-535.

BRESNICK, A. R. 1999. Molecular mechanisms of nonmuscle myosin-II regulation. *Current Opinion in Cell Biology*, 11, 26-33.

BROZZI, F., ARCURI, C., GIAMBANCO, I. & DONATO, R. 2009. S100B Protein Regulates Astrocyte Shape and Migration via Interaction with Src Kinase: IMPLICATIONS FOR ASTROCYTE DEVELOPMENT, ACTIVATION, AND TUMOR GROWTH. *J Biol Chem*, 284, 8797-811.

BRYCE, N. S., SCHEVZOV, G., FERGUSON, V., PERCIVAL, J. M., LIN, J. J.-C., MATSUMURA, F., BAMBURG, J. R., JEFFREY, P. L., HARDEMAN, E. C., GUNNING, P. & WEINBERGER, R. P. 2003. Specification of Actin Filament Function and Molecular Composition by Tropomyosin Isoforms. *Mol. Biol. Cell*, 14, 1002-1016.

BURRIDGE, K. 1981. Are stress fibres contractile? *Nature*, 294, 691-692.

BURRIDGE, K. & WITTCHEM, E. S. 2013. The tension mounts: Stress fibers as force-generating mechanotransducers. *The Journal of Cell Biology*, 200, 9-19.

CABEZÓN, T., CELIS, J. E., SKIBSHØJ, I., KLINGELHÖFER, J., GRIGORIAN, M., GROMOV, P., RANK, F., MYKLEBUST, J. H., MÆLANDSMO, G. M., LUKANIDIN, E. & AMBARTSUMIAN, N. 2007. Expression of S100A4 by a variety of cell types present in the tumor microenvironment of human breast cancer. *International Journal of Cancer*, 121, 1433-1444.

CAI, Y., BIAIS, N., GIANNONE, G., TANASE, M., JIANG, G., HOFMAN, J. M., WIGGINS, C. H., SILBERZAN, P., BUGUIN, A., LADOUX, B. & SHEETZ, M. P. 2006. Nonmuscle Myosin IIA-Dependent Force Inhibits Cell Spreading and Drives F-Actin Flow. *Biophysical Journal*, 91, 3907-3920.

CALDERWOOD, D. A. 2004. Integrin activation. *Journal of Cell Science*, 117, 657-666.

CAMPELLONE, K. G. & WELCH, M. D. 2010. A nucleator arms race: Cellular control of actin assembly. *Nature Reviews Molecular Cell Biology*, 11, 237-251.

CARLO, R. D., MUCCIOLI, G., BELLUSSI, G., PORTALEONE, P., GHI, P., RACCA, S. & CARLO, F. D. 1986. Steroid, Prolactin, and Dopamine Receptors in Normal and Pathologic Breast Tissue. *Annals of the New York Academy of Sciences*, 464, 559-562.

CARMONA-FONTAINE, C., MATTHEWS, H. K., KURIYAMA, S., MORENO, M., DUNN, G. A., PARSONS, M., STERN, C. D. & MAYOR, R. 2008. Contact inhibition of locomotion in vivo controls neural crest directional migration. *Nature*, 456, 957-961.

CESA, C. M., KIRCHGESSNER, N., MAYER, D., SCHWARZ, U. S., HOFFMANN, B. & MERKEL, R. 2007. Micropatterned silicone elastomer substrates for high resolution analysis of cellular force patterns. *Review of Scientific Instruments*, 78, 034301-10.

CHAFFER, C. L. & WEINBERG, R. A. 2011. A Perspective on Cancer Cell Metastasis. *Science*, 331, 1559-1564.

CHANG, S. Y., MCGARY, E. C. & CHANG, S. 1989. Methionine aminopeptidase gene of *Escherichia coli* is essential for cell growth. *J Bacteriol*, 171, 4071-2.

CHEN, B., LI, A., WANG, D., WANG, M., ZHENG, L. & BARTLES, J. R. 1999. Espin Contains an Additional Actin-binding Site in Its N Terminus and Is a Major Actin-bundling Protein of the Sertoli Cell–Spermatid Ectoplasmic Specialization Junctional Plaque. *Molecular Biology of the Cell*, 10, 4327-4339.

CHEN, C., LI, P. P., MADHAVAN, R. & PENG, H. B. 2012. The function of p120 catenin in filopodial growth and synaptic vesicle clustering in neurons. *Molecular Biology of the Cell*, 23, 2680-2691.

CHEN, H.-L., FERNIG, D. G., RUDLAND, P. S., SPARKS, A., WILKINSON, M. C. & BARRACLOUGH, R. 2001. Binding to Intracellular Targets of the Metastasis-Inducing Protein, S100A4 (p9Ka). *Biochemical and Biophysical Research Communications*, 286, 1212-1217.

CHEN, H., CHOUDHURY, D. M. & CRAIG, S. W. 2006. Coincidence of Actin Filaments and Talin Is Required to Activate Vinculin. *Journal of Biological Chemistry*, 281, 40389-40398.

CHEN, P.-C., CHENG, H.-C. & TANG, C.-H. 2013. CCN3 promotes prostate cancer bone metastasis by modulating the tumor–bone microenvironment through RANKL-dependent pathway. *Carcinogenesis*.

CHENG, P., CORZO, C. A., LUETTEKE, N., YU, B., NAGARAJ, S., BUI, M. M., ORTIZ, M., NACKEN, W., SORG, C., VOGL, T., ROTH, J. & GABRILOVICH, D. I. 2008. Inhibition of dendritic cell differentiation

and accumulation of myeloid-derived suppressor cells in cancer is regulated by S100A9 protein. *The Journal of Experimental Medicine*, 205, 2235-2249.

CHEUNG, A., DANTZIG, J. A., HOLLINGWORTH, S., BAYLOR, S. M., GOLDMAN, Y. E., MITCHISON, T. J. & STRAIGHT, A. F. 2002. A small-molecule inhibitor of skeletal muscle myosin II. *Nat Cell Biol*, 4, 83-8.

CHO, Y., GORINA, S., JEFFREY, P. D. & PAVLETICH, N. P. 1994. Crystal structure of a p53 tumor suppressor-DNA complex: understanding tumorigenic mutations. *Science*, 265, 346-55.

CHOU, H.-L., YAO, C.-T., SU, S.-L., LEE, C.-Y., HU, K.-Y., TERNG, H.-J., SHIH, Y.-W., CHANG, Y.-T., LU, Y.-F., CHANG, C.-W., WAHLQVIST, M., WETTER, T. & CHU, C.-M. 2013. Gene expression profiling of breast cancer survivability by pooled cDNA microarray analysis using logistic regression, artificial neural networks and decision trees. *BMC Bioinformatics*, 14, 100.

CIOBANASU, C., FAIVRE, B. & CHRISTOPHE, L. C. 2012. Actin Dynamics Associated with Focal Adhesions. *International Journal of Cell Biology*, 2012.

CLAUDIA SCHÄFER, S. B., CHRISTOPH MÖHL, SEBASTIAN HOUBEN, NORBERT KIRCHGEßNER, RUDOLF MERKEL AND BERND HOFFMANN 2010. **The key feature for early migratory processes** Dependence of adhesion, actin bundles, force generation and transmission on filopodia. *Cell Adhesion & Migration*, 4.

CONDEELIS, J., SINGER, R. H. & SEGALL, J. E. 2005. THE GREAT ESCAPE: When Cancer Cells Hijack the Genes for Chemotaxis and Motility. *Annual Review of Cell and Developmental Biology*, 21, 695-718.

CONTI, M. A., SELLERS, J. R., ADELSTEIN, R. S. & ELZINGA, M. 1991. Identification of the serine residue phosphorylated by protein kinase C in vertebrate nonmuscle myosin heavy chains. *Biochemistry*, 30, 966-70.

COTE, J. F. & VUORI, K. 2007. GEF what? Dock180 and related proteins help Rac to polarize cells in new ways. *Trends Cell Biol*, 17, 383-93.

- COX, L. G., VAN DONKELAAR, C. C., VAN RIETBERGEN, B., EMANS, P. J. & ITO, K. 2012. Decreased bone tissue mineralization can partly explain subchondral sclerosis observed in osteoarthritis. *Bone*, 50, 1152-61.
- CRAMER, L. P. 2010. Forming the cell rear first: breaking cell symmetry to trigger directed cell migration. *Nat Cell Biol*, 12, 628-632.
- CRAMER, L. P. & MITCHISON, T. J. 1995. Myosin is involved in postmitotic cell spreading. *J Cell Biol*, 131, 179-89.
- CRAMER, L. P., SIEBERT, M. & MITCHISON, T. J. 1997. Identification of novel graded polarity actin filament bundles in locomoting heart fibroblasts: implications for the generation of motile force. *J Cell Biol*, 136, 1287-305.
- CRUET-HENNEQUART, S., MAUBANT, S., LUIS, J., GAUDUCHON, P., STAEDL, C. & DEDHAR, S. 2003. alpha(v) integrins regulate cell proliferation through integrin-linked kinase (ILK) in ovarian cancer cells. *Oncogene*, 22, 1688-702.
- DAVIES, B. R., BARRACLOUGH, R. & RUDLAND, P. S. 1994. Induction of Metastatic Ability in a Stably Diploid Benign Rat Mammary Epithelial Cell Line by Transfection with DNA from Human Malignant Breast Carcinoma Cell Lines. *Cancer Research*, 54, 2785-2793.
- DE CURTIS, I. 2011. Function of liprins in cell motility. *Experimental Cell Research*, 317, 1-8.
- DEGUCHI, S. & SATO, M. 2009. Biomechanical properties of actin stress fibers of non-motile cells. *Biorheology*, 46, 93-105.
- DENT, J. Y. 1949. APOMORPHINE TREATMENT OF ADDICTION*. *British Journal of Addiction to Alcohol & Other Drugs*, 46, 15-28.
- DEROSIER, D. J. & EDDS, K. T. 1980. Evidence for fascin cross-links between the actin filaments in coelomocyte filopodia. *Exp Cell Res*, 126, 490-4.
- DIZ-MUÑOZ, A., KRIEG, M., BERGERT, M., IBARLUCEA-BENITEZ, I., MULLER, D. J., PALUCH, E. & HEISENBERG, C.-P. 2010. Control of Directed Cell Migration In Vivo by Membrane-to-Cortex Attachment. *PLoS Biol*, 8, e1000544.

- DOMINGUEZ, R. & HOLMES, K. C. 2011. Actin structure and function. *Annu Rev Biophys*, 40, 169-86.
- DONATO, R. 1986. S-100 proteins. *Cell Calcium*, 7, 123-145.
- DONATO, R. 2001. S100: a multigenic family of calcium-modulated proteins of the EF-hand type with intracellular and extracellular functional roles. *Int J Biochem Cell Biol*, 33, 637-68.
- DONATO, R., ISOBE, T. & OKUYAMA, T. 1985. S-100 proteins and microtubules: analysis of the effects of rat brain S-100 (S-100b) and ox brain S-100a0, S-100a and S-100b on microtubule assembly-disassembly. *FEBS Lett*, 186, 65-9.
- DONATO, R., SORCI, G., RIUZZI, F., ARCURI, C., BIANCHI, R., BROZZI, F., TUBARO, C. & GIAMBANCO, I. 2009. S100B's double life: intracellular regulator and extracellular signal. *Biochim Biophys Acta*, 1793, 1008-22.
- DONEHOWER, L. A., HARVEY, M., SLAGLE, B. L., MCARTHUR, M. J., MONTGOMERY, C. A., JR., BUTEL, J. S. & BRADLEY, A. 1992. Mice deficient for p53 are developmentally normal but susceptible to spontaneous tumours. *Nature*, 356, 215-21.
- DU, M., WANG, G., ISMAIL, T. M., GROSS, S., FERNIG, D. G., BARRACLOUGH, R. & RUDLAND, P. S. 2012. S100P Dissociates Myosin IIA Filaments and Focal Adhesion Sites to Reduce Cell Adhesion and Enhance Cell Migration. *Journal of Biological Chemistry*, 287, 15330-15344.
- DUARTE, W. R., IIMURA, T., TAKENAGA, K., OHYA, K., ISHIKAWA, I. & KASUGAI, S. 1999. Extracellular Role of S100A4 Calcium-Binding Protein in the Periodontal Ligament. *Biochemical and Biophysical Research Communications*, 255, 416-420.
- DUARTE, W. R., SHIBATA, T., TAKENAGA, K., TAKAHASHI, E., KUBOTA, K., OHYA, K., ISHIKAWA, I., YAMAUCHI, M. & KASUGAI, S. 2003. S100A4: a novel negative regulator of mineralization and osteoblast differentiation. *J Bone Miner Res*, 18, 493-501.
- DULYANINOVA, N. G., HOUSE, R. P., BETAPUDI, V. & BRESNICK, A. R. 2007. Myosin-IIA heavy-chain phosphorylation regulates the motility of MDA-MB-231 carcinoma cells. *Mol Biol Cell*, 18, 3144-55.

- DUNNINGTON, D. J., HUGHES, C. M., MONAGHAN, P. & RUDLAND, P. S. 1983. Phenotypic instability of rat mammary tumor epithelial cells. *J Natl Cancer Inst*, 71, 1227-40.
- DUTTA, K., COX, C. J., HUANG, H., BASAVAPPA, R. & PASCAL, S. M. 2002. Calcium Coordination Studies of the Metastatic Mts1 Protein†. *Biochemistry*, 41, 4239-4245.
- EISENMANN, K. M., HARRIS, E. S., KITCHEN, S. M., HOLMAN, H. A., HIGGS, H. N. & ALBERTS, A. S. 2007. Dia-Interacting Protein Modulates Formin-Mediated Actin Assembly at the Cell Cortex. *Current Biology*, 17, 579-591.
- ELLIOTT, PAUL R., IRVINE, ANDREW F., JUNG, HYUN S., TOZAWA, K., PASTOK, MARTYNA W., PICONE, R., BADYAL, SANDIP K., BASRAN, J., RUDLAND, PHILIP S., BARRACLOUGH, R., LIAN, L.-Y., BAGSHAW, CLIVE R., KRIAJEVSKA, M. & BARSUKOV, IGOR L. 2012. Asymmetric Mode of Ca²⁺-S100A4 Interaction with Nonmuscle Myosin IIA Generates Nanomolar Affinity Required for Filament Remodeling. *Structure*, 20, 654-666.
- ELLIS, S. & MELLOR, H. 2000. The novel Rho-family GTPase rif regulates coordinated actin-based membrane rearrangements. *Curr Biol*, 10, 1387-90.
- ENDO, H., TAKENAGA, K., KANNO, T., SATOH, H. & MORI, S. 2002. Methionine Aminopeptidase 2 Is a New Target for the Metastasis-associated Protein, S100A4. *Journal of Biological Chemistry*, 277, 26396-26402.
- EVEN-RAM, S., DOYLE, A. D., CONTI, M. A., MATSUMOTO, K., ADELSTEIN, R. S. & YAMADA, K. M. 2007. Myosin IIA regulates cell motility and actomyosin-microtubule crosstalk. *Nat Cell Biol*, 9, 299-309.
- EZRATTY, E. J., PARTRIDGE, M. A. & GUNDERSEN, G. G. 2005. Microtubule-induced focal adhesion disassembly is mediated by dynamin and focal adhesion kinase. *Nat Cell Biol*, 7, 581-590.
- FISCHER, E., STINGL, A. & KIRKPATRICK, C. 1990. Migration assay for endothelial cells in multiwells. Application to studies on the effect of opioids. *J Immunol Methods*, 128, 235 - 239.
- FLATMARK, K., PEDERSEN, K. B., NESLAND, J. M., RASMUSSEN, H., AAMODT, G., MIKALSEN, S.-O., BJØRNLAND, K., FODSTAD, Ø. & MÆLANDSMO, G. M. 2003. Nuclear localization of the metastasis-

- related protein S100A4 correlates with tumour stage in colorectal cancer. *The Journal of Pathology*, 200, 589-595.
- FLAVAHAN, N. A. 2005. Phenylpropanolamine constricts mouse and human blood vessels by preferentially activating alpha2-adrenoceptors. *J Pharmacol Exp Ther*, 313, 432-9.
- FOORD, S. M., BONNER, T. I., NEUBIG, R. R., ROSSER, E. M., PIN, J.-P., DAVENPORT, A. P., SPEDDING, M. & HARMAR, A. J. 2005. International Union of Pharmacology. XLVI. G Protein-Coupled Receptor List. *Pharmacological Reviews*, 57, 279-288.
- FORD, H., SILVER, D., KACHAR, B., SELLERS, J. & ZAIN, S. 1997. Effect of Mts1 on the structure and activity of nonmuscle myosin II. *Biochemistry*, 36, 16321 - 16327.
- FRANCO, S. J. & HUTTENLOCHER, A. 2005. Regulating cell migration: calpains make the cut. *J Cell Sci*, 118, 3829-38.
- GAO, X.-N., TANG, S.-Q. & ZHANG, X.-F. 2005. S100A4 antisense oligodeoxynucleotide suppresses invasive potential of neuroblastoma cells. *Journal of Pediatric Surgery*, 40, 648-652.
- GARRETT, S. C., VARNEY, K. M., WEBER, D. J. & BRESNICK, A. R. 2006. S100A4, a Mediator of Metastasis. *Journal of Biological Chemistry*, 281, 677-680.
- GEIGER, B., SPATZ, J. P. & BERSHADSKY, A. D. 2009. Environmental sensing through focal adhesions. *Nat Rev Mol Cell Biol*, 10, 21-33.
- GERVAIS, J. L. M., SETH, P. & ZHANG, H. 1998. Cleavage of CDK Inhibitor p21Cip1/Waf1 by Caspases Is an Early Event during DNA Damage-induced Apoptosis. *Journal of Biological Chemistry*, 273, 19207-19212.
- GIBBS, F., BARRACLOUGH, R., PLATT-HIGGINS, A., RUDLAND, P., WILKINSON, M. & PARRY, E. 1995. Immunocytochemical distribution of the calcium-binding protein p9Ka in normal rat tissues: variation in the cellular location in different tissues. *J Histochem Cytochem*, 43, 169 - 180.
- GOECKELER, Z. M., BRIDGMAN, P. C. & WYSOLMERSKI, R. B. 2008. Nonmuscle myosin II is responsible for maintaining endothelial cell basal tone and stress fiber integrity. *American Journal of Physiology - Cell Physiology*, 295, C994-C1006.

GOH THEN SIN, C., HERSCH, N., RUDLAND, P. S., BARRACLOUGH, R., HOFFMANN, B. & GROSS, S. R. 2011. S100A4 downregulates filopodia formation through increased dynamic instability. *Cell Adh Migr*, 5, 439-47.

GOLOMB, E., MA, X., JANA, S. S., PRESTON, Y. A., KAWAMOTO, S., SHOHAM, N. G., GOLDIN, E., CONTI, M. A., SELLERS, J. R. & ADELSTEIN, R. S. 2004. Identification and characterization of nonmuscle myosin II-C, a new member of the myosin II family. *J Biol Chem*, 279, 2800-8.

GONG, H., SHEN, B., FLEVARIS, P., CHOW, C., LAM, S. C., VOYNO-YASENETSKAYA, T. A., KOZASA, T. & DU, X. 2010. G protein subunit G α 13 binds to integrin α 5 β 3 and mediates integrin "outside-in" signaling. *Science*, 327, 340-3.

GREENWAY, S., VAN SUYLEN, R. J., DU MARCHIE SARVAAS, G., KWAN, E., AMBARTSUMIAN, N., LUKANIDIN, E. & RABINOVITCH, M. 2004. S100A4/Mts1 produces murine pulmonary artery changes resembling plexogenic arteriopathy and is increased in human plexogenic arteriopathy. *Am J Pathol*, 164, 253-62.

GRIBENKO, A. V. & MAKHATADZE, G. I. 1998. Oligomerization and divalent ion binding properties of the S100P protein: a Ca²⁺/Mg²⁺-switch model. *Journal of Molecular Biology*, 283, 679-694.

GRIFFITH, E. C., SU, Z., NIWAYAMA, S., RAMSAY, C. A., CHANG, Y. H. & LIU, J. O. 1998. Molecular recognition of angiogenesis inhibitors fumagillin and ovalicin by methionine aminopeptidase 2. *Proc Natl Acad Sci U S A*, 95, 15183-8.

GRIGORIAN, M., ANDRESEN, S., TULCHINSKY, E., KRIAJEVSKA, M., CARLBERG, C., KRUSE, C., COHN, M., AMBARTSUMIAN, N., CHRISTENSEN, A., SELIVANOVA, G. & LUKONIDIN, E. 2001. Tumor suppressor p53 protein is a new target for the metastasis-associated Mts1/S100A4 protein: functional consequences of their interaction. *J Biol Chem*, 276, 22699 - 22708.

GRIGORIAN, M. & LUKANIDIN, E. 2003. Metastasis-Inducing Mts1/S100A4 Protein Binds to Tumor Suppressor p53 Protein. *Russian Journal of Genetics*, 39, 748-755.

GROEGER, G. & NOBES, C. D. 2007. Co-operative Cdc42 and Rho signalling mediates ephrinB-triggered endothelial cell retraction. *Biochemical Journal*, 404, 23-29.

- GROSHEVA, I., VITTITOW, J. L., GOICHBURG, P., GABELT, B. A. T., KAUFMAN, P. L., BORRÁS, T., GEIGER, B. & BERSHADSKY, A. D. 2006. Caldesmon effects on the actin cytoskeleton and cell adhesion in cultured HTM cells. *Experimental Eye Research*, 82, 945-958.
- GROSS, S., SIN, C., BARRACLOUGH, R. & RUDLAND, P. 2013. Joining S100 proteins and migration: for better or for worse, in sickness and in health. *Cellular and Molecular Life Sciences*, 1-29.
- GUAN, J.-L. 1997. Role of focal adhesion kinase in integrin signaling. *The International Journal of Biochemistry & Cell Biology*, 29, 1085-1096.
- GUPTA, G. P. & MASSAGUE, J. 2006. Cancer metastasis: building a framework. *Cell*, 127, 679-95.
- GUPTA, N., WANG, H., MCLEOD, T. L., NAUS, C. C., KYURKCHIEV, S., ADVANI, S., YU, J., PERBAL, B. & WEICHELBAUM, R. R. 2001. Inhibition of glioma cell growth and tumorigenic potential by CCN3 (NOV). *Mol Pathol*, 54, 293-9.
- HAENISCH, B., WALSTAB, J., HERBERHOLD, S., BOOTZ, F., TSCHAIKIN, M., RAMSEGER, R. & BÖNISCH, H. 2010. Alpha-adrenoceptor agonistic activity of oxymetazoline and xylometazoline. *Fundamental & Clinical Pharmacology*, 24, 729-739.
- HALL, A. 1998. Rho GTPases and the actin cytoskeleton. *Science*, 279, 509-14.
- HALL, A. & NOBES, C. D. 2000. Rho GTPases: molecular switches that control the organization and dynamics of the actin cytoskeleton. *Philos Trans R Soc Lond B Biol Sci*, 355, 965-70.
- HELFMAN, D. M. 2011. Niclosamide: An Established Antihelminthic Drug as a Potential Therapy Against S100A4-Mediated Metastatic Colon Tumors. *Journal of the National Cancer Institute*, 103, 991-992.
- HERREN, B., GARTON, K., COATS, S., BOWEN-POPE, D., ROSS, R. & RAINES, E. 2001. ADAM15 overexpression in NIH3T3 cells enhances cell-cell interactions. *Exp Cell Res*, 271, 152 - 160.
- HERTZBERG, R. P. & POPE, A. J. 2000. High-throughput screening: new technology for the 21st century. *Current Opinion in Chemical Biology*, 4, 445-451.
- HOTULAINEN, P. & LAPPALAINEN, P. 2006. Stress fibers are generated by two distinct actin assembly mechanisms in motile cells. *The Journal of Cell Biology*, 173, 383-394.

HOUSE, R. P., POZZUTO, M., PATEL, P., DULYANINOVA, N. G., LI, Z.-H., ZENCHECK, W. D., VITOLO, M. I., WEBER, D. J. & BRESNICK, A. R. 2011. Two Functional S100A4 Monomers Are Necessary for Regulating Nonmuscle Myosin-IIA and HCT116 Cell Invasion. *Biochemistry*, 50, 6920-6932.

HOWARD, J. 2009. Mechanical signaling in networks of motor and cytoskeletal proteins. *Annu Rev Biophys*, 38, 217-34.

HUANG, C., RAJFUR, Z., BORCHERS, C., SCHALLER, M. & JACOBSON, K. 2003. JNK phosphorylates paxillin and regulates cell migration. *Nature*, 424, 219 - 223.

HUMPHRIES, J. D., BYRON, A. & HUMPHRIES, M. J. 2006. Integrin ligands at a glance. *Journal of Cell Science*, 119, 3901-3903.

HUMPHRIES, J. D., WANG, P., STREULI, C., GEIGER, B., HUMPHRIES, M. J. & BALLESTREM, C. 2007. Vinculin controls focal adhesion formation by direct interactions with talin and actin. *J Cell Biol*, 179, 1043-57.

HYNES, R. 1992. Integrins: versatility, modulation, and signaling in cell adhesion. *Cell*, 69, 11 - 25.

IKEBE, M. & HARTSHORNE, D. J. 1985. Phosphorylation of smooth muscle myosin at two distinct sites by myosin light chain kinase. *Journal of Biological Chemistry*, 260, 10027-31.

IKEBE, M., KORETZ, J. & HARTSHORNE, D. J. 1988. Effects of phosphorylation of light chain residues threonine 18 and serine 19 on the properties and conformation of smooth muscle myosin. *Journal of Biological Chemistry*, 263, 6432-6437.

IKENAGA, N., OHUCHIDA, K., MIZUMOTO, K., YU, J., FUJITA, H., NAKATA, K., UEDA, J., SATO, N., NAGAI, E. & TANAKA, M. 2009. S100A4 mRNA is a diagnostic and prognostic marker in pancreatic carcinoma. *J Gastrointest Surg*, 13, 1852-8.

ILIC, D., FURUTA, Y., KANAZAWA, S., TAKEDA, N., SOBUE, K., NAKATSUJI, N., NOMURA, S., FUJIMOTO, J., OKADA, M. & YAMAMOTO, T. 1995. Reduced cell motility and enhanced focal adhesion contact formation in cells from FAK-deficient mice. *Nature*, 377, 539-44.

IMMING, P., SINNING, C. & MEYER, A. 2006. Drugs, their targets and the nature and number of drug targets. *Nat Rev Drug Discov*, 5, 821-34.

ISHIZAKI, T., UEHATA, M., TAMECHIKA, I., KEEL, J., NONOMURA, K., MAEKAWA, M. & NARUMIYA, S. 2000. Pharmacological Properties of Y-27632, a Specific Inhibitor of Rho-Associated Kinases. *Molecular Pharmacology*, 57, 976-983.

ISMAIL, N., KAUR, G., HASHIM, H. & HASSAN, M. 2008a. S100A4 overexpression proves to be independent marker for breast cancer progression. *Cancer Cell International*, 8, 12.

ISMAIL, T. M., FERNIG, D. G., RUDLAND, P. S., TERRY, C. J., WANG, G. & BARRACLOUGH, R. 2008b. The basic C-terminal amino acids of calcium-binding protein S100A4 promote metastasis. *Carcinogenesis*, 29, 2259-2266.

ISMAIL, T. M., ZHANG, S., FERNIG, D. G., GROSS, S., MARTIN-FERNANDEZ, M. L., SEE, V., TOZAWA, K., TYNAN, C. J., WANG, G., WILKINSON, M. C., RUDLAND, P. S. & BARRACLOUGH, R. 2010. Self-association of Calcium-binding Protein S100A4 and Metastasis. *Journal of Biological Chemistry*, 285, 914-922.

IWASAKI, T., MURATA-HORI, M., ISHITOBI, S. & HOSOYA, H. 2001. Diphosphorylated MRLC is required for organization of stress fibers in interphase cells and the contractile ring in dividing cells. *Cell Struct Funct*, 26, 677-83.

KANDA, K., SOBUE, K. & KAKIUCHI, S. 1985. Phosphorylation of myosin light chain and the actin-activated ATPase activity of adrenal medullary myosin. *J Biochem*, 97, 961-4.

KATO, C., KOJIMA, T., KOMAKI, M., MIMORI, K., DUARTE, W. R., TAKENAGA, K. & ISHIKAWA, I. 2005. S100A4 inhibition by RNAi up-regulates osteoblast related genes in periodontal ligament cells. *Biochem Biophys Res Commun*, 326, 147-53.

KATOH, K., KANO, Y., AMANO, M., KAIBUCHI, K. & FUJIWARA, K. 2001a. Stress fiber organization regulated by MLCK and Rho-kinase in cultured human fibroblasts. *Am J Physiol Cell Physiol*, 280, C1669-79.

KATOH, K., KANO, Y., AMANO, M., ONISHI, H., KAIBUCHI, K. & FUJIWARA, K. 2001b. Rho-kinase--mediated contraction of isolated stress fibers. *J Cell Biol*, 153, 569-84.

- KAWANO, Y., FUKATA, Y., OSHIRO, N., AMANO, M., NAKAMURA, T., ITO, M., MATSUMURA, F., INAGAKI, M. & KAIBUCHI, K. 1999. Phosphorylation of Myosin-Binding Subunit (Mbs) of Myosin Phosphatase by Rho-Kinase in Vivo. *The Journal of Cell Biology*, 147, 1023-1038.
- KEE, A. J., SCHEVZOV, G., NAIR-SHALLIKER, V., ROBINSON, C. S., VRHOVSKI, B., GHODDUSI, M., QIU, M. R., LIN, J. J.-C., WEINBERGER, R., GUNNING, P. W. & HARDEMAN, E. C. 2004. Sorting of a nonmuscle tropomyosin to a novel cytoskeletal compartment in skeletal muscle results in muscular dystrophy. *The Journal of Cell Biology*, 166, 685-696.
- KEIRSEBILCK, A., BONNE, S., BRUYNEEL, E., VERMASSEN, P., LUKANIDIN, E., MAREEL, M. & VAN ROY, F. 1998. E-cadherin and metastasin (mts-1/S100A4) expression levels are inversely regulated in two tumor cell families. *Cancer Res*, 58, 4587 - 4591.
- KELLER, H., ZADEH, A. D. & EGGLI, P. 2002. Localised depletion of polymerised actin at the front of Walker carcinosarcoma cells increases the speed of locomotion. *Cell Motil Cytoskeleton*, 53, 189-202.
- KELLEY, C. A., SELLERS, J. R., GARD, D. L., BUI, D., ADELSTEIN, R. S. & BAINES, I. C. 1996. Xenopus nonmuscle myosin heavy chain isoforms have different subcellular localizations and enzymatic activities. *J Cell Biol*, 134, 675-87.
- KIM, E. J. & HELFMAN, D. M. 2003. Characterization of the Metastasis-associated Protein, S100A4. *Journal of Biological Chemistry*, 278, 30063-30073.
- KIM, H. J., KOH, P. O., KANG, S. S., PAIK, W. Y. & CHOI, W. S. 2001. The localization of dopamine D2 receptor mRNA in the human placenta and the anti-angiogenic effect of apomorphine in the chorioallantoic membrane. *Life Sci*, 68, 1031-40.
- KIMURA, K., ENDO, Y., YONEMURA, Y., HEIZMANN, C. W., SCHAFFER, B. W., WATANABE, Y. & SASAKI, T. 2000. Clinical significance of S100A4 and E-cadherin-related adhesion molecules in non-small cell lung cancer. *Int J Oncol*, 16, 1125-31.
- KIMURA, K., ITO, M., AMANO, M., CHIHARA, K., FUKATA, Y., NAKAFUKU, M., YAMAMORI, B., FENG, J., NAKANO, T., OKAWA, K., IWAMATSU, A. & KAIBUCHI, K. 1996. Regulation of myosin phosphatase by Rho and Rho-associated kinase (Rho-kinase). *Science*, 273, 245-8.

- KIRYUSHKO, D., NOVITSKAYA, V., SOROKA, V., KLINGELHOFER, J., LUKANIDIN, E., BEREZIN, V. & BOCK, E. 2006. Molecular mechanisms of Ca(2+) signaling in neurons induced by the S100A4 protein. *Mol Cell Biol*, 26, 3625-38.
- KISS, B., DUELLI, A., RADNAI, L., KÉKESI, K. A., KATONA, G. & NYITRAY, L. 2012. Crystal structure of the S100A4–nonmuscle myosin IIA tail fragment complex reveals an asymmetric target binding mechanism. *Proceedings of the National Academy of Sciences*.
- KLEMKE, R. L., CAI, S., GIANNINI, A. L., GALLAGHER, P. J., LANEROLLE, P. D. & CHERESH, D. A. 1997. Regulation of Cell Motility by Mitogen-activated Protein Kinase. *The Journal of Cell Biology*, 137, 481-492.
- KLIGMAN, D. & HILT, D. C. 1988. The S100 protein family. *Trends Biochem Sci*, 13, 437-43.
- KLINGELHOFER, J., GRUM-SCHWENSEN, B., BECK, M. K., KNUDSEN, R. S., GRIGORIAN, M., LUKANIDIN, E. & AMBARTSUMIAN, N. 2012. Anti-S100A4 antibody suppresses metastasis formation by blocking stroma cell invasion. *Neoplasia*, 14, 1260-8.
- KOLEGA, J. 1998. Cytoplasmic dynamics of myosin IIA and IIB: spatial 'sorting' of isoforms in locomoting cells. *Journal of Cell Science*, 111, 2085-2095.
- KOLEGA, J. 2006. The Role of Myosin II Motor Activity in Distributing Myosin Asymmetrically and Coupling Protrusive Activity to Cell Translocation. *Mol. Biol. Cell*, 17, 4435-4445.
- KOLTZSCHER, M. & GERKE, V. 2000. Identification of Hydrophobic Amino Acid Residues Involved in the Formation of S100P Homodimers in Vivo†. *Biochemistry*, 39, 9533-9539.
- KONDO, T., HAMAOKA, K., KAMIJO, K., KIMURA, H., MORITA, M., TAKAHASHI, M. & HOSOYA, H. 2011. Enhancement of myosin II/actin turnover at the contractile ring induces slower furrowing in dividing HeLa cells. *Biochemical Journal*, 435, 569-576.
- KOVAC, B., TEO, J. L., MAKELA, T. P. & VALLENIUS, T. 2013. Assembly of non-contractile dorsal stress fibers requires alpha-actinin-1 and Rac1 in migrating and spreading cells. *J Cell Sci*, 126, 263-73.

KOVÁCS, M., TÓTH, J., HETÉNYI, C., MÁLNÁSI-CSIZMADIA, A. & SELLERS, J. R. 2004. Mechanism of Blebbistatin Inhibition of Myosin II. *Journal of Biological Chemistry*, 279, 35557-35563.

KOZLOVA, E. N. & LUKANIDIN, E. 1999. Metastasis-associated mts1 (S100A4) protein is selectively expressed in white matter astrocytes and is up-regulated after peripheral nerve or dorsal root injury. *Glia*, 27, 249-58.

KRIAJEVSKA, M., BRONSTEIN, I., SCOTT, D., TARABYKINA, S., FISCHER-LARSEN, M., ISSINGER, O. & LUKANIDIN, E. 2000. Metastasis-associated protein Mts1 (S100A4) inhibits CK2-mediated phosphorylation and self-assembly of the heavy chain of nonmuscle myosin. *Biochim Biophys Acta*, 1498, 252 - 263.

KRIAJEVSKA, M., FISCHER-LARSEN, M., MOERTZ, E., VORM, O., TULCHINSKY, E., GRIGORIAN, M., AMBARTSUMIAN, N. & LUKANIDIN, E. 2002. Liprin β 1, a Member of the Family of LAR Transmembrane Tyrosine Phosphatase-interacting Proteins, Is a New Target for the Metastasis-associated Protein S100A4 (Mts1). *Journal of Biological Chemistry*, 277, 5229-5235.

KRIAJEVSKA, M. V., CARDENAS, M. N., GRIGORIAN, M. S., AMBARTSUMIAN, N. S., GEORGIEV, G. P. & LUKANIDIN, E. M. 1994. Non-muscle myosin heavy chain as a possible target for protein encoded by metastasis-related mts-1 gene. *J Biol Chem*, 269, 19679-82.

KRUEGER, N. X., VAN VACTOR, D., WAN, H. I., GELBART, W. M., GOODMAN, C. S. & SAITO, H. 1996. The transmembrane tyrosine phosphatase DLAR controls motor axon guidance in *Drosophila*. *Cell*, 84, 611-22.

KRUGMANN, S., JORDENS, I., GEVAERT, K., DRIESSENS, M., VANDEKERCKHOVE, J. & HALL, A. 2001. Cdc42 induces filopodia by promoting the formation of an IRSp53:Mena complex. *Curr Biol*, 11, 1645-55.

KUMAR, C. C. 1998. Signaling by integrin receptors. *Oncogene*, 17, 1365-73.

KUO, J.-C., HAN, X., HSIAO, C.-T., YATES III, J. R. & WATERMAN, C. M. 2011. Analysis of the myosin-II-responsive focal adhesion proteome reveals a role for β -Pix in negative regulation of focal adhesion maturation. *Nat Cell Biol*, 13, 383-393.

- KUREISHI, Y., KOBAYASHI, S., AMANO, M., KIMURA, K., KANAIDE, H., NAKANO, T., KAIBUCHI, K. & ITO, M. 1997. Rho-associated Kinase Directly Induces Smooth Muscle Contraction through Myosin Light Chain Phosphorylation. *Journal of Biological Chemistry*, 272, 12257-12260.
- KVERNMO, T., HOUBEN, J. & SYLTE, I. 2008. Receptor-binding and pharmacokinetic properties of dopaminergic agonists. *Curr Top Med Chem*, 8, 1049-67.
- LAKSHMI, M. S., PARKER, C. & SHERBET, G. V. 1997. Expression of the transmembrane glycoprotein CD44 and metastasis associated 18A2/MTS1 gene in B16 murine melanoma cells. *Anticancer Res*, 17, 3451-5.
- LAMPUGNANI, M. G. 1999. Cell migration into a wounded area in vitro. *Methods Mol Biol*, 96, 177-82.
- LAWRIE, A., SPIEKERKOTTER, E., MARTINEZ, E. C., AMBARTSUMIAN, N., SHEWARD, W. J., MACLEAN, M. R., HARMAR, A. J., SCHMIDT, A. M., LUKANIDIN, E. & RABINOVITCH, M. 2005. Interdependent serotonin transporter and receptor pathways regulate S100A4/Mts1, a gene associated with pulmonary vascular disease. *Circ Res*, 97, 227-35.
- LAZARIDES, E. & BURRIDGE, K. 1975. Alpha-actinin: immunofluorescent localization of a muscle structural protein in nonmuscle cells. *Cell*, 6, 289-98.
- LE CLAINCHE, C. & CARLIER, M.-F. 2008. Regulation of Actin Assembly Associated With Protrusion and Adhesion in Cell Migration. *Physiological Reviews*, 88, 489-513.
- LEBER, M. F. & EFFERTH, T. 2009. Molecular principles of cancer invasion and metastasis (review). *Int J Oncol*, 34, 881-95.
- LEWIT-BENTLEY, A., RETY, S., SOPKOVA-DE OLIVEIRA SANTOS, J. & GERKE, V. 2000. S100-annexin complexes: some insights from structural studies. *Cell Biol Int*, 24, 799-802.
- LI, M., BERMAK, J. C., WANG, Z. W. & ZHOU, Q. Y. 2000. Modulation of dopamine D(2) receptor signaling by actin-binding protein (ABP-280). *Mol Pharmacol*, 57, 446-52.
- LI, Z.-H. & BRESNICK, A. R. 2006. The S100A4 Metastasis Factor Regulates Cellular Motility via a Direct Interaction with Myosin-IIA. *Cancer Research*, 66, 5173-5180.

- LI, Z.-H., DULYANINOVA, N. G., HOUSE, R. P., ALMO, S. C. & BRESNICK, A. R. 2010. S100A4 Regulates Macrophage Chemotaxis. *Mol. Biol. Cell*, 21, 2598-2610.
- LI, Z.-H., SPEKTOR, A., VARLAMOVA, O. & BRESNICK, A. R. 2003. Mts1 Regulates the Assembly of Nonmuscle Myosin-IIA⁺. *Biochemistry*, 42, 14258-14266.
- LIM, J. I., SABOURI-GHOMI, M., MACHACEK, M., WATERMAN, C. M. & DANUSER, G. 2010. Protrusion and actin assembly are coupled to the organization of lamellar contractile structures. *Experimental Cell Research*, 316, 2027-2041.
- LIMOUBE, J., STRAIGHT, A., MITCHISON, T. & SELLERS, J. 2004. Specificity of blebbistatin, an inhibitor of myosin II. *Journal of Muscle Research and Cell Motility*, 25, 337-341.
- LIN, C., LEU, S., CHEN, N., TEBEAU, C., LIN, S., YEUNG, C. & LAU, L. 2003. CCN3 (NOV) is a novel angiogenic regulator of the CCN protein family. *J Biol Chem*, 278, 24200 - 24208.
- LIN, J., YANG, Q., WILDER, P. T., CARRIER, F. & WEBER, D. J. 2010. The calcium-binding protein S100B down-regulates p53 and apoptosis in malignant melanoma. *J Biol Chem*, 285, 27487-98.
- LIU, Z., VAN GRUNSVEN, L. A., VAN ROSSEN, E., SCHROYEN, B., TIMMERMANS, J.-P., GEERTS, A. & REYNAERT, H. 2010. Blebbistatin inhibits contraction and accelerates migration in mouse hepatic stellate cells. *British Journal of Pharmacology*, 159, 304-315.
- LLOYD, B. H., PLATT-HIGGINS, A., RUDLAND, P. S. & BARRACLOUGH, R. 1998. Human S100A4 (p9Ka) induces the metastatic phenotype upon benign tumour cells. *Oncogene*, 17, 465-73.
- LO, C.-M., BUXTON, D. B., CHUA, G. C. H., DEMBO, M., ADELSTEIN, R. S. & WANG, Y.-L. 2004. Nonmuscle Myosin IIB Is Involved in the Guidance of Fibroblast Migration. *Mol. Biol. Cell*, 15, 982-989.
- LO, J. F., YU, C. C., CHIOU, S. H., HUANG, C. Y., JAN, C. I., LIN, S. C., LIU, C. J., HU, W. Y. & YU, Y. H. 2011. The epithelial-mesenchymal transition mediator S100A4 maintains cancer-initiating cells in head and neck cancers. *Cancer Res*, 71, 1912-23.

- LOAYZA-PUCH, F., DROST, J., ROOIJERS, K., LOPES, R., ELKON, R. & AGAMI, R. 2013. p53 induces transcriptional and translational programs to suppress cell proliferation and growth. *Genome Biol*, 14, R32.
- LOMBET, A., PLANQUE, N., BLEAU, A.-M., LI, C. L. & PERBAL, B. 2003. CCN3 and calcium signaling. *Cell Communication and Signaling*, 1, 1.
- LOMMEL, S., BENESCH, S., ROTTNER, K., FRANZ, T., WEHLAND, J. & KÜHN, R. 2001. Actin pedestal formation by enteropathogenic Escherichia coli and intracellular motility of Shigella flexneri are abolished in N-WASP-defective cells. *EMBO Reports*, 2, 850-7.
- LOWRY, O. H., ROSEBROUGH, N. J., FARR, A. L. & RANDALL, R. J. 1951. Protein measurement with the Folin phenol reagent. *J Biol Chem*, 193, 265-75.
- LU, K., JONG, K., RAJASEKARAN, A., CLOUGHESY, T. & MISCHEL, P. 2004. Upregulation of tissue inhibitor of metalloproteinases (TIMP)-2 promotes matrix metalloproteinase (MMP)-2 activation and cell invasion in a human glioblastoma cell line. *Lab Invest*, 84, 8 - 20.
- LUCAS-LOPEZ, C., ALLINGHAM, J. S., LEBL, T., LAWSON, C. P. A. T., BRENK, R., SELLERS, J. R., RAYMENT, I. & WESTWOOD, N. J. 2008. The small molecule tool (S)-(-)-blebbistatin: novel insights of relevance to myosin inhibitor design. *Organic & Biomolecular Chemistry*, 6, 2076-2084.
- MA, D., RAJAKUMARASWAMY, N. & MAZE, M. 2005. α 2-Adrenoceptor agonists: shedding light on neuroprotection? *British Medical Bulletin*, 71, 77-92.
- MA, X., YANG, Y., WANG, Y., AN, G. & LV, G. 2010. Small interfering RNA-directed knockdown of S100A4 decreases proliferation and invasiveness of osteosarcoma cells. *Cancer Lett*, 299, 171-81.
- MACHESKY, L. M. & LI, A. 2010. Fascin: Invasive filopodia promoting metastasis. *Communicative & Integrative Biology*, 3, 263-270.
- MACK, G. S. & MARSHALL, A. 2010. Lost in migration. *Nat Biotech*, 28, 214-229.
- MALASHKEVICH, V. N., DULYANINOVA, N. G., RAMAGOPAL, U. A., LIRIANO, M. A., VARNEY, K. M., KNIGHT, D., BRENOWITZ, M., WEBER, D. J., ALMO, S. C. & BRESNICK, A. R. 2010. Phenothiazines

inhibit S100A4 function by inducing protein oligomerization. *Proc Natl Acad Sci U S A*, 107, 8605-10.

MALMENDAL, A., VANDER KOOI, C. W., NIELSEN, N. C. & CHAZIN, W. J. 2005. Calcium-modulated S100 protein-phospholipid interactions. An NMR study of calbindin D9k and DPC. *Biochemistry*, 44, 6502-12.

MALNASI-CSIZMADIA, A. & KOVACS, M. 2010. Emerging complex pathways of the actomyosin powerstroke. *Trends Biochem Sci*, 35, 684-90.

MANARA, M. C., PERBAL, B., BENINI, S., STRAMMIELLO, R., CERISANO, V., PERDICHIZZI, S., SERRA, M., ASTOLFI, A., BERTONI, F., ALAMI, J., YEGER, H., PICCI, P. & SCOTLANDI, K. 2002. The expression of *ccn3(nov)* gene in musculoskeletal tumors. *Am J Pathol*, 160, 849-59.

MARENHOLZ, I., HEIZMANN, C. W. & FRITZ, G. 2004. S100 proteins in mouse and man: from evolution to function and pathology (including an update of the nomenclature). *Biochem Biophys Res Commun*, 322, 1111-22.

MARTIS, E., RADHAKRISHNAN, R. & BADVE, R. 2011. High-throughput screening: the hits and leads of drug discovery-an overview. *Journal of Applied Pharmaceutical Science*, 1, 2-10.

MATHISEN, B., LINDSTAD, R., HANSEN, J., EL-GEWELY, S., MAELANDSMO, G., HOVIG, E., FODSTAD, Ø., LOENNECHEN, T. & WINBERG, J.-O. 2003. S100A4 regulates membrane induced activation of matrix metalloproteinase-2 in osteosarcoma cells. *Clinical and Experimental Metastasis*, 20, 701-711.

MATSUMURA, F. 2005. Regulation of myosin II during cytokinesis in higher eukaryotes. *Trends Cell Biol*, 15, 371-7.

MATSUZAKI, S. & DARCHA, C. 2012. Epithelial to mesenchymal transition-like and mesenchymal to epithelial transition-like processes might be involved in the pathogenesis of pelvic endometriosis. *Human Reproduction*, 27, 712-721.

MATTILA, P. K. & LAPPALAINEN, P. 2008. Filopodia: molecular architecture and cellular functions. *Nat Rev Mol Cell Biol*, 9, 446-54.

MAZZUCHELLI, L. 2002. Protein S100A4: too long overlooked by pathologists? *Am J Pathol*, 160, 7-13.

MCKIERNAN, E., MCDERMOTT, E., EVOY, D., CROWN, J. & DUFFY, M. 2011. The role of S100 genes in breast cancer progression. *Tumor Biology*, 32, 441-450.

MCKILLOP, D. F., FORTUNE, N. S., RANATUNGA, K. W. & GEEVES, M. A. 1994. The influence of 2,3-butanedione 2-monoxime (BDM) on the interaction between actin and myosin in solution and in skinned muscle fibres. *J Muscle Res Cell Motil*, 15, 309-18.

MCLACHLAN, A. D. & KARN, J. 1982. Periodic charge distributions in the myosin rod amino acid sequence match cross-bridge spacings in muscle. *Nature*, 299, 226-31.

MICHAEL, K. E., DUMBAULD, D. W., BURNS, K. L., HANKS, S. K. & GARCIA, A. J. 2009. Focal adhesion kinase modulates cell adhesion strengthening via integrin activation. *Mol Biol Cell*, 20, 2508-19.

MIERKE, C. T., RÖSEL, D., FABRY, B. & BRÁBEK, J. 2008. Contractile forces in tumor cell migration. *European Journal of Cell Biology*, 87, 669-676.

MIKI, H., YAMAGUCHI, H., SUETSUGU, S. & TAKENAWA, T. 2000. IRSp53 is an essential intermediate between Rac and WAVE in the regulation of membrane ruffling. *Nature*, 408, 732-735.

MILLAN, M. J., MAIOFISS, L., CUSSAC, D., AUDINOT, V., BOUTIN, J.-A. & NEWMAN-TANCREDI, A. 2002. Differential Actions of Antiparkinson Agents at Multiple Classes of Monoaminergic Receptor. I. A Multivariate Analysis of the Binding Profiles of 14 Drugs at 21 Native and Cloned Human Receptor Subtypes. *Journal of Pharmacology and Experimental Therapeutics*, 303, 791-804.

MISHRA, S., SIDDIQUE, H. & SALEEM, M. 2012. S100A4 calcium-binding protein is key player in tumor progression and metastasis: preclinical and clinical evidence. *Cancer and Metastasis Reviews*, 31, 163-172.

MITRA, S. K., HANSON, D. A. & SCHLAEPFER, D. D. 2005. Focal adhesion kinase: in command and control of cell motility. *Nat Rev Mol Cell Biol*, 6, 56-68.

- MORACZEWSKA, J., NICHOLSON-FLYNN, K. & HITCHCOCK-DEGREGORI, S. E. 1999. The ends of tropomyosin are major determinants of actin affinity and myosin subfragment 1-induced binding to F-actin in the open state. *Biochemistry*, 38, 15885-15892.
- MORIYAMA-KITA, M., ENDO, Y., YONEMURA, Y., HEIZMANN, C. W., MIYAMORI, H., SATO, H., YAMAMOTO, E. & SASAKI, T. 2005. S100A4 regulates E-cadherin expression in oral squamous cell carcinoma. *Cancer Letters*, 230, 211-218.
- MOSMANN, T. 1983. Rapid colorimetric assay for cellular growth and survival: Application to proliferation and cytotoxicity assays. *Journal of Immunological Methods*, 65, 55-63.
- MOST, P., RAAKE, P., WEBER, C., KATUS, H. A. & PLEGER, S. T. 2013. S100A1 gene therapy in small and large animals. *Methods Mol Biol*, 963, 407-20.
- MSEKA, T., BAMBURG, J. R. & CRAMER, L. P. 2007. ADF/cofilin family proteins control formation of oriented actin-filament bundles in the cell body to trigger fibroblast polarization. *J Cell Sci*, 120, 4332-44.
- MUELLER, A., BACHI, T., HOCHLI, M., SCHAFER, B. W. & HEIZMANN, C. W. 1999. Subcellular distribution of S100 proteins in tumor cells and their relocation in response to calcium activation. *Histochem Cell Biol*, 111, 453-9.
- NAGANO, M., HOSHINO, D., KOSHIKAWA, N., AKIZAWA, T. & SEIKI, M. 2012. Turnover of focal adhesions and cancer cell migration. *Int J Cell Biol*, 2012, 310616.
- NAGASE, H., VISSE, R. & MURPHY, G. 2006. Structure and function of matrix metalloproteinases and TIMPs. *Cardiovascular Research*, 69, 562-573.
- NARDIN, P., TRAMONTINA, A. C., QUINCOZES-SANTOS, A., TORTORELLI, L. S., LUNARDI, P., KLEIN, P. R., WARTCHOW, K. M., BOBERMIN, L. D., GOTTFRIED, C., ELISABETSKY, E. & GONCALVES, C. A. 2011. In vitro S100B secretion is reduced by apomorphine: effects of antipsychotics and antioxidants. *Prog Neuropsychopharmacol Biol Psychiatry*, 35, 1291-6.
- NAUMANEN, P., LAPPALAINEN, P. & HOTULAINEN, P. 2008. Mechanisms of actin stress fibre assembly. *J Microsc*, 231, 446-54.

- NEER, E. J. 1994. G proteins: critical control points for transmembrane signals. *Protein Sci*, 3, 3-14.
- NIEMEYER, G., COTTIER, D. & GERBER, U. 1987. Effects of beta-agonists on b- and c-waves implicit for adrenergic mechanisms in cat retina. *Doc Ophthalmol*, 66, 373-81.
- NIGRO, J. M., BAKER, S. J., PREISINGER, A. C., JESSUP, J. M., HOSTETTER, R., CLEARY, K., BIGNER, S. H., DAVIDSON, N., BAYLIN, S., DEVILEE, P. & ET AL. 1989. Mutations in the p53 gene occur in diverse human tumour types. *Nature*, 342, 705-8.
- NINOMIYA, I., OHTA, T., FUSHIDA, S., ENDO, Y., HASHIMOTO, T., YAGI, M., FUJIMURA, T., NISHIMURA, G., TANI, T., SHIMIZU, K., YONEMURA, Y., HEIZMANN, C. W., SCHAFFER, B. W., SASAKI, T. & MIWA, K. 2001. Increased expression of S100A4 and its prognostic significance in esophageal squamous cell carcinoma. *Int J Oncol*, 18, 715-20.
- NISHIKAWA, M., SELLERS, J. R., ADELSTEIN, R. S. & HIDAKA, H. 1984. Protein kinase C modulates in vitro phosphorylation of the smooth muscle heavy meromyosin by myosin light chain kinase. *J Biol Chem*, 259, 8808-14.
- NOBES, C. D. & HALL, A. 1995. Rho, rac, and cdc42 GTPases regulate the assembly of multimolecular focal complexes associated with actin stress fibers, lamellipodia, and filopodia. *Cell*, 81, 53-62.
- NOVITSKAYA, V., GRIGORIAN, M., KRIAJEVSKA, M., TARABYKINA, S., BRONSTEIN, I., BEREZIN, V., BOCK, E. & LUKANIDIN, E. 2000. Oligomeric Forms of the Metastasis-related Mts1 (S100A4) Protein Stimulate Neuronal Differentiation in Cultures of Rat Hippocampal Neurons. *Journal of Biological Chemistry*, 275, 41278-41286.
- OAKES, P. W., BECKHAM, Y., STRICKER, J. & GARDEL, M. L. 2012. Tension is required but not sufficient for focal adhesion maturation without a stress fiber template. *The Journal of Cell Biology*, 196, 363-374.
- ODA, T., IWASA, M., AIHARA, T., MAEDA, Y. & NARITA, A. 2009. The nature of the globular- to fibrous-actin transition. *Nature*, 457, 441-5.
- OLSON, M. & SAHAI, E. 2009. The actin cytoskeleton in cancer cell motility. *Clinical & Experimental Metastasis*, 26, 273-287.

- ONO, S. & ONO, K. 2002. Tropomyosin inhibits ADF/cofilin-dependent actin filament dynamics. *Journal of Cell Biology*, 156, 1065-1076.
- OPPENHEIMER, S. B. 2006. Cellular basis of cancer metastasis: A review of fundamentals and new advances. *Acta Histochemica*, 108, 327-334.
- OSTAP, E. M. 2002. 2,3-Butanedione monoxime (BDM) as a myosin inhibitor. *J Muscle Res Cell Motil*, 23, 305-8.
- PARKKILA, S., PAN, P.-W., WARD, A., GIBADULINOVA, A., OVECKOVA, I., PASTOREKOVA, S., PASTOREK, J., MARTINEZ, A., HELIN, H. & ISOLA, J. 2008. The calcium-binding protein S100P in normal and malignant human tissues. *BMC Clinical Pathology*, 8, 2.
- PARSONS, J. T., HORWITZ, A. R. & SCHWARTZ, M. A. 2010. Cell adhesion: integrating cytoskeletal dynamics and cellular tension. *Nat Rev Mol Cell Biol*, 11, 633-643.
- PASAPERA, A. M., SCHNEIDER, I. C., RERICHA, E., SCHLAEPFER, D. D. & WATERMAN, C. M. 2010. Myosin II activity regulates vinculin recruitment to focal adhesions through FAK-mediated paxillin phosphorylation. *The Journal of Cell Biology*, 188, 877-890.
- PELLEGRIN, S. & MELLOR, H. 2005. The Rho family GTPase Rif induces filopodia through mDia2. *Curr Biol*, 15, 129-33.
- PELLEGRIN, S. & MELLOR, H. 2007. Actin stress fibres. *J Cell Sci*, 120, 3491-3499.
- PERL, A., WILGENBUS, P., DAHL, U., SEMB, H. & CHRISTOFORI, G. 1998. A causal role for E-cadherin in the transition from adenoma to carcinoma. *Nature*, 392, 190 - 193.
- PICHOT, C. S., ARVANITIS, C., HARTIG, S. M., JENSEN, S. A., BECHILL, J., MARZOUK, S., YU, J., FROST, J. A. & COREY, S. J. 2010. Cdc42-interacting protein 4 promotes breast cancer cell invasion and formation of invadopodia through activation of N-WASp. *Cancer Research*, 70, 8347-8356.
- PLANQUE, N. & PERBAL, B. 2003. A structural approach to the role of CCN proteins in tumorigenesis. *Cancer Cell Int*.
- POHL, J., WINDER, S. J., ALLEN, B. G., WALSH, M. P., SELLERS, J. R. & GERTHOFFER, W. T. 1997. Phosphorylation of calponin in airway smooth muscle. *Am J Physiol*, 272, L115-23.

- PROU, D., GU, W. J., LE CROM, S., VINCENT, J. D., SALAMERO, J. & VERNIER, P. 2001. Intracellular retention of the two isoforms of the D(2) dopamine receptor promotes endoplasmic reticulum disruption. *J Cell Sci*, 114, 3517-27.
- RAMAMURTHY, B., YENGO, C. M., STRAIGHT, A. F., MITCHISON, T. J. & SWEENEY, H. L. 2004. Kinetic Mechanism of Blebbistatin Inhibition of Nonmuscle Myosin IIB⁺. *Biochemistry*, 43, 14832-14839.
- RENSHAW, M. W., PRICE, L. S. & SCHWARTZ, M. A. 1999. Focal adhesion kinase mediates the integrin signaling requirement for growth factor activation of MAP kinase. *J Cell Biol*, 147, 611-8.
- REPEL, M., SASSE, P., PIEKORZ, R., TANG, M., ROELL, W., DUAN, Y., KLETKE, A., HESCHELER, J., NURNBERG, B. & FLEISCHMANN, B. K. 2005. S100A1 enhances the L-type Ca²⁺ current in embryonic mouse and neonatal rat ventricular cardiomyocytes. *J Biol Chem*, 280, 36019-28.
- RESCHER, U. & GERKE, V. 2008. S100A10/p11: family, friends and functions. *Pflugers Arch*, 455, 575-82.
- RIDLEY, ANNE J. 2011. Life at the Leading Edge. *Cell*, 145, 1012-1022.
- RIDLEY, A. J., SCHWARTZ, M. A., BURRIDGE, K., FIRTEL, R. A., GINSBERG, M. H., BORISY, G., PARSONS, J. T. & HORWITZ, A. R. 2003. Cell Migration: Integrating Signals from Front to Back. *Science*, 302, 1704-1709.
- RIVERA ROSADO, L. A., HORN, T. A., MCGRATH, S. C., COTTER, R. J. & YANG, J. T. 2011. Association between $\alpha 4$ integrin cytoplasmic tail and non-muscle myosin IIA regulates cell migration. *Journal of Cell Science*.
- RODRIGUEZ, F. J., LEWIS-TUFFIN, L. J. & ANASTASIADIS, P. Z. 2012. E-cadherin's dark side: Possible role in tumor progression. *Biochimica et Biophysica Acta (BBA) - Reviews on Cancer*, 1826, 23-31.
- ROSENBAUM, D. M., RASMUSSEN, S. G. F. & KOBILKA, B. K. 2009. The structure and function of G-protein-coupled receptors. *Nature*, 459, 356-363.

ROSTY, C., UEKI, T., ARGANI, P., JANSEN, M., YEO, C. J., CAMERON, J. L., HRUBAN, R. H. & GOGGINS, M. 2002. Overexpression of S100A4 in pancreatic ductal adenocarcinomas is associated with poor differentiation and DNA hypomethylation. *Am J Pathol*, 160, 45-50.

ROTTNER, K., BEHRENDT, B., SMALL, J. V. & WEHLAND, J. 1999. VASP dynamics during lamellipodia protrusion. *Nat Cell Biol*, 1, 321-2.

ROTTNER, K., KRAUSE, M., GIMONA, M., SMALL, J. V. & WEHLAND, J. 2001. Zyxin is not colocalized with vasodilator-stimulated phosphoprotein (VASP) at lamellipodial tips and exhibits different dynamics to vinculin, paxillin, and VASP in focal adhesions. *Mol Biol Cell*, 12, 3103-13.

ROUTHIER, A., ASTUCCIO, M., LAHEY, D., MONFREDO, N., JOHNSON, A., CALLAHAN, W., PARTINGTON, A., FELLOWS, K., OUELLETTE, L., ZHIDRO, S., GOODROW, C., SMITH, A., SULLIVAN, K., SIMONE, P., LE, L., VEZULI, B., ZOHNI, M., WEST, E., GLEASON, D. & BRYAN, B. 2010. Pharmacological inhibition of Rho-kinase signaling with Y-27632 blocks melanoma tumor growth. *Oncol Rep*, 23, 861-7.

RUDLAND, P. S., PLATT-HIGGINS, A., RENSHAW, C., WEST, C. R., WINSTANLEY, J. H. R., ROBERTSON, L. & BARRACLOUGH, R. 2000. Prognostic Significance of the Metastasis-inducing Protein S100A4 (p9Ka) in Human Breast Cancer. *Cancer Research*, 60, 1595-1603.

SACK, U., WALTHER, W., SCUDIERO, D., SELBY, M., KOBELT, D., LEMM, M., FICHTNER, I., SCHLAG, P. M., SHOEMAKER, R. H. & STEIN, U. 2011. Novel effect of antihelminthic Niclosamide on S100A4-mediated metastatic progression in colon cancer. *J Natl Cancer Inst*, 103, 1018-36.

SAJID, M., HU, Z., LELE, M. & STOUFFER, G. A. 2000. Protein complexes involving alpha v beta 3 integrins, nonmuscle myosin heavy chain-A, and focal adhesion kinase from in thrombospondin-treated smooth muscle cells. *J Investig Med*, 48, 190-7.

SALEEM, M., KWEON, M.-H., JOHNSON, J. J., ADHAMI, V. M., ELCHEVA, I., KHAN, N., BIN HAFEEZ, B., BHAT, K. M. R., SARFARAZ, S., REAGAN-SHAW, S., SPIEGELMAN, V. S., SETALURI, V. & MUKHTAR, H. 2006. S100A4 accelerates tumorigenesis and invasion of human prostate cancer through the transcriptional regulation of matrix metalloproteinase 9. *Proceedings of the National Academy of Sciences*, 103, 14825-14830.

- SANDQUIST, J. C. & MEANS, A. R. 2008. The C-Terminal Tail Region of Nonmuscle Myosin II Directs Isoform-specific Distribution in Migrating Cells. *Mol. Biol. Cell*, 19, 5156-5167.
- SANDQUIST, J. C., SWENSON, K. I., DEMALI, K. A., BURRIDGE, K. & MEANS, A. R. 2006. Rho Kinase Differentially Regulates Phosphorylation of Nonmuscle Myosin II Isoforms A and B during Cell Rounding and Migration. *Journal of Biological Chemistry*, 281, 35873-35883.
- SANTALA, M., SAARIKOSKI, S. & CASTREN, O. 1990. Decreased numbers of lymphocyte beta 2-adrenoceptors in pregnant women receiving beta 2-adrenergic agonist therapy. *Acta Obstet Gynecol Scand*, 69, 17-21.
- SCHALLER, M. D. 2001. Paxillin: a focal adhesion-associated adaptor protein. *Oncogene*, 20, 6459-6472.
- SCHERKL, R., HASHEM, A. & FREY, H. H. 1990. Apomorphine-induced emesis in the dog-routes of administration, efficacy and synergism by naloxone. *Journal of Veterinary Pharmacology and Therapeutics*, 13, 154-158.
- SCHNEIDER, M., HANSEN, J. & SHEIKH, S. 2008. S100A4: a common mediator of epithelial-mesenchymal transition, fibrosis and regeneration in diseases? *Journal of Molecular Medicine*, 86, 507-522.
- SCHWARTZ, M. A. & ASSOIAN, R. K. 2001. Integrins and cell proliferation: regulation of cyclin-dependent kinases via cytoplasmic signaling pathways. *J Cell Sci*, 114, 2553-60.
- SEABROOK, G. R., KNOWLES, M., BROWN, N., MYERS, J., SINCLAIR, H., PATEL, S., FREEDMAN, S. B. & MCALLISTER, G. 1994. Pharmacology of high-threshold calcium currents in GH4C1 pituitary cells and their regulation by activation of human D2 and D4 dopamine receptors. *Br J Pharmacol*, 112, 728-34.
- SELLERS, J. R. 2000. Myosins: a diverse superfamily. *Biochim Biophys Acta*, 1496, 3-22.
- SELVAKUMAR, P., LAKSHMIKUTTYAMMA, A., DAS, U., PATI, H. N., DIMMOCK, J. R. & SHARMA, R. K. 2009. NC2213: a novel methionine aminopeptidase 2 inhibitor in human colon cancer HT29 cells. *Mol Cancer*, 8, 65.

- SENOLT, L., GRIGORIAN, M., LUKANIDIN, E., SIMMEN, B., MICHEL, B. A., PAVELKA, K., GAY, R. E., GAY, S. & NEIDHART, M. 2006. S100A4 is expressed at site of invasion in rheumatoid arthritis synovium and modulates production of matrix metalloproteinases. *Ann Rheum Dis*, 65, 1645-8.
- SERRA-PAGES, C., KEDERSHA, N. L., FAZIKAS, L., MEDLEY, Q., DEBANT, A. & STREULI, M. 1995. The LAR transmembrane protein tyrosine phosphatase and a coiled-coil LAR-interacting protein co-localize at focal adhesions. *EMBO Journal*, 14, 2827-2838.
- SERRA-PAGÈS, C., MEDLEY, Q. G., TANG, M., HART, A. & STREULI, M. 1998. Liprins, a Family of LAR Transmembrane Protein-tyrosine Phosphatase-interacting Proteins. *Journal of Biological Chemistry*, 273, 15611-15620.
- SHANG, X., CHENG, H. & ZHOU, R. 2008. Chromosomal mapping, differential origin and evolution of the S100 gene family. *Genetics Selection Evolution*, 40, 449 - 464.
- SHEMESH, T., VERKHOVSKY, A. B., SVITKINA, T. M., BERSHADSKY, A. D. & KOZLOV, M. M. 2009. Role of Focal Adhesions and Mechanical Stresses in the Formation and Progression of the Lamellum Interface. *Biophysical Journal*, 97, 1254-1264.
- SHERBET, G. & LAKSHMI, M. 1998. S100A4 (MTS1) calcium binding protein in cancer growth, invasion and metastasis. *Anticancer Res*, 18, 2415 - 2421.
- SHUTOVA, M., YANG, C., VASILIEV, J. M. & SVITKINA, T. 2012. Functions of Nonmuscle Myosin II in Assembly of the Cellular Contractile System. *PLoS ONE*, 7, e40814.
- SIEG, D. J., HAUCK, C. R., ILIC, D., KLINGBEIL, C. K., SCHAEFER, E., DAMSKY, C. H. & SCHLAEPFER, D. D. 2000. FAK integrates growth-factor and integrin signals to promote cell migration. *Nat Cell Biol*, 2, 249-56.
- SIMONS, M., WANG, M., MCBRIDE, O. W., KAWAMOTO, S., YAMAKAWA, K., GDULA, D., ADELSTEIN, R. S. & WEIR, L. 1991. Human nonmuscle myosin heavy chains are encoded by two genes located on different chromosomes. *Circ Res*, 69, 530-9.
- SIN, N., MENG, L., WANG, M. Q. W., WEN, J. J., BORNMANN, W. G. & CREWS, C. M. 1997. The anti-angiogenic agent fumagillin covalently binds and inhibits the methionine aminopeptidase, MetAP-2. *Proceedings of the National Academy of Sciences*, 94, 6099-6103.

- SIN, W.-C., TSE, M., PLANQUE, N., PERBAL, B., LAMPE, P. D. & NAUS, C. C. 2009. Matricellular Protein CCN3 (NOV) Regulates Actin Cytoskeleton Reorganization. *Journal of Biological Chemistry*, 284, 29935-29944.
- SIONOV, R. V. & HAUPT, Y. 1999. The cellular response to p53: the decision between life and death. *Oncogene*, 18, 6145-57.
- SMALL, J. V. & KAVERINA, I. 2003. Microtubules meet substrate adhesions to arrange cell polarity. *Curr Opin Cell Biol*, 15, 40-7.
- SNAPPER, S. B., TAKESHIMA, F., ANTON, I., LIU, C. H., THOMAS, S. M., NGUYEN, D., DUDLEY, D., FRASER, H., PURICH, D., LOPEZ-ILASACA, M., KLEIN, C., DAVIDSON, L., BRONSON, R., MULLIGAN, R. C., SOUTHWICK, F., GEHA, R., GOLDBERG, M. B., ROSEN, F. S., HARTWIG, J. H. & ALT, F. W. 2001. N-WASP deficiency reveals distinct pathways for cell surface projections and microbial actin-based motility. *Nat Cell Biol*, 3, 897-904.
- SONTAG, J. M., SANDERSON, P., KLEPPER, M., AUNIS, D., TAKEDA, K. & BADER, M. F. 1990. Modulation of secretion by dopamine involves decreases in calcium and nicotinic currents in bovine chromaffin cells. *The Journal of Physiology*, 427, 495-517.
- STAHL, S. M. 1998. Mechanism of action of serotonin selective reuptake inhibitors: Serotonin receptors and pathways mediate therapeutic effects and side effects. *Journal of Affective Disorders*, 51, 215-235.
- STERNLICHT, M. D., LOCHTEST, A., SYMPSON, C. J., HUEY, B., ROUGIER, J. P., GRAY, J. W., PINKEL, D., BISSELL, M. J. & WERB, Z. 1999. The stromal proteinase MMP3/stromelysin-1 promotes mammary carcinogenesis. *Cell*, 98, 137-146.
- SUMI, T., MATSUMOTO, K. & NAKAMURA, T. 2001. Specific Activation of LIM kinase 2 via Phosphorylation of Threonine 505 by ROCK, a Rho-dependent Protein Kinase. *Journal of Biological Chemistry*, 276, 670-676.
- SVOBODA, P., TEISINGER, J., NOVOTNÝ, J., BOUROVÁ, L., DRMOTA, T., HEJNOVÁ, L., MORAVCOVÁ, Z., LISÝ, V., RUDAJEV, V., STÖHR, J., VOKURKOVÁ, A., SVANDOVÁ, I. & DURCHÁNKOVÁ, D. 2004.

Biochemistry of transmembrane signaling mediated by trimeric G proteins. *Physiological research / Academia Scientiarum Bohemoslovaca*, 53 Suppl 1, S141-52.

SZYMAŃSKI, P., MARKOWICZ, M. & MIKICIUK-OLASIK, E. 2011. Adaptation of High-Throughput Screening in Drug Discovery—Toxicological Screening Tests. *International Journal of Molecular Sciences*, 13, 427-452.

TAKÁCS, B., BILLINGTON, N., GYIMESI, M., KINTSES, B., MÁLNÁSI-CSIZMADIA, A., KNIGHT, P. J. & KOVÁCS, M. 2010. Myosin complexed with ADP and blebbistatin reversibly adopts a conformation resembling the start point of the working stroke. *Proceedings of the National Academy of Sciences*, 107, 6799-6804.

TAKENAGA, K., NAKAMURA, Y. & SAKIYAMA, S. 1994. Expression of a Calcium Binding Protein pEL98 (mts1) During Differentiation of Human Promyelocytic Leukemia HL-60 Cells. *Biochemical and Biophysical Research Communications*, 202, 94-101.

TAKENAGA, K., NAKAMURA, Y. & SAKIYAMA, S. 1997a. Expression of antisense RNA to S100A4 gene encoding an S100-related calcium-binding protein suppresses metastatic potential of high-metastatic Lewis lung carcinoma cells. *Oncogene*, 14, 331-337.

TAKENAGA, K., NAKANISHI, H., WADA, K., SUZUKI, M., MATSUZAKI, O., MATSUURA, A. & ENDO, H. 1997b. Increased expression of S100A4, a metastasis-associated gene, in human colorectal adenocarcinomas. *Clin Cancer Res*, 3, 2309 - 2316.

TAMAKI, Y., IWANAGA, Y., NIIZUMA, S., KAWASHIMA, T., KATO, T., INUZUKA, Y., HORIE, T., MOROOKA, H., TAKASE, T., AKAHASHI, Y., KOBUE, K., ONO, K., SHIOI, T., SHEIKH, S. P., AMBARTSUMIAN, N., LUKANIDIN, E., KOSHIMIZU, T. A., MIYAZAKI, S. & KIMURA, T. 2013. Metastasis-associated protein, S100A4 mediates cardiac fibrosis potentially through the modulation of p53 in cardiac fibroblasts. *J Mol Cell Cardiol*, 57, 72-81.

TARABYKINA, S., KRIAJEVSKA, M., SCOTT, D. J., HILL, T. J., LAFITTE, D., DERRICK, P. J., DODSON, G. G., LUKANIDIN, E. & BRONSTEIN, I. 2000. Heterocomplex formation between metastasis-related protein S100A4 (Mts1) and S100A1 as revealed by the yeast two-hybrid system. *FEBS Lett*, 475, 187-91.

TARABYKINA, S., SCOTT, D. J., HERZYK, P., HILL, T. J., TAME, J. R., KRIAJEVSKA, M., LAFITTE, D., DERRICK, P. J., DODSON, G. G., MAITLAND, N. J., LUKANIDIN, E. M. & BRONSTEIN, I. B. 2001. The dimerization interface of the metastasis-associated protein S100A4 (Mts1): in vivo and in vitro studies. *J Biol Chem*, 276, 24212-22.

TEOH, C. M., TAM, J. K. C. & TRAN, T. 2012. Integrin and GPCR Crosstalk in the Regulation of ASM Contraction Signaling in Asthma. *Journal of Allergy*, 2012, 9.

TESTER, A. M., RUANGPANIT, N., ANDERSON, R. L. & THOMPSON, E. W. 2000. MMP-9 secretion and MMP-2 activation distinguish invasive and metastatic sublines of a mouse mammary carcinoma system showing epithelial-mesenchymal transition traits. *Clin Exp Metastasis*, 18, 553-60.

TOGO, T. & STEINHARDT, R. A. 2004. Nonmuscle Myosin IIA and IIB Have Distinct Functions in the Exocytosis-dependent Process of Cell Membrane Repair. *Molecular Biology of the Cell*, 15, 688-695.

TOJKANDER, S., GATEVA, G. & LAPPALAINEN, P. 2012. Actin stress fibers – assembly, dynamics and biological roles. *Journal of Cell Science*, 125, 1855-1864.

TOMAR, A. & SCHLAEPFER, D. D. 2009. Focal adhesion kinase: switching between GAPs and GEFs in the regulation of cell motility. *Curr Opin Cell Biol*, 21, 676-83.

TOTSUKAWA, G., YAMAKITA, Y., YAMASHIRO, S., HARTSHORNE, D. J., SASAKI, Y. & MATSUMURA, F. 2000. Distinct roles of ROCK (Rho-kinase) and MLCK in spatial regulation of MLC phosphorylation for assembly of stress fibers and focal adhesions in 3T3 fibroblasts. *J Cell Biol*, 150, 797-806.

TSOPORIS, J. N., MOHAMMADZADEH, F. & PARKER, T. G. 2010. Intracellular and Extracellular Effects of S100B in the Cardiovascular Response to Disease. *Cardiovascular psychiatry and neurology*, 2010, 206073.

UEHATA, M., ISHIZAKI, T., SATOH, H., ONO, T., KAWAHARA, T., MORISHITA, T., TAMAKAWA, H., YAMAGAMI, K., INUI, J., MAEKAWA, M. & NARUMIYA, S. 1997. Calcium sensitization of smooth muscle mediated by a Rho-associated protein kinase in hypertension. *Nature*, 389, 990-994.

- VALLELY, K. M., RUSTANDI, R. R., ELLIS, K. C., VARLAMOVA, O., BRESNICK, A. R. & WEBER, D. J. 2002. Solution Structure of Human Mts1 (S100A4) As Determined by NMR Spectroscopy†. *Biochemistry*, 41, 12670-12680.
- VALLENIUS, T. 2013. Actin stress fibre subtypes in mesenchymal-migrating cells. *Open Biology*, 3.
- VAN DIECK, J., TEUFEL, D. P., JAULENT, A. M., FERNANDEZ-FERNANDEZ, M. R., RUTHERFORD, T. J., WYSLOUCH-CIESZYNSKA, A. & FERSHT, A. R. 2009. Posttranslational modifications affect the interaction of S100 proteins with tumor suppressor p53. *J Mol Biol*, 394, 922-30.
- VENOT, C., MARATRAT, M., DUREUIL, C., CONSEILLER, E., BRACCO, L. & DEBUSSCHE, L. 1998. The requirement for the p53 proline-rich functional domain for mediation of apoptosis is correlated with specific PIG3 gene transactivation and with transcriptional repression. *EMBO J*, 17, 4668-79.
- VERKHOVSKY, A. B. & BORISY, G. G. 1993. Non-sarcomeric mode of myosin II organization in the fibroblast lamellum. *J Cell Biol*, 123, 637-52.
- VICENTE-MANZANARES, M., CHOI, C. K. & HORWITZ, A. R. 2009a. Integrins in cell migration - the actin connection. *J Cell Sci*, 122, 199-206.
- VICENTE-MANZANARES, M. & HORWITZ, A. R. 2010. Myosin light chain mono- and di-phosphorylation differentially regulate adhesion and polarity in migrating cells. *Biochemical and Biophysical Research Communications*, 402, 537-542.
- VICENTE-MANZANARES, M. & HORWITZ, A. R. 2011a. Adhesion dynamics at a glance. *Journal of Cell Science*, 124, 3923-3927.
- VICENTE-MANZANARES, M. & HORWITZ, A. R. 2011b. Adhesion dynamics at a glance. *J Cell Sci*, 124, 3923-7.
- VICENTE-MANZANARES, M., KOACH, M. A., WHITMORE, L., LAMERS, M. L. & HORWITZ, A. F. 2008. Segregation and activation of myosin IIB creates a rear in migrating cells. *The Journal of Cell Biology*, 183, 543-554.
- VICENTE-MANZANARES, M., MA, X., ADELSTEIN, R. S. & HORWITZ, A. R. 2009b. Non-muscle myosin II takes centre stage in cell adhesion and migration. *Nat Rev Mol Cell Biol*, 10, 778-90.

- VICENTE-MANZANARES, M., ZARENO, J., WHITMORE, L., CHOI, C. K. & HORWITZ, A. F. 2007. Regulation of protrusion, adhesion dynamics, and polarity by myosins IIA and IIB in migrating cells. *J Cell Biol*, 176, 573-80.
- VIGNJEVIC, D., KOJIMA, S., ARATYN, Y., DANCIU, O., SVITKINA, T. & BORISY, G. G. 2006. Role of fascin in filopodial protrusion. *J Cell Biol*, 174, 863-75.
- WANG, G., PLATT-HIGGINS, A., CARROLL, J., DE SILVA RUDLAND, S., WINSTANLEY, J., BARRACLOUGH, R. & RUDLAND, P. S. 2006. Induction of Metastasis by S100P in a Rat Mammary Model and Its Association with Poor Survival of Breast Cancer Patients. *Cancer Research*, 66, 1199-1207.
- WANG, G., RUDLAND, P. S., WHITE, M. R. & BARRACLOUGH, R. 2000. Interaction in Vivo and in Vitro of the Metastasis-inducing S100 Protein, S100A4 (p9Ka) with S100A1. *Journal of Biological Chemistry*, 275, 11141-11146.
- WANG, G., ZHANG, S., FERNIG, D. G., MARTIN-FERNANDEZ, M., RUDLAND, P. S. & BARRACLOUGH, R. 2004. Mutually antagonistic actions of S100A4 and S100A1 on normal and metastatic phenotypes. *Oncogene*, 24, 1445-1454.
- WANG, K., ASH, J. F. & SINGER, S. J. 1975. Filamin, a new high-molecular-weight protein found in smooth muscle and non-muscle cells. *Proceedings of the National Academy of Sciences*, 72, 4483-4486.
- WANG, Y. Y., YE, Z. Y., ZHAO, Z. S., TAO, H. Q. & CHU, Y. Q. 2010. High-level expression of S100A4 correlates with lymph node metastasis and poor prognosis in patients with gastric cancer. *Ann Surg Oncol*, 17, 89-97.
- WANG, Z. & GRIFFIN, M. 2013. The Role of TG2 in Regulating S100A4-Mediated Mammary Tumour Cell Migration. *PLoS ONE*, 8, e57017.
- WATANABE, T., HOSOYA, H. & YONEMURA, S. 2007. Regulation of myosin II dynamics by phosphorylation and dephosphorylation of its light chain in epithelial cells. *Mol Biol Cell*, 18, 605-16.

- WATANABE, T., NORITAKE, J. & KAIBUCHI, K. 2005. Regulation of microtubules in cell migration. *Trends Cell Biol*, 15, 76-83.
- WATANABE, T. M., TOKUO, H., GONDA, K., HIGUCHI, H. & IKEBE, M. 2010. Myosin-X induces filopodia by multiple elongation mechanism. *J Biol Chem*, 285, 19605-14.
- WATANABE, Y., USADA, N., MINAMI, H., MORITA, T., TSUGANE, S., ISHIKAWA, R., KOHAMA, K., TOMIDA, Y. & HIDAKA, H. 1993. Calvasculin, as a factor affecting the microfilament assemblies in rat fibroblasts transfected by src gene. *FEBS Lett*, 324, 51-5.
- WEAR, M. A., YAMASHITA, A., KIM, K., MAÉDA, Y. & COOPER, J. A. 2003. How Capping Protein Binds the Barbed End of the Actin Filament. *Current Biology*, 13, 1531-1537.
- WEI, Z., ZHENG, S., SPANGLER, SAMANTHA A., YU, C., HOOGENRAAD, CASPER C. & ZHANG, M. 2011. Liprin-Mediated Large Signaling Complex Organization Revealed by the Liprin- α /CASK and Liprin- α /Liprin- β Complex Structures. *Molecular Cell*, 43, 586-598.
- WELLMAN, P. J., MCMAHON, L. R., GREEN, T. & TOLE, A. 1997. Effects of the alpha 1a-adrenoceptor antagonist RS-17053 on phenylpropanolamine-induced anorexia in rats. *Pharmacol Biochem Behav*, 57, 281-4.
- WHEELER, A. P. & RIDLEY, A. J. 2004. Why three Rho proteins? RhoA, RhoB, RhoC, and cell motility. *Exp Cell Res*, 301, 43-9.
- WICKSTEAD, B. & GULL, K. 2011. The evolution of the cytoskeleton. *The Journal of Cell Biology*, 194, 513-525.
- WIESNER, S., LANGE, A. & FÄSSLER, R. 2006. Local call: from integrins to actin assembly. *Trends in Cell Biology*, 16, 327-329.
- WIESNER, S., LEGATE, K. R. & FÄSSLER, R. 2005. Integrin-actin interactions. *Cellular and Molecular Life Sciences*, 62, 1081-1099.
- WOLF, R., RUZICKA, T. & YUSPA, S. H. 2011. Novel S100A7 (psoriasin)/S100A15 (koebnerisin) subfamily: highly homologous but distinct in regulation and function. *Amino Acids*, 41, 789-96.

- WOLFENSON, H., HENIS, Y. I., GEIGER, B. & BERSHADSKY, A. D. 2009. The heel and toe of the cell's foot: A multifaceted approach for understanding the structure and dynamics of focal adhesions. *Cell Motility and the Cytoskeleton*, 66, 1017-1029.
- WONG, K., PERTZ, O., HAHN, K. & BOURNE, H. 2006. Neutrophil polarization: spatiotemporal dynamics of RhoA activity support a self-organizing mechanism. *Proc Natl Acad Sci U S A*, 103, 3639-44.
- WORTHYLAKE, R. A. & BURRIDGE, K. 2003. RhoA and ROCK Promote Migration by Limiting Membrane Protrusions. *Journal of Biological Chemistry*, 278, 13578-13584.
- WOZNIAK, M. A., MODZELEWSKA, K., KWONG, L. & KEELY, P. J. 2004. Focal adhesion regulation of cell behavior. *Biochim Biophys Acta*, 1692, 103-19.
- XUE, C., PLIETH, D., VENKOV, C., XU, C. & NEILSON, E. G. 2003. The gatekeeper effect of epithelial-mesenchymal transition regulates the frequency of breast cancer metastasis. *Cancer Res*, 63, 3386-94.
- YAM, P. T., WILSON, C. A., JI, L., HEBERT, B., BARNHART, E. L., DYE, N. A., WISEMAN, P. W., DANUSER, G. & THERIOT, J. A. 2007. Actin-myosin network reorganization breaks symmetry at the cell rear to spontaneously initiate polarized cell motility. *J Cell Biol*, 178, 1207-21.
- YAMAGUCHI, H., WYCKOFF, J. & CONDEELIS, J. 2005. Cell migration in tumors. *Current Opinion in Cell Biology*, 17, 559-564.
- YAMASHIRO, S., YAMAKITA, Y., ONO, S. & MATSUMURA, F. 1998. Fascin, an actin-bundling protein, induces membrane protrusions and increases cell motility of epithelial cells. *Mol Biol Cell*, 9, 993-1006.
- YAMMANI, R. R., CARLSON, C. S., BRESNICK, A. R. & LOESER, R. F. 2006. Increase in production of matrix metalloproteinase 13 by human articular chondrocytes due to stimulation with S100A4: Role of the receptor for advanced glycation end products. *Arthritis & Rheumatism*, 54, 2901-2911.
- YARROW, J., PERLMAN, Z., WESTWOOD, N. & MITCHISON, T. 2004. A high-throughput cell migration assay using scratch wound healing, a comparison of image-based readout methods. *BMC Biotechnology*, 4, 21.

- YARROW, J. C., LECHLER, T., LI, R. & MITCHISON, T. J. 2003. Rapid de-localization of actin leading edge components with BDM treatment. *BMC Cell Biol*, 4, 5.
- YOKOTA, J. 2000. Tumor progression and metastasis. *Carcinogenesis*, 21, 497-503.
- YONEMURA, Y., ENDOU, Y., KIMURA, K., FUSHIDA, S., BANDOU, E., TANIGUCHI, K., KINOSHITA, K., NINOMIYA, I., SUGIYAMA, K., HEIZMANN, C. W., SCHAFFER, B. W. & SASAKI, T. 2000a. Inverse expression of S100A4 and E-cadherin is associated with metastatic potential in gastric cancer. *Clin Cancer Res*, 6, 4234-42.
- YONEMURA, Y., ENDOU, Y., KIMURA, K., FUSHIDA, S., BANDOU, E., TANIGUCHI, K., KINOSHITA, K., NINOMIYA, I., SUGIYAMA, K., HEIZMANN, C. W., SCHAFFER, B. W. & SASAKI, T. 2000b. Inverse Expression of S100A4 and E-Cadherin Is Associated with Metastatic Potential in Gastric Cancer. *Clinical Cancer Research*, 6, 4234-4242.
- ZHANG, H.-Y., ZHENG, X.-Z., WANG, X.-H., XUAN, X.-Y., WANG, F. & LI, S.-S. 2011. S100A4 mediated cell invasion and metastasis of esophageal squamous cell carcinoma via the regulation of MMP-2 and E-cadherin activity. *Molecular Biology Reports*, 1-10.
- ZHANG, S., WANG, G., FERNIG, D. G., RUDLAND, P. S., WEBB, S. E. D., BARRACLOUGH, R. & MARTIN-FERNANDEZ, M. 2005. Interaction of metastasis-inducing S100A4 protein in vivo by fluorescence lifetime imaging microscopy. *European Biophysics Journal*, 34, 19-27.
- ZHAO, J. H., REISKE, H. & GUAN, J. L. 1998. Regulation of the cell cycle by focal adhesion kinase. *J Cell Biol*, 143, 1997-2008.
- ZHU, F., SHI, Z., QIN, C., TAO, L., LIU, X., XU, F., ZHANG, L., SONG, Y., ZHANG, J., HAN, B., ZHANG, P. & CHEN, Y. 2012. Therapeutic target database update 2012: a resource for facilitating target-oriented drug discovery. *Nucleic Acids Res*, 40, D1128-36.
- ZIGMOND, S. H. & SULLIVAN, S. J. 1979. Sensory adaptation of leukocytes to chemotactic peptides. *J Cell Biol*, 82, 517-27.
- ZOLESE, G., TANGORRA, A., CURATOLA, G., GIAMBANCO, I. & DONATO, R. 1988. Interaction of S-100b protein with cardiolipin vesicles as monitored by electron spin resonance, pyrene fluorescence and circular dichroism. *Cell Calcium*, 9, 149-57.

ZOU, M., AL-BARADIE, R. S., AL-HINDI, H., FARID, N. R. & SHI, Y. 2005. S100A4 (Mts1) gene overexpression is associated with invasion and metastasis of papillary thyroid carcinoma. *Br J Cancer*, 93, 1277-1284.

ZOU, M., FAMULSKI, K. S., PARHAR, R. S., BAITEI, E., AL-MOHANNA, F. A., FARID, N. R. & SHI, Y. 2004. Microarray Analysis of Metastasis-Associated Gene Expression Profiling in a Murine Model of Thyroid Carcinoma Pulmonary Metastasis: Identification of S100A4 (Mts1) Gene Overexpression as a Poor Prognostic Marker for Thyroid Carcinoma. *J Clin Endocrinol Metab*, 89, 6146-6154.